Experimental Study of Basalt Carbonatization

Gabrielle J. Stockmann

Université de Toulouse

THÈSE

En vue de l'obtention du

DOCTORAT DE L'UNIVERSITÉ DE TOULOUSE

Délivré par :
Université Toulouse 3 Paul Sabatier (UT3 Paul Sabatier)

Cotutelle internationale avec :
University of Iceland, Islande

Présentée et soutenue par :
Gabrielle J. STOCKMANN
Le mercredi 16 mai 2012

Titre :

Experimental study of basalt carbonatization
(Étude expérimentale de la carbonatation du basalte)

ED SDU2E : Sciences de la Terre et des Planètes Solides

Unité de recherche :
Géosciences Environnement Toulouse (GET)

Directeur(s) de Thèse :

OELKERS, Dr. Eric H.
GISLASON, Dr. Sigurdur Reynir

Rapporteurs :
BENNING, Prof. Liane G.,
MÉNEZ, Prof. Bénédicte

Autre(s) membre(s) du jury :

WOLFF-BOENISCH, Dr. Domenik,
BURTON, Prof. Kevin, et ARNÓRSSON, Prof. Stefán

Résumé

La concentration croissante de CO_2 dans l'atmosphère et les dangers potentiels qu'elle représente pour la terre au travers des changements climatiques, l'acidification des océans et l'élévation du niveau de la mer a conduit à un certain nombre de projets qui tentent de trouver un moyen sûr et inoffensifs pour capturer et stocker le CO_2 dans des formations géologiques. Une de ces tentatives se déroule actuellement en Islande à la centrale géothermique Hellisheiði, située à proximité de la capitale, Reykjavik (le projet CarbFix). Le dioxyde de carbone et d'autres gaz comme H_2S, N_2, H_2, CH_4, et Ar sont des sous-produits de l'exploitation de l'énergie géothermique et l'objectif est de stocker tout ce CO_2 dans les formations basaltiques qui se situent sous Hellisheiði. Le CO_2 est dissous dans un courant d'eau injecté par pompage dans puits jusqu'à à 350 mètres de profondeur et qui s'écoule ensuite au sein d'horizons mixtes de verre basaltique et de basalte cristallin. Les roches basaltiques sont caractérisées par des teneurs élevées en cations divalents comme Mg^{2+}, Fe^{2+} et Ca^{2+} et des vitesses de dissolution relativement rapides. L'eau acide chargée en CO_2 dissout le basalte, libérant ainsi des cations qui peuvent réagir avec les ions carbonates pour former des minéraux carbonatés (magnésite, sidérite, calcite, ankérite ainsi que des solutions solides (Ca-Mg-Fe)CO_3)). Si on admet que c'est la dissolution des roches basaltiques qui contrôle ce processus de séquestration du carbone, on peut en déduire que tout ce qui pourra limiter cette dissolution sera préjudiciable à l'ensemble du processus de confinement du CO_2.

Mon rôle dans le projet CarbFix a été d'examiner les effets de la formation de revêtements de carbonate de calcium sur la dissolution des phases primaires de basalte. Je me suis concentrée sur le verre basaltique et le clinopyroxène, diopside, afin de comparer des phases cristallines et non cristallines. En outre, une série d'expériences ont été menées pour étudier l'effet de la structure du minéral primaire sur la nucléation de calcite. Ces expériences ont été faites pour vérifier si les différentes structures de silicate conduiraient à une différente étendue de la nucléation et croissance de la calcite à la surface des silicates. Enfin, de nombreuses expériences de dissolution de verre basaltique ont été menées en présence de bactéries hétérotrophes mortes et vivantes, *Pseudomonas reactans,* afin de déterminer l'effet des bactéries sur la dissolution des roches dans le système des eaux souterraines du site Hellisheiði.

Les expériences de dissolution de verre basaltique et de diopside ont été réalisés à 25 et 70 °C pour un pH de 7-8 dans des réacteurs à circulation alimentés en solutions de forces ioniques > 0,03 mol / kg contenant $CaCl_2 \pm NaHCO_3$. Deux séries d'essais ont été menés simultanément, une série appelée essais de 'précipitations' au cours de laquelle la solution dans le réacteur était sursaturée par rapport à la calcite, et l'autre série appelée essais de 'contrôle', pour laquelle la modélisation PHREEQC ne prévoyait pas formation de minéraux secondaires. Ainsi, il a été possible de comparer les vitesses de dissolution du verre basaltique et du diopside à 25 °C avec et sans la formation de carbonate de calcium et d'autres minéraux secondaires afin d'en déduire leur effet sur les vitesses de dissolution. Les images de microscopie électronique à balayage ont montré que des quantités importantes de carbonate de calcium ont précipité au cours des expériences de 'précipitations' mais, dans le cas du verre basaltique la croissance primaire se présente sous forme gros amas discrets de calcite et d'aragonite qui ne se forment pas sur le verre lui-même. Par contre, plusieurs des cristaux de diopside ont été largement envahis par des revêtements de calcite sans aragonite décelable. Dans les deux cas, la présence de calcite / aragonite n'a pas eu d'incidence sur les vitesses de dissolution du verre basaltique et de diopside qui sont les mêmes que celles mesurées dans la série 'contrôle'. Il semblerait que la couverture discontinue et poreuse de carbonates permet aux ions des phases primaires de continuer à diffuser sans entrave à travers la couche secondaire.

Pour mieux évaluer l'effet de la surface des silicates sur la nucléation de la calcite, les vitesses de dissolution de six minéraux et roches silicatés ont été mesurées à 25 °C dans des réacteurs à circulation en présence de solutions de pH ~ 9,1 sursaturées par rapport à la calcite. Les phases silicatées étaient les suivantes: olivine, enstatite, augite, labradorite, verre basaltique et péridotite. Les résultats montrent que le temps d'induction pour la nucléation de calcite et l'étendue de la couverture de carbonatée avec le temps varient selon la phase silicatée. Dans un même laps de temps l'olivine, l'enstatite et la péridotite (principalement composé d'olivine riche en Mg) étaient les plus couvertes par les précipitations de calcite, suivis par l'augite, la labradorite et enfin le verre basaltique. Toute la croissance de calcite a eu lieu sur la surface du silicate, y compris sur le verre basaltique. La cinétique favorise la croissance de calcite par nucléation sur les minéraux orthorhombiques (enstatite et olivine) par rapport aux minéraux monocliniques et tricliniques. Les plus faibles

quantités de calcite ont été trouvées sur le verre qui n'a pas de structure silicatée ordonnée.

Des bactéries hétérotrophes, *Pseudomonas reactans* ont été extraites de l'un des puits de contrôle à Hellisheiði et ont ensuite été séparées, purifiées et cultivées en laboratoire. Avec le bouillon de culture utilisé, les conditions de croissance optimales de cette bactérie sont 5-37 ºC et un pH de 7,0 à 8. Cette bactérie, très commune dans l'eau et le sol, est une bonne candidate pour tester l'impact des bactéries hétérotrophes en général lors de la séquestration du CO_2 dans un aquifère naturel comme en Islande. Les vitesses de dissolution du verre basaltique ont été mesurés à 25 ºC dans des nouveaux réacteurs à circulation permettant d'opérer en présence de bactéries (BMFR) dans des solutions tamponnées transportant 0,1 à 0,4 g/L de bactéries mortes et 0,9 à 19 g/L de bactéries vivantes à $4 \leq pH \leq 10$. Les résultats ont montré que la présence de ces bactéries n'avait quasiment pas d'effet effet sur la vitesse de dissolution.

La conclusion générale de cette étude est que ni les revêtements de carbonate, ni les bactéries n'ont d'impact majeur sur les vitesses de dissolution des phases primaires silicatées. Ainsi, leur effet devrait être négligeable sur le processus de séquestration du CO_2 sur le site Hellisheiði en Islande. Le basalte cristallin pourrait être recouvert plus rapidement en carbonate de calcium, mais le verre basaltique pourrait aussi servir de support pour la nucléation de calcite.

Abstract

The increasing levels of CO_2 in the atmosphere and the potential dangers this pose to the Earth through climate change, ocean acidification and sea-level rise has lead to a substantial number of projects attempting to find a safe and benign way to capture and store CO_2 in geological formations, also referred to as the CCS (Carbon Capture Storage) technology. One of these CCS attempts is currently taking place in Iceland at the geothermal power plant Hellisheiði, located close to the capital Reykjavik (the CarbFix project). CO_2 and other gasses (H_2S, N_2, H_2, CH_4) are waste products of the geothermal energy exploitation and the aim is with time to store all of this anthropogenic-made CO_2 in the basaltic formations underlying Hellisheiði. The CO_2 is dissolved in groundwater as it is pumped down to 350 meters depth and then injected into mixed horizons of basaltic glass and crystalline basalt. The basaltic rocks are characterized by high contents of divalent cations like Mg^{2+}, Fe^{2+} and Ca^{2+} and relatively fast dissolution rates. The acidic CO_2-loaded water will dissolve the basalt thereby releasing cations, which can react with the aqueous carbonate ions to form carbonate minerals (magnesite, siderite, calcite, ankerite and Ca-Mg-Fe solid solutions). The rate-limiting step of this carbon sequestration process is thought to be the dissolution of basaltic rocks, thus any effect that could potentially limit basalt dissolution would be detrimental to the overall CO_2 sequestration process.

My part of the CarbFix project has been to look at the effects the formation of calcium carbonate coatings would have on the dissolution of the primary phase, in this case basaltic glass and the clinopyroxene diopside, so there would be a glass phase to compare with the results of a mineral phase. Furthermore, a series of experiments were conducted where we tested the primary mineral structure's affect on calcite nucleation. This was done in order to test if different silicate structures would lead to different extent of calcite nucleation and growth. Finally, extensive series were conducted on the dissolution of basaltic glass in the presence of dead and live heterotrophic bacteria, *Pseudomonas reactans* in order to determine the potential effect of bacteria on the carbon storage effort at the Hellisheiði site.

The basaltic glass and diopside dissolution experiments were run at 25 and 70 ºC and pH 7-8 in mixed-flow reactors connected to solutions containing $CaCl_2$±$NaHCO_3$ with ionic strengths > 0.03 mol/kg. Two sets of experimental series were run simultaneously, one series called the "precipitation" experiments in which

the solution inside the reactor was supersaturated with respect to calcite, and the other series called the "control" experiments, where PHREEQC modeling foretold no major secondary mineral formation. By this, it was possible to compare dissolution rates of basaltic glass and diopside at 25 ºC with and without calcium carbonate and other secondary mineral formation in order to deduce the effect on their dissolution rates. Scanning electron microscope images showed substantial amounts of calcium carbonate had precipitated in the "precipitation" experiments, but in the case of basaltic glass the primary growth appeared as big, discrete cluster of calcite and aragonite with no growth on the glass itself. Opposed to this, several of the diopside crystals were extensively overgrown by calcite coatings and no aragonite was found. In neither cases did the presence of calcite/aragonite have an effect on the dissolution rates of basaltic glass and diopside when compared to the "control' dissolution rates. It appears the discontinuous cover of the carbonate allows the ions of the primary phases to continue to diffuse through the secondary layer unhindered.

To further assess the effect of silicate surface on the nucleation of calcite, the dissolution rates of six selected silicate minerals and rocks were measured in mixed-flow reactors in solutions supersaturated with respect to calcite at 25 ºC and pH ~9.1. The silicate phases were: Mg-rich olivine, enstatite, augite, labradorite, basaltic glass and peridotite. The results show different onset time of calcite nucleation and thus different extent of carbonate coverage with elapsed time depending on silicate phase. Within the same timeframe olivine, enstatite and peridotite (mainly composed of Mg-rich olivine) were the most covered by calcite precipitations, followed by augite, labradorite and finally basaltic glass. All calcite growth took place on the silicate surface including on the basaltic glass. Kinetics favor calcite nucleation growth on the orthorhombic minerals (enstatite and olivine) over the monoclinic and triclinic minerals. Least calcite was found on the glass, which has no ordered silicate structure.

Heterotrophic bacteria, *Pseudomonas reactans* was extracted from one of the monitoring wells at Hellisheiði, and then separated, purified and cultured in the laboratory. Its optimal growth conditions were found to be 5-37 ºC and pH 7.0-8.2 on Brain Heart Broth nutrient. Being a common water- and soil bacteria it offered a good candidacy to test what could be expected of heterotrophic bacteria in general when storing CO_2 in a natural aquifers like the one at the Hellisheiði site, in Iceland. Basaltic glass dissolution rates were measured at 25 ºC in newly developed Bacterial Mixed-Flow reactors (BMFR) in buffer solutions carrying 0.1–0.4 g/L of dead

bacteria and 0.9–19 g/L of live bacteria at $4 \leq pH \leq 10$. The results show that the presence had either no or a slightly rate-limiting effect.

The overall conclusion is that neither the carbonate coatings nor the bacteria had major impact on the measured dissolution rates of the primary silicate phases, thus their effect are expected to be negligible on the CO_2 sequestration process in basalt. Crystalline basalt might be faster covered by calcium carbonate, but also basaltic glass can act as a nucleation platform for calcite nucleation.

Ágrip

Aukinn styrkur koltvíoxíðs í andrúmslofti hefur leitt til aukinna gróðurhúsaáhrifa og þar með hlýnunar loftslags, hækkunar á yfirborði sjávar og súrnunar úthafanna. Til þess að stemma stigu við frekari aukningu á styrk koltvíoxíðs (CO_2) í andrúmslofti hafa verið gerðar nokkrar tilraunir til að fanga og binda koltvíoxíð í bergi. Svokallað Carbfix verkefni á Hellisheiði er ein slík tilraun. Við Hellisheiðarvirkjun losna jarðhitalofttegundir eins og CO_2, H_2S, N_2, H_2, CH_4, and Ar. Í ráði er að skilja gastegundinar að og dæla CO_2 undir þrýstingi niður á um 350 m dýpi, þar sem gasið blandast vatni sem dælt er niður í bergið. Koltvíoxíðið leysist upp í vatninu, en við það verður vatnið hvarfgjarnt og leysir tvígildar jónir úr berginu. Styrkur jónanna Mg^{2+}, Fe^{2+} og Ca^{2+} er hlutfallslega mikill í berggrunninum á Hellisheiði, sem gerður er úr basalti. Jónirnar ganga í efnasamband við kolefni í vatnslausninni og mynda karbónatsteindir sem falla út og geta verið stöðugar í þúsundir ára. Þar með er koltvíoxíðið steinrunnið. Talið er að leysing tvígildra jóna úr bergi ráði hraða steinrenningarinnar. Það er því brýnt að rannsaka þau ferli, sem hugsanlega gætu haft áhrif á leysnihraða jónanna úr berginu.

Í þessum hluta CarbFix verkefnisins voru áhrif karbónatsteinda og baktería á leysingu basalts rannsökuð með tilraunum á ransóknarstofu. Sérstök áhersla var lögð á að rannsaka leysingu bergsins þegar yfirborð þess var þakið karbónatútfellingum. Tilraunir voru gerðar með leysnihraða basaltglers og díopsíðs, til þess að bera saman áhrif útfellinga á leysnihraða glers og kristals, sem eru rík af Ca^{2+} og Mg^{2+} jónum. Enn fremur voru áhrif kristalbyggingar bergs á nýmyndun kalsítútfellinga rannsökuð með tilraunum á rannsóknarstofu. Og loks voru áhrif bakteríunnar *Pseudomonas reactans* á leysnihraða basaltglers rannsökuð. Bakteríurnar voru einangraðar úr grunnvatni frá Hellisheiði og voru þær ýmist dauðar eða lifandi í tilraununum.

Leysnihraði basaltglers og díopsíðs var mældur við 25° og 70°C, og pH 7 til 8 í hvarfakútum með hræringu og gegnumflæði lausnar. Jóníska styrkur lausnarinnar, $CaCl_2 \pm NaHCO_3$, var meiri en 0,03 mól/L. Tvær tilraunaraðir voru keyrðar samtímis, önnur kölluð „útfelling“, þar sem lausnin var mettuð miðað við útfellingarsteindina kalsít, en hin tilraunaröðin, kölluð „viðmið“, var undirmettuð miðað við kalsít samkvæmt reiknilíkaninu PHREEQC. Með þessu var hægt að bera saman leysnihraða díopsíðs og basaltglers, með eða án kalsítútfellinga. Rafeindasmásjármyndir sýndu töluverðar útfellingar í lok útfellingatilrauna en ekki í viðmiðunartilraununum. Kalsít og aragónít útfellingar mynduðust

ekki á yfirborði basaltglersins en mynduðu sérstaka klasa. Kalsít óx hins vegar á yfirborði díopsíðs en ekkert aragónít myndaðist. Viðmiðunartilraunin sýndi að útfellingarnar höfðu ekki marktæk áhrif á leysnihraða díopsíðs eða basaltglers. Útfellingarnar mynduðu lauslega tengda kristalsklasa eða gropna himnu sem höfðu hvorki áhrif á leysingu basaltglersins né díopsíðsins.

Áhrif kristalbyggingar sex mismunandi leysnifasa á nýmyndun kalsítútfellinga var rannsökuð í hvarfakútum með hræringu og gegnumflæði lausnar, sem var yfirmettuð miðað við kalsít við 25°C og pH 9,1. Tilraunin var gerð á steindunum ólivíni, enstatíti, ágíti og labradoríti og svo á basaltgleri. Bergtegundin perídótít var einnig notuð til samanburðar en hún var að mestu Mg-ríkt ólivín. Nýmyndun kalsíts var háð kristalbyggingu leysnifasans. Kalsít féll fyrst út á ólivíni, enstatíti og perídótíti. Því næst myndaðist kalsít á ágíti, þá labradoríti og síðast á basaltgleri. Útfellingar mynduðust á yfirborði allra leysnifasanna, þar með talið á yfirborði basaltglersins. Nýmyndun kalsíts gengur greiðlegar fyrir sig á steindum með orþórombíska kristalbyggingu (ólivín og enstatít) en á steindum með mónóklíníska og tríklíníska byggingu. Minnst myndaðist af kalsíti á yfirborði glersins, sem hefur takmarkaðri reglu í uppröðun frumeinda sinna en kristallarnir.

Ófrumbjarga bakteríunni *Pseudomonas reactans* var safnað úr einni af vöktunarborholunum á Hellisheiði, hún var síðan einangruð og ræktuð á rannsóknarstofu. Kjöraðstæður hennar eru við 5 − 37ºC, pH 7.0 − 8.2 og hún var nærð á „Brain Heart Broth“. Bakterían er algeng í jarðvegi og grunnvatni og ætti því að gefa góða mynd af viðbrögðum baktería við niðurdælingu koltvíoxíðs í berg og áhrifum baktería á leysnihraða basalts. Leysnihraði basaltglers var mældur í sérstökum bakteríuhvarfakútum með hræringu og gegnumflæði við 25°C og pH frá 4 til 10. Styrkur baktería í lausn sem dælt var í gegnum hvarfakútinn var 0,9–19 g/L af lifandi bakteríum en 0,1–0,4 g/L af dauðum bakteríum. Bakteríurnar höfðu ýmist engin eða lítillega letjandi áhrif á leysnihraða basaltglersins.

Heildarniðurstöður þessarar rannsóknar eru að karbónatútfellingar og bakteríur hafa ekki afgerandi áhrif á leysnihraða þeirra frumsteinda basalts og basaltglers sem rannsakaðar voru. Útfellingarnar og bakteríurnar ættu því ekki að letja steinrenningu koltvísýrings í basalti. Kalsít fellur hraðar út á kristölluðu basalti en á glerjuðu, en þrátt fyrir það myndast einnig kalsít á yfirborði basaltglers.

Acknowledgement

There are several people I would like to acknowledge in connection with this PhD project. First of all, I sincerely want to thank my supervisors, Sigurður Reynir Gíslason at the University of Iceland and Eric H. Oelkers at GET/CNRS, Université Paul Sabatier for enrolling me in the CarbFix project and providing me with a first-class PhD project. It was a long-lived dream of mine to return to a career in research, and I have never regretted for one second that I left my well-paid job in Copenhagen for a PhD position in Iceland, despite economic collapse etc. It has been quite an adventurous and interesting time of my life. I owe my former supervisor from the Master's study in Denmark, Susan Stipp special thanks for encouraging me to return to a career in science and for recommending me to the PhD position in Iceland.

I was recommended at the end of my Master's project to improve my kinetic skills, so it felt great to get under the supervision of two kinetic experts like Siggi and Eric during this PhD project. They have provided me with the exact knowledge I was looking for and needed in order to become a better scientist. Furthermore, they have taught me how to "cut it to the bone" and get a message across in scientific writing. Eric and Siggi have always emphasized the importance of networking and been excellent in sending PhD students to conferences and meetings, as well as getting us involved in European networks for young researchers. Hence, we now benefit from a super network of fellow scientists around the world.

Two other scientists have functioned as co-supervisors during the PhD and been of great help; Domenik Wolff-Boenisch at the University of Iceland and Oleg Pokrovsky at GET/CNRS in Toulouse. Domenik Wolff-Boenisch was my daily supervisor in Iceland and has been a tremendous help both in setting up the experiments, discussing results and having the patience to explain the science I found difficult to understand. He has always helped me, when I needed it and furthermore been a really good friend along with the rest of his family. Oleg Pokrovsky got me involved in the biogeochemistry experiments in Toulouse, which I am very grateful for. It has been fun and inspiring to work with Oleg and Liudmila Shirokova, and they have opened a whole new world for me; the world of bacteria-mineral interaction.

There are so many colleagues from Iceland and France I want to thank and the list is too long for this text. However, I really want to name a few: Eydís Salome Eiríksdóttir, Hanna Kassalainen, Nicole Keller, Snorri Guðbrandsson, Helgi Arnar

Alfreðsson, Júlia Katrin Björke, Alex Gysi, Nicole Hurtig, Ívar Örn Benediktsson, Anders Schomacker, Marie Kløve Keiding, Jakob Kløve Jakobsen, Gro Birkefeldt Møller Pedersen, Sylvia Lebon, Kate Smith, Ólafur Ingólfsson, Andri Stefánsson, Ingvi Gunnarson, Iwona Galeczka, Kiflom Mesfin, Mahnaz Rezvani Khalilabad, Guðrún Gísladóttir, and Halldór Ólafsson. They have all been excellent company in Iceland and helped in many different ways.

Valuable technical support was provided by Þorsteinn Jónsson (Steini), who among others made all my reactors for the flow-through experiments in Iceland. I want to thank both Anna Eiríksdóttir and Magnús Birgisson for helping with salary and other important financial issues.

Therese K. Flaathen introduced me to the French life in Toulouse, helped to set up experiments in the LMTG/GET lab, and showed me how to run the different analysis instruments there. I owe her a thousand thanks for all her help. It took some time to get settled in France, but in the end I really enjoyed it. Thanks to good colleagues like Vassilis Mavromatis, Markus Aretz, Quentin Gautier, Sam Parry, Allison Haus, Sigurður H. Markusson, Chris Pearce, Giuseppe Saldi, Morgan Jones, Teresa Roncal Herrero, Elena Bazarkina, Irina Bundeleva, Pascale Bénézeth, and Jacques Schott (who generously shared his impressive knowledge of science and taught me how to pronounce my name correctly in French).

This thesis would probably not have been possible without the help of Clare Desplat in Toulouse, and she deserves special thanks for all the practical things she has helped me with, which are numerous.

Reykjavik Energy and the Research Fund of the University of Iceland are gratefully acknowledged for providing me with the main funding and making this PhD project possible. Rikke Pedersen and the Nordic Volcanological Center (NordVulk) helped me financially at the end of the project, so I could finish my PhD. Thus Rikke Pedersen and NordVulk deserve special thanks for helping me, when I most desperately needed it.

Caroline Hem from the University of Copenhagen, David Cornell and Johan Hogmalm from the University of Gothenburg deserve my sincere thanks for providing technical assistance in connection with XRD and SEM analysis.

My family and friends from Denmark, Sweden and the Netherlands have all been very supportive and furthermore been frequent visitors both in Iceland and in France. When the economical collapse of Iceland threatened my plans of working in

France on my PhD, relatives in the Netherlands stepped in and supported me financially. My parents have always encouraged me to go abroad and embrace life as an adventure, which is the philosophy I have tried to take with me. This PhD has most certainly brought me in contact with so many great new people, and most importantly my husband, Erik Sturkell, whom I met only two days after arriving in Iceland. Erik has been a fantastic support over the years, and moreover gotten me involved in all of his interesting work on volcanoes in Iceland and meteorite craters in Sweden.

And in conclusion, with all my efforts to improve my English, Icelandic, French and Swedish I sometimes wonder if this PhD project has been just as much a course in language skills as an education in science. Thank You / Takk fyrir / Merci beacoup / Tack så mycket!

Gabrielle Jarvik Stockmann

Gothenburg, Sweden, May 2012

Table of Contents

1. Introduction

1.1 CO_2 emissions and consequences

The CO_2 level of the atmosphere has been constantly increasing over the last century reaching, as of February 2012, a concentration of 393 ppm according to measurements at the Mauna Loa Observatory on Hawaii, as opposed to ~280 ppm in pre-industrial times (e.g. Etheridge et al., 1996; MacFarling Meure et al., 2006; "Scripps CO_2 Program" (http://scrippsco2.ucsd.edu)).

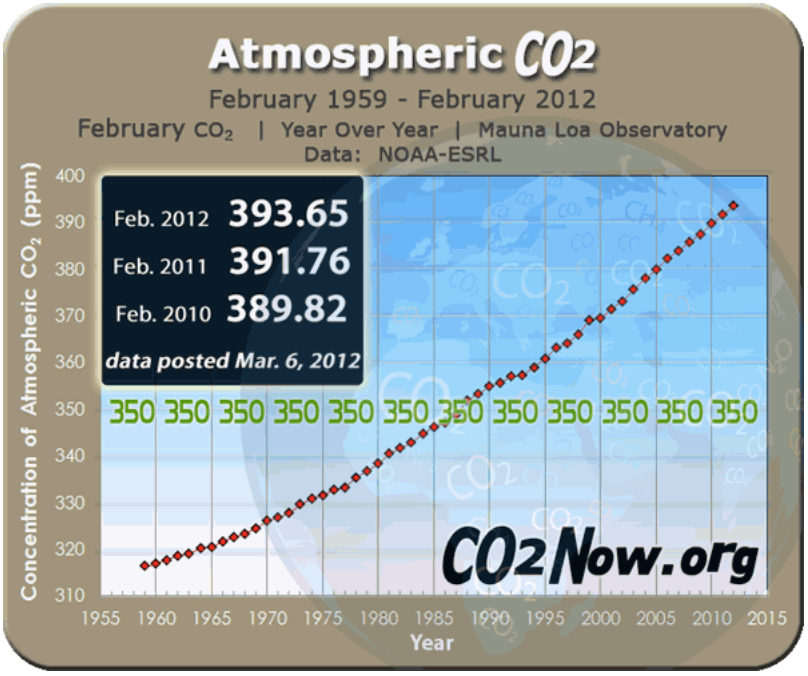

Fig. 1 Atmospheric CO_2 measurements dating back to 1959 from the Mauna Loa Observatory, Hawaii. *Source: CO2now.org*

The increase in atmospheric CO_2 mainly stems from the combustion of fossil fuels (coal, oil and gas) and others processes of anthropogenic origin such as cement production and land use changes. On a global scale, demand for energy and associated services are increasing to meet social and economic development, human welfare and health. All societies around the globe require energy services to meet basic human needs (e.g., lighting, cooking, transportation and communication) and to serve production processes. Since ~1850, global use of fossil fuels has increased to be the dominating energy supply, leading to a rapid growth in carbon dioxide emissions

(IPCC, 2011). The fourth IPCC Assessment Report concluded that "Most of the observed increase in global average temperature since the mid-20th century is very likely due to the observed increase in anthropogenic greenhouse gas concentrations" (IPCC, 2007). Changes in global climate are considered to cause changes to the oceans and ecosystems through acidification of oceans, sea level changes, shrinking sea ice cover, and extreme weather conditions, among others (IPCC, 2007).

Increasing efforts are directed towards the development of alternative energy sources like windmills, solar panels, hydropower, bio fuel, geothermal exploitation, and nuclear power plants. Furthermore, considerable funding and research are currently going into projects attempting to find methods to reduce industrial CO_2 emissions and mitigate the consequences of increasing CO_2 levels. One method is to capture and store CO_2 in geological formations, also referred to as CCS (Carbon Capture and Storage; IPCC, 2005) technology. Promising geological formations with large storage capacities have been identified both onshore and offshore in deep saline aquifers, depleted oil and gas reservoirs, unmineable coal seems, and in basaltic and ultramafic rocks.

1.2 CCS efforts around the world

There are currently some CCS projects already injecting CO_2 into geological formations, several pilot studies testing CO_2 injection on a time-limited smaller scale in different geological settings, and extensive experimental work being carried out in laboratories around the world. CO_2 can be injected either as a gas ($CO_2(g)$), a supercritical fluid ($scCO_2$), or dissolved in water ($CO_2(aq)$). The preferred method is to inject CO_2 as a supercritical liquid, which means at critical pressures of at least 7.4 MPa, corresponding to depths of 740 meters below the water table. Injecting it as a supercritical fluid has the advantage that CO_2 has the density of a fluid but behaves as a gas, and this makes it possible to inject large quantities of CO_2 (Fig.2). Once injected into a geological formation, $scCO_2$ is buoyant, and it has the tendency to migrate upward through pores and fractures and will displace any pre-existing fluid (water, oil, gas). Thus, reservoir stability, retention time and risk of leakage are important factors, when identifying a suitable geological formation for CO_2 storage.

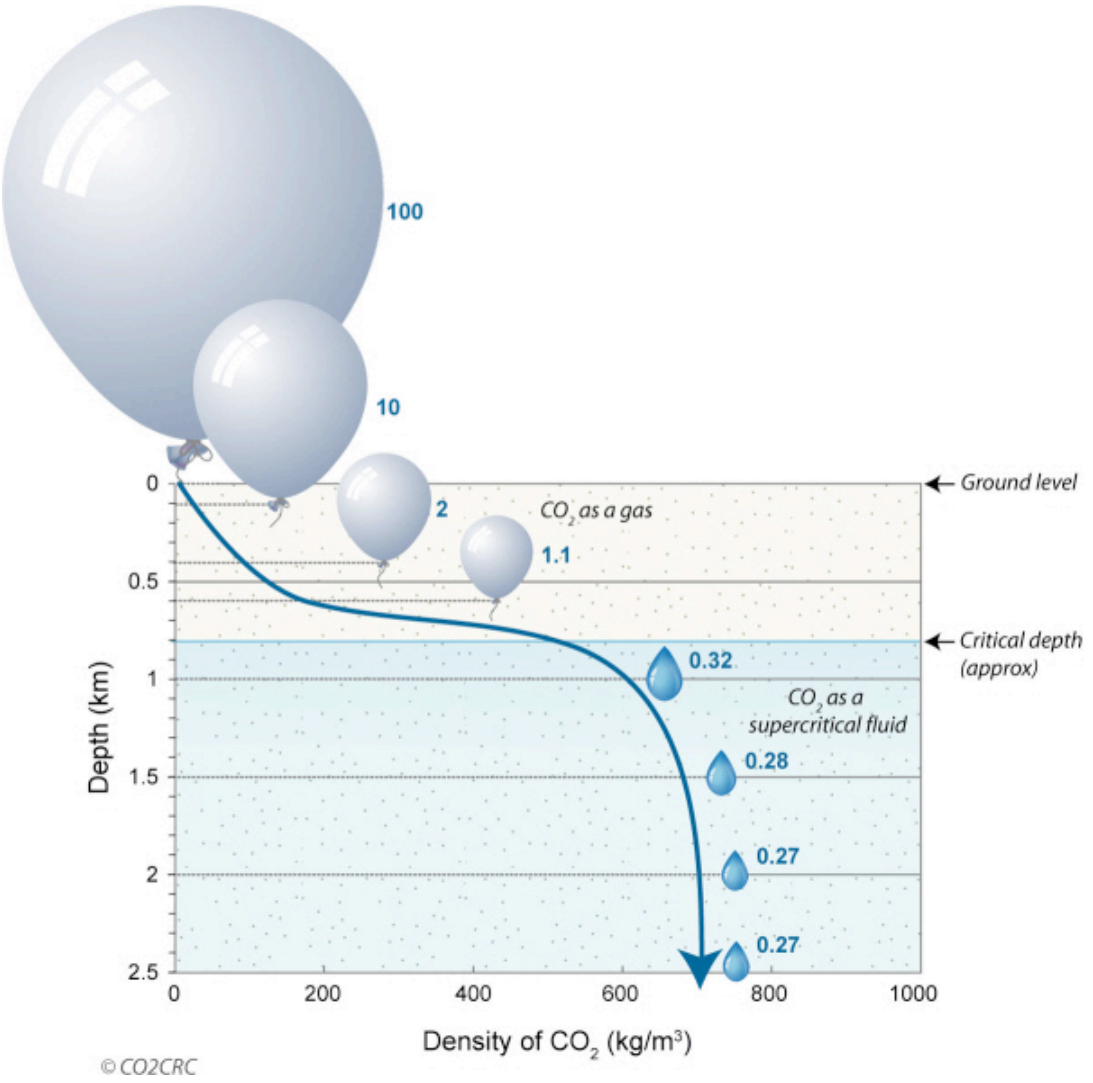

Fig. 2 CO_2 becomes a dense supercritical fluid around 800 meters depth. Its volume reduces from 1000 m^3 at the surface to 2.7 m^3 at 2 km's depth. *Source: CO2CRC*.

However, injecting CO_2(g) or scCO_2 requires a sealing cap rock above the geological formation where the CO_2 is injected into, because buoyancy properties will make the gas move upwards and may pose potential threats to the integrity and quality of underground sources for drinking water (Lu et al., 2009). Besides, CO_2 in concentrated amounts in air is toxic and escape back to the surface could therefore be lethal. With time, CO_2 will slowly dissolve in the host fluid leading to solubility trapping and eventually mineral trapping through the formation of carbonates as shown in Figure 3. However, the chemical reactions leading to dissolution of the CO_2

in an aquifer might take hundreds of years, and the mineralization even longer (IPCC, 2005).

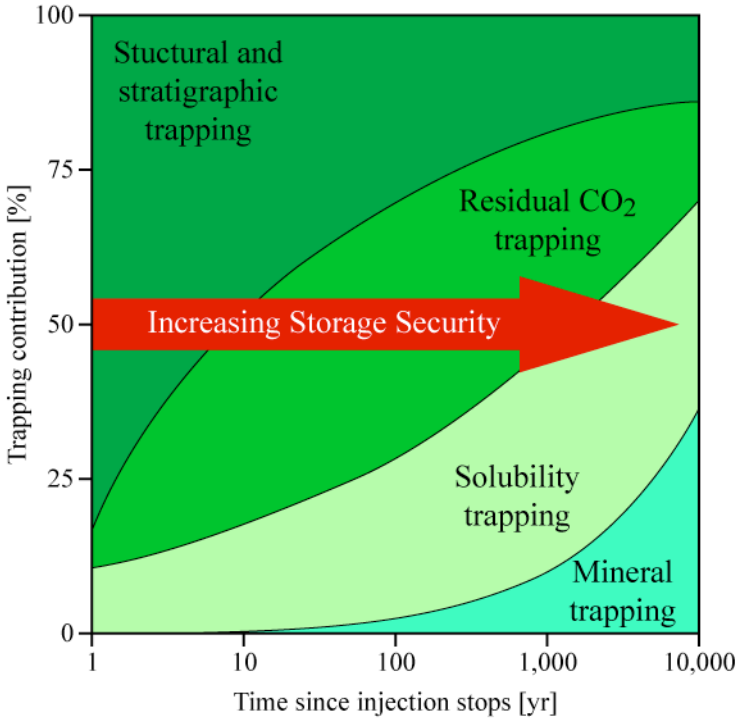

Fig. 3 A diagram illustrating storage security depending on trapping method. *Source: IPCC (2005)*

It will not be possible to describe all active CCS projects and pilot studies but below follows a description of some of the better known currently running CCS projects and selected pilot studies.

1.2.1 Permanent CO_2 injection fields:

- The Sleipner project, Utsira formation, Norway (Statoil Hydro)
- The Weyburn Enhanced Oil Recovery project, Williston Basin Oilfield, Canada (Cenovus Energy / EnCana)
- The In Salah project, Krechba field, Algeria (BP, Sonatrach and Statoil)
- The Snøhvit field, Barents Sea, Norway (Statoil Hydro)

1.2.2 Selected pilot studies of CO_2 injection:

- The Frio formation, US Gulf Coast
- The Ketzin project, Germany
- The Nagaoka project, Japan

- The Ogachi hydrothermal area, Japan
- The Hellisheiði basaltic formations, Iceland

Furthermore, investigations are underway of injecting CO_2 into the Deccan flood basalts in India (McGrail et al., 2006; Prasad et al., 2009), the Columbia River flood basalts in the US (McGrail et al., 2006; Schaef and McGrail, 2009; Schaef et al., 2009; 2010; 2011), and into ultramafic rocks in Oman (Kelemen and Matter, 2008; Matter and Kelemen, 2009; Rudge et al., 2011), among others. Studies are also looking at methods to store CO_2 in oceanic basalts (MORB) (e.g. Goldberg et al., 2008; Wolff-Boenisch et al., 2011) or simply by pumping CO_2 into the deeper parts of the ocean (Adams and Caldeira, 2008). This will store CO_2 for a time, but eventually ocean overturn will bring the CO_2 back to the surface. Thus, it is not a permanent storage solution, but one that can buy time until more promising techniques have been developed.

1.2.1.1 The Sleipner project, Norway

The Sleipner project in run by the Statoil Hydro oil company and is the first industrial CCS operation and the longest running permanent CO_2 injection project (e.g. Chadwick et al., 2004; Bickle et al., 2007; Hermanrud et al., 2009; Boait et al., 2011). The storage site is located offshore the west coast of Norway close to Stavanger. Carbon dioxide is separated from the natural gas extracted from the production wells in the Sleipner Field in order to meet quality specifications for sale. Back-injection of carbon dioxide started in 1996 with approximately 1 million tons/year (Mt/y) and by now more than 12 Mt of CO_2 have been injected into the Utsira sand formation at ~1000 meters depth below seafloor (Boait et al., 2011). The injection site is constantly monitored with geophysical methods and modeling simulations. Seismic imaging shows that so far no leakage of CO_2 has been detected, and in fact the seismograms indicate that CO_2 is slowly being dissolved into the saline aquifer (Boait et al., 2011).

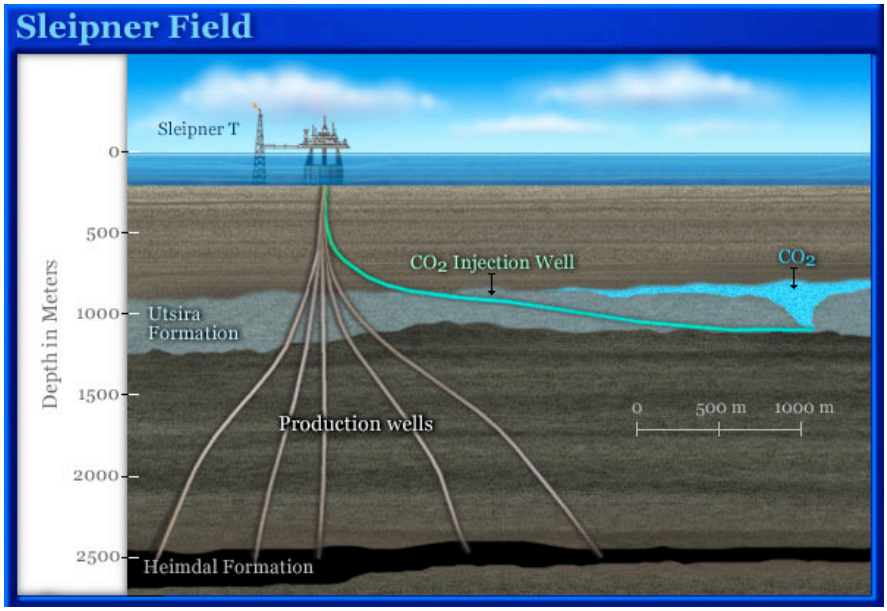

Fig. 4 Cross section of the CO_2 injection site at the Sleipner Field. *Source: planetseed.com*

The Utsira Formation consists of sandstones with 90-98% sand and has an average porosity of 35-40% (Hermanrud et al., 2009). It is overlain by the Nordland shale, which acts as a cap rock. The sandstones are mainly composed of quartz (75%), K-feldspar (13%) and calcite (3%) (Chadwick et al., 2004). Reactive transport modeling of carbon dioxide injected into the Utsira Formation indicates that after 10,000 years, 95% will be dissolved in the brine and stored by solubility trapping, whereas only 5% will be trapped as carbonate minerals (Audigane et al., 2007). The low percentage of secondary carbonates is due to the slow reactivity of primary minerals (quartz and K-feldspar) and their low content of divalent cations. Estimations of the total capacity and running time of the Sleipner Field production accumulates to a total amount of 20 Mt of CO_2 eventually being stored in the Utsira Formation (Chadwick et al., 2004).

1.2.1.2 The Weyburn Field, Canada

The Weyburn project is a combined CO_2 storage and enhanced oil recovery (CO_2-EOR) program now run by the company Cenovus Energy, but previously owned by EnCana Corporation, and has been in operation since 2000 (e.g., Emberley et al., 2004; Cantucci et al., 2009; Whittaker et al., 2011). In 2005, the adjacent Midale Oil Field (owned by Apache Canada) was also incorporated into the storage

project, and they now run together as the "IEA GHG Weyburn-Midale CO_2 Monitoring and Storage Project" (Whittaker et al., 2011).

The Weyburn field is one of a number of large oilfields that lie along the Mississippian subcrop belt on the northern extent of the Williston Basin. The Weyburn field is located approximately 130 km southeast of Regina, Saskatchewan, Canada, where crude oil is produced from the Midale beds of the Mississippian Charles Formation (Emberley et al., 2004). $scCO_2$ is injected into a nearly depleted oil field at 1500 meters depth to increase the pressure and in that way enhance the amount of oil production (Cantucci et al., 2009). The Weyburn Field consists of marine carbonates formed in shallow water, and the presence of scCO2 causes these carbonates to dissolve according to monitoring data and predictions from chemical modeling (Cantucci et al., 2009). Geochemical simulations indicate that the CO_2 will eventually be immobilized by solubility trapping and in minerals like dawsonite ($NaAlCO_3(OH)_2$) (Cantucci et al., 2009).

EnCana started injecting in 2000 with an injection rate of 1.8 Mt/yr of $scCO_2$/yr. By 2010 it was estimated that ~18 Mt of CO_2 had been stored in the geological reservoir (Whittaker et al., 2011). The Weyburn Field and the Midale Oild Field are scheduled to continue as CO_2-EOR projects until 2035 and maybe even beyond, where an expected amount of more than 40 Mt of CO_2 will have been stored in these two carbonate reservoirs by then (Whittaker et al., 2011).

1.2.1.3 The In Salah project, Krechba Field, Algeria

In Salah is a joint venture by BP, Sonatrach and Statoil and is one of the biggest on-shore CCS operations to this day (e.g. Iding and Ringrose, 2010; Durucan et al., 2011; Mathieson et al., 2011; Shi et al., 2012). Injection has been running in the Sahara desert in Algeria since 2004 and more than 3 Mt of CO_2, separated during gas production, have been stored in a deep saline formation at almost 2 km depth. The Krechba gas field holds an estimated 160 billion m^3 of gas with an expected operational life of 20 years. As the natural gas contains small amounts (1-10%) of CO_2, it is necessary to separate the CO_2 to meet purity standards for sale. About 1.4 million m^3 per day of CO_2 are produced from the gas processing facility at Krechba. Before being re-injected into the Krechba reservoir the $CO_2(g)$ is compressed to a very high pressure of 185 bars to force it into the reservoir's low permeability

sandstone as a supercritical fluid. The reservoir at 1850-1950 m depth comprises a 20 m thick Carboniferous sandstone, with medium porosity (13-20%) and low permeability (10 mD) (Mathieson et al., 2011). The sandstone is sealed by 950 m of Carboniferous mudstones, followed by 900 m of Cretaceous sandstone and mudstone.

Surface uplift has been detected over all three of the In Salah CO_2 injection wells with corresponding subsidence observed across the gas production area (Mathieson et al., 2011; Shi et al., 2012). The observed surface uplift rate is around 3 mm/year (Shi et al., 2012). Furthermore, CO_2 leaked from an old uncemented appraisal well in 2007. The well was properly plugged and since then no CO_2 leakage has been detected (Mathieson et al., 2011). A detailed monitoring program of geophysical methods and modeling have been set up to follow and interpret subsurface movement of the CO_2 plume and hydro-mechanical responses to the CO_2 injection. The aim is to store a total of 17 Mt of CO_2 in the Krechba Field over the next 20 years (Mathieson et al., 2011).

1.2.1.4 The Snøhvit Field, Barents Sea, Norway (Statoil Hydro)

Statoil's Snøhvit project is constructed to exploit the resources of three gas fields in the Barents Sea: Snøhvit, Albatross and Askeladd, which lie about 140 km northwest of Hammerfest in Norway. The Snøhvit and Albatross fields came onstream in 2007, while the Askeladd is due to come onstream in 2014-15 (www.statoilhydro.com). The natural gas, which is piped from the Snøhvit field to the Melkøya island outside Hammerfest contains 5-8% of CO_2. The project has a carbon dioxide capture and storage facility located 2600 m beneath the seabed of the Snøhvit field and a 153 km pipeline for re-injection. At the onshore plant on Melkøya, CO_2 is separated from the natural gas and piped back to a formation, called the Tubåen Formation, which lies somewhat beneath the gas-bearing formations on the Snøhvit Field. The first injection of $scCO_2$ into the Tubåen Formation started in 2008 (Pham et al., 2011).

Tubåen formation consists of sandstone dominated by quartz with minor amounts of feldspars, and has a porosity of ~15% (Pham et al., 2011). A shale cap (Nordmela Formation) overlying the sandstone acts as a seal above the reservoir to ensure that CO_2 stays underground without migrating to the surface. At full capacity, 0.7 Mt/y CO_2 will be stored corresponding to over 20 Mt CO_2 over the 30 year period the

Snøhvit Field is estimated to be running (Pham et al., 2011).

1.2.2 Pilot projects of CO_2 injection

1.2.2.1 The Frio Formation, US Gulf Coast

The Frio experimental site is located on the southeast flank of a salt dome within the South Liberty oil field, near Dayton, Texas, a region of the US Gulf Coast. The aim of this pilot project was to test storage of carbon dioxide in an onshore saline sedimentary aquifer (Kharaka et al., 2006; 2009; Xu et al., 2010). The injection layer hosts poorly cemented subarkosic sandstone, belonging to the Frio Formation, comprised dominantly of fine-grained, moderately sorted quartz with minor amounts of illite/smectite, feldspar and calcite (Kharaka et al., 2006). The mean porosity of the sandstone is 32% with a concomitant very high permeability of 2000-3000 mD. Cap rock and main barrier to CO_2 leakage are overlying thick marine shale beds of the Miocene–Oligocene Anahuac Formation (Hovorka et al., 2005).

In 2004, 1600 tons of CO_2 were injected at 1500 m depth into a 24 m section of the Frio Formation (Kharaka et al., 2006). This led to a sharp pH drop and increase in alkalinity and aqueous Fe concentration (Kharaka et al., 2006). There were also mobilization of other metals, including Zn and Pb, which are commonly adsorbed to iron oxyhydroxides (Kharaka et al., 2009). Injected $scCO_2$ also mobilized toxic organic compounds such as toluene and benzene because it is a very good organic solvent. Future environmental impacts of this pilot injection may be of concern if large brine volumes with mobilized toxic metals and organics migrate into potable groundwater (Kharaka et al., 2009).

Geochemical modeling of the $scCO_2$ plume predicted that Frio Formation water would have dropped as low as pH ~3 if not being buffered by dissolution of calcite and Fe oxyhydroxides. Post-injection analysis indicated that the brine gradually returned to pre-injection composition (Kharaka et al., 2006).

1.2.2.2 The Ketzin project, Germany

The Ketzin project is an on-shore pilot study injecting CO_2 into a saline aquifer near the town of Ketzin, 40 km west of Berlin, Germany (e.g. Schilling et al., 2009; Kempka et al., 2010; Lengler et al., 2010; Würdemann et al., 2010; Zemke et al.,

2010). This pilot project was launched in 2008 as part of the European CO_2SINK program sponsored by the European Commission.

In northern Germany, salt structures have formed in anticlinal structures that can act as natural traps for oil or gas, and the Ketzin anticline is such a geological structure. In the past, natural gas was present in the Ketzin area at depths between 250 and 400 m. The target zone for the CO_2 storage, however, is a deeper sandstone reservoir of the Stuttgart Formation. A previous exploration well at the site encountered this sandstone unit at a depth of about 700 m. Sandstone samples are generally fine-grained with porosities between 17 and 32% and permeabilities between 1 and 100 mD (Zemke et al., 2010). The cap rocks ensuring sealing of this reservoir comprise gypsum and clay belonging to the Weser Formation (Förster et al., 2006).

Up to 18 March 2012, an amount of 59,521 tons of CO_2 have been injected into the underground sandstone reservoir at depths of 650 m (www.co2ketzin.de). High-purity CO_2 ($\geq$99.9%) was bought for the testing purpose, and it had to be heated and gasified prior to injection, as part of the CO_2 was injected as CO_2(g). The project, CO_2SINK, was concluded in March 2010 after 5 years of operation, and the Ketzin project now runs as a collaborative effort by six scientific institutions, continuing CO_2 injection, research and development work at the pilot site in Ketzin. A combination of site-specific geophysical (seismic, geoelectric, thermal), geochemical and biological monitoring techniques follow the evolution of the CO_2 plume in space and time as part of a detailed monitoring program set up for the Ketzin site (Würdemann et al., 2010).

1.2.2.3 The Nagaoka project, Haizume Formation, Japan

The Minami Nagaoka field is an active oil and gas field operated by Teikoku Oil extracting gas from 5000 m depth and re-injecting scCO_2 into a saline aquifer in the Pleistocene sandstones in the Haizume Formation at 1100 m depth with a mean porosity of 23% and permeability of 7 mD (e.g. Mito et al., 2008; Mito and Xue, 2011; Sato et al., 2011). The Nagaoka reservoir has a complex mineralogy comprised of quartz, feldspar, pyroxene, biotite, and hornblende among others. This was a test site injecting 10,400 tons of CO_2 in the period from 2003 to 2005. Geochemical modeling estimates 81% of the CO_2 will be trapped by solubility and ionic trapping in

100 year's time, whereas 18% will be trapped in carbonate minerals (Sato et al., 2011).

1.2.2.4 The Ogachi Hot Dry Rock project, Ogachi area, Japan

In a pilot study in the Ogachi hydrothermal area, CO_2(aq) was injected into the Ogachi granodiorite rocks consisting of quartz (45%), K-feldspar (11%), plagioclase (20%) plus minor amounts of secondary minerals (Wakahama et al., 2009). Injection took place at ~1000 m depth and at a temperature of ~200 °C and is referred to as the Ogachi Hot-Dry Rock site. The injected CO_2-charged water was diluted with the reservoir fluid within 3 days. Ca concentration in the water samples increased from 10 to 80 mg/L within one day and then quickly decreased to background levels. This observation combined with *in-situ* experiments on calcite precipitation led to the conclusion that the majority of CO_2 was deposited as calcite by interaction with granitic rocks due to high temperature and water-rock ratio, causing high reactivity (Wakahama et al., 2009). The authors concluded that CO_2 can be sequestered as carbonates in hydrothermal conditions in a fracture-type geothermal reservoir like the Ogachi site.

All of these pilot studies, except for the Ogachi hydrothermal project, are injections of either CO_2(g) or $scCO_2$ into saline aquifers, thus depending very much on the sealing capacity of the cap rock. The general approach has been that if the sealing rock could trap oil and gas in the past, then it should also be able to withstand the pressure of CO_2 in the storage formation. However, much lower interfacial tension of the CO_2-water system compared to the original hydrocarbon-water system reduces the sealing capacity of the cap rock significantly (Li et al., 2006). Buoyancy properties of CO_2 will make it migrate upwards and be trapped underneath the cap rock. Any failure or fracture in the sealing cap rock could release CO_2 into shallower aquifer systems leading to acidification, and toxic metal and organic compound releases. These aquifers will then lose their potential for serving as underground sources of drinking water and their integrity is vital (Lu et al., 2009). A few storage projects like Ogachi, Japan and CarbFix, Iceland offer CO_2 sequestration through *in-situ* mineralization, which improves long-term stability of CO_2 and therefore reduces the risks of leakage considerably.

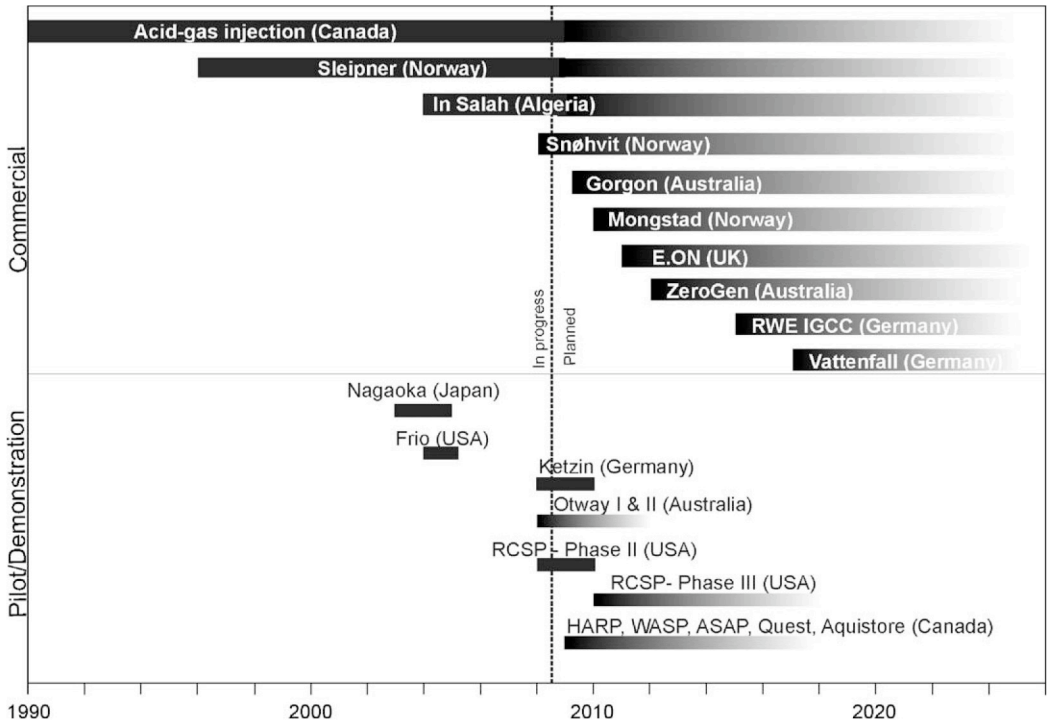

Fig. 5 Overview of past and planned future implementation of CO_2 geological storage in saline aquifers (Michael et al., 2010).

1.3 The CarbFix project in Iceland

The CarbFix project in Iceland is a joint venture between, Reykjavik Energy, University of Iceland, The Earth Institute at Columbia University in New York, US and the Centre National de la Recherche Scientifique, Université Paul Sabatier in France to develop a long-term, safe, and cost-effective technology to store carbon dioxide through *in-situ* mineralization in basalts in Iceland (Oelkers et al., 2008; Matter et al., 2009; 2011; Gislason et al., 2010; Aradóttir et al., 2011; 2012). The project was launched in 2007, and CO_2 injection started close to the Hellisheidi geothermal power plant in SW-Iceland in January 2012.

The Hellisheidi geothermal power plant is located approximately 20 km east of the capital Reykjavik. From a series of deep wells, mixed water and steam are brought to the surface and led through pipes to the power plant. Waste products connected to the geothermal heat production are a mixture of gases consisting of CO_2, H_2S, H_2, N_2, CH_4 and Ar. Most of these gases originate from the magma situated at few km depth. Currently, the Hellisheidi geothermal power plant is producing 40,000 tons of CO_2 per year that is released into the atmosphere. The ambition is with time to store all of this industrial CO_2 in the basaltic formations underlying Hellisheidi.

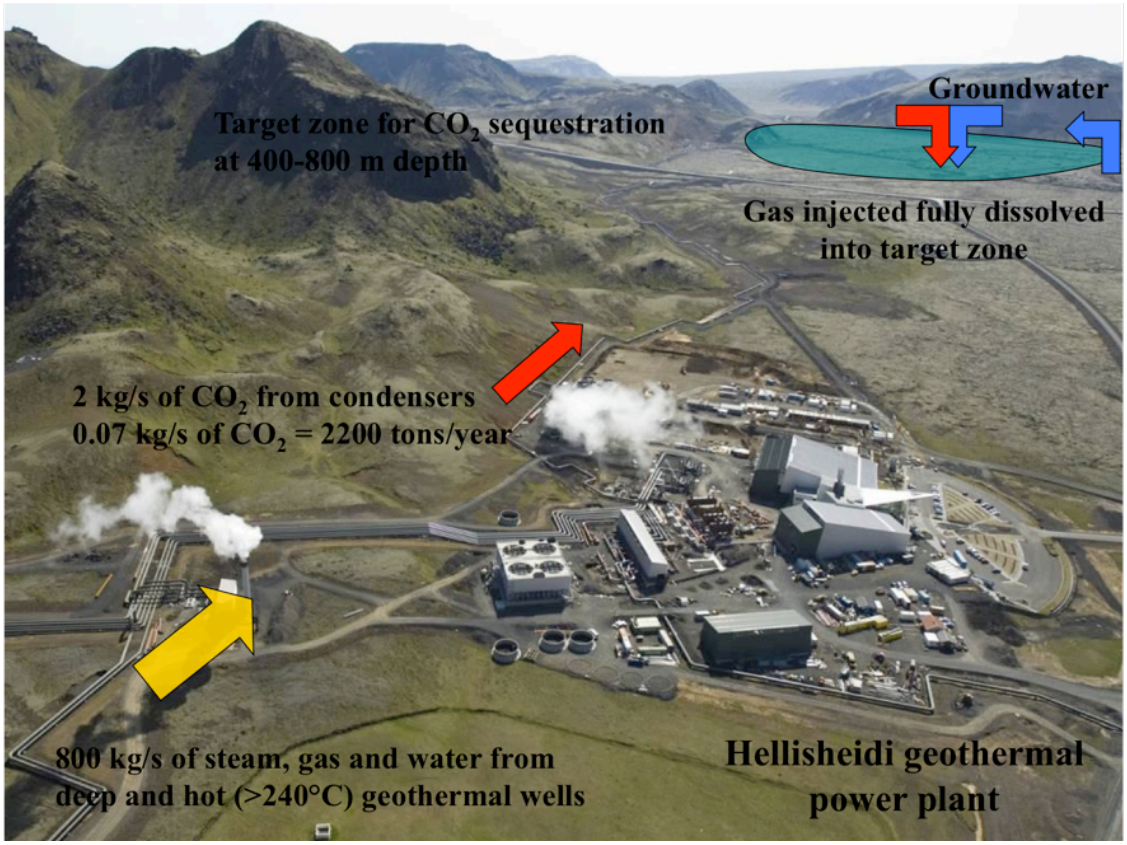

Fig. 6 Aerial overview of the Hellisheidi geothermal power plant and the CarbFix injection site.

In January 2012, a pilot study injecting 170 tons of pure CO_2 at Hellisheidi was initiated. The injection ran for approximately one month, and the gas injected was bought for the purpose. Several water samples were collected with close time intervals from injection and monitoring wells and are now in the process of being analyzed. Further injection of a CO_2-H_2S gas mixture will commence later this year.

CO_2 injection at Hellisheidi differs from the majority of other storage sites by fully dissolving CO_2(g) before injecting the carbonated solution into the target aquifer. Groundwater is extracted from an adjacent groundwater well HN-01, which is then pumped with the CO_2 gas stream down into the injection well HN-02 (Fig. 7). A method has been developed where the CO_2(g) is turned into tiny bubbles to minimize the buoyancy forces and coagulation tendency of the carbon dioxide gas bubbles as they are being injected into the water stream at 350 m depth. The gas-water mix is carried further down to 550 m depth, where carbonation is completed. At injection depth, the CO_2(aq) follows along the aquifer flow path towards the sea in the south. From the injection site to the sea, reaction of basalt dissolution and carbonate

precipitation is expected to take place. According to geochemical modeling, the CO_2-loaded water will have a pH of ~3-4 when it enters the ~40 °C warm aquifer at depth, running through geological layers of glassy and crystalline basalt.

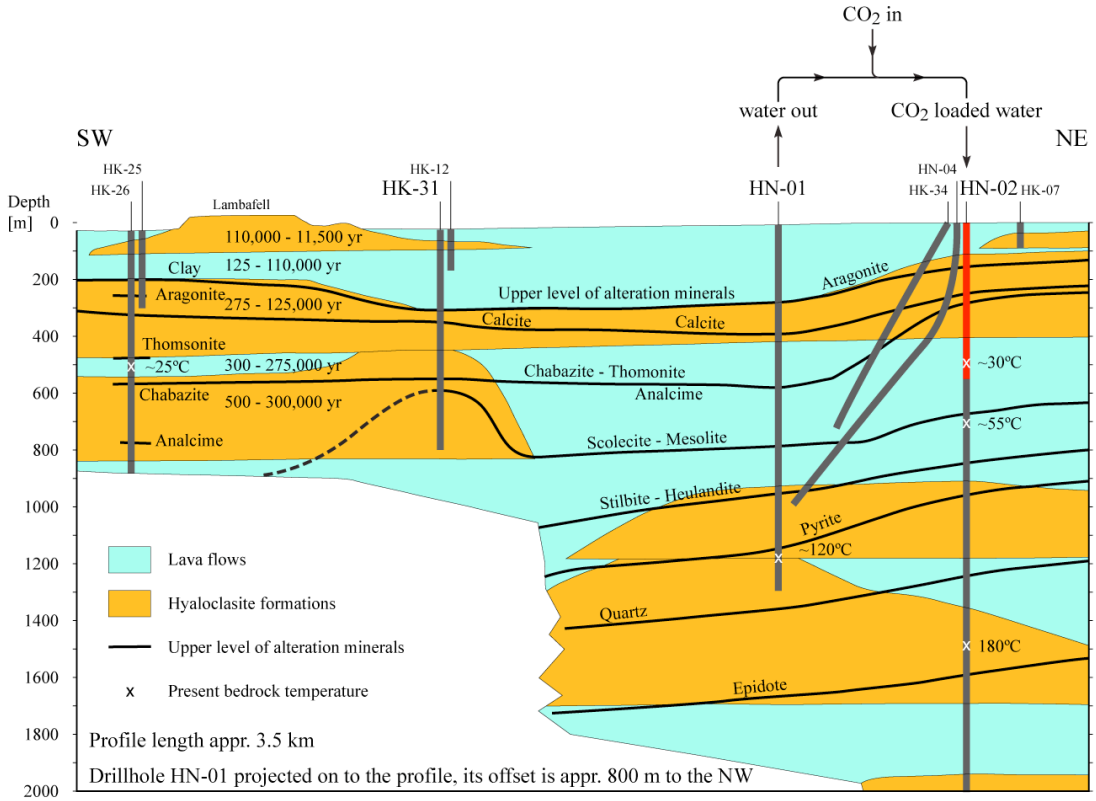

Fig. 7 A cross-section of the basaltic rocks and wells at the injection site. HN-01 is the groundwater source, HN-02 is the injection well, and HK-31 and HK-26 are monitoring wells along the flow path. *Modified from Alfredsson et al. (2008).*

The chemical reactions associated with the mineralization of CO_2 follow several steps. First comes the carbonation process and dissociation of carbonic acid:

$$CO_2(g) + H_2O = H_2CO_3^*(aq) = HCO_3^- + H^+ \quad (1)$$

where $H_2CO_3^*$ refers to the total concentration of $CO_2(aq)$ and $H_2CO_3(aq)$, carbonic acid. The carbonic acid dissociates and forms bicarbonate ions (HCO_3^-). Then follows the dissolution process of the basaltic crystalline (Ca,Mg,Fe)-silicates and basaltic glass:

$$Mg_2SiO_4(s) + 4H^+ = 2Mg^{2+} + SiO_2\,(aq) + 2H_2O \quad (2a)$$

Forsterite

$CaAl_2Si_2O_8(s) + 8H^+ = Ca^{2+} + 2Al^{3+} + 2SiO_2(aq) + 4H_2O$ (2b)

Ca-plagioclase

$CaMgSi_2O_6 + 4H^+ = Ca^{2+} + Mg^{2+} + 2SiO_2(aq) + 2H_2O$ (2c)

Clinopyroxene

$Si_{1.00}Al_{0.36}Ti_{0.02}Fe(III)_{0.02}Ca_{0.26}Mg_{0.28}Fe(II)_{0.17}Na_{0.08}K_{0.008}O_{3.36}(s) + 6.72H^+ =$

Basaltic glass $Si^{4+} + 0.36Al^{3+} + 0.02Ti^{4+} + 0.02Fe^{3+} + 0.17Fe^{2+} + 0.26Ca^{2+} +$

$0.28Mg^{2+} + 0.08Na^+ + 0.008K^+ + 3.36H_2O$ (3)

And finally the released divalent cations can react with the dissolved CO_2 to precipitate carbonates:

$(Ca, Mg, Fe)^{2+} + H_2CO_3^*(aq) = (Ca,Mg,Fe)CO_3(s) + 2H^+$ (4)

The carbonates formed can either be calcite ($CaCO_3$), magnesite ($MgCO_3$), siderite ($FeCO_3$), ankerite ($CaFe(CO_3)_2$), dolomite ($CaMg(CO_3)_2$) or Ca-Mg-Fe carbonate solid solution depending on the divalent cation ratios, pH, and temperature. Reaction (4) not only forms carbonates, but protons as well, and reaction (4) can only continue as long as the protons are consumed, thereby forcing the reaction to the right. Dissolution of basaltic rocks consumes protons as illustrated by reactions (2) and (3). Hence, it is essential for successful carbon storage to have the dissolution of basalts continuously running. Any effect decreasing basalt dissolution could be detrimental to the CO_2 sequestration process.

1.4 Effects of carbonate coatings and bacteria on basalt dissolution

The rate-limiting process of carbon storage in basalt is thought to be the dissolution of basaltic rocks and the ensuing release of divalent cations (c.f., Oelkers et al., 2008). Thus, any reaction that could potentially change the reactive surface area of basalt and/or trap the cations meant for carbonate formation could alter the CO_2 sequestration process.

One of these potential dissolution rate-limiting processes is the formation of secondary minerals. From observations in nature and laboratory experiments, basaltic rocks are known to weather into clay minerals and zeolites (Kristmannsdóttir and Tómasson, 1978; Kristmannsdóttir, 1982; Gislason et al., 1993; Neuhoff et al., 1999, Alfredsson et al., 2008). Calcite is also found as a secondary product of Icelandic basalts, but typically in warm water environments (Kristmannsdóttir and Tómasson, 1978; Kristmannsdóttir, 1982). Calcite or other secondary minerals can cover the primary silicate surface with coatings and limit the dissolution of the primary basaltic rock. In areas with highly altered Icelandic basalts, permeability and most available pore spaces are clogged by secondary mineral precipitates (Neuhoff et al., 1999; Franzson et al., 2010), thus leaving limited space for CO_2 storage. However, at the Hellisheidi injection site, the rocks are relatively young somewhat altered but still porous. Hydrological models suggest that the effective matrix porosity of this lava formation is 8.5% (Aradóttir et al., 2012).

If carbonates instantaneously form passivating coatings on the primary silicate surface, then the storage process could be very short-lived. An increasing number of studies are looking into the effect of carbonate coatings on silicates of importance to carbon storage efforts (i.e. olivine, pyroxenes, plagioclases, glasses). There is no unambiguous conclusion on the effect of carbonate coatings from the literature. Some studies found no effect on the dissolution rates by carbonate coatings (Giammar et al., 2005; Daval et al., 2009a), whereas other studies found that mixed coating layers of carbonate and amorphous silica were able to effectively stall the surface dissolution (Béarat et al., 2006; Andreani et al., 2009; Daval et al., 2009b; 2011).

Bacteria present in the aquifer of the CO_2 injection site at Hellisheidi have been considered as another potential factor that could alter basaltic dissolution, either by increasing or decreasing dissolution rates. Several studies have found an impact by bacteria in geological processes, especially iron-reducing or oxidizing bacteria (e.g. Brock and Gustafson, 1976; Bridge and Johnson, 1998; Kalinowski et al., 2000; Kappler and Newman, 2004). Bacteria can affect by several different processes, i.e. by adsorbing ions from solution on the bacteria surface, and by complexing aqueous ions with organic molecules originating from bacteria. In the case of basaltic glass and plagioclase, Al^{3+} is of particular importance as the rate of basaltic glass and Ca-rich plagioclase dissolution is affected by the exchange of three protons (H^+) for one Al^{3+}. Thus, any bacterial-induced change to the aqueous Al concentration could affect

the basaltic glass dissolution rates. Previous studies on basaltic glass have shown oxalic and fluoride ions are capable of complexing Al ions at acidic pH, thereby increasing basaltic glass dissolution rates (Oelkers and Gislason, 2001;Wolff-Boenisch et al., 2004; Wolff-Boenisch et al., 2011). The same effect was found in the presence of SO_4^{2-} ions at pH < 7 (Flaathen et al., 2010). Another characteristic behavior of certain bacteria is their ability to produce a biofilm composed of exopolysaccharides (Welch and Vandevivere, 1994; Hutchens et al., 2010). These biofilms can either complex ions or form a protective layer on the silicate surface, and like mineral coatings limit mineral dissolution. The effects of carbonate coatings and bacteria on basaltic glass and silicate minerals, and their implications for the CO_2 sequestration efforts at Hellisheidi, have been studied in several specific experiments within this thesis work as part of the CarbFix project.

1.5 Outline of Thesis

This thesis is subdivided into five chapters following the introduction; four chapters each representing an article either published, submitted or in preparation for submission to international peer-reviewed journals, and finally concluding remarks and perspectives:

Chapter 1: Introduction.

Chapter 2: **Gabrielle J. Stockmann**, Domenik Wolff-Boenisch, Sigurdur R. Gislason, Eric H. Oelkers (2011). Do carbonate precipitates affect dissolution kinetics? 1: Basaltic glass. *Chemical Geology* 284, 306-316.

Chapter 3: **Gabrielle J. Stockmann**, Domenik Wolff-Boenisch, Sigurdur R. Gislason, Eric H. Oelkers (2012). Do carbonate precipitates affect dissolution kinetics? 2: Diopside. *(submitted to Chemical Geology)*

Chapter 4: **Gabrielle J. Stockmann**, Liudmila S. Shirokova, Oleg S. Pokrovsky, Pascale Bénézeth, Nicolas Bovet, Sigurdur R. Gislason, Eric H. Oelkers (2012). Does the presence of heterotrophic bacterium *Pseudomonas reactans* affect basaltic glass dissolution rates? *Chemical Geology* 296-297, 1–18.

Chapter 5: **Gabrielle J. Stockmann**, Eric H. Oelkers, Domenik Wolff-Boenisch, Nicolas Bovet, Sigurdur R. Gislason (2012). The role of mineral surfaces on calcite nucleation kinetics. *(draft manuscript to be submitted when completed)*.

Chapter 6: Concluding remarks and perspectives.

In addition, an extended abstract and supplementary solution chemistry data have been added in three appendices (I to III):

Appendix I: **Stockmann, G.**, Wolff-Boenisch, D., Gíslason, S.R. and Oelkers, E.H. (2008). Dissolution of diopside and basaltic glass: the effect of carbonate coating. *Mineralogical Magazine* 72, 135-139 (extended abstract).

Appendix II: Chemistry of solutions from diopside dissolution experiments at 70 °C.

Appendix III: Growth of *Pseudomonas reactans* (HK 31.3) in the presence of extract of basalt (filtered solution) at different conditions.

In Chapter 2 and 3, the effects of calcium carbonate coatings on the dissolution rates of basaltic glass and diopside, respectively, were described from experiments at 70 °C and 25 °C and pH 7-8. In the 70 °C experiments, basaltic glass and diopside were dissolved with a $NaHCO_3$ inlet solution and the silicates were the sole Ca-source, similar to field scale sequestration operations like the one at Hellisheidi. PHREEQC modeling predicted solutions would be saturated with respect to calcite. At 25 °C a different concept was used, where two inlets, one containing $CaCl_2$ and the other $NaHCO_3$, created a solution supersaturated with respect to calcite inside the reactor vessel. These "precipitation" experiments were compared with simultaneous "control" dissolution experiments where the aim was not to form any secondary minerals. It was thus possible to compare dissolution rates from experiments with and without calcite and other secondary minerals forming. Finally, a series of basaltic glass dissolution experiments were conducted with a $NaHCO_3/Na_2CO_3$ inlet solution at 25 °C and pH 10, to simulate some of the highly alkaline, basic springs found in Iceland. The glass was once again the only Ca-source.

In Chapter 4, extensive series of basaltic glass dissolution were conducted in the presence of the heterotrophic bacterium *Pseudomonas reactans* at 25 °C and in the pH range 4 to 10, to deduce the effect of natural occurring heterotrophic bacteria on the carbon storage process. *Pseudomonas reactans* was selected as it represents a typical soil and water bacterium from an Icelandic aquifer in basalt. It was extracted from water sampled in one of the monitoring wells (HK-31) at Hellisheidi, and then purified and grown on heart broth nutrient in the laboratory. In our experiments, both live and dead bacteria were used to test their effect on the basaltic glass dissolution rates. We developed a new mixed-flow reactor setup for these experiments, the "Bacterial Mixed-Flow Reactor" (BMFR). Rates were measured in the presence of 0 g/L to 0.43 g/L dead bacteria and 0 g/L to 19 g/L live bacteria concentrations. These concentrations cover and even exceed normal bacteria concentrations found in nature.

In Chapter 5, the role of mineral structure on calcite nucleation and growth was investigated using different silicates under identical experimental conditions. Similar to the experiments described in Chapter 2 and 3, two inlets of $CaCl_2$ and $NaHCO_3/Na_2CO_3$ were used to create a solution saturated with respect to calcite inside the reactor at 25 °C. The pH of the mixed solution was ~9. Six different silicates plus calcite were tested; enstatite, olivine, augite, labradorite, basaltic glass and peridotite. By conducting similar experiments within the same timeframe, it was possible to identify the effect of the primary silicate on calcite nucleation. The silicates were chosen to represent different crystal systems; orthorhombic, monoclinic, triclinic and non-ordered silicate framework (glass). Calcite is a trigonal mineral, thus any growth of calcite on the silicates were expected to be non-epitaxial due to non-matching structures, whereas calcite growth on calcite crystals should be epitaxial. These experiments were carried out for a better understanding of what differences can be expected from carbonate precipitation on crystalline basalt versus basaltic glass in the Hellisheidi basaltic formations during CO_2 sequestration.

References

Adams, E.E., Caldeira, K., 2008. CO_2 sequestration in deep sedimentary formations. Elements 4, 319–324

Alfredsson, H.A., Hadrarson, B.S., Franzson, H., Gislason, S.R., 2008. CO_2 sequestration in basaltic rock at the Hellisheidi site in SW Iceland: stratigraphy and chemical composition of the rocks at the injection site. Min. Mag. 72, 1–5.

Andreani, M., Liquot, L., Gouze, P., Godard, M., Hoise, E., Gibert, B., 2009. Experimental study of carbon sequestration reactions controlled by the percolation of CO_2-rich brine through peridotites. Eviron. Sci. Technol. 43, 1226–1231.

Aradóttir, E.S.P., Sigurdardóttir, H., Sigfússon, B., Gunnlaugsson, E., 2011. CarbFix - a CCS pilot project imitating and accelerating natural CO_2 sequestration. Greenhouse Gases: Science and Technology 1, 105–118.

Aradóttir, E. S., Sonnenthal, E., Björnsson, G., Jonsson, H., 2012. Multidimensional reactive transport modeling of CO_2 mineral sequestration in basalts at the Hellisheidi geothermal field, Iceland. Int. J. Greenhouse Gas Control 9, 24-40.

Audigane, P., Gaus, I., Czernichowski-Lauriol, I., Pruess, K., Xu, T., 2007. Two dimensional reactive transport modelling of CO_2 injection in a saline aquifer at the Sleipner site, North Sea. Am. J. Sci. 307, 974-1008.

Bickle, M., Chadwick, A., Huppert, H.E., Hallworth, M., Lyle, S., 2007. Modelling carbon dioxide accumulation at Sleipner: Implications for underground carbon storage. Earth Planet. Sci. Let. 255, 164–176.

Boait, F., White, N., Chadwick, A., Noy, D., Bickle, M., 2011. Layer spreading and dimming within the CO_2 plume at the Sleipner Field in the North Sea. Energy Procedia 4, 3254–3261.

Bridge, T.A.M., Barrie Johnson, D., 1998. Reduction of Soluble Iron and Reductive Dissolution of Ferric Iron-Containing Minerals by Moderately Thermophilic Iron-Oxidizing Bacteria. Appl. Env. Microbiol. 64, 2181-2186.

Brock, T.D., Gustafson, J., 1976. Ferric iron reduction by sulfur- and iron-oxidizing bacteria. Appl. Env. Microbiol. 32, 567-571.

Béarat, H., McKelvey, M.J., Chizmeshya, A.V., Gormley, D., Nunez, R., Carpenter, R.W., Squires, K., Wolf, G.H., 2006. Carbon sequestration via aqueous olivine mineral carbonation: role of passivating layer formation. Eviron. Sci. Technol. 40, 4802–4808.

Cantucci, B., Montegrossi, G., Vaselli, O., Tassi, F., Quattrocchi, F., Perkins, E.H., 2009. Geochemical modeling of CO_2 storage in deep reservoirs; The Weyburn Project (Canada) case study. Chem. Geol. 265, 181–197.

Chadwick, R.A., Zweigel, P., Gregersen, U., Kirby, G.A., Holloway, S., Johannessen, P.N., 2004. Geological reservoir characterization of a CO2 storage site: The Utsira Sand, Sleipner, northern North Sea. Energy 29, 1371-1381.

Daval, D., Martinez, I., Corvisier, J., Findling N., Goffe, B., Guyot, F., 2009a. Carbonation of Ca-bearing silicates, the case of wollastonite: Experimental investigations and kinetic modeling. Chem. Geol. 265, 63-78.

Daval, D., Martinez, I., Guigner, J.-M., Hellmann, R., Corvisier, J., Findling N., Dominici, C., Goffe, B., Guyot, F., 2009b. Mechanism of wollastonite carbonation deduced from micro- to nanometer length scale observations. Amer. Min. 94, 1707-1726.

Daval, D., Sissmann, O., Menguy, N., Saldi, G.D., Guyot, F., Martinez, I., Corvisier, J., Garcia, B., Machouk, I., Knauss, K.G., Hellmann, R.. 2011. Influence of amorphous silica layer formation on the dissolution rate of olivine at 90 °C and elevated pCO_2. Chem. Geol. 284, 193–209.

Durucan, S., Shi, J.-Q., Sinayuc, C., Korre, A., 2011. In Salah CO_2 storage JIP: Carbon dioxide plume extension around KB-502 well - New insights into reservoir behaviour at the In Salah storage site. Energy Procedia 4, 3379–3385.

Emberley, S., Hutcheon, I., Shevalier, M., Durocher, K., Mayer, B., Gunter, W.D., Perkins, E.H., 2004. Geochemical monitoring of fluid-rock interaction and CO_2 storage at the Weyburn CO_2-injection enhanced oil recovery site, Saskatchewan, Canada. Energy 29, 1393-1401.

Etheridge, D. M., Steele, L.P., Langenfelds, R.L., Francey, R.J., Barnola, J.-M., Morgan, V.I., 1996. Natural and anthropogenic changes in atmospheric CO_2 over the last 1000 years from air in Antarctic ice and firn. Journal of Geophys. Res. 101, doi:10.1029/95JD03410

Flaathen, T.K., Gislason, S.R., Oelkers, E.H., 2010. The effect of aqueous sulphate on basaltic glass dissolution rates. Chem. Geol. 277, 345–354.

Förster, A., Norden, B., Zinck-Jørgensen, K., Frykman, P., Kulenkampff, J., Spangenberg, E., Erzinger, J., Zimmer, M., Kopp, J., Borm, G., Juhlin, C., Cosma, C.-G., Hurter, S., 2006. Baseline characterization of the CO2SINK geological storage site at Ketzin, Germany. Environ. Geosci. 13 (3), 145–161.

Franzson, H., Gudfinnsson, G. H., Helgadottir, H. M., 2010. Porosity, density and chemical composition relationships in altered Icelandic hyaloclastites. In: Water-Rock Interaction XIII – Birkle, P. and Torres-Alvarado, I. S. (eds). CRC Press Inc., ISBN 978-0-415-60426-0

Giammar, D.E., Bruant Jr., R.G., Peters, C.A., 2005. Forsterite dissolution and magnesite precipitation at conditions relevant for deep saline aquifer storage and sequestration of carbon dioxide. Chem. Geol. 217, 257-276.

Gislason, S.R., Veblen, D.R., Livi, K.J.T., 1993. Experimental meteoric water–basalt interactions: characterization and interpretation of alteration products. Geochim. Cosmochim. Acta 57, 1459–1471.

Gislason, S.R., Wolff-Boenisch, D., Stefansson, A., Oelkers, E.H., Gunnlaugsson, E., Sigurdardóttir, H., Sigfússon, G., Brocker, W.S., Matter, J., Stute, M., Axelsson, G., Fridriksson, T., 2010. Mineral sequestration of carbon dioxide in basalt: A pre-injection overview of the CarbFix project. Int. J. Greenhouse Gas Control 4, 537-545.

Goldberg, D.S., Takahashi, T., Slagle, A.L., 2008. Cabon dioxide sequestration in deep-sea basalt. PNAS 105, 9920-9925.

Hermanrud, C., Andresen, T., Eiken, O., Hansen, H., Janbu, A., Lippard, J., Bolås, H.N., Simmenes, T.H., Teige, G.M.T., Østmo, S., 2009. Storage of CO_2 in

saline aquifers – lessons learned from 10 years of injection into the Utsira Formation in the Sleipner area. Energy Procedia 1, 1997-2004.

Hovorka, S.D., Doughty, C.K., Sakurai, S., Holtz, M., 2005. Frio brine pilot: field validation of numerical simulation of CO_2 storage. Abstract, AAPG Annual Convention; June 19–22, 2005, Calgary, Alberta, Canada.

Hutchens, E., Gleeson, D., McDermott, F., Miranda-CasoLuengo, R., Clipson, N., 2010. Meter-scale diversity of microbial communities on a weathered pegmatite granite outcrop in the Wicklow Mountains, Ireland; Evidence for mineral induced selection? Geomicrobiol. J. 27, 1-14.

Iding, M., Ringrose, P., 2010. Evaluating the impact of fractures on the performance of the In Salah CO_2 storage site. Int. J. of Greenhouse Gas Control 4, 242–248.

IPCC, 2005. Summary for Policymakers. In: Metz, B., Davidson, O., Coninck, H., Loos, M., Meyer, L. (eds) IPCC Special Report on Carbon Dioxide Capture and Storage, prepared by Working Group III of the Intergovernmental Panel on Climate Change. Cambridge University Press, Cambridge, UK, and New York, USA, pp 3-15.

IPCC, 2007. Climate Change 2007; Synthesis Report. Contribution of working Groups I, II and III to the Fourth Assessment Report of the Intergovernmental Panel on Climate Change (Eds.) Pachauri, R.K., Reisinger, A. IPCC, Geneva, Switzerland, 104 pp.

IPCC, 2011. Summary for Policymakers. In: IPCC Special Report on Renewable Energy Sources and Climate Change Mitigation [O. Edenhofer, R. Pichs-Madruga, Y. Sokona, K. Seyboth, P. Matschoss, S. Kadner, T. Zwickel, P. Eickemeier, G. Hansen, S. Schlömer, C. von Stechow (eds)], Cambridge University Press, Cambridge, United Kingdom and New York, NY, USA.

Kalinowski, B.E., Liermann, L.J., Givens, S., Brantley S.L., 2000. Rates of bacteria-promoted solubilization of Fe from minerals: a review of problems and approaches. Chem. Geol. 169, 357-370.

Kappler, A., Newman, D.K., 2004. Formation of Fe(III)-minerals by Fe(II)-oxidizing photoautotrophic bacteria. Geochim. Cosmochim. Acta 68, 1217–1226.

Kelemen, P.B., Matter, J., 2008. In situ carbonation of peridotite for CO_2 storage. PNAS 105, 17295-17300.

Kempka, T., Kühn, M., Class, H., Frykman, P., Kopp, A., Nielsen, C.M., Probst, P., 2010. Modelling of CO_2 arrival time at Ketzin – Part I. Int. J. of Greenhouse Gas Control 4, 1007–1015.

Kharaka, Y.K., Cole, D.R., Thordsen, J.J., Kakouros, E., Nance, H.S, 2006. Gas-water-rock interactions in sedimentary basins: CO_2 sequestration in the Frio Formation, Texas, USA. J. Geochem. Expl. 89, 183-186.

Kharaka, Y.K., Thordsen, J.J., Hovorka, S.D., Nance, H.S., Cole, D.R., Phelps, T.J., Knauss, K.G., 2009. Potential environmental issues of CO_2 storage in deep saline aquifers: Geochemical results from the Frio-I Brine Pilot test, Texas, USA. Appl. Geochem. 24, 1106-1112.

Kristmannsdóttir, H., Tómasson, J., 1978. Zeolite zones in geothermal areas in Iceland. In Natural Zeolites, Occurrences, Properties, Use (eds. L. Sand and F. Mumpton), pp. 277–284. Pergamon.

Kristmannsdóttir, H., 1982. Alteration in the IRDP drill hole compared with other drill holes in Iceland. J. Geophys. Res. 87, 6525–6531.

Lengler, U., De Lucia, M., Kühn, M., 2010. The impact of heterogeneity on the distribution of CO_2: Numerical simulation of CO_2 storage at Ketzin. Int. J. Greenhouse Gas Control 4, 1016–1025.

Li, Z., Dong, M., Li, S., Huang, S., 2006. CO_2 sequestration in depleted oil and gas reservoirs – caprock characterization and storage capacity. Energy Conversion and Management 47, 1372-1382.

Lu, J., Partin, J.W., Hovorka, S.D., Wong, C., 2009. Potential risks to freshwater resources as a result of leakage from CO_2 geological storage: a batch-reaction experiment. Env. Earth Sci. 60, 335–348.

MacFarling Meure, C., Etheridge, D., Trudinger, C., Steele, P., Langenfelds, R., van Ommen, T., Smith, A., Elkins, J., 2006. Law Dome CO, CH and NO ice core records extended to 2000 years BP. Geophys. Res. Lett. 33, L14810, doi:10.1029/2006GL026152.

Mathieson, A., Midgely, J., Wright, I., Saoula, N., Ringrose, P., 2011. In Salah CO_2 Storage JIP: CO_2 sequestration monitoring and verification technologies applied at Krechba, Algeria. Energy Procedia 4, 3596–3603.

Matter, J.M., Kelemen, P.B., 2009. Permanent storage of carbon dioxide in geological reservoirs by mineral carbonation. Nature Geoscience, doi: 10.1038/NGEO683.

Matter, J.M., Broecker, W.S., Stute, M., Gíslason, S.R., Oelkers, E.H., Stefánsson, A., Wolff-Boenisch, D., Gunnlaugsson, E., Axelsson, G., Björnsson, G., 2009. Permanent carbon dioxide storage into basalt: the CarbFix pilot project, Iceland. Energy Procedia 1, 3641–3646.

Matter, J.M., Broecker, W.S., Gislason, S.R., Gunnlaugsson, E., Oelkers, E.H., Stute, M., Sigurdardóttir, H., Stefansson, A., Alfredsson, H.A., Aradóttir, E.S., Axelsson, G., Sigfusson, B., Wolff-Boenisch, D., 2011. The CarbFix Pilot Project – Storing Carbon Dioxide in Basalt. Energy Procedia 4, 5579-5585.

McGrail, B.P., Schaef, H.T, Ho, A.M., Chien, Yi-Ju, Dooley, J.J., Davidson, C.L., 2006. Potential for carbon dioxide sequestration in flood basalts. JGR Res. 111. B12201, doi:10.1029/2005JB004169.

Michael, K., Golab, A., Shulakova, V., Ennis-King, J., Allinson, G., Sharma, S., Aiken, T., 2010. Geological storage of CO_2 in saline aquifers—A review of the experience from existing storage operations. Int. J. Greenhouse Gas Control 4, 659–667.

Mito, S., Xue, Z., Ohsumi, T., 2008. Case study of geochemical reactions at the Nagaoka CO_2 injection site, Japan. Int. J. Greenhouse Gas Control 2, 309-318.

Mito, S., Xue, Z., 2011. Post-Injection Monitoring of Stored CO_2 at the Nagaoka Pilot Site: 5 Years Time-Lapse Well Logging Results. Energy Procedia 4, 3284–3289.

Neuhoff, P.S., Fridriksson, T., Arnorsson, S., Bird, D.K., 1999. Porosity evolution and mineral paragenesis during low-grade metamorphism of basaltic lavas at Teigarhorn, Eastern Iceland. Am. J. Sci. 299, 467–501.

Oelkers, E.H., Gislason, S.R., 2001. The mechansim, rates and consequences of basaltic glass dissolution: I. An experimental study of the dissolution rates of basaltic glass as as function of aqueous Al, Si and oxalic acid concentration at 25 °C and pH = 3 and 11. Geochim. Cosmochim. Acta 65, 3671-3681.

Oelkers, E.H., Gislason, S.R., Matter, J., 2008. Mineral carbonation of CO_2. Elements 4, 333-337.

Pham, T.H.M., Maast, T.E, Hellevang, H., Aagaard, P., 2011. Numerical modeling including hysteresis properties for CO_2 storage in Tubåen formation, Snøhvit field, Barents Sea. Energy Procedia 4, 3746–3753.

Prasad, P.S.R., Srinivasa Sarma, D., Sudhakar, L., Basavaraju, U., Singh, R.S., Begum, Z., Archana, K.B., Chavan, C.D., Charan, S.N., 2009. Geological sequestration of carbon dioxide in Deccan basalts: preliminary laboratory study. Current Sci. 96, 288-292.

Rudge, J.F., Kelemen, P.B., Spiegelman, M., 2011. A simple model of reaction-induced cracking applied to serpentinization and carbonation of peridotite. Earth Planet. Sci. Let. 291, 215–227.

Sato, K., Mito, S., Horie, T., Ohkuma, H., Saito, H., Watanabe, J., Yoshimura, T., 2011. Monitoring and simulation studies for assessing macro- and meso-scale migration of CO_2 sequestered in an onshore aquifer: Experiences from the Nagaoka pilot site, Japan. Int. J. Greenhouse Gas Control 5, 125–137.

Schaef, H.T., McGrail, B.P., Owen, A.T., 2009. Basalt-CO_2-H_2O Interactions and Variability in Carbonate Mineralization Rates. Energy Procedia 1, 4899-4906.

Schaef, H.T., McGrail, B.P., 2009. Dissolution of Columbia River Basalt under mildly acidic conditions as a function of temperature: Experimental results relevant to the geological sequestration of carbon dioxide. Appl. Geochem. 24, 980-987.

Schaef, H.T., McGrail, B.P., Owen, A.T., 2010. Carbonate mineralization of volcanic province basalts. Int. J. Greenhouse Gas Control 4, 249-261.

Schaef, H.T., McGrail, B.P., Owen, A.T., 2011. Basalt Reactivity Variability with Reservoir Depth in Supercritical CO_2 and Aqueous Phases. Energy Procedia 4, 4977–4984.

Schilling, F., Borm, G., Würdemann, H., Möller, F., Kühn, M., and CO_2SINK Group, 2009. Status Report on the First European on-shore CO_2 Storage Site at Ketzin (Germany). Energy Procedia 1, 2029–2035.

Shi, J.-Q., Sinayuc, C., Durucan, S., Korre, A., 2012. Assessment of carbon dioxide plume behaviour within the storage reservoir and the lower caprock around the KB-502 injection well at In Salah. Int. J. Greenhouse Gas Control 7, 115–126.

Wakahama, H., Mito, S., Ohsumi, T., Ueda, A., Yajima, T., Satoh, H., Sugiyama, K., Ozawa, A., Ajima, S., Todaka, N., Sato, T., Kato, M., Kaji, Y., Tokumarui, T., Kaieda, H., Kubota, K., 2009. A concept of CO_2 Georeactor sequestration at the Ogachi HDR site, NE Japan. Energy Procedia 3683–3689.

Welch, S.A., Vandevivere, P., 1994. Effect of microbial and other naturally occurring polymers on mineral dissolution. Geomicrobiol. J. 12, 227-238.

Whittaker, S., Rostron, B., Hawkes, C., Gardner, C., White, D., Johnson, J., Chalaturnyk, R., Seeburger, D., 2011. A decade of CO_2 injection into depleting oil fields: monitoring and research activities of the IEA GHG Weyburn-Midale CO_2 Monitoring and Storage Project. Energy Procedia 4, 6069–6076.

Wolff-Boenisch, D., Gislason, S.R., Oelkers, E.H., 2004. The effect of fluoride on the dissolution rates of natural glasses at pH 4 and 25°C. Geochim. Cosmochim. Acta 68, 4571–4582.

Wolff-Boenisch, D., Wenau, S., Gislason, S.R., Oelkers, E.H., 2011. Dissolution of basalts and peridotite in seawater, in the presence of ligands, and CO_2: Implications for mineral sequestration of carbon dioxide. Geochim. Cosmochim. Acta 75, 5510–5525.

Würdemann, H., Möller, F., Kühn, M., Heidug, W., Christensen, N.P., Borm, G., Schilling, F.R., the CO_2SINK Group, 2010. CO_2SINK—From site characterisation and risk assessment to monitoring and verification: One year of operational experience with the field laboratory for CO_2 storage at Ketzin, Germany. Int. J. Greenhouse Gas Control 4, 938–951.

Xu, T., Kharaka, Y.K., Doughty, C., Freifeld, B.M., Daley, T.M., 2010. Reactive transport modeling to study changes in water chemistry induced by CO_2 injection at the Frio-I Brine Pilot. Chem. Geol. 271, 153–164.

Zemke, K., Liebscher, A., Wandrey, M., the CO_2SINKGroup, 2010. Petrophysical analysis to investigate the effects of carbon dioxide storage in a subsurface saline aquifer at Ketzin, Germany (CO_2SINK). Int. J. Greenhouse Gas Control 4, 990–999.

Chapter 2

Do carbonate precipitates affect dissolution kinetics? 1: Basaltic glass

Gabrielle J. Stockmann, Domenik Wolff-Boenisch, Sigurdur R. Gislason and Eric H. Oelkers

Chemical Geology 284 (2011), 306-316

ABSTRACT

Basaltic glass dissolution rates were measured in mixed-flow reactors at basic pH and at 25 °C and 70 °C in aqueous solutions supersaturated with respect to calcite for up to 140 days. Inlet solutions were comprised of $NaHCO_3$±$CaCl_2$ with ionic strengths >0.03 mol kg^{-1}. Scanning Electron Microscope images show that significant $CaCO_3$ precipitated during these experiments. This precipitate grew on the basaltic glass in experiments performed in Ca-free inlet solutions, but nucleated and grew independently of the glass surfaces in experiments performed in Ca-bearing inlet solutions. In those experiments where $CaCO_3$ precipitated on the glass surface, it grew as discrete crystals; no pervasive $CaCO_3$ layers were observed. The lack of structural match between glass and calcium carbonate favors $CaCO_3$ nucleation and growth as discrete crystals. Measured basaltic glass dissolution rates based on either Si, Al, or Mg were both 1) independent of time during the experiments, and 2) equal to that of corresponding control experiments performed in $NaHCO_3$-free inlet solutions. Taken together, these observations show that basaltic glass dissolution rates are unaffected by the precipitation of secondary $CaCO_3$ precipitation. It seems therefore likely that carbonate precipitation will not slow basaltic glass dissolution during mineral sequestration efforts in basaltic rocks.

Chemical Geology 284 (2011) 306–316

Contents lists available at ScienceDirect

Chemical Geology

journal homepage: www.elsevier.com/locate/chemgeo

Research paper

Do carbonate precipitates affect dissolution kinetics? 1: Basaltic glass

Gabrielle J. Stockmann [a,*], Domenik Wolff-Boenisch [a], Sigurður R. Gislason [a], Eric H. Oelkers [b]

[a] Institute of Earth Sciences, University of Iceland, Sturlugata 7, 101 Reykjavík, Iceland
[b] GET-Université de Toulouse-CNRS-IRD-OMP, 14 Avenue Edouard Belin, 31400 Toulouse, France

ARTICLE INFO

Article history:
Received 1 October 2010
Received in revised form 9 March 2011
Accepted 10 March 2011
Available online 17 March 2011

Editor: U. Brand

Keywords:
Glass dissolution rates
CO_2 storage
Carbonate coating
Carbonatization
Mineral-carbon sequestration
Mixed-flow reactors

ABSTRACT

Basaltic glass dissolution rates were measured in mixed-flow reactors at basic pH and at 25 °C and 70 °C in aqueous solutions supersaturated with respect to calcite for up to 140 days. Inlet solutions were comprised of $NaHCO_3 \pm CaCl_2$ with ionic strengths >0.03 mol kg^{-1}. Scanning Electron Microscope images show that significant $CaCO_3$ precipitated during these experiments. This precipitate grew on the basaltic glass in experiments performed in Ca-free inlet solutions, but nucleated and grew independently of the glass surfaces in experiments performed in Ca-bearing inlet solutions. In those experiments where $CaCO_3$ precipitated on the glass surface, it grew as discrete crystals; no pervasive $CaCO_3$ layers were observed. The lack of structural match between glass and calcium carbonate favors $CaCO_3$ nucleation and growth as discrete crystals. Measured basaltic glass dissolution rates based on either Si, Al, or Mg were both 1) independent of time during the experiments, and 2) equal to that of corresponding control experiments performed in $NaHCO_3$-free inlet solutions. Taken together, these observations show that basaltic glass dissolution rates are unaffected by the precipitation of secondary $CaCO_3$ precipitation. It seems therefore likely that carbonate precipitation will not slow basaltic glass dissolution during mineral sequestration efforts in basaltic rocks.

1. Introduction

This study has been designed to elucidate the effect of secondary mineral precipitation on the dissolution rate of primary phases. The dissolution rates of minerals and glasses are commonly believed to be proportional to their surface area in contact with reactive fluid (e.g. Pačes, 1983; Helgeson et al., 1984; Lasaga, 1984; Siegel and Pfannkuch, 1984; Gautier et al., 2001; Oelkers, 2001; Schott et al., 2009). It seems likely therefore, that the precipitation of secondary phases could alter significantly the dissolution rates of those primary phases on which they precipitate. To test this possibility, the dissolution rates of basaltic glass have been measured in aqueous solutions that were supersaturated with respect to calcite.

Numerous studies have been performed in an attempt to determine the effect of secondary mineral precipitation on the dissolution rates of primary minerals in natural systems. Several authors suggested that the presence of mineral coatings is in part responsible for an apparent difference in laboratory versus natural mineral weathering rates (e.g. Nugent et al., 1998; White and Brantley, 2003). In contrast, Lee et al. (2008) concluded such coatings would be insufficiently continuous to significantly affect feldspar dissolution rates. Slow feldspar weathering rates in natural aquifers have been attributed to the coupling of secondary mineral precipitation to the dissolution of primary silicates (e.g. Zhu, 2005; Zhu et al., 2006, 2010). Velbel (1993) emphasized that the molar volume ratio of product to reactant has to be >1 to provide the volume needed to completely passivate the reactant surface.

Similarly, numerous studies have focused on the effect of secondary mineral precipitation on dissolution rates in the laboratory; these studies commonly present conflicting observations. For example, Murakami et al. (1998) suggested that secondary mineral formation could increase anorthite dissolution rates. In contrast, Hodson (2003) determined that the presence of iron-rich coatings had little effect on anorthite dissolution rates. Giammar et al. (2005) concluded that secondary magnesite precipitated as discrete particles would not limit forsterite dissolution in their experiments. Daval et al. (2009a) observed that secondary calcite coatings have only minor effects on the dissolution rates of wollastonite at acidic conditions, but could be significant at neutral pH. Daval et al. (2009b) described the formation of a non-passivating pseudomorphic silica-rich rim around wollastonite crystals. Both Béarat et al. (2006) and Andreani et al. (2009) reported that silica-rich layer formation on dissolving olivine surfaces slowed carbonate formation, and eventually inhibited olivine dissolution. Park and Fan (2004) suggested that silica-layers inhibited serpentine dissolution. Numerous studies have observed the slowing of glass dissolution rates due to the formation of pervasive leached layers (e.g. Cailleteau et al., 2008; Verney-Carron et al., 2010). Cubillas et al. (2005) concluded that the degree to which secondary mineral precipitation affects the dissolution rates of primary minerals depends on the relative structure of the precipitating versus the dissolving

* Corresponding author. Tel.: +354 525 5248; fax: +354 562 9767.
E-mail address: gjs3@hi.is (G.J. Stockmann).

0009-2541/$ – see front matter © 2011 Elsevier B.V. All rights reserved.
doi:10.1016/j.chemgeo.2011.03.010

Table 1
Chemical composition of the basaltic glass as measured with X-ray Fluorescence spectrometry (XRF).

	Stapafell Mountain, Iceland [a]	Stapafell Mountain, Iceland [b]
	Weight%	Weight%
SiO_2	48.25	48.12
Al_2O_3	14.95	14.62
CaO	11.85	11.84
Fe_2O_3	12.25	1.11
FeO		9.82
K_2O	0.309	0.29
MgO	9.50	9.08
MnO	0.187	0.191
Na_2O	2.01	1.97
P_2O_5	0.207	0.195
TiO_2	1.63	1.564
Total	101.14	99.89

[a] Glass used in this study. Iron was measured after oxidation of all Fe(II) to Fe(III) and thus Fe_2O_3 represents total Fe.
[b] XRF analysis results of Stapafell basaltic glass published by Oelkers and Gislason (2001).

mineral. If the precipitating mineral has a similar structure to the dissolving mineral, the secondary mineral can form a thin impermeable layer through an epitaxial growth mechanism arresting the dissolution of the underlying mineral. The degree that epitaxial growth occurs on a surface may also be affected by the degree of supersaturation (Lasaga, 1998). Similarly, Putnis (2009) found that the replacement of one mineral by another is closely related to the mineral structure and the relative volumes of the phases involved.

This study is focused on the dissolution of basaltic glass coupled to calcium carbonate precipitation. This system has been selected because of its potential application to carbon storage as part of *in-situ* mineral sequestration efforts (e.g. McGrail et al., 2006; Marini, 2007; Matter et al., 2007; Goldberg et al., 2008; Oelkers and Schott, 2005; Oelkers and Cole, 2008; Oelkers et al., 2008; Schaef and McGrail, 2009; Schaef et al., 2009; Gislason et al., 2010; Schaef et al., 2010). Carbon mineralization in basalts involves dissolution of the host rock releasing divalent metal cations such as Ca^{2+}, Mg^{2+}, and Fe^{2+} to solution. These ions can react with dissolved CO_2 and precipitate as carbonate minerals. The rate-limiting step for this reaction is thought to be the release of divalent cations (c.f., Oelkers et al., 2008). As such, any process that can potentially slow the dissolution rates of the basalt, such as secondary carbonate precipitation, would be detrimental to carbon storage efforts.

Towards the improved understanding of the effect of secondary minerals on the dissolution rates of primary solids, long-term basaltic glass dissolution experiments were performed in aqueous solutions supersaturated with respect to calcite in mixed-flows reactors. The purpose of this paper is to report the results of this experimental study and to apply these results to assess the potential effect of secondary carbonate precipitation on carbon mineralization efforts.

2. Theoretical background

The standard state adopted in this study is that of unit activity of pure minerals and H_2O at any temperature and pressure. For aqueous species other than H_2O, the standard state is unit activity of species in a hypothetical 1 mol kg^{-1} solution referenced to infinite dilution at any temperature and pressure. All thermodynamic calculations reported in this study were performed using the PHREEQC 2.14 computer code (Parkhurst and Appelo, 1999) together with its phreeqc.dat database to which thermodynamic data have been added for magnesite, thomsonite, scolecite, mesolite, laumontite, heulandite, analcime, Ca-stilbite, Ca-mordenite, Ca-clinoptilolite, Fe-celadonite, antigorite, amorphous FeOOH, allophane, and imogolite taken from Gysi and Stefansson (submitted for publication) and dawsonite from Benezeth et al. (2007). The thermodynamic properties of hydrated leached basaltic glass with the composition, $SiAl_{0.365}O_2(OH)_{1.095}$, was also added to this phreeqc.dat database. The equilibrium constant (K) for the leached glass dissolution reaction given by:

$$SiAl_{0.365}O_2(OH)_{1.095} + 1.095H^+ + 0.905H_2O = 0.365Al^{3+} + H_4SiO_4 \quad (1)$$

was calculated from the stoichiometric sum of the equilibrium constants of amorphous SiO_2 and amorphous $Al(OH)_3$ hydrolysis reactions (Wolff-Boenisch et al., 2004a). log K for reaction (1) is 1.23 with a ΔH_r equal to −24.04 kJ/mol at 25 °C.

3. Materials and methods

The basaltic glass used in this study was collected from the same location on the Stapafell Mountain in SW Iceland as that studied by Oelkers and Gislason (2001) and Gislason and Oelkers (2003). The chemical composition of the glass (Table 1) was determined by X-ray fluorescence spectrometry (XRF) and can be expressed as: $Si_{1.000}$ $Al_{0.365}$ $Fe_{0.191}$ $Mn_{0.003}$ $Mg_{0.294}$ $Ca_{0.263}$ $Na_{0.081}$ $K_{0.008}$ $Ti_{0.025}$ $P_{0.004}$ $O_{3.405}$. Iron is listed as total Fe as no attempt at determining Fe^{2+} was undertaken. However, the Fe^{2+}/Fe^{3+}-ratio in Stapafell basaltic glass was measured by Oelkers and Gislason (2001), and they showed Fe to be predominantly Fe^{2+} (see Table 1).

The basaltic glass was crushed in plastic bags using a plastic hammer. After crushing, the material was sieved and the 45–125 μm size fraction obtained. Fine particles were removed from this glass fraction by first gravity settling and then by ultrasonically cleaning the glass powder with cycles of water and then acetone. Altogether five water cycles and five acetone cycles were performed and the ultra fine suspension discarded at the end of each cycle. The final glass powder was then dried overnight at 60 °C. Solids before and after each experimental series were analyzed by Scanning Electron Microscopy (SEM) using a LEO Supra 25 and a JEOL 6360 LV Scanning Electron Microscope. The solids were coated with gold prior to this analysis. Energy Dispersive X-ray Spectroscopy (EDX) was used together with SEM to identify primary and secondary minerals. Selected samples were analyzed by X-ray diffraction (XRD) using an INEL CPS 120 to confirm the identity of secondary minerals. Fig. 1a shows the resulting glass powder after sieving and cleaning to be fine-particle free with an even distribution of all particle sizes from 45 to 125 μm. The specific surface area of the cleaned powder was determined to 5878 cm^2/g by 3-point krypton adsorption using the BET method. The density of this glass, as reported by Wolff-Boenisch et al. (2006), is 3.05 g/cm^3. The geometric surface area of the basaltic glass used in this study, A_{geo}, calculated using equations reported by Wolff-Boenisch et al. (2004a) is 251 cm^2/g. Dividing the BET surface area by the geometric surface area yields a roughness factor of 23. Although the glass surface appears smooth, the difference between BET and geometric surface area likely stems from fine scale porosity and roughness as can be seen in large magnification SEM images (see Fig. 1b).

The mixed-flow reactor system used for all experiments is illustrated in Fig. 2. This reactor system is similar to those used in past dissolution rate studies (e.g., Wolff-Boenisch et al., 2004a,b; Cubillas et al., 2005; Pokrovsky et al., 2005; Chaïrat et al., 2007; Gautelier et al., 2007). All reactors, connectors, and tubing were thoroughly cleaned in a 0.1 M HCl bath for ~24 h and rinsed with Millipore™ water prior to each experiment. All outlet fluid sample bottles went through the same cleaning procedure prior to sampling to prevent contamination. Basaltic glass dissolution experiments were initiated by placing either 5 or 10 g of cleaned basaltic glass powder and the selected inlet solution into the 300 mL polyethylene mixed-flow reactors. These reactors were sealed and placed into a temperature controlled water bath. Temperature was kept constant during the experiment at either 25 or 70 °C. Teflon™ coated floating stir bars from Nalgene™ were placed on the bottom of the reactors and propelled at stirring rates

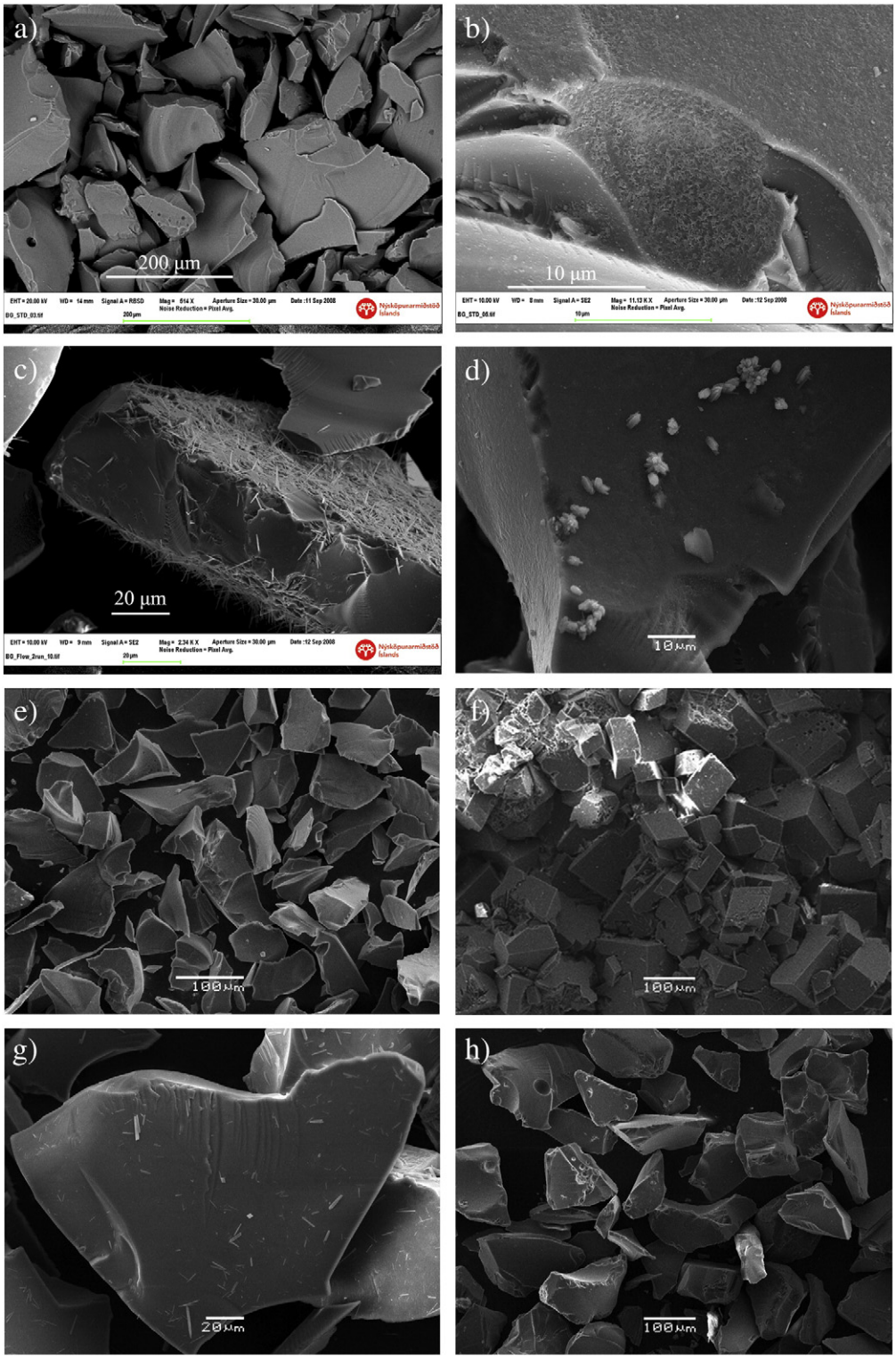

Fig. 1. Scanning electron images of the basaltic glass used in this study. Images a and b are of the basaltic glass before experiment. Image b is a magnification of image a showing surface roughness. Image c shows secondary silica-rich precipitates growing on the surfaces of glass following its dissolution during experimental series 2 at 70 °C, which is the only series, where other secondary phases than carbonates were observed. Image d depicts small $CaCO_3$ crystals growing out of the glass surface following its dissolution during series 8 at pH 10. Image e represents the surface of basaltic glass after dissolution during control series 9 at pH 10. Images f and g illustrate the morphology of $CaCO_3$ precipitates recovered from series 4 and 6. Calcite clusters as in f ranged in size from 10 to 1000 µm. Image h shows the surfaces of basaltic glass following its dissolution for ~164 days in control Exp. 7.

around 300 rpm using a multi-position magnetic stirrer located underneath the water bath. Floating stir bars were used to avoid grinding of the basaltic glass grains during the experiments.

Inlet solutions were comprised of Millipore™ water and Merck/Sigma-Aldrich analytical grade $NaHCO_3$, Na_2CO_3, NH_4Cl, $CaCl_2$, NaCl, NaOH, and/or HCl with ionic strengths ranging from 0.01 to 0.09 mol kg^{-1}. Compositions of the inlet solutions were based on calculations made using PHREEQC to yield the desired pH and ionic strength. The inlet solutions were stored in 8 or 12 L compressible plastic bags. Inlet solutions containing $CaCl_2$ were continuously

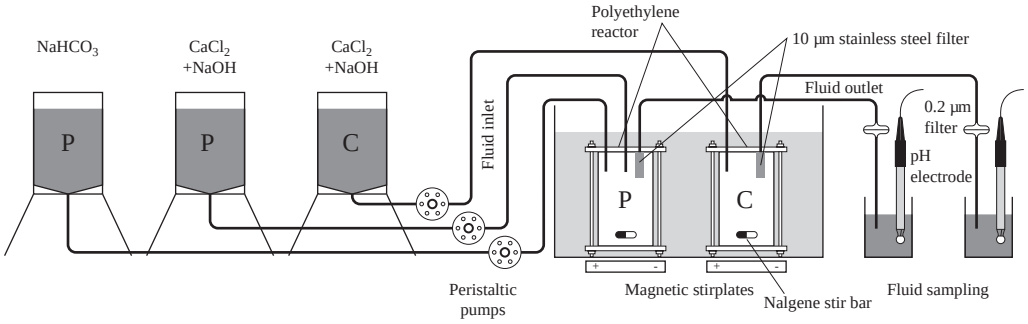

Fig. 2. Experimental setup of the precipitation (P) and control (C) experiments used for experimental series 4 through 7 at 25 °C. Supersaturation of calcite in the precipitation experiments is obtained by mixing two inlet solutions comprised of $NaHCO_3$ and $CaCl_2$, respectively, inside the reactor. The control experiments ran with a $CaCl_2$ inlet solution designed to dissolve basaltic glass without secondary precipitate formation. Both P and C reactors contained approximately 10 g of basaltic glass powder.

purged with N_2 to prevent atmospheric CO_2 from dissolving into this solution and to keep the pH stable. This effort was only partially successful as the pH in these solutions fluctuated ± 1 pH unit from the target pH. Inlet solutions were injected into the reactors at a constant rate using Masterflex™ cartridge pumps. In some experiments two inlet solutions (one Ca-rich and the second carbonate-rich) were used to create a solution supersaturated with respect to calcite in the reactor.

Experiments in this study were performed in series consisting of a sequence of runs performed on a single basaltic glass powder. For each experiment in a series the temperature and inlet solution flow rate were kept constant while the chemical composition of the inlet solution was changed. Two different types of experiments were performed: 'precipitation' and control 'experiments'. 'Precipitation' experiments were designed to measure basaltic glass dissolution rates during carbonate precipitation. To attain calcite saturation, carbonate ±calcium were provided to the system by the inlet solutions. 'Control' experiments were designed to measure basaltic glass dissolution rates in the absence of secondary phase precipitation and were carried out in carbonate-free inlet solutions. Details of all nine experimental series are provided in Tables 2–4. Each series is denoted by a number, and each experiment within a series is indicated by a letter, i.e. Exp. 7a–e are five experiments within series 7.

Outlet fluids were regularly sampled during all experiments. Three residence times or more separated each sampling. The residence time is defined as the volume of the reactor divided by the fluid flow rate. The outlet solutions were filtered through a 0.2 μm cellulose acetate membrane filter into a 100 mL polyethylene bottle and acidified with concentrated supra-pure HNO_3. The major element concentrations of inlet and outlet fluids were determined using a Spectro Ciros Vision Inductively Coupled Plasma Optical Emission Spectrometer (ICP-OES). Analytical uncertainties on ICP-OES analyses are estimated to be 3–5%.

Glass dissolution rates based on the release of the *i*th element ($r_{+,i,j}$) were calculated from:

$$r_{+,i,j} = \frac{C_i \cdot fr}{\nu_i \cdot A_j \cdot m} \quad (2)$$

where C_i stands for the concentration of the *i*th element in the outlet solution, *fr* refers to the fluid flow rate, ν_i is the stoichiometric factor of the *i*th element, A_j designates the specific surface area of the basaltic glass, and *m* denotes the mass of glass used in the experiment. The

Table 2
Composition of the inlet fluids for the all experiments performed in this study.

Experiment[a]	$NaHCO_3$ (mol/kg)	NH_4Cl (mol/kg)	$CaCl_2$ (mol/kg)	Na_2CO_3 (mol/kg)	NaCl (mol/kg)	NaOH (mol/kg)	HCl (mol/kg)[c]	Ionic strength (mol/kg)	pH (21 °C)
1a-P	0.035							0.035	8.45
1b-P	0.035						n.m.	0.035	6.35
2-P	0.035							0.035	8.54
3-C		0.010						0.010	5.74
4-P[b]	0.035		0.010					0.033	8.15
5a-C			0.014			1.0E−06		0.042	7.29
5b-C			0.020			1.4E−06		0.060	7.22
6a-P[b]	0.035		0.010			1.2E−07		0.033	n.m.
6b-P[b]	0.035		0.020			1.6E−07		0.048	n.m.
6c-P	0.010							0.010	8.54
6d-P		0.010					n.m.	0.010	3.81
7a-C			0.020			1.6E−07		0.060	7.92
7b-C			0.030			1.7E−07		0.090	8.33
7c-C			0.030					0.090	5.83
7d-C	0.010							0.010	8.54
7e-C		0.010					n.m.	0.010	3.81
8a-P	0.010			0.010				0.040	10.12
8b-P	0.010			0.010				0.040	10.13
8c-P	0.010							0.010	8.54
9a-C					0.035	1.3E−07		0.035	10.18
9b-C					0.035	1.3E−07		0.035	10.19
9c-C	0.010							0.010	8.54

n.m. = not measured.
[a] The '-P' and '-C' designates precipitation and control experiments, respectively.
[b] Two-inlet system, i.e. the concentration of the fluid entering the reactor is half of each inlet.
[c] HCl was added until the desired pH was reached, but the exact concentration was not measured.

index *j* refer to rates calculated either using the measured BET surface area, A_{BET} or the geometric surface area, A_{geo}.

Thermodynamic calculations suggest the some of the outlet fluids at both 25 and 70 °C were supersaturated with respect to several secondary phases including gibbsite, hematite, goethite, zeolites and clay minerals. These are minerals that occur naturally in the Hellisheidi basalts (Alfredsson et al., 2008). Secondary iron phases were supersaturated in most experiments and often a reddish-brown precipitate was observed on the stainless steel filters inside the mixed-flow reactors. Thermodynamic calculations also indicate that the outlet fluids were all strongly undersaturated with respect to the dissolving basaltic glass itself with a chemical affinity; $A^* \geq 10$ kJ/mol in all experiments, where A^* refers to the chemical affinity of the hydrated surface layer (c.f., Gislason and Oelkers, 2003).

4. Experimental results

In total, 19 steady-state dissolution experiments were performed as part of 9 experimental series. The chemical compositions of the inlet fluids, their pH and ionic strength are listed in Table 2. Compositions of the outlet fluids at steady-state and calculated steady-state basaltic glass dissolution rates for all 19 experiments are listed in Tables 3a and b. The saturation state of calcite in the outlet fluids and other selected minerals are provided in Table 4. These experimental results will be discussed in detail below.

4.1. Basaltic glass dissolution in aqueous carbonate inlet fluids at 70 °C (experimental series 1 and 2)

Experimental series 1 and 2 dissolved basaltic glass in 0.035 mol kg^{-1} $NaHCO_3$ inlet solutions. Experimental series 1 was previously described by Stockmann et al. (2008), a preliminary report of this study. Results for this experimental series in the current manuscript differ somewhat from those previously reported because they have been corrected for loss of dissolving basaltic glass mass during the experiment. The initial mass of 9.9 g of basaltic glass was reduced by dissolution to 8.8 g during the experiment, which makes a notable difference in calculated rates. Mass-corrected results of experimental series 1 are shown as a function

Table 3
Physical conditions, steady-state solution compositions, and measured basaltic glass dissolution rates of all experiments performed in the present study.

a. Physical conditions and steady-state fluid compositions of the basaltic glass dissolution experiments performed in this study.

Exp.[c]	T (°C)	m_{BG} (g)	S_{BET} (m^2)	*fr* (g/min)	t_{exp} (days)	pH_{out} in-situ T[a]	$[Si]_{out}$ (μmol/kg)	$[Al]_{out}$ (μmol/kg)	$[Ca]_{out}$ (μmol/kg)	$[Mg]_{out}$ (μmol/kg)	$[Fe]_{out}$ (μmol/kg)	A* (kJ/mol)[a]	log (a^2_{H+}/a_{Al3+})[a]
1a-P	70	9.93	5.84	0.56	42	8.2	244.82	78.47	19.47	62.04	0.15	13.4	−6.3
2-P	70	9.82	5.77	0.57	26	8.1	129.72	38.38	20.90	30.37	0.04	15.1	−6.1
3-C	70	5.00	2.94	1.17	10	5.2	19.71	0.10	3.31	2.86	0.26	21.7	−5.6
4-P	25	9.98	5.87	0.51	64	7.1	5.03	0.09	2370.25[b]	9.53[b]	0.05	20.2	−9.2
5a-C	25	9.92	5.83	0.51	12	6.8	5.86	0.33	n.m.[b]	22.90[b]	0.05	17.7	−9.2
5b-C	25	9.92	5.83	0.51	48	6.8	8.75	1.17	n.m.[b]	30.20[b]	0.03	16.0	[d]
6a-P	25	9.53	5.60	0.50	29	7.2	7.47	0.14	2517.38[b]	9.29[b]	0.10	18.5	−8.6
6b-P	25	9.53	5.60	0.50	40	7.0	4.26	0.23	5913.36[b]	15.79[b]	0.08	19.1	−8.9
6c-P	25	5.09	2.99	0.63	8	8.6	4.24	1.57	53.82	1.31	0.06	20.6	−8.3
6d-P	25	5.09	2.99	0.64	5	8.1	4.64	1.36	794.66	1.61	0.03	19.4	−8.7
7a-C	25	9.85	5.79	0.45	32	7.7	14.93	3.83	n.m.[b]	30.70[b]	0.08	14.9	[d]
7b-C	25	9.85	5.79	0.49	114	7.9	14.54	4.31	n.m.[b]	42.18[b]	0.04	15.5	[d]
7d-C	25	5.13	3.02	0.63	9	8.5	4.63	1.70	n.m.	1.12	0.29	20.3	−8.3
8a-P	25	9.75	5.73	0.48	146	10.0	14.86	2.76	4.66	3.60	b.d.	22.9	−7.0
8b-P	25	5.01	2.94	0.72	7	10.1	11.75	2.12	7.46	2.92	b.d.	23.7	−6.9
8c-P	25	5.01	2.94	0.72	5	8.6	5.15	1.21	7.09	2.33	0.12	20.5	−8.1
9a-C	25	9.41	5.53	0.47	132	9.9	11.79	3.54	n.m.	2.14	0.03	18.8	−7.2
9b-C	25	5.03	2.96	0.70	7	10.0	11.48	3.59	n.m.	1.96	0.16	22.6	−7.2
9c-C	25	5.03	2.96	0.69	5	8.5	4.11	0.83	n.m.	1.66	0.02	21.4	−8.0

b. Steady-state basaltic glass dissolution rates (log r_+) in mol/cm^2/s obtained in this study

Exp.	T (°C)	pH_{out} at in-situ T	log $r_{+,Si,BET}$	log $r_{+,Si,geo}$	log $r_{+,Al,BET}$	log $r_{+,Al,geo}$	log $r_{+,Ca,BET}$	log $r_{+,Ca,geo}$	log $r_{+,Mg,BET}$	log $r_{+,Mg,geo}$	log $r_{+,Fe,BET}$	log $r_{+,Fe,geo}$
1a-P	70	8.2	−13.4	−12.0	−13.5	−12.1	−13.9	−12.6	−13.5	−12.1	−15.9	−14.5
2-P	70	8.1	−13.7	−12.3	−13.8	−12.4	−13.9	−12.5	−13.8	−12.4	−16.5	−15.1
3-C	70	5.2	−13.9	−12.5	−15.7	−14.4	−14.1	−12.7	−14.2	−12.8	−15.0	−13.7
4-P	25	7.1	−15.1	−13.8	−16.4	−15.1					−16.4	−15.1
5a-C	25	6.8	−15.1	−13.7	−15.9	−14.5					−16.4	−15.0
5b-C	25	6.8	−14.9	−13.5	−15.3	−14.0					−16.6	−15.3
6a-P	25	7.2	−15.0	−13.6	−16.2	−14.9					−16.1	−14.7
6b-P	25	7.0	−15.2	−13.8	−16.0	−14.7					−16.2	−14.8
6c-P	25	8.6	−14.8	−13.5	−14.8	−13.5	−13.1	−11.8	−14.8	−13.4	−16.0	−14.6
6d-P	25	8.1	−14.8	−13.4	−14.9	−13.5	−12.0	−10.6	−14.7	−13.3	−16.3	−14.9
7a-C	25	7.7	−14.7	−13.3	−14.9	−13.5					−16.3	−14.9
7b-C	25	7.9	−14.7	−13.3	−14.8	−13.4					−16.5	−15.2
7d-C	25	8.5	−14.8	−13.4	−14.8	−13.4			−14.9	−13.5	−15.3	−13.9
8a-P	25	10.0	−14.7	−13.3	−15.0	−13.6	−14.6	−13.2	−14.8	−13.4		
8b-P	25	10.1	−14.3	−13.0	−14.6	−13.3	−13.9	−12.6	−14.4	−13.0		
8c-P	25	8.6	−14.7	−13.3	−14.9	−13.5	−14.0	−12.6	−14.5	−13.1	−15.6	−14.2
9a-C	25	9.9	−14.8	−13.4	−14.9	−13.5			−15.0	−13.6	−16.7	−15.3
9b-C	25	10.0	−14.3	−13.0	−14.4	−13.0			−14.6	−13.2	−15.5	−14.1
9c-C	25	8.5	−14.8	−13.4	−15.1	−13.7			−14.7	−13.3	−16.4	−15.0

n.m. = not measured. b.d. = below detection limit.
[a] Computed with PHREEQC version 2.14.
[b] Ca and Mg concentrations arise from $CaCl_2$ inlet solution.
[c] The '-P' and '-C' designates precipitation and control experiments, respectively.
[d] No stable value, not included.

Table 4
Saturation indices (SI) of selected minerals in the outlet fluids of all experiments reported in this study.[a,b,c]

Exp.[d]	Calcite	Aragonite	Gibbsite	Amorph. $Al(OH)_3$	Goethite	Hematite	Amorph. FeOOH[e]	Amorph. SiO_2	Chlorite	Kaolinite	Mesolite[e]	Scolecite[e]	Thomsonite[e]	Other minerals super-saturated according to modeling[a]
1a-P	−0.02	−0.14	0.37	−1.97	5.46	13.11	−0.09	−1.26	6.10	1.22	1.44	1.64	3.69	Allophane, analcime, chrysotile, dawsonite, dolomite, imogolite, Ca-mordenite, magnesite, talc
2-P	−0.05	−0.16	0.21	−2.13	5.23	12.66	−0.32	−1.51	2.18	0.40	0.16	0.38	1.15	Allophane, analcime, dawsonite, dolomite, imogolite, magnesite, talc
3-C			−0.35	−2.68	−4.10	−6.02	−9.66	−2.33	−33.50	−2.34	−10.66	−9.29	−21.82	
4-P	0.24	0.10	−0.10	−2.79	5.25	12.51	−0.65	−2.57	−23.34	−1.98	−5.58	−4.52	−10.44	
5a-C			1.10	−1.59	4.48	10.96	−1.43	−2.52	−22.25	0.52	−5.58	−1.87	−7.94	Allophane, imogolite
5b-C			1.52	−1.17	4.45	10.90	−1.46	−2.37	−20.13	1.66	−3.98	−0.41	−4.44	Allophane, imogolite
6a-P	0.45	0.30	0.59	−1.04	5.24	12.50	−0.65	−2.51	−22.03	−0.49	−3.97	−2.89	−6.55	Dawsonite, imogolite
6b-P	0.50	0.36	0.83	−0.80	4.96	11.92	−0.95	−2.68	−22.65	−0.34	−4.07	−2.90	−6.30	Dawsonite, imogolite
6c-P	0.10	−0.04	0.15	−2.54	6.10	14.21	0.20	−2.69	−13.09	−1.72	−3.76	−3.13	−6.04	
6d-P	−5.83	−5.97	0.57	−2.12	−1.29	−0.57	−7.19	−2.63	−16.30	−0.76	−4.57	−1.95	−6.23	
7a-C			1.28	−1.41	5.89	13.79	−0.01	−2.11	−10.91	1.70	−1.79	1.73	0.32	Allophane, imogolite
7b-C			1.14	−1.55	5.80	13.60	−0.11	−2.15	−9.07	1.35	−1.78	1.82	0.52	Allophane, imogolite
7d-C	−0.24	−0.39	0.17	−2.52	6.72	15.44	0.81	−2.67	−13.78	−1.65	−3.96	−3.43	−6.67	
8a-P	−0.06	−0.21	−1.19	−3.88				−2.63	−1.35	−4.28	−4.10	−4.29	−7.85	
8b-P	0.04	−0.11	−1.27	−3.96				−2.71	−1.69	−4.59	−4.37	−4.52	−8.29	
8c-P	−0.65	−0.79	−0.03	−2.72	6.49	14.99	0.59	−2.58	−10.67	−1.86	−4.13	−3.78	−7.51	
9a-C			−0.91	−3.60	4.96	11.92	−0.95	−2.62	−0.49	−3.70	−3.19	−3.21	−5.43	
9b-C			−0.95	−3.64	5.53	13.06	−0.38	−2.66	−0.46	−3.84	−3.02	−2.90	−4.77	
9c-C	−0.82	−0.97	−0.23	−2.92	5.56	13.13	−0.34	−2.80	−14.42	−2.68	−5.54	−5.20	−10.49	

[a] Computed with PHREEQC version 2.14.
[b] Saturation index is defined as: $SI = \log(IAP/K_{sp})$, where IAP is the ion activity product and K_{sp} refers to the solubility product of the solid phase.
[c] Uncertainty on SI is estimated to ±0.10 log units.
[d] The '-P' and '-C' designates precipitation and control experiments, respectively.
[e] Based on data from Gysi and Stefansson (submitted for publication).

of time in Fig. 3a. Basaltic glass dissolution rates based on Si, Al, and Mg release are similar and thus consistent with the stoichiometric dissolution of the glass during the first 42 days of the experiment. The pH of the outlet fluid was constant and equal to 8.2 during the experiment. The dissolution of the glass also released Ca to solution. The combination of this Ca release and the HCO_3^- present in the inlet solution resulted in the reactive fluid being saturated with respect to calcite (Fig. 3b). The dissolution rates based on Ca shown in Fig. 3a are 0.5 log units slower than that of the other elements, consistent with the precipitation of a calcium carbonate phase. Calculations indicate that the reactive fluids are also supersaturated with respect to gibbsite, goethite, hematite, dawsonite, dolomite, magnesite, chlorite, chrysotile, talc, kaolinite, allophane, imogolite and several zeolites. Dissolution rates based on Fe are not shown in Fig. 3a as their concentration in the outlet fluids are at or below the analytical detection limit suggesting Fe-oxyhydroxide precipitation. In contrast the relative dissolution rates based on Si, Al, and Mg are consistent with the absence of significant quantities of Mg or Al bearing secondary phases.

After 42 days, the original inlet solution was replaced by a 0.035 mol kg^{-1} $NaHCO_3$ solution to which sufficient HCl was added to lower its pH to 6.4. This pH pulse had distinct effects on the dissolution rates measured from Si, Al, and Mg versus Ca concentrations. The dissolution rates calculated from Si, Al, and Mg release decreased following this pH pulse consistent with the decrease of basaltic glass dissolution rates over this pH range (c.f. Gislason and Oelkers, 2003), whereas dissolution rates from Ca release increased following this pH pulse consistent with the relatively rapid re-dissolution of a calcium carbonate phase. Note that the solubility of calcium carbonate phases increase dramatically with decreasing pH at these conditions (Plummer and Busenberg, 1982).

If all the non-stoichiometric Ca release is attributed to calcium carbonate precipitation, mass balance considerations indicate that 0.14 g of calcite precipitated during the first 42 days of experimental series 1. This mass of calcite, if homogeneously precipitated over the whole basaltic glass BET surface area, would have lead to a 1 μm thick secondary calcite layer on the ~8.9 g of glass present in the reactor. Nevertheless, Si release suggests that this precipitation has little effect on the glass dissolution rates. This observation suggests that the precipitated calcium carbonate is not passivating. This observation would be consistent with either the precipitation of the calcium carbonate independently from the glass surface or heterogeneously on this surface.

Experimental series 2 ran for 26 days as a replicate of series 1, but dissolution rates for this experiment suggest not only retention of Ca, but also of Si, Mg and Al in secondary mineral phases. Steady-state glass dissolution rates based on Si, Mg and Al are systematically 0.3 log units lower than the rates obtained in series 1. The steady-state dissolution rates based on Ca release of this series are identical to those observed in experimental series 1 consistent with calcite saturation. PHREEQC calculations indicate the reactive fluid was supersaturated with respect to calcite, dawsonite, gibbsite, clays and zeolites; SEM images coupled with EDX substantiated the precipitation of a secondary silica-rich phase as depicted in Fig. 1c. It was not possible, however, to identify this needle-shaped precipitate due to crystal size. The observed silicate needles do, however, exhibit the morphology of the zeolites mesolite and scolecite, which are supersaturated in the outlet solution. It seems likely that this precipitate is responsible for the lower Si and Al release rates observed in this experimental series relative to experimental series 1. EDX also detected carbon on the glass surface, but no carbonate crystals were visible. More sensitive surface analysis techniques might reveal the identity of the needles and the carbon phases on the glass surface. This is the only experiment where mineral phases other than calcium carbonate were observed. It is noteworthy that these secondary Si-rich precipitates do not form massive coatings on the glass surface. In contrast, passivating silica rims have been reported in

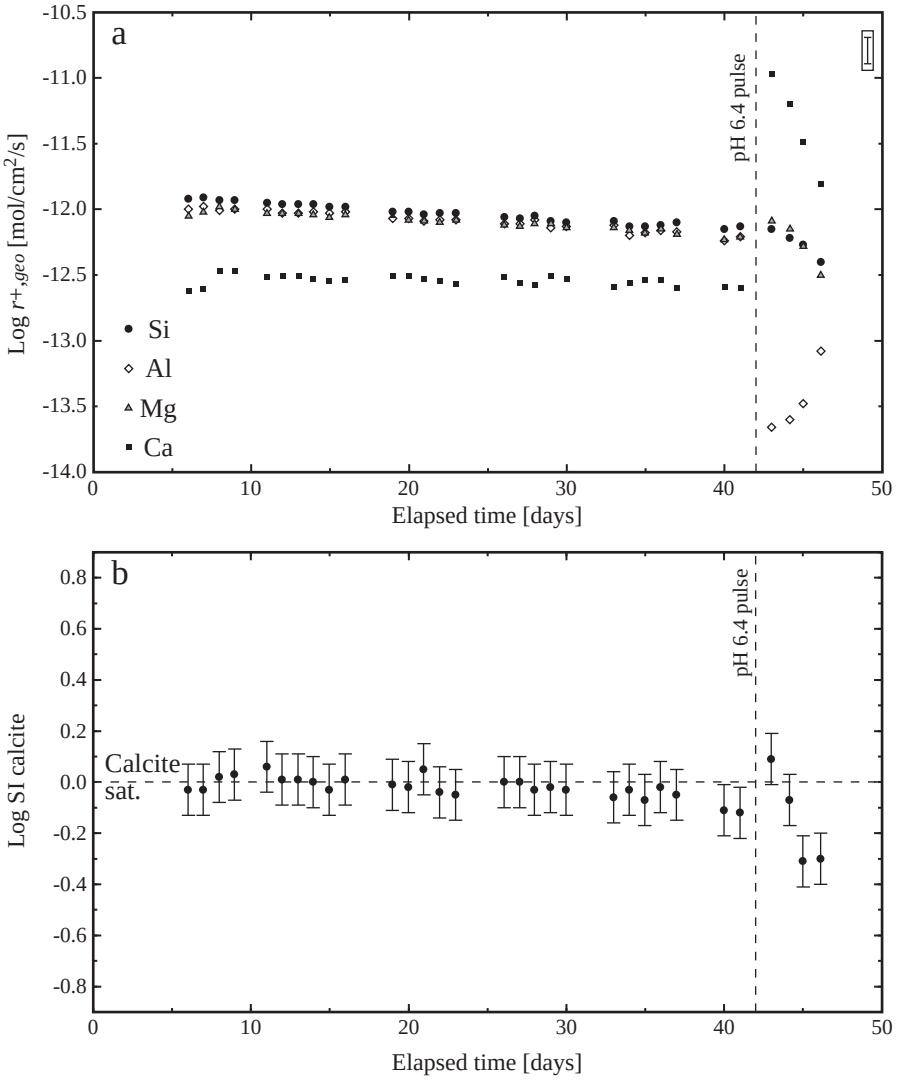

Fig. 3. a) Basaltic glass dissolution rates during experiment 1 at 70 °C and pH 8.2. A pH 6.4-pulse was added after 42 days of experiment. The uncertainty in the measured rates is ± 0.15 log units as illustrated by the error bar in the top-right corner of the plot. b) Calculated calcite saturation state of the reactive fluid during experiment 1. The error bars in this plot correspond to ± 0.10 uncertainty in log SI calcite values.

some previous studies (e.g. Béarat et al., 2006; Andreani et al., 2009; Daval et al., 2009b).

4.2. Basaltic glass dissolution in carbonate-rich fluids at 25 °C (experimental series 8 and 9)

Experimental series 8 consisted of the dissolution of basaltic glass in a solution containing 0.01 mol kg^{-1} $NaHCO_3$ and 0.01 mol kg^{-1} Na_2CO_3. The resulting inlet solution had a pH of 10.0. The results of experiment 8a are presented as a function of time in Fig. 4a. Dissolution rates from Si, Mg, and Ca release are similar and consistent with stoichiometric dissolution of the glass during the first 100 days duration of the experiment. After 100 days, Ca appears to be preferentially released from the glass. The reason for this preferential Ca release is unclear, but post-experimental SEM images (e.g., Fig. 1d) clearly indicate that calcium carbonate precipitated on the basaltic glass surface. This is also corroborated by calculations showing that the reactive fluid was saturated with calcite throughout the experiment. Dissolution rates calculated from Al release are relatively low suggesting precipitation of an Al-bearing phase. As was the case for experimental series 1, Si and Mg release appear nearly constant during the 140-day experiment.

A parallel control experiment, experimental series 9, was performed by dissolving basaltic glass in a pH 9.9 solution comprised of 0.035 mol kg^{-1} NaCl + 0.13 mmol kg^{-1} NaOH. Dissolution rates based on Si release from experiment 9a are compared to those of experiment 8a in Fig. 4b. It can be seen that dissolution rates from Si release from both experiments are identical within experimental uncertainty. SEM images of basaltic glass powders following experimental series 9 show the basalt surfaces to be free of secondary minerals (Fig. 1e).

4.3. Basaltic glass dissolution in calcium-bearing aqueous carbonate fluids at 25 °C (experimental series 4 and 6)

In an attempt to assess the effect of thicker calcium carbonate layers on basaltic glass dissolution, two further sets of basaltic glass dissolution experiments were carried out using calcium bearing aqueous carbonate inlet fluids at 25 °C (series 4 and 6). Two inlet solutions were connected to the mixed-flow reactor; one injecting an aqueous 0.035 mol kg^{-1} $NaHCO_3$ solution and the other aqueous solution containing 0.01 to 0.03 mol kg^{-1} $CaCl_2$ and sufficient NaOH to attain the target pH. The compositions of these inlet solutions are listed in Table 2.

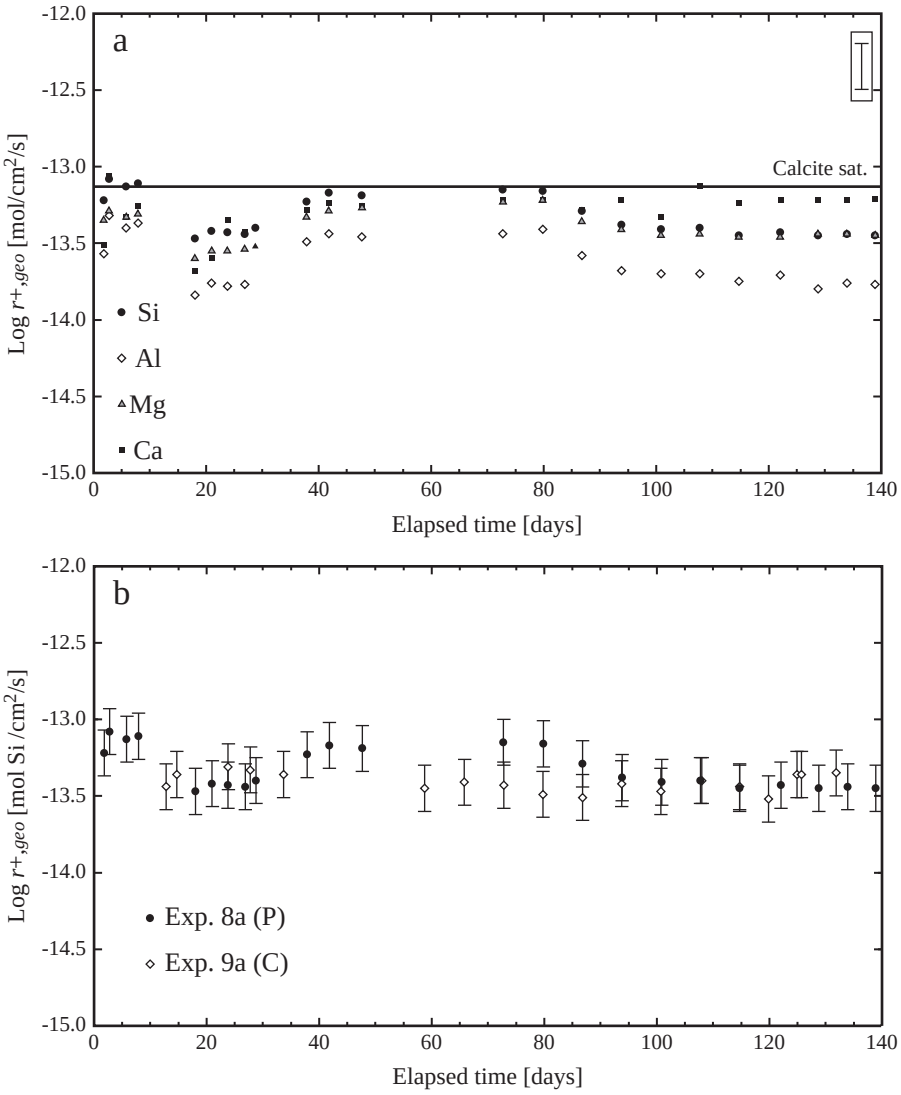

Fig. 4. a) Measured basaltic glass dissolution rates based on Si, Mg, Al, and Ca during experiment 8a (P) at 25 °C and pH 10.0. The error bars in this plot correspond to ± 0.15 log units uncertainty on the rates, and the solid line represents the Ca release rate needed to reach calcite saturation. b) Comparison of the dissolution rates based on Si release during experiment 8a (P) with the Si rates of the corresponding control experiment 9a (C) at 25 °C. 'P' and 'C' refers to precipitation and control experiments, respectively.

Basaltic glass dissolution rates based on Si during experimental series 4 and 6 are shown in Fig. 5, together with corresponding rates from control experiments (series 5 and 7, c.f. Table 3). Basaltic glass dissolution rates in precipitation and control experiments are identical within uncertainty and are invariant over time.

SEM images of both 'precipitation' and 'control' experiments are shown in Fig. 1f, g and h. No secondary minerals are evident in the 'control' experiments (series 5 and 7, Fig. 1h), and only calcium carbonate minerals (calcite and aragonite, based on morphology) are apparent in the 'precipitation' experiments (series 4 and 6, Fig. 1f and g). In contrast to the SEM images of the glass after experimental series 8, the calcium carbonate precipitates in series 4 and 6 did not grow on the basaltic glass surface but as individual crystals. This differing behavior may stem from two factors. First, the source of calcium in the fluids of experimental series 8 is the dissolution of the basaltic glass rather than the inlet fluid. Secondary, the inlet fluid in experimental series 4 and 6 are far more supersaturated with respect to calcite than the fluid in experimental series 8. This higher degree of supersaturation could provoke heterogeneous nucleation of calcium carbonate in the fluid of experimental series 4 and 6. Indeed, the weight of the solids after the experimental series 6 indicated that approximately 5 g of carbonates had precipitated inside the reactor; this estimate was qualitatively corroborated by Ca mass balance calculations that suggested that ~10 g of calcite precipitated during the 69-day duration of experiments 6a and 6b. Despite the fact that the mass of precipitated carbonates was substantial, glass dissolution rates were not affected. XRD analysis of post-experiment samples confirmed the presence of calcite in both experiments, whereas aragonite and vaterite, a third polymorph of $CaCO_3$, were not detected by XRD. However, the presence of aragonite in these experiments is very probable because the elongated crystals, seen in Fig. 1g are typical of orthorhombic aragonite (Palache et al., 1951). No cation impurities such as Mg or Sr, that could help distinguish between calcite and aragonite in the crystal structure, were detected with EDX (Gobac et al., 2009).

4.4. Comparison with previously published basaltic glass dissolution rates

The logarithm of steady state dissolution rates obtained in this study at 25 °C are plotted in Fig. 6 as a function of $\log\cdot(a_{H^+}^3 / a_{Al^{3+}})$ where a_i refers to the activity of the subscripted aqueous species. Only data for those outlet fluids where Si and Al release was stoichiometric

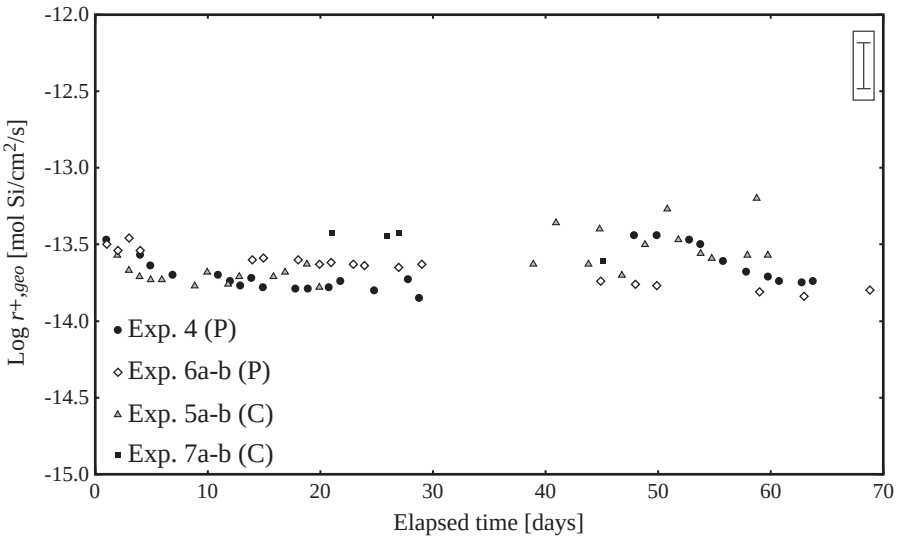

Fig. 5. Comparison of measured basaltic glass dissolution rates from Si release during experiments 4 and 6a–b with Si release during the corresponding control experiments 5a–b and 7a–b at 25 °C and pH ~ 7. The uncertainty on the rates is ±0.15 log units as illustrated by the error bar in the top-right corner. 'P' and 'C' refers to precipitation and control experiments, respectively.

are plotted in Fig. 6 to avoid potential ambiguities due to potential secondary mineral precipitation. Consistent with the dissolution mechanism and rate equations provided by Oelkers and Gislason (2001) and Gislason and Oelkers (2003) the far-from-equilibrium dissolution rates from the 'precipitation' as well as 'control' series can be expressed as

$$r_{Si,geo} = k\left(\frac{a_{H^+}^3}{a_{Al^{3+}}}\right)^n \quad (3)$$

where k denotes a rate constant and n a reaction order equal to 0.33. Eq. (3) is based on the assumption that the rate limiting step of basaltic glass dissolution is the breaking of partially liberated Si-tetrahedras through proton/aluminum exchange reactions (Oelkers, 2001; Wolff-Boenisch et al., 2004b; Schott et al., 2009). It can be seen in Fig. 6 that the dissolution rates of basaltic glass measured in the presence of precipitating $CaCO_3$ are similar to those measured in the 'control' experiments.

Several past studies reported dissolution rates of glasses similar to that used in this study at similar temperatures and pH. A compilation of these rates is given in Table 5. Rates normalized to BET surface area are comparable to those determined in this study, whereas rates normalized to geometric surface area are approximately one log unit lower than those obtained in this study.

A comparison of measured basaltic glass dissolution rates based on Si release as a function of fluid phase ionic strength is illustrated in Fig. 7. No effect of ionic strength is apparent.

5. Discussion

The results summarized above suggest that the presence of calcite precipitating on or near the surfaces of basaltic glass does not affect its dissolution rate. What calcium carbonate is observed to precipitate on these surfaces forms prisms rather than pervasive coatings covering

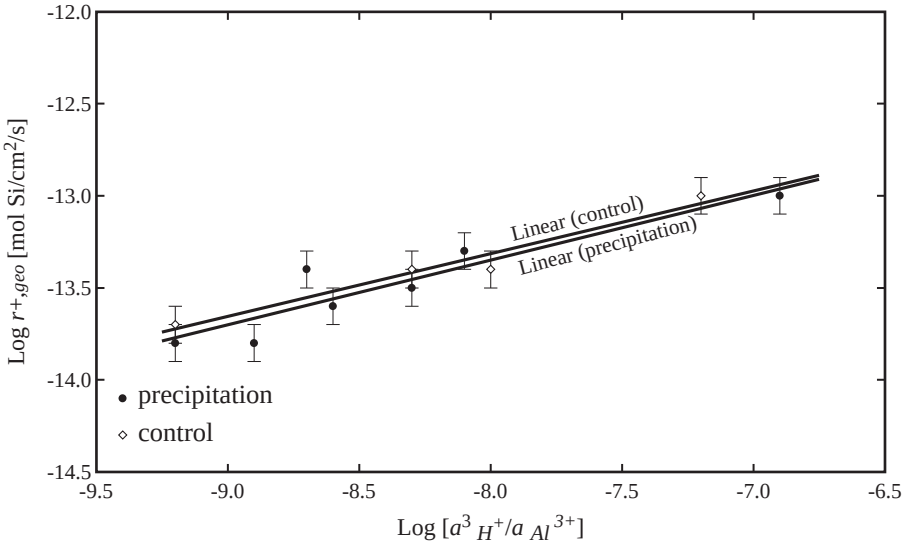

Fig. 6. Variation of measured basaltic glass dissolution rates, based on Si release, as a function of log $(a_{H^+}^3/a_{Al^{3+}})$ for all experiments at 25 °C for which stoichiometric Si/Al release was observed (see Table 3a). The uncertainty on the rates is ±0.15 log units as illustrated by the error bars. The linear equation for the control data is $\log r_{+,geo} = 0.34 \log (a_{H^+}^3/a_{Al^{3+}}) - 10.59$, $R^2 = 0.96$, and the corresponding equation for the precipitation data is $\log r_{+,geo} = 0.35 \log (a_{H^+}^3/a_{Al^{3+}}) - 10.53$, $R^2 = 0.86$.

Table 5
Steady-state Si dissolution rates (log r_+) in mol/cm^2/s at 25 °C reported in the literature.

pH	log $r_{+,BET}$ [a]	log $r_{+,BET}$ [b]	log $r_{+,geo}$ [b]	pH [c]	log $r_{+,BET}$ [c]	log $r_{+,geo}$ [c]
7.0	−15.1	−14.9	−12.9	7.0	−15.1	−13.7
8.0	−14.8	−14.6	−12.6	7.9	−14.7	−13.3
8.5		−14.4	−12.4	8.6	−14.8	−13.4
10.0	−14.1	−13.9	−11.9	10.1	−14.3	−13.0

[a] From Oelkers and Gislason (2001).
[b] From Gislason and Oelkers (2003), a roughness factor of 92 is used to calculate $r_{+,geo}$ from $r_{+,BET}$.
[c] This study, average of values given in Table 3b. The basaltic glass roughness factor is 23.

the whole original surface. These observations are consistent with those of Cubillas et al. (2005) who concluded that substantial inhibition of mineral dissolution by a precipitating phase is only efficient when there is a close crystal structural match between the dissolving and precipitating phase. As basaltic glass has a far different structure than precipitating calcium carbonate phases there is little thermodynamic drive to precipitate pervasive coatings on the surface of the primary mineral.

Another interesting observation is that the location of secondary precipitates apparently depends on the source of the material used to create the secondary phase and/or the degree of supersaturation of the fluid phase. In experiments where Ca was sourced from the dissolving basaltic glass (e.g. experimental series 8) precipitating calcite formed on the surfaces of the dissolving glass (see Fig. 1d). In contrast, in experiments where calcite was externally sourced and the fluids had higher degrees of supersaturation, calcite formed as distinct crystals separated from the glass surface (see Fig. 1f). This suggests that the location of secondary precipitates in natural systems may hold information on the source of its constituent elements. This conclusion is consistent with that of Putnis (2009) who reported that mineral replacement reactions are favored when the primary phase contributes elements to the secondary phase.

The observation that the presence of calcium carbonate precipitates does not inhibit basaltic glass dissolution favors the use of basalt for CO_2 carbonatization. This carbonatization process involves the release of Ca, Mg, and Fe from basalt by dissolution. These divalent metals can then react with dissolved CO_2 in the fluid phase to form stable carbonate minerals. It has been argued that basalt dissolution is the slowest and thus rate-limiting step of this coupled process. The observation that calcium carbonate precipitates do not create passivating layers on the basaltic glass surface suggests that Ca, Mg, and Fe release will not be slowed by carbonate precipitation at least at the initial part of the injection. The calcite growth may become more extensive with time, as was observed on basaltic grains by Schaef et al. (2009), though dissolution rates were not reported in this previous study.

6. Conclusions

The presence of calcite precipitate either on or adjacent to basaltic glass does not affect the dissolution rates of the primary phase. In fact the dissolution rates of basalt glass appear to be constant for at least 144 days despite the precipitation of substantial calcite during the experiments. This result favors long-term mineral sequestration in glassy volcanic rocks. In addition, the measured steady-state BET rates match those previously reported in the literature; supporting their application to describing chemical mass transfer rates in natural systems.

The observations presented above also confirm previous conclusions that non-pervasive secondary precipitates do not significantly influence the dissolution rates of the primary phase. This contrasts to the behavior of those systems where pervasive passivating surface precipitates form. In these latter systems rates can be slowed dramatically (c.f., Cubillas et al., 2005). It appears, therefore that the key to determining if a secondary precipitate will affect the dissolution rates of a primary phase is the understanding of the morphology and location of the secondary precipitates which is likely a function of 1) the relative structures of the primary and secondary phases, 2) the degree of supersaturation of the reactive fluid with respect to the secondary phase, and 3) the location of the source of the elements comprising the secondary phase. Further experiments attempting to illuminate the affect of calcium carbonate precipitation on the dissolution rates of other solids will be reported in future publications.

Acknowledgments

This study is part of the CarbFix project (www.carbfix.com) in Iceland, and we would like to thank all colleagues and co-workers within this project, in particular Helgi A. Alfredsson, Therese K. Flaathen, Snorri Guðbrandsson, Alex P. Gysi, Mahnaz Rezvani Khalilabad, Jürg

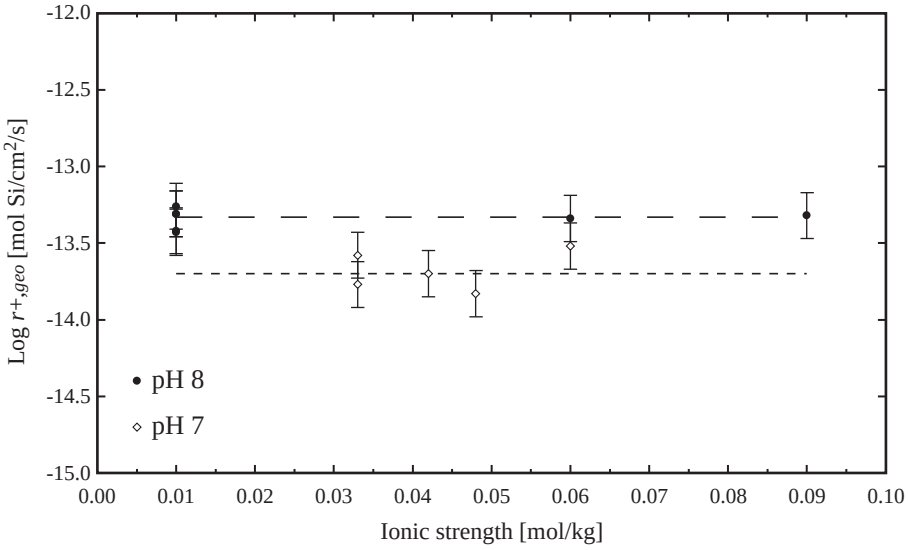

Fig. 7. Variation of measured steady-state basaltic glass Si dissolution rates as a function of ionic strength at 25 °C and pH 7 and 8. Rates were obtained from both 'precipitation' and 'control' experiments and the error bars on this plot correspond to ±0.15 log units uncertainty on the rates. The dashed lines are added to aid the reader.

Matter, Andri Stefánsson and Martin Stute. We thank the editor, Uwe Brand, and two anonymous reviewers, whose comments greatly improved this manuscript. We would also like to thank several colleagues for their help, in particular Eydís Salome Eiríksdóttir and Ingvi Gunnarsson at the University of Iceland, and Hólmfríður Sigurðardóttir at Reykjavík Energy. We are grateful for the SEM technical support provided by Jón Matthíasson at the Innovation Center Iceland and Sophie Gouy at LMTG-CNRS in Toulouse, France. We are also indebted to Caroline Piper Hem at the University of Copenhagen and Vasileios Mavromatis at LMTG-CNRS in Toulouse for assistance with XRD interpretations. We would also like to thank Erik Sturkell for graphical assistance and continued support. Reykjavík Energy, Nordurál and Hitaveita Suðurnesja and the European Community through the MIN-GRO Research and Training Network (MRTN-CT-2006-035488) are gratefully acknowledged for their financial support.

References

Alfredsson, H.A., Hadrarson, B.S., Franzson, H., Gislason, S.R., 2008. CO_2 sequestration in basaltic rock at the Hellisheidi site in SW Iceland: stratigraphy and chemical composition of the rocks at the injection site. Min. Mag. 72, 1–5.

Andreani, M., Liquot, L., Gouze, P., Godard, M., Hoise, E., Gibert, B., 2009. Experimental study of carbon sequestration reactions controlled by the percolation of CO_2-rich brine through peridotites. Eviron. Sci. Technol. 43, 1226–1231.

Béarat, H., McKelvey, M.J., Chizmeshya, A.V., Gormley, D., Nunez, R., Carpenter, R.W., Squires, K., Wolf, G.H., 2006. Carbon sequestration via aqueous olivine mineral carbonation: role of passivating layer formation. Eviron. Sci. Technol. 40, 4802–4808.

Benezeth, P., Palmer, D.A., Anovitz, L.M., Horita, J., 2007. Dawsonite synthesis and reevaluation of its thermodynamic properties from solubility measurements: implications for mineral trapping of CO_2. Geochim. Cosmochim. Acta 71, 4438–4455.

Cailleteau, C., Angeli, F., Devreux, F., Gin, S., Jestin, J., Jollivet, P., Spalla, O., 2008. Insight into silicate-glass corrosion mechanisms. Nat. Mat. 7, 978–983.

Chaïrat, C., Schott, J., Oelkers, E.H., Lartigue, J.-E., Harouiya, N., 2007. Kinetics and mechanism of natural fluorapatite dissolution at 25 °C and pH from 3 to 12. Geochim. Cosmochim. Acta 71, 5901–5912.

Cubillas, P., Köhler, S., Prieto, M., Causserand, C., Oelkers, E.H., 2005. How do mineral coatings affect dissolution rates? An experimental study of coupled $CaCO_3$ dissolution–$CdCO_3$ precipitation. Geochim. Cosmochim. Acta 69, 5459–5476.

Daval, D., Martinez, I., Corvisier, J., Findling, N., Goffe, B., Guyot, F., 2009a. Carbonation of Ca-bearing silicates, the case of wollastonite: experimental investigations and kinetic modeling. Chem. Geol. 265, 63–78.

Daval, D., Martinez, I., Guigner, J.-M., Hellmann, R., Corvisier, J., Findling, N., Dominici, C., Goffe, B., Guyot, F., 2009b. Mechanism of wollastonite carbonation deduced from micro- to nanometer length scale observations. Am. Mineral. 94, 1707–1726.

Gautelier, M., Oelkers, E.H., Schott, J., 2007. An experimental study of dolomite dissolution rates at 80 °C as a function of chemical affinity and solution composition. Chem. Geol. 242, 509–517.

Gautier, J.-M., Oelkers, E.H., Schott, J., 2001. Are quartz dissolution rates proportional to BET surface areas? Geochim. Cosmochim. Acta 65, 1059–1070.

Giammar, D.E., Bruant Jr., R.G., Peters, C.A., 2005. Forsterite dissolution and magnesite precipitation at conditions relevant for deep saline aquifer storage and sequestration of carbon dioxide. Chem. Geol. 217, 257–276.

Gislason, S.R., Oelkers, E.H., 2003. Mechanism, rates and consequences of basaltic glass dissolution: II. An experimental study of the dissolution rates of basaltic glass as a function of pH and temperature. Geochim. Cosmochim. Acta 67, 3817–3832.

Gislason, S.R., Wolff-Boenisch, D., Stefansson, A., Oelkers, E.H., Gunnlaugsson, E., Sigurdardóttir, H., Sigfússon, G., Brocker, W.S., Matter, J., Stute, M., Axelsson, G., Fridriksson, T., 2010. Mineral sequestration of carbon dioxide in basalt: a pre-injection overview of the CarbFix project. Int. J. Greenhouse Gas Control 4, 537–545.

Gobac, Ž.Ž., Posilović, H., Bermanec, V., 2009. Identification og biogenetic calcite and aragonite using SEM. Geol. Croat. 62 (3), 201–206.

Goldberg, D.S., Takahashi, T., Slagle, A.L., 2008. Carbon dioxide sequestration in deep-sea basalt. Proc. Natl Acad. Sci. 105, 9920–9925.

Gysi, A., Stefansson, A., submitted for publication. CO_2–water–basalt interaction II. Numerical simulation of low temperature CO_2 sequestration into basalts. Reaction modeling, *submitted to Geochim. Cosmochim. Acta*.

Helgeson, H.C., Murphy, W.M., Aagaard, P., 1984. Thermodynamic and kinetic constraints on reaction rates among minerals and aqueous solutions. II. Rate constants, effective surface area, and the hydrolysis of feldspars. Geochim. Cosmochim. Acta 48, 2405–2432.

Hodson, M.E., 2003. The influence of Fe-rich coatings on the dissolution of anorthite at pH 2.6. Geochim. Cosmochim. Acta 67, 3355–3363.

Lasaga, A.C., 1984. Chemical kinetics of water–rock interactions. J. Geophys. Res. 89 (B6), 4009–4025.

Lasaga, A.C., 1998. Kinetic Theory in the Earth Sciences. Princeton Series in GeochemistryPrinceton University Press, Princeton, New Jersey. 811 pp.

Lee, M.R., Brown, D.J., Hodson, M.E., MacKenzie, M., Smith, C.L., 2008. Weathering microenvironments on feldspar surfaces: implications for understanding fluid-mineral reactions in soils. Min. Mag. 71, 1319–1328.

Marini, L., 2007. Geological Sequestration of Carbon Dioxide. Thermodynamics, Kinetics and Reaction Path modeling. Elsevier, Amsterdam. 470 pp.

Matter, J.M., Takahashi, T., Goldberg, D., 2007. Experimental evaluation of in situ CO_2–water–rock reactions during CO_2 injection in basaltic rocks: implications for geological CO_2 sequestration. Geochem. Geophys. Geosyst. 8, Q02001. doi:10.1029/2006GC001427.

McGrail, B.P., Schaef, H.T., Ho, A.M., Chien, Yi-Ju, Dooley, J.J., Davidson, C.L., 2006. Potential for carbon dioxide sequestration in flood basalts. J. Geophys. Res. 111. doi:10.1029/2005JB004169 B12201.

Murakami, T., Kogure, T., Kadohara, H., Ohnuki, T., 1998. Formation of secondary minerals and its effect on anorthite dissolution. Am. Mineral. 83, 1209–1219.

Nugent, M.A., Brantley, S.L., Pantano, C.G., Maurice, P.A., 1998. The influence of natural mineral coatings on feldspar weathering. Nature 395, 588–591.

Oelkers, E.H., 2001. General kinetic description of multioxide silicate mineral and glass dissolution. Geochim. Cosmochim. Acta 65, 3703–3719.

Oelkers, E.H., Cole, D.R., 2008. Carbon dioxide sequestration: a solution to a global problem. Elements 4, 305–310.

Oelkers, E.H., Gislason, S.R., 2001. The mechansim, rates and consequences of basaltic glass dissolution: I. An experimental study of the dissolution rates of basaltic glass as a function of aqueous Al, Si and oxalic acid concentration at 25 °C and pH = 3 and 11. Geochim. Cosmochim. Acta 65, 3671–3681.

Oelkers, E.H., Schott, J., 2005. Geochemical aspects of CO_2 sequestration. Chem. Geol. 217, 183–186.

Oelkers, E.H., Gislason, S.R., Matter, J., 2008. Mineral carbonation of CO_2. Elements 4, 333–337.

Pačes, T., 1983. Rate constants of dissolution derived from the measurements of mass balance in hydrological catchments. Geochim. Cosmochim. Acta 47, 1855–1863.

Palache, C., Berman, H., Frondel, C., 1951. The system of mineralogy of James Dwight Dana and Edward Salisbury Dana, 7th Edition. Halides, Nitrates, Borates, Carbonates, Sulfates, Phosphates, Arsenates, Tungstates, Molibdates, etc., Vol. 2. John Wiley and Sons, New York. 1124 pp.

Park, A.-H.A., Fan, L.-S., 2004. CO_2 mineral sequestration: physically activated dissolution of serpentine and pH swing process. Chem. Eng. Sci. 59, 5241–5247.

Parkhurst, D.L., Appelo, C.A.J., 1999. User's Guide to PHREEQC (version 2) — A Computer Program for Speciation, Batch-reaction, One-dimensional Transport, and Inverse Geochemical Calculations. USGS-Report 99-4259.

Plummer, L.N., Busenberg, E., 1982. The solubilities of calcite, aragonite and vaterite in CO_2–H_2O solutions between 0 and 90 °C, and an evaluation of the aqueous model for the system $CaCO_3$–CO_2–H_2O. Geochim. Cosmochim. Acta 46, 1011–1040.

Pokrovsky, O.S., Schott, J., Castillo, A., 2005. Kinetics of brucite dissolution at 25 C in the presence of organic and inorganic ligands and divalent metals. Geochim. Cosmochim. Acta 69, 905–918.

Putnis, A., 2009. Mineral replacement reactions. Rev. Mineral. Geochem. 70, 87–124.

Schaef, H.T., McGrail, B.P., 2009. Dissolution of Columbia River Basalt under mildly acidic conditions as a function of temperature: experimental results relevant to the geological sequestration of carbon dioxide. Appl. Geochem. 24, 980–987.

Schaef, H.T., McGrail, B.P., Owen, A.T., 2009. Basalt–CO_2–H_2O interactions and variability in carbonate mineralization rates. Energy Procedia 1, 4899–4906.

Schaef, H.T., McGrail, B.P., Owen, A.T., 2010. Carbonate mineralization of volcanic province basalts. Int. J. Greenhouse Gas Control 4, 249–261.

Schott, J., Pokrovsky, O.S., Oelkers, E.H., 2009. The link between mineral dissolution/precipitation kinetics and solution chemistry. Rev. Mineral. Geochem. 70, 207–258.

Siegel, D.I., Pfannkuch, H.O., 1984. Silicate dissolution influence on Filson Creek chemistry, northeastern Minnesota. Geol. Soc. Am. Bull. 95, 1446–1453.

Stockmann, G.J., Wolff-Boenisch, D., Gíslason, S.R., Oelkers, E.H., 2008. Dissolution of diopside and basaltic glass: the effect of carbonate coating. Min. Mag. 72, 139–143.

Velbel, M.A., 1993. Formation of protectiye surface layers during silicate-mineral weathering under well-leached oxidizing conditions. Am. Mineral. 78, 405–414.

Verney-Carron, A., Gin, S., Frugier, P., Libourel, G., 2010. Long-term modelling of alteration-transport coupling: application to a fractured Roman glass. Geochim. Cosmochim. Acta 74, 2291–2315.

White, A.F., Brantley, S.L., 2003. The effect of time on the weathering of silicate minerals: why do weathering rates differ in the laboratory and field? Chem. Geol. 202, 479–506.

Wolff-Boenisch, D., Gislason, S.R., Oelkers, E.H., Putnis, C.V., 2004a. The dissolution rates of natural glasses as a function of their composition at pH 4 and 10.6, and temperatures from 25 to 74 °C. Geochim. Cosmochim. Acta 68, 4843–4858.

Wolff-Boenisch, D., Gislason, S.R., Oelkers, E.H., 2004b. The effect of fluoride on the dissolution rates of natural glasses at pH 4 and 25 °C. Geochim. Cosmochim. Acta 68, 4571–4582.

Wolff-Boenisch, D., Gislason, S.R., Oelkers, E.H., 2006. The effect of crystallinity on dissolution rates and CO_2 consumption capacity of silicates. Geochim. Cosmochim. Acta 70, 858–870.

Zhu, C., 2005. In situ feldspar dissolution rates in an aquifer. Geochim. Cosmochim. Acta 69, 1435–1453.

Zhu, C., Veblen, D.R., Blum, A.E., Chipera, S.L., 2006. Naturally weathered feldspar surfaces in the Navajo sandstone aquifer, Black Mesa Arizona: electron microscopic characterization. Geochim. Cosmochim. Acta 70, 4600–4616.

Zhu, C., Lu, P., Zheng, Z., Ganor, J., 2010. Coupled alkali feldspar dissolution and secondary mineral precipitation in batch systems: 4. Numerical modeling of kinetic reaction paths. Geochim. Cosmochim. Acta 74, 3963–3983.

Chapter 3

Do carbonate precipitates affect dissolution kinetics? 2: Diopside

Gabrielle J. Stockmann, Domenik Wolff-Boenisch, Sigurdur R. Gislason and Eric H. Oelkers

(submitted to Chemical Geology)

ABSTRACT

Diopside dissolution rates were measured in mixed-flow reactors at neutral and basic pH at 25 ºC and 70 ºC. Experiments were performed in aqueous solutions 1) supersaturated with respect to calcite for up to 63 days, and 2) strongly undersaturated with respect to calcite and other secondary phases for up to 164 days. Inlet solutions were comprised of $CaCl_2 \pm NaHCO_3$ with ionic strengths ≥ 0.02 mol/kg. In the experiments performed at 25 ºC, calcite nucleated and grew extensively on the diopside surfaces and as > 1000 μm discrete crystals in experiments performed in CO_3-bearing inlet solutions but no precipitates were formed on or adjacent to the diopside in experiments performed in CO_3-free inlet solutions. Measured diopside dissolution rates in calcite precipitating experiments based on Si are both 1) time independent, and 2) equal to that of corresponding control experiments performed in $NaHCO_3$-free inlet solutions. These observations indicate that diopside dissolution rates are unaffected by the simultaneous precipitation of calcite. Calcite likely forms a porous coating on diopside, which allows ions from the dissolving diopside to diffuse readily to the bulk fluid. It seems therefore likely that carbonate precipitation will not slow pyroxene dissolution during carbon storage efforts.

Do carbonate precipitates affect dissolution kinetics? 2: Diopside

(*submitted to Chemical Geology*)

Gabrielle J. Stockmann [a,b,*], Domenik Wolff-Boenisch [c], Sigurdur R. Gislason [c], Eric H. Oelkers [b,c]

[a] *Nordic Volcanological Center, Institute of Earth Sciences, University of Iceland, Sturlugata 7, 101 Reykjavík, Iceland*

[b] *GET-Université de Toulouse-CNRS-IRD-OMP, 14 Avenue Edouard Belin, 31400 Toulouse, France*

[c] *Institute of Earth Sciences, University of Iceland, Sturlugata 7, 101 Reykjavík, Iceland*

ABSTRACT

Diopside dissolution rates were measured in mixed-flow reactors at neutral and basic pH at 25 ºC and 70 ºC. Experiments were performed in aqueous solutions 1) supersaturated with respect to calcite for up to 63 days, and 2) strongly undersaturated with respect to calcite and other secondary phases for up to 164 days. Inlet solutions were comprised of $CaCl_2 \pm NaHCO_3$ with ionic strengths ≥ 0.03 mol/kg. In the experiments performed at 25 ºC, calcite nucleated and grew extensively on the diopside surfaces and as > 1000 μm discrete crystals in experiments performed in CO_3-bearing inlet solutions but no precipitates were formed on or adjacent to the diopside in experiments performed in CO_3-free inlet solutions. Measured diopside dissolution rates in calcite precipitating experiments based on Si are both 1) time independent, and 2) equal to that of corresponding control experiments performed in $NaHCO_3$-free inlet solutions. These observations indicate that diopside dissolution rates are unaffected by the simultaneous precipitation of calcite. Calcite likely forms a porous coating on diopside, which allows ions from the dissolving diopside to be transported readily to the bulk fluid. It seems therefore likely that carbonate precipitation will not slow pyroxene dissolution during carbon storage efforts.

Keywords: Diopside, calcite coating, dissolution kinetics, mixed-flow reactors, carbonatization, CO_2 sequestration

---

1. INTRODUCTION

A large number of recent studies have been aimed at providing the scientific basis for the *in-situ* carbonatization of CO_2 in an effort to attenuate the consequences of anthropogenic carbon emissions (e.g. Oelkers and Schott, 1995; McGrail et al., 2006; Wolff-Boenisch et al., 2006; 2011; Marini, 2007; Matter et al., 2007; Kelemen and Matter, 2008; Goldberg et al., 2008; Oelkers and Cole, 2008; Oelkers et al., 2008; Wakahama et al., 2009; Schaef and McGrail, 2009; Schaef et al., 2009; 2010; 2011; Flaathen et al., 2010; Gislason et al., 2010; Matter et al., 2011; Rudge et al., 2011; Gysi and Stefansson, 2011; 2012, Aradottir et al., 2012). *In-situ* CO_2 carbonatization is promoted by the dissolution of silicate rocks that release divalent metal cations such as Ca^{2+}, Mg^{2+}, and Fe^{2+} to the fluid phase. These ions can react with dissolved CO_2 and precipitate as carbonate minerals. The rate-limiting step for this reaction is commonly thought to be the release of divalent cations (c.f., Oelkers et al., 2008). As such, any process that can potentially slow the dissolution rates of divalent metal bearing silicate minerals, such as secondary carbonate precipitation, could be detrimental to carbon storage efforts.

The dissolution rates of minerals and glasses are commonly believed to be proportional to their interfacial surface area (e.g. Pačes, 1983; Helgeson et al., 1984; Siegel and Pfannkuch, 1984; Lasaga 1984; Schott and Oelkers, 1995; Oelkers, 2001; Schott et al., 2009). It seems likely therefore, that the precipitation of secondary phases, such as calcite during subsurface carbon storage efforts, could potentially decrease the dissolution rates of those phases on which they precipitate. Such precipitates could, therefore, be detrimental to mineral carbonatization efforts. This study is aimed at determining the extent to which diopside dissolution rates are affected by calcite precipitation on its surfaces. Towards this goal, diopside has been dissolved over time periods of up to 5 months in aqueous fluids that are either saturated or undersaturated with respect to calcite. The goal of this paper is to report

the results of this experimental study and to use these results to assess the degree to which carbonate precipitation on silicate minerals might affect the efficiency of subsurface carbon storage efforts.

Diopside dissolution rates have received considerable attention in the literature (Schott et al., 1981; Eggleston et al., 1989; Knauss et al., 1993; Chen and Brantley, 1998; Golubev et al., 2005; Golubev and Pokrovsky, 2006; Dixit and Carroll, 2007; Daval et al., 2010). For example, Knauss et al. (1993) reported diopside dissolution rates as a function of pH at 25, 50, and 70 ºC. Measured diopside dissolution rates decrease with increasing pH to at least pH ~7. At higher pH, rates are either pH independent or decrease weakly with increasing pH (Knauss et al., 1993; Golubev et al., 2005). Chen and Brantley (1998) reported diopside dissolution rates as a function of pH at 25 and 90 ºC; these rates also decrease with increasing pH at pH <7 but they are approximately one order of magnitude lower than corresponding rates reported in other studies. Chen and Brantley (1998) suggested that this difference was most likely due to their rates being normalized to the BET surface area of the post-experiment powders, whereas the majority of other studies normalized rates to the BET surface area of the initial solids. Knauss et al. (1993) reported that diopside dissolution rates are independent of aqueous CO_2 concentration. Daval et al. (2010) found that diopside dissolution rates varied significantly as a function of solution saturation state (ΔG_r) at acidic conditions and 90 ºC.

A number of past studies have focused on the effect of mineral coatings on the dissolution rates of divalent metal bearing silicates, in part due to the significance of this process to the carbonatization of ultramafic and mafic rocks. These studies include efforts on basaltic glasses (Stockmann et al., 2011; Gysi and Stefansson, 2011; 2012), crystalline basalts (McGrail et al., 2006; Schaef et al., 2009; 2010; 2011), wollastonite (Daval et al., 2009a,b), olivine (Giammar et al., 2005; Béarat et al., 2006; Andreani et al., 2009; Daval et al., 2011), serpentine (Park and Fan, 2004), and anorthite (Hodson, 2003). These past studies provide ambiguous results; in some cases dissolution rates are unaffected by coatings, but in others significant effects are observed. The presence of carbonate precipitates on basaltic glass (Stockmann et al., 2011), olivine (Giammar et al., 2005), and wollastonite at acidic pH conditions (Daval et al. 2009a) were reported to have no effect on the dissolution rates of the primary minerals as these coatings formed discontinuous and porous layers. Similarly,

Hodson (2003) observed that the presence of discontinuous iron-rich coatings had little effect on anorthite dissolution rates. In contrast, Daval et al. (2011) reported that olivine dissolution rates decreased by two orders of magnitude by the presence of an amorphous silicate layer. Daval et al. (2009a, b) reported that wollastonite dissolution rates were significantly decreased at neutral and basic conditions due to the presence of a surface coating consisting of amorphous silica and calcite. Park and Fan (2004) suggested that the presence of silica-rich layers inhibited serpentine dissolution rates. Both Béarat et al. (2006) and Andreani et al. (2009) reported that silica-rich layers on dissolving olivine surfaces slowed carbonate formation, and inhibited olivine dissolution. It suggests that crystallographic properties might play an important role in this process, especially in the early stages of dissolution-precipitation, in whether a secondary layer has the potential to armor the primary surface. For example, Cubillas et al. (2005) showed that $CaCO_3$ dissolution rates were strongly affected by otavite ($CdCO_3$) precipitation on its surface because there was a close structural match between the dissolving and precipitating phase. Putnis (2009) noted that the replacement of one mineral by another is closely related to the mineral structure and the relative volumes of the phases involved, whereas Velbel (1993) emphasized that the molar volume ratio of product to reactant has to be > 1 to provide the volume needed to completely passivate the reactant surface. This study aims to provide further insight into this coupled process through a series of diopside dissolution experiments performed in the presence and absence of co-precipitating calcite.

2. MATERIALS AND METHODS

The standard state adopted in this study is that of unit activity of pure minerals and H_2O at any temperature and pressure. For aqueous species other than H_2O, the standard state is unit activity of species in a hypothetical 1 mol/kg solution referenced to infinite dilution at any temperature and pressure. All thermodynamic calculations reported in this study were performed using the PHREEQC 2.17 computer code (Parkhurst and Appello, 1999) together with its llnl.dat database.

The diopside crystals used in this study were obtained from the Transbaikal region of Russia and are identical to those studied by Golubev et al. (2005) and Golubev and Pokrovsky (2006). Golubev et al. (2005) determined the chemical

composition of the diopside to be: $Ca_{0.99}Mg_{0.98}Fe_{0.02}Cr_{0.01}Si_2O_6$ with minor amounts of Al_2O_3 (0.15 wt%), MnO (0.03 wt%), Na_2O (0.4 wt%), and TiO_2 (0.03 wt%).

Prior to the experiments, the diopside crystals were reacted in concentrated HCl for several hours to remove impurities from the crystal surfaces. Following this acid cleaning, the diopside crystals were rinsed with MilliQ™ water and dried at 60 ºC before being crushed with an agate mortar and pestle. After crushing, the material was sieved and the 45-125 μm size fraction obtained. Fine particles were removed from this powder by ultrasonically cleaning in acetone. Several ultrasonic cleaning cycles were performed and the ultra-fine suspension was discarded at the end of each cycle. The cleaning cycles were repeated until the discarded fluid phase appeared clear. The resulting diopside powder was dried overnight at 60 ºC. A representative Scanning Electron Microscope (SEM) image of this diopside powder is displayed in Fig. 1a, and this image shows the resulting diopside powder to be free of fine particles. All SEM images in this study were performed using a LEO Supra 25, JEOL 6360 LV or a HITACHI S3400N Scanning Electron Microscope after particles were coated with a fine gold layer. Further analysis of the solids in this study was performed using Energy Dispersive X-ray Spectroscopy (EDX/EDS) and X-ray diffraction (XRD) using an INEL CPS 120.

The specific surface area of the cleaned dried diopside powder is 1013 ± 40 cm^2/g as determined by 3-point krypton adsorption using the BET method. Golubev et al. (2005) reported a BET specific surface area of 1250 ± 20 cm^2/g for their cleaned 50-100 μm size fraction of this diopside; Golubev and Pokrovsky (2006) reported a BET specific surface area of 1045 ± 50 cm^2/g for their cleaned 100-200 μm size fraction of this diopside. The average density of diopside, as reported by Klein (2002), is 3.27 g/cm^3. Taking account of this density and equations reported by Wolff-Boenisch et al. (2004a), the geometric surface area of the diopside used in this study, A_{geo}, is calculated to be 234 cm^2/g. Dividing the BET surface area by this geometric surface area yields a roughness factor of 4.3.

The mixed-flow reactor system used in this study is illustrated in Fig. 2. This reactor system is similar to that used in past dissolution rate measurement studies (e.g., Wolff-Boenisch et al., 2004a,b; Cubillas et al., 2005; Pokrovsky et al., 2005; Chairat et al., 2007; Gautelier et al., 2007). The physical and chemical conditions of the experiments performed in this study were identical to those of basaltic glass

experiments described in Stockmann et al. (2011). All reactors, connectors, and tubing were thoroughly cleaned in a 0.1 M HCl bath for ~ 24 hours and rinsed with MilliQ™ water prior to each experiment. All outlet fluid sample bottles went through the same cleaning procedure prior to sampling to prevent contamination. Diopside dissolution experiments were initiated by placing between five and ten grams of cleaned diopside powder and a quantity of the selected inlet solution into the 300 mL polyethylene mixed-flow reactors. These reactors were sealed and placed into a temperature controlled water bath. Temperature was kept constant during the experiment at either 25 or 70 ºC. Teflon®coated floating stir-bars from Nalgene® were placed on the bottom of the reactors and rotated at ~300 rpm using a multi-position magnetic stirrer located underneath the water bath.

Inlet fluids were comprised of Millipore™ water and Merck/Sigma-Aldrich analytical grade $NaHCO_3$, $CaCl_2$, NH_4Cl, NaOH, and/or HCl with ionic strengths ranging from 0.01 to 0.09 mol/kg; the composition of all inlet fluids is listed in Table 1. Compositions of the inlet fluids were based on calculations made using PHREEQC to yield the desired pH and ionic strength. The inlet fluids were stored in 8 or 12 L compressible plastic bags. Inlet fluids containing $CaCl_2$ were continuously purged with N_2 to prevent atmospheric CO_2 from dissolving into this solution and to keep the pH stable. The inlet fluids were injected into the reactors at a constant rate using multi-cartridge Masterflex™ peristaltic pumps. In some experiments two inlet fluids (one Ca-rich and one carbonate-rich) were injected simultaneously to create a reactive fluid supersaturated with respect to calcite in the reactor.

Each experiment reported in this study was performed at a constant temperature, inlet fluid flow rate, and inlet fluid composition. All experiments were run until and beyond a steady-state outlet fluid composition was obtained. Steady state is defined as the outlet fluid concentration remaining constant, within analytical uncertainty, for at least 10 residence times. The residence time is defined as the reactor volume divided by the fluid flow rate. In selected experiments, the inlet fluid composition was changed after a steady-state concentration profile was attained. Two different types of experiments were performed: ’precipitation‘ (P) and ’control‘ (C) experiments. ’Precipitation‘ experiments were designed to measure diopside dissolution rates during carbonate precipitation. To achieve calcite saturation, carbonate ± calcium were provided to the system by the inlet fluids. ’Control‘

197 experiments were designed to measure diopside dissolution rates at the same physical
198 and chemical conditions as the corresponding 'precipitation' experiment but in the
199 absence of aqueous carbonate.
200 Outlet fluids were regularly sampled during all experiments. Three residence
201 times or more separated each sampling. The outlet solutions were filtered through a
202 0.2 μm cellulose acetate membrane filter into 100 ml polyethylene sample bottles and
203 acidified with concentrated supra-pure HNO_3 prior to analysis. The major element
204 concentrations of inlet and outlet fluids were determined using a Spectro Ciros Vision
205 Inductively Coupled Plasma Optical Emission Spectrometer (ICP-OES). Analytical
206 uncertainties on ICP-OES analyses are estimated to be 3-5%.
207 At the end of the experiments, all diopside powders from the reactors were rinsed
208 several times with 10 mM $NaHCO_3$ and then with MilliQ™ water, before being dried
209 at 40 ºC. After drying, the sample weight was registered and the powders kept for
210 SEM, EDX, and XRD analysis.
211
212 **3. EXPERIMENTAL RESULTS**
213
214 In total, 9 steady-state dissolution experiments and 2 short-term pH pulses at the
215 end of selected dissolution experiments were performed as part of five experimental
216 series. The chemical composition, pH, and ionic strength of the inlet fluids are listed
217 in Table 1. Compositions of the outlet fluids at steady-state and calculated steady-
218 state diopside dissolution rates for all 9 experiments are listed in Table 2a-b together
219 with the results of chemical speciation calculations. The saturation state of calcite and
220 other selected minerals in the outlet fluids are provided in Table 3. The diopside
221 dissolution rates based on the release of the *i*th element ($r_{+,i,j}$) listed in these tables
222 were calculated from:
223

224 $$r_{+,i,j} = \frac{C_i \cdot fr}{\nu_i \cdot A_j \cdot m} \quad (1)$$

225
226 where C_i stands for the concentration of the *i*th element in the outlet fluid, *fr* refers to
227 the fluid flow rate, ν_i represents the stoichiometric factor of the *i*th element, A_j
228 designates the specific surface area of the diopside, and *m* denotes the mass of

diopside used in the experiment. The index *j* refers to rates calculated either using the measured BET surface area, A_{BET} or the geometric surface area, A_{geo}. These experimental results will be discussed in detail below.

3.1 Diopside dissolution in calcium ±carbonate-bearing aqueous fluids at 25 ºC (Experimental series 4 and 5)

The temporal evolution of diopside dissolution rates based on Si release at pH 7 and 25 ºC in 'precipitation' and 'control' experiments is illustrated in Fig. 3. In the 'precipitation' experiments, two inlet fluids were connected to the mixed-flow reactor; one injecting an aqueous 0.035 mol/kg $NaHCO_3$ solution and the other aqueous solution containing $CaCl_2$ and sufficient NaOH to attain the target pH, whereas the 'control' experiment was run by injecting a single $CaCl_2$-bearing, CO_3-free aqueous solution. The 'precipitation' experimental series 4a-b ran for 63 days in total. For the first 29 days the inlet fluid contained 0.1 mol/kg $CaCl_2$, and for the subsequent 34 days the inlet fluid contained 0.2 mol/kg $CaCl_2$. The 'control' experimental series 5a-c ran for 164 days. For the first 32 days the inlet fluid contained 0.2 mol/kg $CaCl_2$, and for the next 132 days the inlet fluid contained 0.3 mol/kg $CaCl_2$. Comparison of Figs. 3a and b show there is no significant difference in diopside dissolution rates observed between the 'control' and the 'precipitation' experiments, and the effect of changing $CaCl_2$ concentration in the inlet fluids had at most a small effect on measured rates. The steady-state diopside dissolution rate found in these experiments was log $r_{+,BET}$ = -15.1 ± 0.15 (mol/cm^2/s) and -15.2 ± 0.15 (mol/cm^2/s) for the 'control' and 'precipitation' experiments, respectively. Calcite precipitation occurred during the 'precipitation' experiments as seen in Fig. 1c-g. In general, calcite grew as discrete crystals on almost all diopside surfaces and some surfaces were completely overgrown with calcite (see Fig. 1c-e). Calcite was the only calcium carbonate phase present according to XRD analysis. This conclusion is confirmed by SEM photos showing that the precipitated phase consists of rhombohedral crystals consistent with the calcite structure (see Fig. 1e-g). SEM-EDX analysis showed some of the calcite contains minor amounts of Mg (<0.5 wt%). Mass balance calculations suggest that ~5 grams of calcite were precipitated inside the reactor during the 'precipitation' experiments. Precipitation occurred inside the

reactor as well as in the outlet fluid tubing, which eventually clogged ending the experiment.

Approximately half of powder recovered from experiments 5a-c was subsequently returned to the mixed-flow reactor and reacted with a 0.01 mol/kg $NaHCO_3$ inlet fluid of pH 8.4 and 25 ºC. After 9 days the inlet fluid was changed to a fluid having a pH of 3.81. The results of these experiments (5d and e) are illustrated in Fig. 4. Steady-state diopside dissolution rates, based on Si release are ~ 10^{-15} mol/cm^2/s, whereas corresponding steady-state rates based on Mg release, are $10^{-14.6}$ mol/cm^2/s in Exp. 5d, consistent with a preferential release of Mg over Si at these conditions. The addition of the acid leads to an increase in instantaneous diopside dissolution rates to ~ $10^{-14.2}$ mol/cm^2/s in Exp. 5e based on either Si, Mg and/or Fe release (see Table 2b), consistent with stoichiometric dissolution of diopside.

The variation of 25 ºC diopside steady-state dissolution rates based on Si release with reactive fluid ionic strength, calcium concentration, and diopside saturation state is illustrated in Fig 5. The distribution of data points in this figure suggests that there is no significant effect of these parameters on the steady-state diopside dissolution rates generated in this study at 25 ºC. Within experimental uncertainty, all measured rates at pH 6-8 are equal to ~$10^{-15.1}$ mol/cm^2/s.

3.2 Diopside dissolution in aqueous carbonate inlet fluids at 70 ºC (Experimental series 1 to 3)

Experimental series 1-3 were originally designed to provoke the precipitation of calcite by the dissolution of diopside in $NaHCO_3$ inlet solutions. Series 1 and 2 dissolved at 70 ºC diopside powder in 0.035 mol/kg $NaHCO_3$ and series 3 in 0.010 mol/kg $NaHCO_3$ inlet solutions. These experiments, however, failed to precipitate carbonate minerals, as evidenced by the saturation state of calcite in the outlet fluid samples, which are all undersaturated with respect to calcite and magnesite, and analysis of the solids recovered from the experiments by SEM and XRD. As such, these experiments are effectively pure diopside dissolution experiments.

The temporal evolution of instantaneous diopside dissolution rates based on Si, Ca, and Mg release during experimental series 1-3 is shown in Fig. 6. The results shown in this figure indicate that all exhibited an initial preferential Si release over

Mg and Ca. This preferential Si release attenuates and eventually disappears as the diopside dissolution rates based on Si decrease to match those based on Ca and Mg release after 45 days of dissolution in experiment 1a (see Fig. 6a). A similar behavior of preferential release of Si over Mg and Ca was reported by Knauss et al. (1993) for diopside dissolution at pH 8.9 and 70 ºC, though they did not observe a final stoichiometric dissolution phase of their experiments, as they stopped their experiment after 17 days. Oelkers et al. (2009) observed that Si was initially preferentially released from diopside at basic pH, but Mg and Ca were initially preferentially released at acidic pH. A preferential release of Si over Mg was reported in enstatite dissolution experiments performed by Oelkers and Schott (2001) at 70º C and neutral to basic pH; dissolution eventually became stoichiometric as Si release rates decreased to equal those of Mg. As further evidence of the lack of carbonate precipitation during these experiments, a HCl pulse of pH 6.4 was added to the inlet fluid at the end of experimental series 1. This pH pulse led to an increase in diopside dissolution rates based on Si, Ca, and Mg release. As rates based of Ca and Mg rates are similar to those based on Si release, and that the rates of carbonate dissolution are far faster than those of diopside at acid pH, it can be concluded that no dissolving carbonates phases were present.

3.3 Fluid saturation states during the experiments

Results of thermodynamic calculations, as listed in Table 3, suggest some of the outlet fluids at 25 ºC were supersaturated with respect to a number of carbonate minerals including calcite, aragonite, dolomite, and dawsonite. The only secondary precipitate observed by SEM, EDX and XRD analysis on post-experimental solids was calcite. In contrast, the outlet fluids of the 70 ºC experiments were in general undersaturated with respect to these carbonates, and none were observed on the post-experiment solids. Fe-hydroxides (i.e. hematite, goethite), Al-hydroxides (i.e. diaspore, gibbsite), Ti- and Mn oxides, and clay minerals (i.e. nontronite) were also calculated to be supersaturated in experiments performed at 25 and 70 ºC. The Fe, Al, Na, Mn and Ti release rates from the dissolving diopside in this study however, are low so therefore only minor quantities of non-carbonate secondary minerals are likely to have formed. Thermodynamic calculations indicate that the outlet fluids were all

undersaturated with respect to the dissolving diopside with a chemical affinity; $-\Delta G_r \geq$ ~40 kJ/mol in all experiments.

4. DISCUSSION

4.1 Comparison with previously published diopside dissolution rates

A comparison of steady-state diopside dissolution rates generated in this study and those reported in the literature can be made with the aid of Fig. 7. Rates in this study are consistent with those of Knauss et al. (1993) and Golubev et al. (2005) at 25 ºC, and those of Knauss et al. (1993) at 70 ºC. All rates tend to decrease mildly with increasing pH, though some of the data sets suggest that this decrease lessens at alkaline conditions at 25 ºC. The rates reported by Chen and Brantley (1998) are ~1 order of magnitude lower than corresponding rates reported in other sources. As mentioned above, these authors attributed this difference to differences in the normalizing surface area used in the different studies. Similarly, diopside dissolution rates obtained from experimental series 1-3 at 70 ºC are consistent with those of Knauss et al. (1993), as can be seen in Fig 7b.

4.2 Comparison of the effect of carbonate precipitation on diopside versus basaltic glass

Similar coupled dissolution-calcite precipitation experiments were carried out on basaltic glass (Stockmann et al., 2011) and diopside (this study) at 25 ºC. In the basaltic glass experiments, calcite mainly formed individual discrete clusters and did not precipitate on the glass surfaces, whereas calcite grew extensively on the diopside crystal surfaces in the present study. This difference suggests that diopside is a better nucleation template for calcite than basaltic glass. The difference may stem from the structure of these solids. Glass has a non-ordered silica framework whereas diopside has an ordered monoclinic structure. Diopside dissolution creates a rippled surface (see Fig. 1b), and it can be seen in Figs. 1d and f that these surfaces are favorable calcite precipitation sites. Putnis (2009) emphasized the importance of structural control on secondary mineral formation on the surfaces of primary minerals. In

addition, Putnis (2009) reported that mineral replacement reactions are favored when the primary phase contributes elements to the secondary phase. Both diopside and basaltic glass contain Ca^{2+} and Mg^{2+} that could potentially form carbonates. The lack of carbonate precipitates on the glass suggests that a local source of elements is not itself sufficient to provoke secondary mineral precipitation on the dissolving surface. Another difference between carbonate precipitation in the basaltic glass versus the diopside experiments is that aragonite was also observed to form in the former. This may be due to the presence of various metals released during glass dissolution.

4.3 Why does calcite precipitation have little effect on diopside dissolution rates?

A major result of this study is that the precipitation of calcite on and near the surfaces of diopside has little effect on its dissolution rates. These results appear to be consistent with the conclusions of Cubillas et al. (2005) who proposed that there will not be an inhibition of dissolution rates of the primary minerals unless there is an exact match of the crystallographic properties of the dissolving and precipitating phase leading to epitaxial growth. Other studies suggest that dissolution rates may be inhibited by the formation of amorphous Si layers, as observed on wollastonite and olivine surfaces (Park and Fan, 2004; Béarat et al., 2006; Andreani et al., 2009; Daval et al., 2009a, b; 2011). The match between the dissolving diopside and the precipitating carbonate in this study appears therefore to be sufficient to promote nucleation on these surfaces yet insufficient to form the impermeable layer required to arrest the dissolution of the primary phase despite the precipitation of over 5 g of calcite in Experimental series 4.

4.4 Implications for carbon storage

This study demonstrates that calcite precipitation does not significantly slow diopside dissolution rates. Stockmann et al. (2011) reported that carbonate precipitation does not affect basaltic glass dissolution rates. These two observations favor carbon storage via the carbonatization of basaltic and ultramafic rocks. This carbonatization process involves the release of Ca, Mg, and Fe from silicate minerals by dissolution. These divalent metals can then react with dissolved CO_2 in the fluid

phase to form stable carbonate minerals. It has been argued that silicate mineral dissolution is the slowest and thus rate-limiting step of this coupled process. The observation that calcium carbonate precipitates do not create compact armoring layers on diopside and basaltic glass surfaces suggests that Ca, Mg, and Fe release will not be slowed by carbonate precipitation, at least in the early stage, during mineral sequestration efforts in basalts, as currently being pursued in Iceland and in the Northwest of the United States (McGrail et al., 2006; Oelkers et al., 2008; Alfredsson et al., 2008; 2011; Schaef and McGrail, 2009; Schaef et al., 2009; 2010; 2011; Matter et al., 2009; 2011; Flaathen et al., 2010; Gislason et al., 2010; Gudbrandsson et al., 2011; Gysi and Stefansson, 2011; 2012a,b,c; Aradóttir et al., 2011; 2012a,b).

5. CONCLUSIONS

The results summarized above suggest that the presence of calcite precipitating on or near the surfaces of diopside does not affect its dissolution rates. Calcite is observed to precipitate both in the form of discrete prisms and as pervasive coatings covering the whole diopside surface. These observations are consistent with those of Cubillas et al. (2005) who concluded that substantial inhibition of mineral dissolution by a precipitating phase is only efficient when there is a close crystal structural match between the dissolving and precipitating phase. The observation that diopside dissolution rates are unaffected by calcite precipitation, favors carbon storage in crystalline basaltic and ultramafic rocks.

ACKNOWLEDGEMENTS

This study is part of the CarbFix project (www.carbfix.com) in Iceland, and we would like to thank all colleagues and co-workers within this project. We are grateful for the SEM technical support provided by Jón Matthíasson at the Innovation Center Iceland, Sophie Gouy at GET-CNRS in Toulouse, France, and David Cornell at Geovetarcentrum, University of Gothenburg in Sweden. We are also indebted to Caroline Piper Hem at the University of Copenhagen for assistance with XRD interpretations. Finally, we would sincerely like to thank Erik Sturkell for graphical assistance and continued support. The Environmental and Energy Fund of Reykjavík

Energy, the Research Fund of the University of Iceland, the Nordic Council of Ministers through NORDVULK, and the European Community through the MIN-GRO Research and Training Network (MRTN-CT-2006-035488) and the ERASMUS student mobility program are gratefully acknowledged for their financial support.

REFERENCES

Alfredsson, H.A., Hadrarson, B.S., Franzson, H., Gislason, S.R., 2008. CO_2 sequestration in basaltic rock at the Hellisheidi site in SW Iceland: stratigraphy and chemical composition of the rocks at the injection site. Min. Mag. 72, 1–5.

Alfredsson, H.A., Wolff-Boenisch, D., Stefansson, A., 2011. CO_2 sequestration in basaltic rocks in Iceland: Development of a piston-type downhole sampler for CO_2 rich fluids and tracers. Energy Procedia 4, 3510–3517.

Andreani, M., Liquot, L., Gouze, P., Godard, M., Hoise, E., Gibert, B., 2009. Experimental study of carbon sequestration reactions controlled by the percolation of CO_2-rich brine through peridotites. Eviron. Sci. Technol. 43, 1226–1231.

Aradóttir, E.S.P., Sigurdardóttir, H., Sigfússon, B., Gunnlaugsson, E., 2011. CarbFix - a CCS pilot project imitating and accelerating natural CO_2 sequestration. Greenhouse Gases: Science and Technology 1, 105–118.

Aradóttir, E.S.P., Sonnenthal, E.L., Jónsson, H.I., 2012a. Development and evaluation of a thermodynamic dataset for phases of interest in CO_2 sequestration in basaltic rocks. Chem. Geol. 304–305, 26–38.

Aradóttir, E.S.P., Sonnenthal, E.L., Björnsson, G., Jónsson, H., 2012b. Multidimensional reactive transport modeling of CO_2 mineral sequestration in basalts at the Hellisheidi geothermal field, Iceland. Int. J. Greenhouse Gas Control 9, 24-40.

Béarat, H., McKelvey, M.J., Chizmeshya, A.V., Gormley, D., Nunez, R., Carpenter, R.W., Squires, K., Wolf, G.H., 2006. Carbon sequestration via aqueous olivine mineral carbonation: role of passivating layer formation. Eviron. Sci. Technol. 40, 4802–4808.

Chaïrat, C., Schott, J., Oelkers, E.H., Lartigue, J.-E., Harouiya, N., 2007. Kinetics and mechanism of natural fluorapatite dissolution at 25°C and pH from 3 to 12. Geochim. Cosmochim. Acta 71, 5901-5912.

Chen, Y., Brantley, S.L., 1998. Diopside and anthophyllite dissolution at 25° and 90°C and acid pH. Chem. Geol. 147, 233-248.

Cubillas, P., Köhler, S., Prieto, M., Causserand, C., Oelkers, E.H., 2005. How do mineral coatings affect dissolution rates? An experimental study of coupled $CaCO_3$ dissolution – $CdCO_3$ precipitation. Geochim. Cosmochim. Acta 69, 5459–5476.

467 Daval, D., Martinez, I., Corvisier, J., Findling N., Goffe, B., Guyot, F., 2009a.
468 Carbonation of Ca-bearing silicates, the case of wollastonite: Experimental
469 investigations and kinetic modeling. Chem. Geol. 265, 63-78.

470 Daval, D., Martinez, I., Guigner, J.-M., Hellmann, R., Corvisier, J., Findling N.,
471 Dominici, C., Goffe, B., Guyot, F., 2009b. Mechanism of wollastonite
472 carbonation deduced from micro- to nanometer length scale observations. Amer.
473 Min. 94, 1707-1726.

474 Daval, D., Hellmann, R., Corvisier, J., Tisserand, D., Martinez, I., Guyot, F., 2010.
475 Dissolution kinetics of diopside as a function of solution saturation state:
476 Macroscopic measurements and implications for modeling of geological storage
477 of CO_2. Geochim. Cosmochim. Acta 74, 2615–2633.

478 Daval, D., Sissmann, O., Menguy, N., Saldi, G.D., Guyot, F., Martinez, I., Corvisier,
479 J., Garcia, B., Machouk, I., Knauss, K.G., Hellmann, R.. 2011. Influence of
480 amorphous silica layer formation on the dissolution rate of olivine at 90 °C and
481 elevated pCO_2. Chem. Geol. 284, 193–209.

482 Dixit, S., Caroll, S.A., 2007. Effect of solution saturation state and temperature on
483 diopside dissolution. Geochem. Trans. doi:10.1186/1467-4866-8-3.

484 Eggleston, C.M., Hochella Jr., M.F., George, P.A., 1989. Sample preparation and
485 aging effects on the dissolution rate and surface composition of diopside.
486 Geochim. Cosmochim. Acta 53, 797–804.

487 Flaathen, T.K., Gislason, S.R., Oelkers, E.H., 2010. The effect of aqueous sulphate on
488 basaltic glass dissolution rates. Chem. Geol. 277, 345–354.

489 Gautelier, M., Oelkers, E.H., Schott, J., 2007. An experimental study of dolomite
490 dissolution rates at 80 °C as a function of chemical affinity and solution
491 composition. Chem. Geol. 242, 509-517.

492 Giammar, D.E., Bruant Jr., R.G., Peters, C.A., 2005. Forsterite dissolution and
493 magnesite precipitation at conditions relevant for deep saline aquifer storage
494 and sequestration of carbon dioxide. Chem. Geol. 217, 257-276.

495 Gislason, S.R., Wolff-Boenisch, D., Stefansson, A., Oelkers, E.H., Gunnlaugsson, E.,
496 Sigurdardóttir, H., Sigfússon, G., Brocker, W.S., Matter, J., Stute, M., Axelsson,
497 G., Fridriksson, T., 2010. Mineral sequestration of carbon dioxide in basalt: A
498 pre-injection overview of the CarbFix project. Int. J. Greenhouse Gas Control 4,
499 537-545.

500 Goldberg, D.S., Takahashi, T., Slagle, A.L., 2008. Carbon dioxide sequestration in
501 deep-sea basalt. Proc. Natl. Acad. Sci. 105, 9920-9925.

502 Golubev, S.V., Pokrovsky, O.S., Schott, J., 2005. Experimental determination of the
503 effect of dissolved CO_2 on the dissolution kinetics of Mg and Ca silicates at 25
504 °C. Chem. Geol. 217, 227-238.

505 Golubev, S.V., Pokrovsky, O.S., 2006. Experimental study of the effect of organic
506 ligands on diopside dissolution kinetics. Chem. Geol. 235, 377-389.

507 Gudbrandsson, S., Wolff-Boenisch, D., Gislason, S.R., Oelkers, E.H., 2011. An
508 experimental study of crystalline basalt dissolution from $2 \leq pH \leq 11$ and
509 temperatures from 5 to 75 °C. Geochim. Cosmochim. Acta 75, 5496-5509.

Gysi, A.P., Stefansson, A., 2011. CO_2–water–basalt interaction. Numerical simulation of low temperature CO_2 sequestration into basalts. Geochim. Cosmochim. Acta 75, 4728–4751.

Gysi, A.P., Stefansson, A., 2012a. CO_2-water-basalt interaction. Low temperature experiments and implications for CO_2 sequestration into basalts. Geochim. Cosmochim. Acta. 81, 129-152.

Gysi, A.P., Stefansson, A., 2012b. Mineralogical aspects of CO_2 sequestration during hydrothermal basalt alteration - An experimental study at 75 to 250 °C and elevated pCO_2. Chem. Geol. 306-307, 146–159.

Gysi, A.P., Stefansson, A., 2012c. Experiments and geochemical modeling of CO_2 sequestration during hydrothermal basalt alteration. Chem. Geol. 306-307, 10–28.

Helgeson, H.C., Murphy, W.M., Aagaard, P., 1984. Thermodynamic and kinetic constraints on reaction rates among minerals and aqueous solutions. II. Rate constants, effective surface area, and the hydrolysis of feldspars. Geochim. Cosmochim. Acta 48, 2405-2432.

Hodson, M.E., 2003. The influence of Fe-rich coatings on the dissolution of anorthite at pH 2.6. Geochim. Cosmochim. Acta 67, 3355-3363.

Kelemen, P.B., Matter, J., 2008. In situ carbonation of peridotite for CO_2 storage. PNAS 105, 17295–17300.

Klein, C., 2002. Manual of Mineral Science, 22nd edition. John Wiley & sons, Inc., New York, 642 pp.

Knauss, K.G., Nguyen, S.N., Weed, H.C., 1993. Diopside dissolution kinetics as a function of pH, CO_2, temperature, and time. Geochim. Cosmochim. Acta 57, 285-294.

Lasaga, A.C., 1984. Chemical kinetics of water-rock interactions. J. Geophys. Res. 89(B6), 4009-4025.

Marini, L., 2007. Geological Sequestration of Carbon Dioxide. In: Thermodynamics, Kinetics and Reaction Path modeling. Elsevier, Amsterdam, 470 pp.

Matter, J.M., Takahashi, T., Goldberg, D., 2007. Experimental evaluation of in-situ CO_2-water-rock reactions during CO_2 injection in basaltic rocks: Implications for geological CO_2 sequestration. Geochem. Geophy. Geosys. 8, Q02001, doi: 10.1029/2006GC001427.

Matter, J.M., Broecker, W.S., Stute, M., Gíslason, S.R., Oelkers, E.H., Stefánsson, A., Wolff-Boenisch, D., Gunnlaugsson, E., Axelsson, G., Björnsson, G., 2009. Permanent carbon dioxide storage into basalt: the CarbFix pilot project, Iceland. Energy Procedia 1, 3641–3646.

Matter, J.M., Broecker, W.S., Gislason, S.R., Gunnlaugsson, E., Oelkers, E.H., Stute, M., Sigurdardóttir, H., Stefansson, A., Alfredsson, H.A., Aradóttir, E.S., Axelsson, G., Sigfusson, B., Wolff-Boenisch, D., 2011. The CarbFix Pilot Project – Storing Carbon Dioxide in Basalt. Energy Procedia 4, 5579-5585.

551 McGrail, B.P., Schaef, H.T, Ho, A.M., Chien, Yi-Ju, Dooley, J.J., Davidson, C.L.,
552 2006. Potential for carbon dioxide sequestration in flood basalts. JGR Research
553 111. B12201, doi:10.1029/2005JB004169.

554 Oelkers, E.H., 2001. General kinetic description of multioxide silicate mineral and
555 glass dissolution. Geochim. Cosmochim. Acta 65, 3703-3719.

556 Oelkers, E.H., Schott, J., 2001. An experimental study of enstatite dissolution rates as
557 a function of pH, temperature, and aqueous Mg and Si concentration, and the
558 mechanism of pyroxene/pyroxenoid dissolution. Geochim. Cosmochim. Acta
559 65, 1219-1231.

560 Oelkers, E.H., Cole, D.R., 2008. Carbon dioxide sequestration: A solution to a global
561 problem. Elements 4, 305-310.

562 Oelkers, E.H., Gislason, S.R., Matter, J., 2008. Mineral carbonation of CO_2. Elements
563 4, 333-337.

564 Oelkers E.H. Golubev, S.V., Chairat, C., Pokrovsky, O.S., Schott, J., 2009. The
565 surface chemistry of multi-oxide silicates. Geochim. Cosmochim Acta, 73, 4617-
566 4634.

567 Oelkers E.H., Schott J., 2005. Geochemical Aspects of CO_2 Sequestration. Chem.
568 Geo. 217, 183-186.

569 Pačes, T., 1983. Rate constants of dissolution derived from the measurements of mass
570 balance in hydrological catchments. Geochim. Cosmochim. Acta 47, 1855-1863.

571 Park, A.-H.A., Fan, L.-S., 2004. CO_2 mineral sequestration: physically activated
572 dissolution of serpentine and pH swing process. Chem. Eng. Sci. 59, 5241-5247.

573 Parkhurst, D.L., Appelo, C.A.J., 1999. User's guide to PHREEQC (Version 2) – A
574 computer program for speciation, batch-reaction, one-dimensional transport, and
575 inverse geochemical calculations. USGS-Report 99-4259.

576 Pokrovsky, O.S., Schott, J., Castillo, A., 2005. Kinetics of brucite dissolution at 25 °C
577 in the presence of organic and inorganic ligands and divalent metals. Geochim.
578 Cosmochim. Acta 69, 905-918.

579 Putnis, A., 2009. Mineral Replacement Reactions. Rev. Min. Geochem. 70, 87-124.

580 Rudge, J.F., Kelemen, P.B., Spiegelman, M., 2011. A simple model of reaction-
581 induced cracking applied to serpentinization and carbonation of peridotite. Earth
582 Planet. Sci. Let. 291, 215–227.

583 Schaef, H.T., McGrail, B.P., Owen, A.T., 2009. Basalt-CO_2-H_2O Interactions and
584 Variability in Carbonate Mineralization Rates. Energy Procedia 1, 4899-4906.

585 Schaef, H.T., McGrail, B.P., 2009. Dissolution of Columbia River Basalt under
586 mildly acidic conditions as a function of temperature: Experimental results
587 relevant to the geological sequestration of carbon dioxide. Appl. Geochem. 24,
588 980-987.

589 Schaef, H.T., McGrail, B.P., Owen, A.T., 2010. Carbonate mineralization of volcanic
590 province basalts. Int. J. Greenhouse Gas Control 4, 249-261.

Schaef, H.T., McGrail, B.P., Owen, A.T., 2011. Basalt Reactivity Variability with Reservoir Depth in Supercritical CO_2 and Aqueous Phases. Energy Procedia 4, 4977–4984.

Schott, J., Berner, R.A., Sjöberg, E.L., 1981. Mechanism of pyroxene and amphibole weathering—I. Experimental studies of iron-free minerals. Geochim. Cosmochim. Acta 45, 2123-2135.

Schott J., Oelkers E.H., 1995. Dissolution and crystallization rates of silicate minerals as a function of chemical affinity. Pure App. Chem., 67, 903-910.

Schott, J., Pokrovsky, O.S., Oelkers, E.H., 2009. The link between mineral dissolution/precipitation kinetics and solution chemistry. Rev. Min. Geochem. 70, 207-258.

Siegel, D.I., Pfannkuch, H.O., 1984. Silicate dissolution influence on Filson Creek chemistry, northeastern Minnesota. Geol. Soc. Am. Bull. 95, 1446-1453.

Stockmann, G.J., Wolff-Boenisch, D., Gislason, S.R., Oelkers, E.H., 2011. Do carbonate precipitates affect dissolution kinetics? 1: Basaltic glass. Chem. Geol. 284, 306-316.

Velbel, M.A., 1993. Formation of protectiye surface layers during silicate-mineral weathering under well-leached oxidizing conditions. Am. Min. 78, 405-414.

Wakahama, H., Mito, S., Ohsumi, T., Ueda, A., Yajima, T., Satoh, H., Sugiyama, K., Ozawa, A., Ajima, S., Todaka, N., Sato, T., Kato, M., Kaji, Y., Tokumarui, T., Kaieda, H., Kubota, K., 2009. A concept of CO_2 Georeactor sequestration at the Ogachi HDR site, NE Japan. Energy Procedia 3683–3689.

Wolff-Boenisch, D., Gislason, S.R., Oelkers, E.H., Putnis, C.V., 2004a. The dissolution rates of natural glasses as a function of their composition at pH 4 and 10.6, and temperatures from 25 to 74°C. Geochim. Cosmochim. Acta 68, 4843–4858.

Wolff-Boenisch, D., Gislason, S.R., and Oelkers, E.H., 2004b. The effect of fluoride on the dissolution rates of natural glasses at pH 4 and 25°C. Geochim. Cosmochim. Acta 68, 4571–4582.

Wolff-Boenisch D., Gislason S.R., Oelkers, E.H., 2006. The effect of crystallinity on dissolution rates and CO_2 consumption capacity of silicates. Geochim. Cosmochim. Acta, 70, 858-870.

Wolff-Boenisch, D., Wenau, S., Gislason, S.R., Oelkers, E.H., 2011. Dissolution of basalts and peridotite in seawater, in the presence of ligands, and CO_2: Implications for mineral sequestration of carbon dioxide. Geochim. Cosmochim. Acta 75, 5510–5525.

Table 1

Composition of inlet fluids used in this study

Experiment	Type of experiment [a]	$NaHCO_3$ (mol/kg)	NH_4Cl (mol/kg)	$CaCl_2$ (mol/kg)	NaOH (mol/kg)	HCl (mol/kg) [c]	Ionic strength (mol/kg)	pH (22 ºC)
1a	P	0.035					0.035	8.45
1b	P	0.035				n.m.	0.036	6.35
2	P	0.035					0.035	8.54
3	C	0.010					0.010	8.60
4a [b]	P	0.035		0.010	1.2E-07		0.033	n.m.
4b [b]	P	0.035		0.020	1.6E-07		0.048	n.m.
5a	C			0.020	1.6E-07		0.060	7.92
5b	C			0.030	1.7E-07		0.090	8.47
5c	C			0.030	1.7E-07		0.090	5.83
5d	C	0.010					0.010	8.54
5e	C		0.010			n.m.	0.010	3.81

[a] 'P' and 'C' designates precipitation and control experiments, respectively

[b] Two-inlet system, i.e. the concentration of the fluid entering the reactor is half of each inlet

[c] HCl was added until the desired pH was reached, but the exact concentration was not measured

n.m. = not measured

Table 2a

Physical conditions and steady-state results of the diopside dissolution experiments performed in this study [a]

Exp.	T (ºC)	*m* (g)	S_{BET} (m^2)	*fr* (g/min)	t_{exp} (days)	pH_{out} (22 ºC)	pH_{out} in-situ T [b]	$[Si]_{out}$ (µmol/kg)	$[Ca]_{out}$ (µmol/kg)	$[Mg]_{out}$ (µmol/kg)	$[Fe]_{out}$ (µmol/kg)	$-\Delta G_r$ (kJ/mol) [b]	Log (a^2_{H+}/a_{Ca2+}) [b]	Log (a^2_{H+}/a_{Mg2+}) [b]
1a	70	10.00	1.01	0.56	53	8.74	8.46	15.36	5.61	5.70	0.013	36.4	-10.8	-11.1
1b [d]	70	10.00	1.01	0.55	6	7.30	7.19	23.38	11.84	13.28	b.d.	62.0	*-9.1*	*-9.1*
2	70	9.81	0.99	0.58	26	8.57	8.31	8.71	1.61	2.58	b.d.	49.0	-10.1	-10.5
3	70	4.67	0.47	1.13	13	8.58	8.29	3.68	0.87	1.23	b.d.	53.7	-10.1	-10.4
4a [c]	25	9.68	0.98	0.52	29	7.10	7.08	3.04	1942.38	9.11	0.030	67.9		
4b [c]	25	9.68	0.98	0.50	34	6.91	6.89	1.45	5102.16	13.81	0.056	73.0		
5a [c]	25	9.92	1.00	0.49	32	7.33	7.25	3.09	~20000	28.2	0.034	56.0		
5b [c]	25	9.92	1.00	0.45	114	7.94	7.84	2.32	~30000	38.32	0.018	42.9		
5c	25	9.92	1.00	0.47	18	6.37	6.34	2.00	~30000	1.54	0.008	85.4		
5d	25	5.05	0.51	0.64	9	8.57	8.53	0.93	n.m.	1.07	b.d.	59.6		
5e [d]	25	5.05	0.51	0.64	5	4.33	4.33	5.25	n.m.	2.67	0.076	142.3		

[a] The data reported are the temperature (T), the initial mass of diopside (*m*), the initial BET surface area of the diopside (S_{BET}), the flow rate (*fr*), the total duration of the experiment (t_{exp}), measured pH of outlet solution, calculated pH of the outlet solution at in-situ T, the concentration of elements in the outlet solution in µmol/kg, and the chemical affinity of diopside ($-\Delta G_r$).
[b] Computed with PHREEQC version 2.17
[c] The high Ca and Mg concentrations arise from the $CaCl_2$ powder used for making the inlet solution
[d] pH pulse added at the end of experiment (end point data provided)
n.m. = not measured
b.d. = below detection limit

Table 2b

Logarithms of measured steady-state diopside dissolution rates (r_+) in mol/cm^2/s based on the release rates of elected elements

Exp.	T (ºC)	pH_{out} at in-situ T	Log $r_{+,Si,\ BET}$	Log $r_{+,Si,\ geo}$	Log $r_{+,Ca,BET}$	Log $r_{+,Ca,geo}$	Log $r_{+,Mg,BET}$	Log $r_{+,Mg,geo}$	Log $r_{+,Fe,BET}$	Log $r_{+,Fe,geo}$
1a	70	8.46	-14.2	-13.5	-14.3	-13.6	-14.3	-13.6	-15.5	-14.8
1b [a]	70	7.19	-14.0	-13.3	-14.0	-13.3	-13.9	-13.3		
2	70	8.31	-14.4	-13.7	-14.8	-14.1	-14.6	-13.9		
3	70	8.29	-14.1	-13.5	-14.5	-13.8	-14.3	-13.6		
4a	25	7.08	-14.9	-14.2					-15.1	-14.5
4b	25	6.89	-15.2	-14.6					-14.9	-14.2
5a	25	7.25	-14.9	-14.2					-15.1	-14.5
5b	25	7.84	-15.1	-14.4					-15.4	-14.8
5c	25	6.34	-15.1	-14.5			-14.9	-14.3	-15.8	-15.1
5d	25	8.53	-15.0	-14.4			-14.6	-14.0		
5e [a]	25	4.33	-14.3	-13.6			-14.2	-13.6	-14.4	-13.7

[a] pH pulse added at the end of experiment (end point data provided)

Table 3

Saturation indices (SI) of selected minerals in the steady-state fluids in all experiments a,b,c

Exp.	calcite	aragonite	dolomite	magnesite	goethite	hematite	$Fe(OH)_3$	$SiO_2(a)$	chrysotile	talc	Ca-saponite	diaspore	Other minerals supersaturated according to modeling [a]
1a	-0.36	-0.51	0.89	-0.14	5.78	12.75	1.19	-2.57	-2.45	-3.66	-2.89	-1.06	Anatase, andradite, cronstedtite, ferrite, magnetite, nontronite, rutile, MnO_2
1b	-1.21	-1.36	-1.04	-1.22	-	-	-	-2.17	-9.05	-9.43	-8.72	0.28	Anatase, rutile
2	-1.02	-1.16	-0.23	-0.60	-	-	-	-2.77	-4.71	-6.30	-5.62	-1.12	Anatase, rutile
3	-1.43	-1.58	-1.24	-1.19	-	-	-	-3.15	-5.80	-8.15	-7.33	-1.12	Anatase, rutile
4a	0.25	0.11	-0.60	-2.48	3.29	7.56	-1.82	-2.64	-15.12	-15.83	-14.57	1.34	Anatase, magnetite, nontronite, dawsonite, boehmite, gibbsite, rutile
4b	0.43	0.29	-0.50	-2.56	2.94	6.86	-2.17	-3.10	-16.86	-18.51	-17.00	1.61	Anatase, magnetite, nontronite, dawsonite, boehmite, gibbsite, rutile
5a	-	-	-	-	3.55	8.09	-1.56	-2.78	-13.13	-14.13	-12.61	1.32	Gibbsite, anatase, boehmite, magnetite, nontronite, rutile
5b	-	-	-	-	3.49	7.97	-1.62	-2.91	-9.62	-10.87	-9.23	0.90	Gibbsite, anatase, boehmite, magnetite, nontronite, rutile
5c	-	-	-	-	0.98	2.94	-4.13	-2.96	-22.78	-24.14	-22.65	1.91	Gibbsite, anatase, boehmite, rutile
5d	-	-	-	-	-	-	-	-3.32	-10.67	-12.76	-	-	none
5e	-	-	-	-	-9.35	-17.71	-14.46	-2.53	-32.81	-33.31	-34.29	-1.53	none

[a] Computed with PHREEQC version 2.17

[b] Saturation index is defined as: SI = log (IAP/K_{sp}), where IAP is the ion activity product and K_{sp} refers to the solubility product of the solid phase

[c] Uncertainty is estimated to ± 0.10 log unit

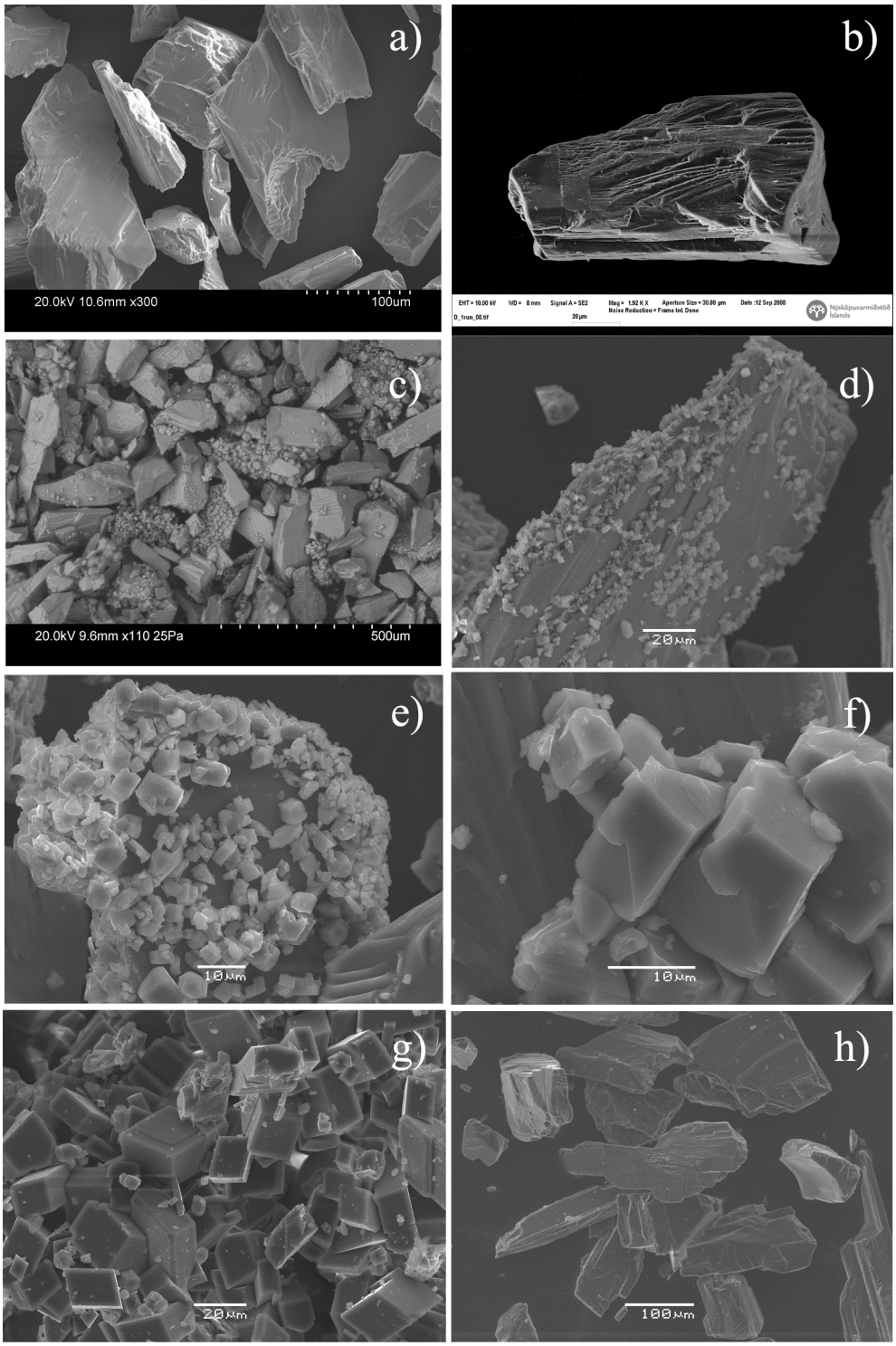

Fig. 1. Scanning electron images of diopside samples from this study. Image a) is of the cleaned diopside powder prior to experiments. Image b) is of a diopside grain after its dissolution during experimental series 1 for ~60 days at 70 ºC. Images c-f) shows secondary calcite precipitates growing on the surfaces of diopside following its dissolution during experimental series 4 at 25 ºC and pH 7. Image f) is a close-up of image e) illustrating how the $CaCO_3$ crystals grow preferentially on topographical features ('surface ripples') on diopside surfaces. Image g) illustrates the morphology of $CaCO_3$ precipitates recovered from experimental series 4. Calcite clusters, like in g), ranged in size from 10 to 1000 μm. Image h) shows the surfaces of diopside following its dissolution for 164 days in control experimental series 5 at 25 ºC.

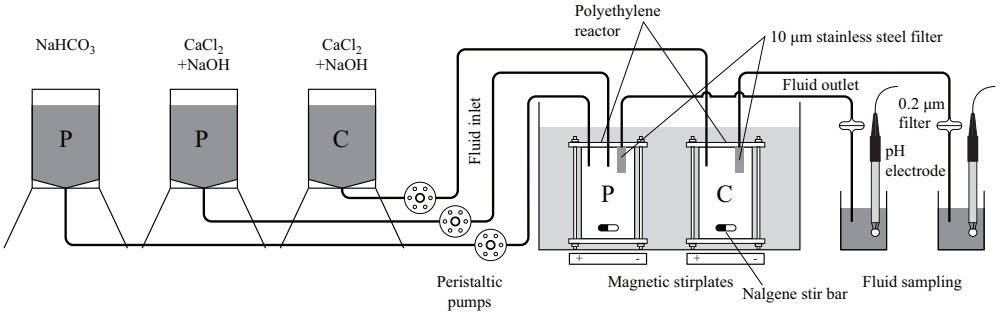

Fig. 2. Schematic illustration of the reactors used in the present study. Supersaturation of calcite in the precipitation experiments is obtained by mixing two inlet solutions comprised of $NaHCO_3$ and $CaCl_2$, respectively, inside the reactor. The control experiments ran with a $CaCl_2$ inlet solution designed to dissolve diopside without secondary precipitate formation. The 70 ºC experiments were performed using an identical reactor system with only one inlet solution connected to the reactor comprised of $NaHCO_3$. In those experiments, diopside was the Ca-source in attempts to achieve calcite saturation inside the reactor.

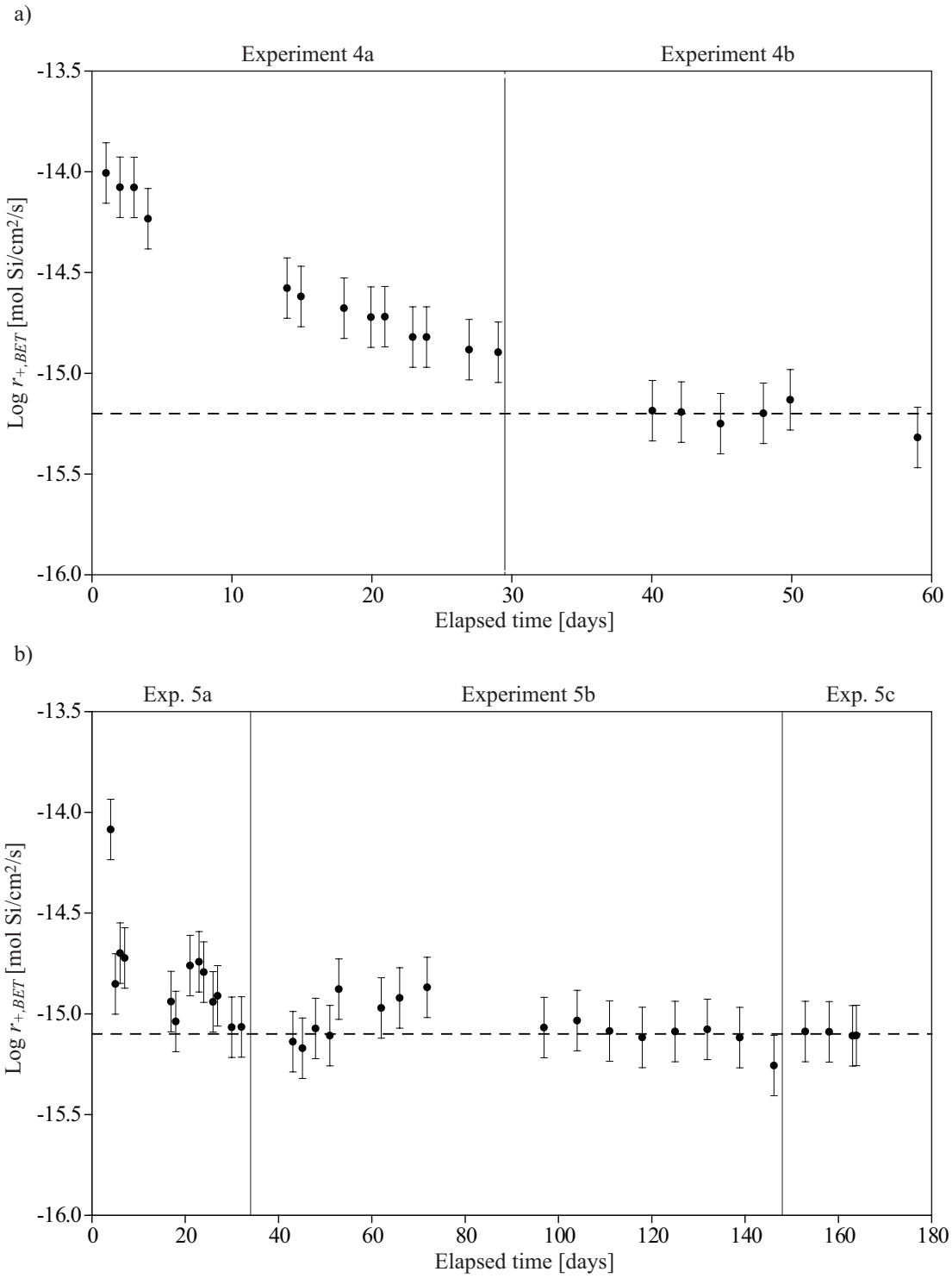

Fig. 3. Measured instantaneous diopside dissolution rates based on Si release during precipitation and control experiments performed at 25 ºC and pH 7.0. a) Rates from experiments 4a and b performed in the presence of precipitating calcite. The dashed line corresponds to a final steady-state rate of $10^{-15.2}$. b) Rates from experiments 5a, b and c performed in the absence of precipitating calcite. The dashed line corresponds to a final steady-state rate of $10^{-15.1}$. The error bars on both plots correspond to ±0.15 log units uncertainty on the rates.

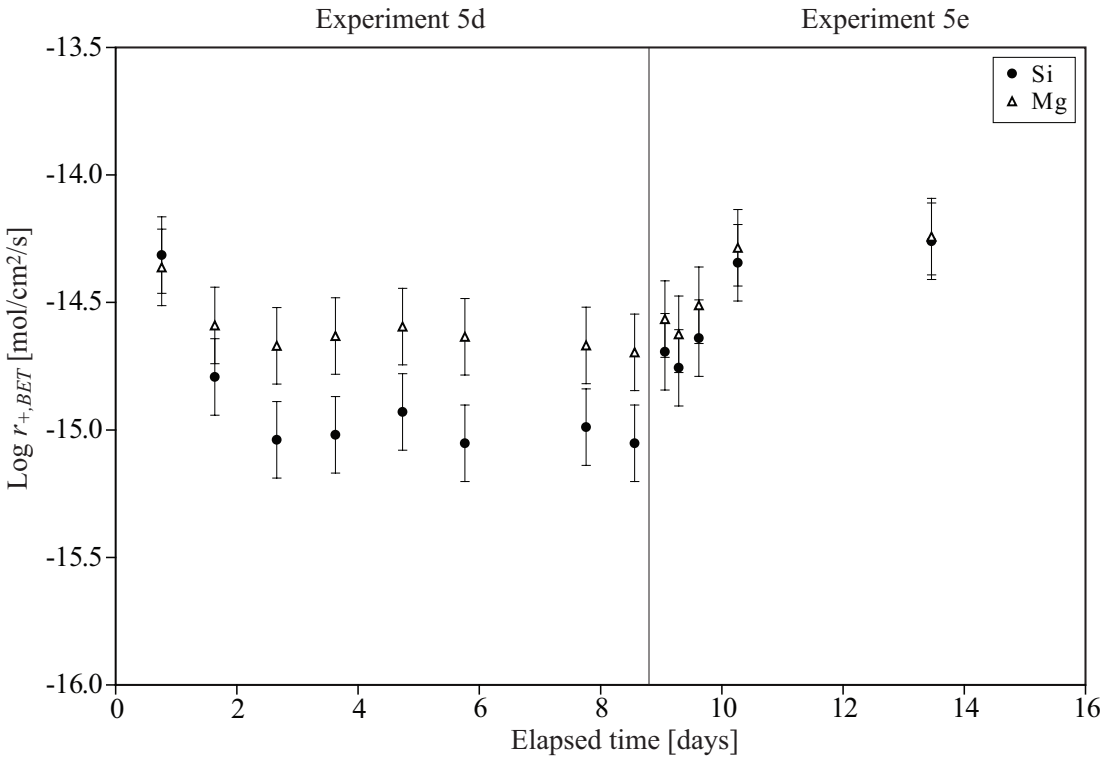

Fig. 4. Measured instantaneous diopside dissolution rates based on Si and Mg release during experiments 5d and e performed at 25 ºC and pH 8.5 and pH ~4, respectively.

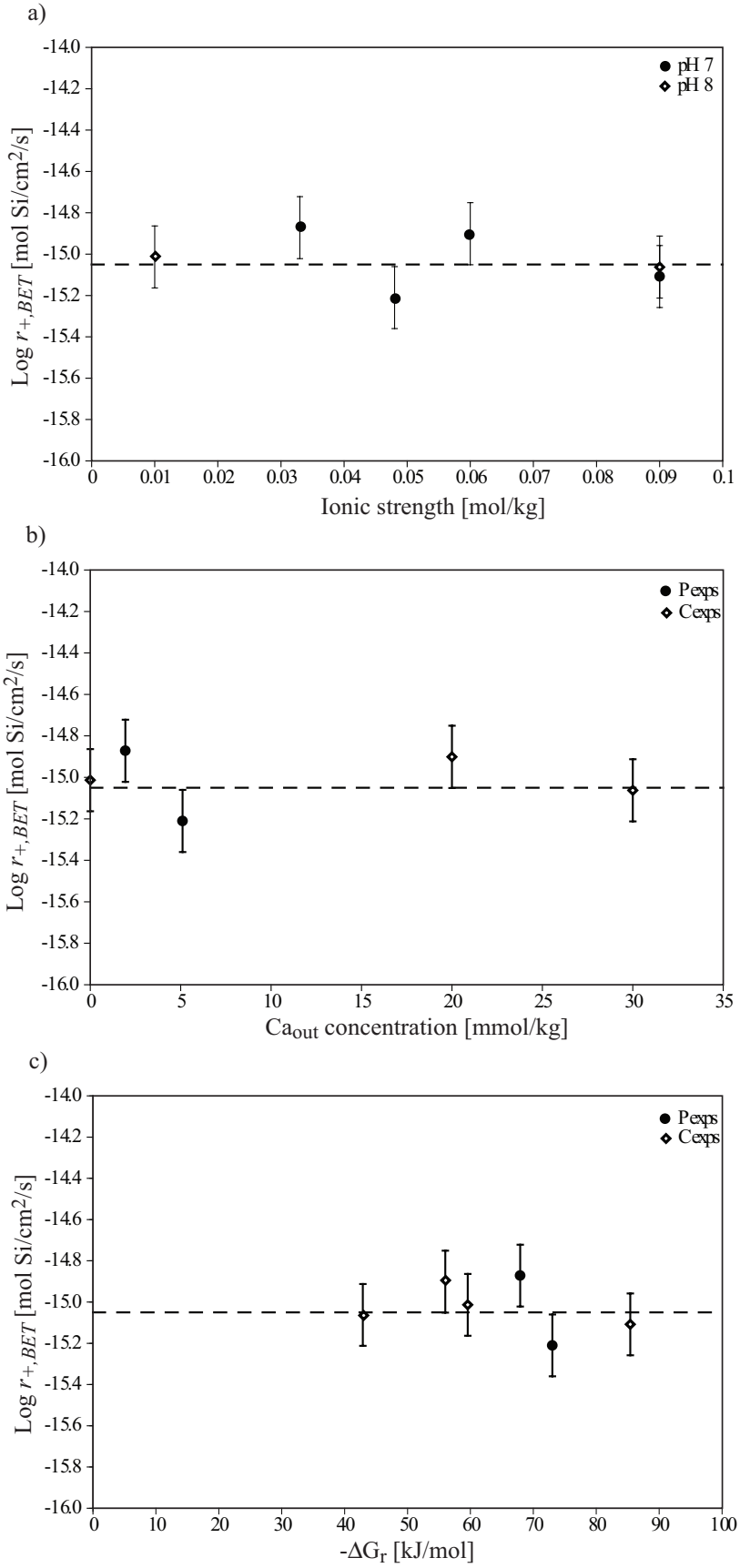

Fig. 5. Measured steady-state diopside dissolution rates based on Si release at pH 7 to 8 as a function of (a) solution ionic strength, (b) reactive fluid Ca concentration of outlet solution, and (c) diopside saturation state. The error bars on these plots correspond to ±0.15 log unit uncertainty. The dashed line in these figures corresponds to a rate of $10^{-15.1}$ mol/cm^2/s. 'P' and 'C' refer to precipitation and control experiments, respectively.

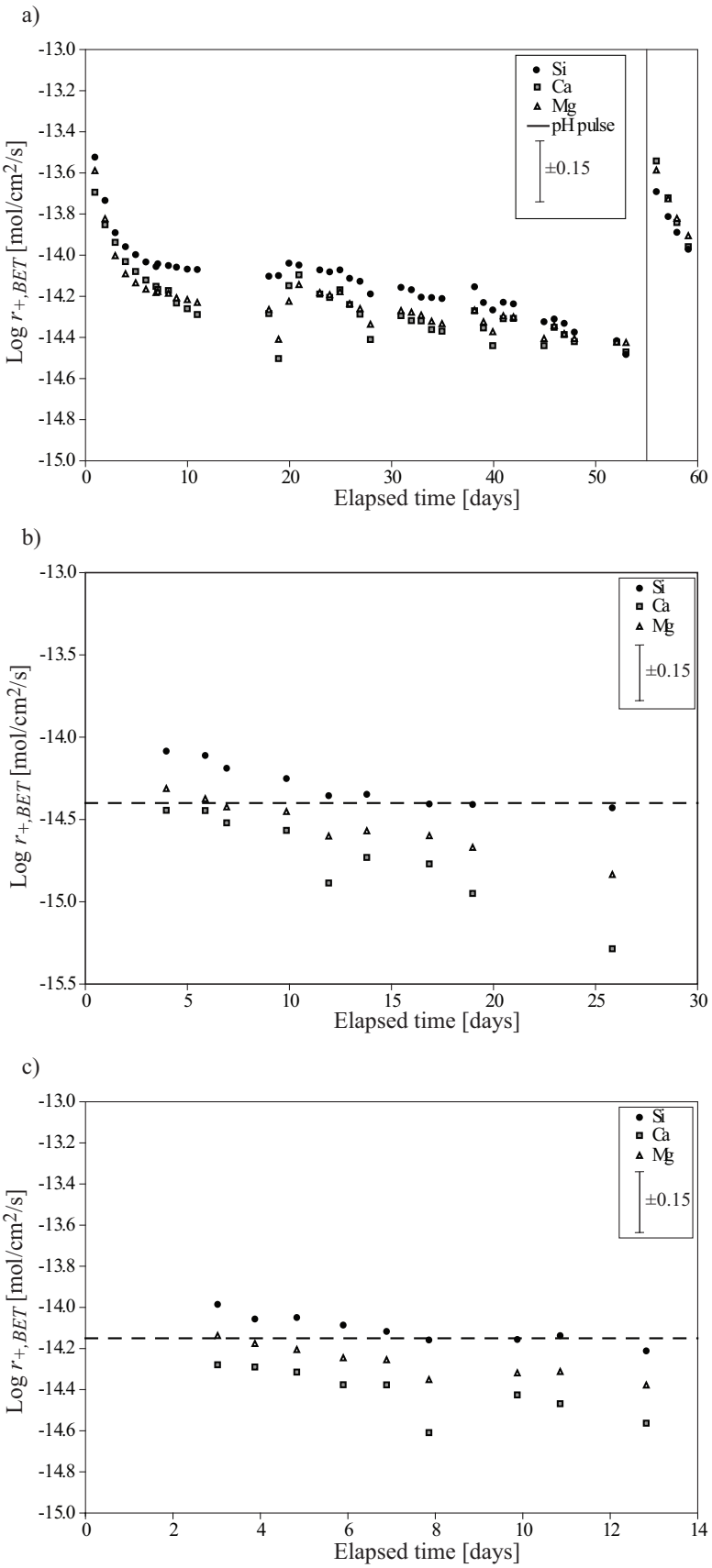

Fig. 6. Measured instantaneous diopside dissolution rates based on Si, Ca, and Mg release during precipitation experiments performed at 70 ºC and pH 8.5. a) Rates from experiments 1a and b, where 1b represents a pH-pulse of pH 6.4. b) Rates from experiment 2, and c) rates from experiment 3. The dashed line in plot b) and c) are drawn at a steady-state Si rate at $10^{-14.40}$ mol/cm^2/s and $10^{-14.15}$ mol/cm^2/s, respectively. The uncertainty on the measured rates is ±0.15 log units as illustrated by the error bar in the top-right corner of the plots.

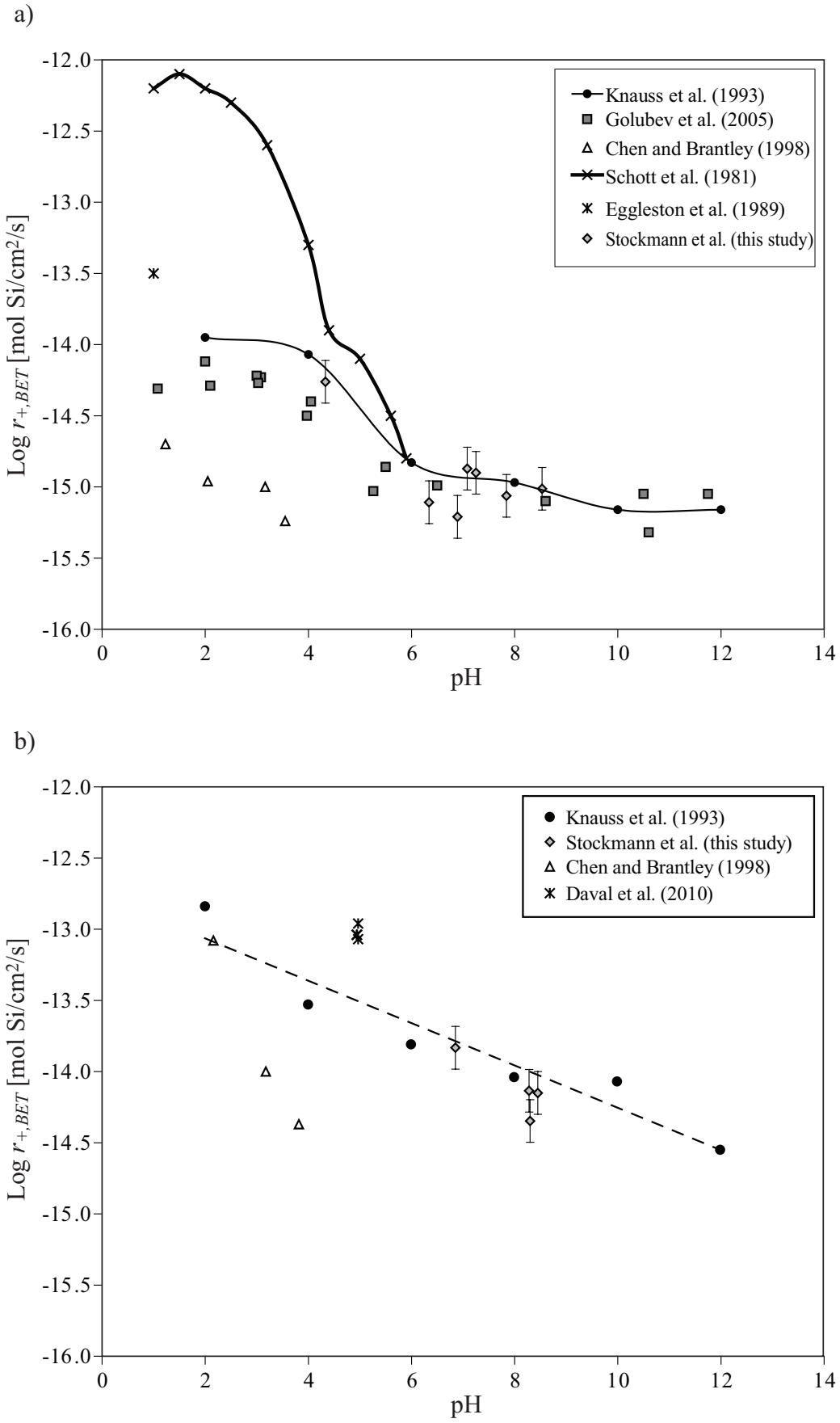

Fig. 7. a) Compilation of diopside dissolution rates at 20-25 ºC reported in the literature and in this study. b) Compilation of diopside dissolution rates near 70 ºC reported in the literature and in this study. The data points from Chen and Brantley (1998) and Daval et al. (2010) were measured at 90 ºC. The dashed trend line is based on the plotted data from Knauss et al. (1993).

Chapter 4

Does the presence of heterotrophic bacterium *Pseudomonas reactans* affect basaltic glass dissolution rates?

Gabrielle J. Stockmann, Liudmila S. Shirokova, Oleg S. Pokrovsky, Pascale Bénézeth, Nicolas Bovet, Sigurdur R. Gislason and Eric H. Oelkers

Chemical Geology 296-297 (2012), 1-18

(reprinted with permission by Elsevier Science Ltd)

ABSTRACT

Far-from-equilibrium steady-state basaltic glass dissolution rates were measured using newly developed Bacterial Mixed-Flow Reactors (BMFR) at 25 °C. Experiments were performed in aqueous pH 4, 6, 8, and 10 buffer solutions with and without nutrients and in: 1) the absence of bacteria, 2) the presence of 0.1–0.4 $g_{we}t$/L dead *Pseudomonas reactans*, and 3) in the presence of 0.9–19.0 g_{wet}/L live *P. reactans* extracted from a deep subsurface oxygen-bearing basaltic aquifer. The BMFR allows steady-state rate measurements at constant concentrations of live or dead bacteria. Experiments ran for 30–60 days on a single basaltic glass powder, initially at bacteria- and nutrient-free conditions until Si steady-state glass dissolution was achieved. Then, in 2–4 steps, either live or dead *P. reactans* were added via nutrient-rich or nutrient-free inlet solutions, and the flux of Si and other mineral constituents from the basaltic glass were measured until a new chemical steady state was attained. Scanning Electron Microscope and X-ray Photoelectron Spectroscopic techniques verified the presence of live bacteria on the basaltic glass surfaces through biofilm formation, bacterial dissolution imprints, and enrichment of surface layers in C and N. The presence of either live or dead *P. reactans* lowers constant pH steady-state basaltic glass dissolution rates by no more than ~0.5 log units which is close to combined analytical and experimental uncertainties of the experiments. The presence of bacteria did not cause any significant modification in trace element release rates from dissolving basaltic glass within the uncertainty of the measurements. Experiments in nutrient-rich solutions yielded close to stoichiometric release of all major elements from basaltic glass at pH 6–8 likely as a result of organic ligand complexation with aqueous Al and Fe, which would otherwise form hydroxy-precipitates. As the results of this work suggest, at most, a small inhibiting effect of live or dead *P. reactans* on basaltic glass dissolution rates, geochemical modeling of mineral reactivity in basaltic aquifers likely does not require explicit provision for the presence of heterotrophic bacteria on basaltic glass reactivity.

Chemical Geology 296-297 (2012) 1–18

Contents lists available at SciVerse ScienceDirect

Chemical Geology

journal homepage: www.elsevier.com/locate/chemgeo

Does the presence of heterotrophic bacterium *Pseudomonas reactans* affect basaltic glass dissolution rates?

Gabrielle J. Stockmann [a,b,*], Liudmila S. Shirokova [b,c], Oleg S. Pokrovsky [b], Pascale Bénézeth [b], Nicolas Bovet [d], Sigurdur R. Gislason [e], Eric H. Oelkers [b,e]

[a] Nordic Volcanological Center, Institute of Earth Sciences, University of Iceland, Sturlugata 7, 101 Reykjavík, Iceland
[b] GET-Université de Toulouse-CNRS-IRD-OMP, 14 Avenue Edouard Belin, 31400 Toulouse, France
[c] Institute of Ecological Problems of the North, 23 Nab. Severnoy Dviny, Russian Academy of Science, Arkhangelsk, Russia
[d] Nano-Science Center, Department of Chemistry, University of Copenhagen, Universitetsparken 5, 2100 Copenhagen, Denmark
[e] Institute of Earth Sciences, University of Iceland, Sturlugata 7, 101 Reykjavík, Iceland

ARTICLE INFO

Article history:
Received 23 July 2011
Received in revised form 11 December 2011
Accepted 12 December 2011
Available online 26 December 2011

Editor: J. Fein

Keywords:
Basaltic glass
Pseudomonas reactans
Mineral–bacteria interaction
Dissolution kinetics
Bacterial mixed-flow reactors
CO_2 sequestration

ABSTRACT

Far-from-equilibrium steady-state basaltic glass dissolution rates were measured using newly developed Bacterial Mixed-Flow Reactors (BMFR) at 25 °C. Experiments were performed in aqueous pH 4, 6, 8, and 10 buffer solutions with and without nutrients and in: 1) the absence of bacteria, 2) the presence of 0.1–0.4 g_{wet}/L dead *Pseudomonas reactans*, and 3) in the presence of 0.9–19.0 g_{wet}/L live *P. reactans* extracted from a deep subsurface oxygen-bearing basaltic aquifer. The BMFR allows steady-state rate measurements at constant concentrations of live or dead bacteria. Experiments ran for 30–60 days on a single basaltic glass powder, initially at bacteria- and nutrient-free conditions until Si steady-state glass dissolution was achieved. Then, in 2–4 steps, either live or dead *P. reactans* were added via nutrient-rich or nutrient-free inlet solutions, and the flux of Si and other mineral constituents from the basaltic glass were measured until a new chemical steady state was attained. Scanning Electron Microscope and X-ray Photoelectron Spectroscopic techniques verified the presence of live bacteria on the basaltic glass surfaces through biofilm formation, bacterial dissolution imprints, and enrichment of surface layers in C and N. The presence of either live or dead *P. reactans* lowers constant pH steady-state basaltic glass dissolution rates by no more than ~0.5 log units which is close to combined analytical and experimental uncertainties of the experiments. The presence of bacteria did not cause any significant modification in trace element release rates from dissolving basaltic glass within the uncertainty of the measurements. Experiments in nutrient-rich solutions yielded close to stoichiometric release of all major elements from basaltic glass at pH 6–8 likely as a result of organic ligand complexation with aqueous Al and Fe, which would otherwise form hydroxy-precipitates. As the results of this work suggest, at most, a small inhibiting effect of live or dead *P. reactans* on basaltic glass dissolution rates, geochemical modeling of mineral reactivity in basaltic aquifers likely does not require explicit provision for the presence of heterotrophic bacteria on basaltic glass reactivity.

1. Introduction

The role of bacteria on geochemical processes is receiving increasing attention as it has become apparent that bacteria can act as both a catalyst and an inhibitor of mineral precipitation and dissolution reactions (Ehrlich, 1981; Kalinowski et al., 2000; Ganor et al., 2009). Numerous laboratory and field studies have shown that bacteria can significantly affect alumino-silicate and metal oxide dissolution rates at Earth-surface conditions (Bennett and Casey, 1994; Vandevivere et al., 1994; Welch and Vandevivere, 1994; Grantham et al., 1997; Hutchens et al., 2003; Edwards et al., 2004; Rogers and Bennett, 2004; Wu et al., 2007, 2008; Hutchens, 2009; Uroz et al., 2009; Hutchens et al., 2010). These observations may be due to several and sometimes competing effects including: a) fluid pH changes due to bacterial acid production or proton consumption (Wu et al., 2007, 2008), b) bacterial exometabolites and lysis production which may complex aqueous ions at the mineral surface and in the fluid phase, thereby changing the fluid saturation state with respect to the dissolving solid and/or secondary minerals, c) metal adsorption on cell walls (e.g. Fein et al., 1997) which together with aqueous metal complexation can alter multi-oxide mineral dissolution rates due to their dissolution mechanism (Gout et al., 1997; Oelkers and Schott, 1998; Schott et al., 2009), and d) biofilm formation, composed of exopolysaccharides (EPS), which could inhibit dissolution by blocking mineral surface–fluid interface (Welch and Vandevivere, 1994; Lee and Fein,

* orresponding author at: Nordic Volcanological Center, Institute of Earth Sciences, University of Iceland, Sturlugata 7, 101 Reykjavik, Iceland. Tel.: +354 857 4079; fax: +354 562 9767.
E-mail address: gjs3@hi.is (G.J. Stockmann).

0009-2541/$ – see front matter © 2011 Elsevier B.V. All rights reserved.
doi:10.1016/j.chemgeo.2011.12.011

2000; Buchardt et al., 2001; Hutchens et al., 2010). Certain soil Gram-positive bacteria have also been observed to promote silicate dissolution via acidic exopolysaccharide production (Belkanova et al., 1985, 1987; Malinovskaya et al., 1990). Due to the large number of bacterial influenced processes effecting mineral dissolution rates, bacteria may have distinct effects depending on its environment (Hutchens et al., 2006). In addition, certain bacteria have been observed to diversify their biofilm composition depending on the ions available to them (Liermann et al., 2000b).

To further our understanding of bacterial–surface interaction, this study reports basaltic glass dissolution rates in the presence and absence of heterotrophic bacteria. Generally, one would expect a different effect of bacteria on alumino-silicate reactivity compared to Al-free, Ca- and Mg-bearing "basic silicate" reactivity due to their different dissolution mechanisms (e.g., see Pokrovsky et al., 2009, 2010; Berner, 2010 for recent discussion). Basaltic glass represents an intermediate case between the alumino- and "basic" silicates, because its dissolution requires removal of both Al, and Ca and Mg from the surface (c.f. Oelkers, 2001).

An additional motivation for this study is the potential for using basalts for carbon storage via mineral carbonatization (c.f. Oelkers and Schott, 2005; Oelkers et al., 2008a). This possibility is currently being tested at the Hellisheidi geothermal power plant in Iceland (Gislason et al., 2010). Heterotrophic aerobic bacteria, extracted from groundwater collected from well HK-31 at the Hellisheidi power plant (see Fig. 1), were used in this study of basaltic glass dissolution. Basaltic glass contains a large variety of major and trace elements allowing direct evaluation of the extent that weathering may be influenced by the solid's nutritional potential (i.e. Bennett et al., 2001; Bailey et al., 2009).

Despite the fact that basaltic glass leaching in biotic soil and marine systems has been extensively investigated (Thorseth et al., 1992; Benedetti et al., 2003 and references therein), there are few laboratory studies of basalt and basaltic glass interaction with bacteria available in the literature (Thorseth et al., 1995; Aouad et al., 2006; Wu et al., 2007). These studies, however, used batch reactors, in which the reactor fluid composition evolved continuously during the experiments. This approach prevents the rigorous determination of the dissolution rates required for the predictive modeling of water–rock interaction processes. The present work is aimed at overcoming these limitations by performing rate measurements in newly developed Bacterial Mixed-Flow Reactors (BMFR). BMFR reactors allow determination of water–rock reaction rates at constant bacterial concentrations and at steady-state conditions. The purpose of this paper is to present the results of basaltic glass dissolution rate measurements performed in these reactors and to use these results to better understand the role of bacteria on these rates.

2. Theoretical background

The standard state adopted in this study is that of unit activity of pure minerals and H_2O at any temperature and pressure. For aqueous species other than H_2O, the standard state is unit activity of species in a hypothetical 1.0 mol/kg solution referenced to infinite dilution at any temperature and pressure. Thermodynamic calculations reported in this study were performed using the PHREEQC 2.17 computer code (Parkhurst and Appelo, 1999) together with its llnl.dat and minteqv4.dat databases. The thermodynamic properties of hydrated leached basaltic glass with the composition, $SiAl_{0.35}O_2(OH)_{1.05}$, was added to the minteqv4 database. The equilibrium constant (K) for the leached glass dissolution reaction given by:

$$SiAl_{0.35}O_2(OH)_{1.05} + 1.05H^+ + 0.95H_2O = 0.35Al^{3+} + H_4SiO_4^0 \quad (1)$$

was calculated from the stoichiometric sum of the equilibrium constants of amorphous SiO_2 and amorphous $Al(OH)_3$ hydrolysis reactions (see

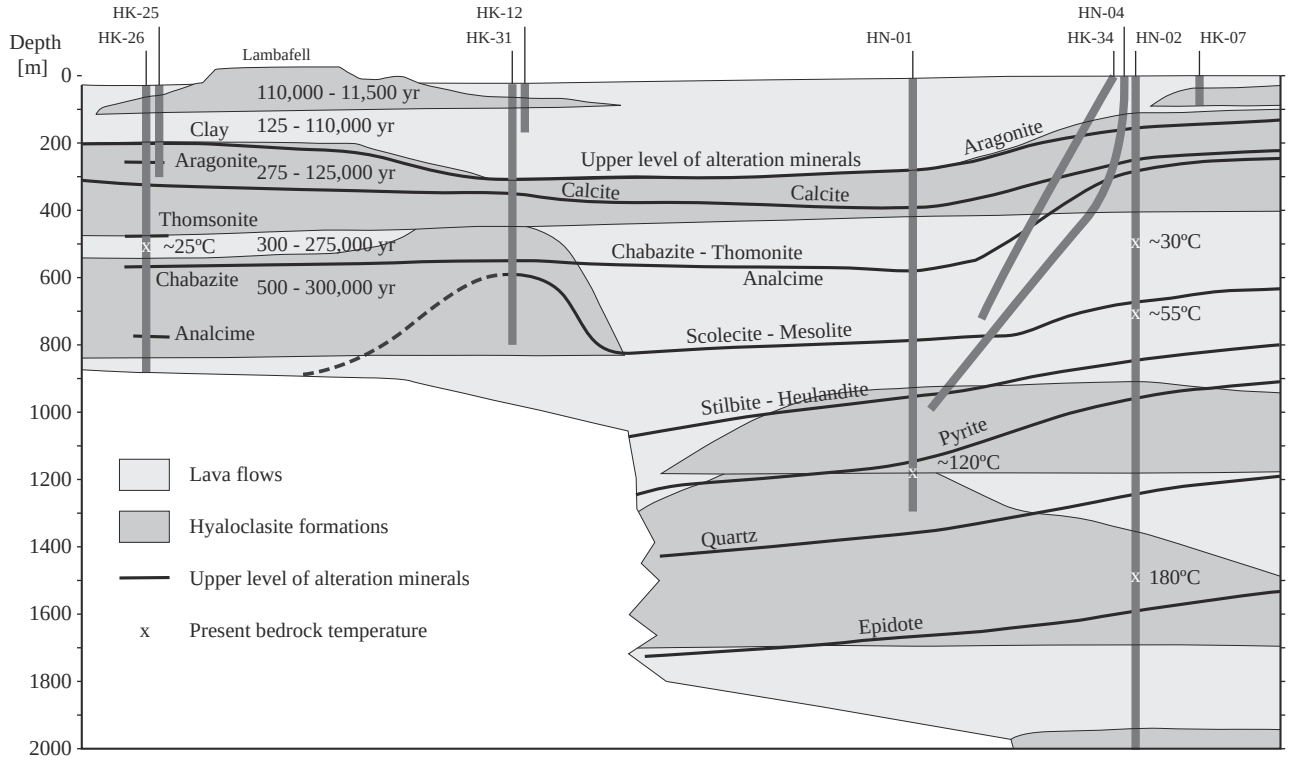

Fig. 1. Cross-section of the geological setting for the CO_2 injection at the Hellisheidi geothermal power plant in Iceland. The *Pseudomonas reactans* bacteria used for this study was extracted from water collected from well HK-31 at 400–800 m depth. Well HN-02 is the CO_2 injection well, HN-01 is the groundwater source, and HN-04, HK-34, HK-31 and HK-26 are the monitoring wells.
Modified from Alfredsson et al. (2008).

Bourcier et al., 1990; Wolff-Boenisch et al., 2004b and references therein). Log K for reaction (1) is calculated to be 1.07 and its corresponding ΔH_r to −22.47 kJ/mol at 25 °C.

Glass dissolution rates based on the release of the *i*th element ($r_{+,i,j}$) were calculated from:

$$r_{+,i,j} = \frac{\Delta C_i \cdot fr}{\nu_i \cdot A_j \cdot m} \quad (2)$$

where ΔC_i stands for the concentration of the *i*th element in the outlet fluid minus its concentration in the inlet fluid, *fr* refers to the fluid flow rate, ν_i is a stoichiometric factor equal to the number of moles of the *i*th element in 1 mol of the glass (assumed to contain one Si atom), A_j designates the specific surface area of the basaltic glass, and *m* denotes the mass of glass used in the experiment. The index *j* refer to rates calculated either using the measured BET surface area, A_{BET} or the geometric surface area, A_{geo}.

Consistent with the dissolution mechanism and rate equations provided by Oelkers and Gislason (2001) and Gislason and Oelkers (2003), surface area normalized far-from-equilibrium basaltic glass dissolution rates can be quantified using:

$$r_{+,Si,j} = k\left(\frac{a^3_{H^+}}{a_{Al^{3+}}}\right)^{\frac{1}{3}} \quad (3)$$

where *k* denotes a rate constant, and *j* refer to rates normalized to either the BET surface area, A_{BET} or the geometric surface area, A_{geo}. Eq. (3) is based on the assumption that the rate-limiting step for basaltic glass dissolution is the liberation of partially detached Si tetrahedrons formed by the exchange of one adjacent Al with three aqueous protons (Oelkers, 2001; Oelkers and Gislason, 2001; Wolff-Boenisch et al., 2004b, 2006; Schott et al., 2009). According to Eq. (3), basaltic glass dissolution rates exhibit a U-shaped curve as a function of pH, which reaches a minimum around pH 6–7 at 25 °C. At high pH, the rates increase due to aqueous Al^{3+} complexation with hydroxide ions forming $Al(OH)_4^-$. Similar U-shaped dissolution rate versus pH curves are found for other aluminum-containing silicates, i.e. feldspars (Oelkers and Schott, 1998) and muscovite (Oelkers et al., 2008b). Any complexing of aqueous Al^{3+} at low pH with anions like F^- and SO_4^{2-}, or organic molecules leads to increased basaltic glass dissolution rates (Oelkers and Gislason, 2001; Wolff-Boenisch et al., 2004a, 2011; Flaathen et al., 2010), whereas at high pH aqueous Al–OH complexing is strong and the rates are relatively unaffected by other complexing ions (Wolff-Boenisch et al., 2004a; Flaathen et al., 2010; Wolff-Boenisch et al., 2011).

The elements released by basaltic glass dissolution in the presence of bacteria and exometabolites can a) remain free aqueous ions, b) complex with cell exometabolites, c) adsorb on the bacteria surface, d) be consumed and assimilated into bacteria cells and/or e) be sequestered by secondary minerals (Neaman et al., 2005a,b, 2006; Shirokova et al., 2012). Bacterial surfaces contain large quantities of functional groups including carboxyl, hydroxyl, and phosphoryl groups (Fein et al., 1997), and exometabolites comprised of long organic sugar molecules, together with pieces of lysed and dead bacteria cells. Both surface complexes and exometabolites could affect mineral dissolution, through complexing with the aqueous Al^{3+} and divalent cations, primarily Ca^{2+}, Mg^{2+} and Fe^{2+}. Complexing aqueous Al^{3+} could lead to increased dissolution rates of basaltic glass at low pH as described by Wolff-Boenisch et al. (2004a) and Flaathen et al. (2010), whereas bacterial surface adsorption or intracellular consumption of divalent cations would decrease element availability for secondary mineral precipitation. Surface passivation via binuclear or multinuclear complex formation is another possible rate inhibition mechanism of microorganisms and their exometabolites and lysis products.

3. Material and methods

3.1. Basaltic glass

The basaltic glass used in this study was collected from the Stapafell Mountain in Southwest Iceland and is the same material as was previously described by Oelkers and Gislason (2001), Gislason and Oelkers (2003), and Stockmann et al. (2011). A size fraction of 45–125 μm basaltic glass was used for all experiments performed in this study. The grinding, sieving, and cleaning procedures of this glass powder were described in detail by Stockmann et al. (2011). The chemical composition of the basaltic glass, as determined by X-ray Fluorescence analysis, is listed in Table 1 and is consistent with the formula: $Si_{1.000}$ $Al_{0.350}$ $Fe_{0.187}$ $Mn_{0.003}$ $Mg_{0.292}$ $Ca_{0.263}$ $Na_{0.076}$ $K_{0.007}$ $Ti_{0.024}$ $P_{0.004}$ $O_{3.371}$. The Fe^{2+}/Fe^{3+}-ratio of this glass was not determined, but Oelkers and Gislason (2001) reported iron in Stapafell basaltic glass to be predominantly Fe^{2+}. Trace element analysis is included in Table 1 and selected trace elements were chosen to test the effect of bacteria uptake and absorption in this study.

The specific surface area, A_{BET}, of the cleaned basaltic glass powder was determined to 5878 ± 400 cm^2/g by the multi-point krypton adsorption BET method, and the geometric surface area, A_{geo}, was calculated to 251 cm^2/g (Stockmann et al., 2011). Dividing the BET surface area by the geometric yields a roughness factor of 23. Surface roughness and fine-scale porosity within the glass are the likely reasons for the higher BET surface area compared to the geometric surface area. Dissolution rates of basaltic glass based on both BET and geometric surface areas are reported in this study. However, BET dissolution rates are shown in figures to be consistent with previous reports of abiotic basaltic glass dissolution (Oelkers and Gislason, 2001; Gislason and Oelkers, 2003; Stockmann et al., 2011). Additional BET measurements were performed on the basaltic glass at the end of selected experiments to assess if the dissolution in the presence of bacteria had dramatically affected surface areas.

3.2. Bacterial culture

Bacteria were extracted from groundwater collected from well HK-31 at the Hellisheidi power plant from 400 to 800 m depth (see Fig. 1). Water chemistry data from HK-31 at the time of sampling is provided in Table 2. Heterotrophic aerobic Gram-negative strain of *Pseudomonas reactans* (called HK 31.3), as identified by DNA extracting (UltraClean® Microbial DNA Isolation Kit MO BIO) and 16S rRNA gene amplifying (Shirokova et al., 2012), was separated and purified

Table 1
Chemical composition of basaltic glass from the Stapafell Mountain, SW Iceland. Results of X-ray fluorescence analysis (XRF).

Major elements [a,b]	Weight %	Trace elements							
			ppm		ppm		ppm		ppm
SiO_2	48.55	Ag	0.031	Hf	1.89	Sr	201	Cs	<0.1
Al_2O_3	14.43	As	0.126	Hg	0.004	Ta	0.717	Pr	3.42
CaO	11.94	Au	0.005	Li	4.27	Te	0.016	Nd	15.1
Fe_2O_3	12.08	B	1.06	Mo	0.901	Th	0.944	Sm	3.74
FeO	–	Ba	79.6	Nb	15.5	Tl	0.011	Eu	1.31
K_2O	0.274	Be	0.704	Ni	153	U	0.248	Gd	4.26
MgO	9.51	Bi	0.008	Pb	0.841	V	296	Tb	0.653
MnO	0.192	Cd	0.147	Rb	6.84	W	0.253	Dy	4.17
Na_2O	1.91	Co	51.9	Re	0.001	Y	21.6	Ho	0.817
P_2O_5	0.199	Cr	646	S	326	Zn	162	Er	2.51
TiO_2	1.570	Cu	136.2	Sb	0.054	Zr	95.3	Tm	0.345
		Ga	15.5	Sc	40.4	La	11.9	Yb	2.15
Total	100.00	Ge	1.90	Sn	1.92	Ce	26.3	Lu	0.331

[a] Major elements were re-analyzed at the University of Edinburgh, 2011 and thus differs slightly from values in Stockmann et al. (2011).
[b] Fe_2O_3 represents total Fe in the glass. Oelkers and Gislason (2001) determined Fe to be predominantly Fe^{2+} in Stapafell basaltic glass.

Table 2
Water chemistry data for well HK-31 at Hellisheidi, Iceland.
source: Shirokova et al. (2012) except for O_2 which was obtained by H.A. Alfredsson (personal comm., 2011).

pH_{exit}	9.44
T_{exit}	18.2 °C
Na	46 mg/l
Si	16 mg/l
Ca	3.6 mg/l
Mg	0.6 mg/l
Al	50 μg/l
Fe	8 μg/l
O_2	0.081 mmol/L
DOC	0.44 ppm

using agar plate technique and cultured under laboratory conditions in nutrient broth-rich (NB) media. *P. reactans* is a common rod-shaped groundwater and soil bacteria averaging 2 μm in size; it has already reported to occur in underground Siberian water repositories (Nazina et al., 2006, 2010). A further description of *P. reactans* is provided by Shirokova et al. (2012). Freshly-grown bacterial cultures having the identical age, physiological, and initial nutritional status were used in all experiments.

Dead (heat-killed) cells were produced via autoclaving a freshly grown bacterial biomass for 30 min at 130 °C, followed by thorough rinsing in sterile 0.1 M NaCl. Although the heat-killing procedure can significantly modify the cell surface structure, it still remains a widely used method for producing biological control material (e.g. Ngwenya, 2007; Martinez et al., 2008; Pokrovsky et al., 2008; Kenward et al., 2009; Martinez et al., 2010). Scanning electron and optical microscopic examination showed that heat-killed cells maintained their integrity and shape after heat treatment. Inactivated cells were produced using 0.01 M sodium azide (NaN_3) during selected experiments. The use of NaN_3 as metabolic inhibitor for heterotrophic bacteria is well established in the literature (i.e., Urrutia Mera et al., 1992; Johnson et al., 2007).

Active bacteria number counts (colony forming-units, CFU/mL) were performed using Petri dish inoculation on nutrient agar (0.1, 0.2, and 0.5 mL of sampled solution in three replicates) in a laminar hood box. Inoculation of blanks was routinely performed to assure the absence of external contamination. The biomass of live bacteria suspensions was also quantified by measuring wet (after it was centrifuged 15 min at 10,000 rpm) and freeze-dried weight in duplicates. The conversion ratio wet/freeze-dried weight of the studied microorganisms is equal to 8.4 ± 0.5. The conversion factor of optical density (600 nm, 10 mm path) and wet biomass (g_{wet}/L) to the cell number (CFU/mL) was equal to $(5 \pm 1) \times 10^8$ and $(8.0 \pm 1.5) \times 10^7$, respectively as determined by triplicate measurements. Live biomass concentration during BMFR experiments ranged from 0.9 to 19 g_{wet}/L. Before the preparation of the inlet fluid for BMFR experiments, cells were rinsed twice in either the appropriate fresh culture media or a sterile 0.1 M NaCl solution using centrifugation with ~500 mL of solution for 1 g of wet biomass, to remove adsorbed metals and cell exudates from the surface.

3.3. Dissolution rate experiments in Bacterial Mixed-Flow Reactors (BMFR)

Steady-state basaltic glass dissolution rates were obtained at distinct fluid compositions and pH using a Bacterial Mixed-Flow Reactor (BMFR) system; the design of this system is shown in Fig. 2. This system consists of a 40 ml mixed-flow reaction vessel immersed in a water bath held at a constant temperature of 25.0 ± 0.5 °C. This reactor is fitted with 10 or 20 μm poresize Magna Millipore Nylon outlet filters to allow bacteria to pass while retaining the 45–125 μm glass powder in the reactor. This reactor system thus maintained a constant biomass concentration in the reactor, equal to that of the inlet fluid. The input fluids were kept in 1 L polypropylene bottles closed with Biosilico® ventilated caps. These fluids were stirred continuously during the experiments and were changed typically each 7 days. This allowed maintenance of a constant and stable stationary phase bacterial culture in the bacteria-bearing inlet fluids. Bacteria concentration was verified by periodic sampling of inlet and outlet fluids for cell optical density (total biomass) and live cell numbers (via agar plate counting). Prior to each

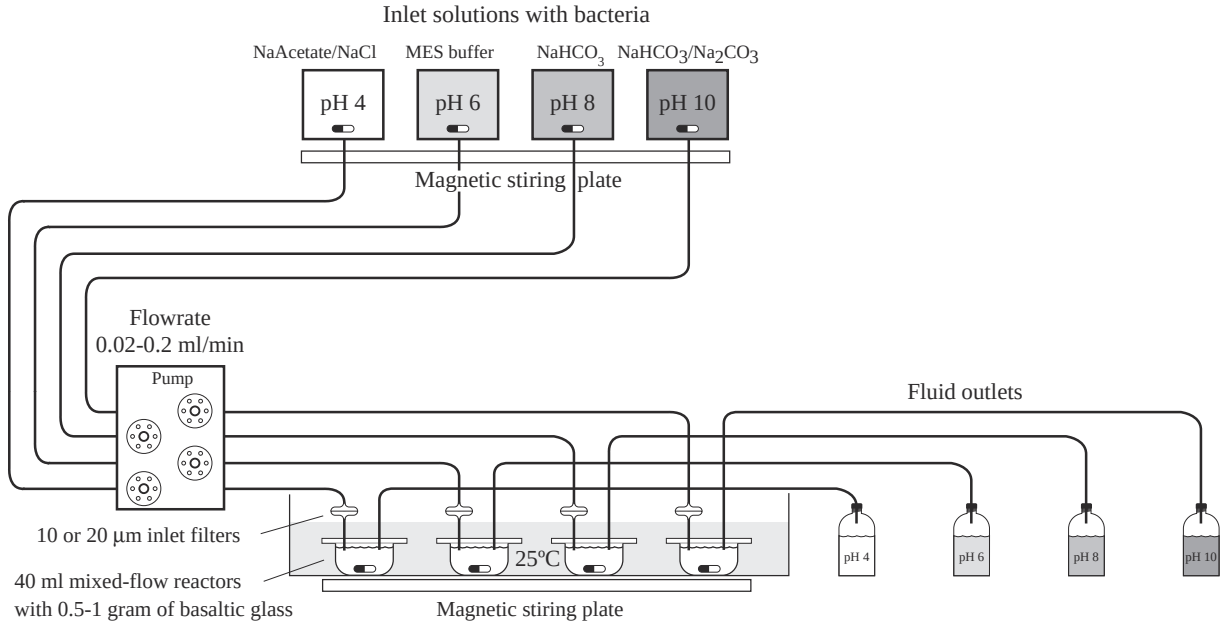

Fig. 2. Reactor system used for the experiments performed in this study. Inlet solutions containing bacteria were continuously stirred to keep solutions homogenous. Outlet solutions passed through 10 or 20 μm filters, which allow bacteria to pass while retaining the basaltic glass powder.

Table 3a
Summary of experimental results at steady state for all the basaltic glass dissolution experiments performed in this study. All experiments were performed at 25 °C.

Exp.[a]	m_{BG}	S_{BET}	Fr	Duration	pH_{in}	pH_{out}	$Bact_{in}$[b]	Bact. status[c]	$Nutr_{in}$	$Bact_{out}$[b]	DOC_{out}	[Si][d]	[Al][d]	[Ca][d]	[Mg][d]	[Fe][d]
	(g)	(m^2)	(g/min)	(days)			(mg_{wet}/L)		(%)	(CFU/mL)	(mg/L)	(μmol/kg)	(μmol/kg)	(μmol/kg)	(μmol/kg)	(μmol/kg)
4-1	1.00	0.59	0.03	15	4.07	4.33	0		0			36.57	15.64	22.95	26.75	10.8
4-2	0.97	0.57	0.02	14	4.58	4.63	100	Dead	0			17.19	1.85	b.d.	3.99	0.61
4-3	0.97	0.57	0.03	11	4.28	4.58	430	Dead	0			10.79	1.38	5.30	2.80	0.43
4-4[e]	0.89	0.53	0.02	22	4.18	7.44	700	Live	0	1.0E + 07		11.14	0.39	2.17	4.70	0.22
6-1	0.52	0.30	0.33	4	5.86	5.92	0		0			0.60				
6-2	0.52	0.30	0.21	3	5.81	5.98	0		0			0.84				
6-3	0.52	0.30	0.21	3	6.22	6.38	0		1			0.58				
6-4	0.52	0.30	0.21	6	6.33	6.44	0		10			1.30				
6-5	0.94	0.55	0.23	7	6.05	6.04	0		0			1.98	0.06		0.51	
6-6	0.94	0.55	0.22	9	6.12	6.15	11.8	Dead	0			0.63	0.06		0.21	
6-7	0.94	0.55	0.22	4	6.12	6.17	100	Dead	0			0.62	0.11			
6-8	0.94	0.55	0.22	2	6.16	6.19	198	Dead	0			0.68				
6-9	0.94	0.55	0.22	15	6.40	6.35	368	Dead	0			b.d.	0.21		0.87	
6-10	1.05	0.62	0.02	21	6.10	6.19	0		0			13.10	0.14	5.09	3.29	0.04
6-11	1.00	0.59	0.02	26	6.23	6.32	200	Dead	0			b.d.	b.d.	b.d.	0.92	0.004
6-12	1.00	0.59	0.02	11	6.10	6.24	430	Dead	0			6.72	0.04	6.71	1.46	b.d.
6-13[e]	0.94	0.55	0.02	22	6.08	6.02	700	Live	0	2.8E + 07		4.45	0.58	b.d.	3.75	0.15
E5-1	0.98	0.57	0.02	8	n.m.	6.59	0		0			23.00	0.67	7.29	7.24	0.93
E5-2	0.98	0.57	0.02	7	n.m.	6.22	870	Live	0	6.0E + 07		15.90	0.29	11.4	2.80	0.34
E5-3	0.98	0.57	0.02	12	n.m.	7.15	6500	Live	0			8.51	0.52	9.63	2.80	0.70
E3-1	1.03	0.61	0.02	13	n.m.	7.43	0		10			18.16	6.38	7.56	11.44	2.22
E3-2	1.03	0.61	0.02	12	n.m.	7.78	8900	Live	10	9.0E + 08		18.65	3.45	5.89	5.06	2.17
E3-3	1.03	0.61	0.02	6	n.m.	7.62	12,000	Live	10			19.19	1.96	6.69	6.05	2.20
8-1	0.50	0.3	0.42	4	7.92	7.92	0		0			1.23				
8-2	0.50	0.3	0.28	3	7.94	7.91	0		0			1.18				
8-3	0.50	0.3	0.28	3	7.83	7.34	0		1			0.79				
8-4	0.50	0.3	0.28	6	7.89	7.67	0		10			0.46				
8-5	0.96	0.56	0.26	7	8.55	8.37	0		0			3.41	1.19		0.81	
8-6	0.96	0.56	0.26	9	8.46	8.24	12	Dead	0			2.41	0.78		0.49	
8-7	0.96	0.56	0.26	4	8.33	8.04	70	Dead	0			1.70	0.40			
8-8	0.96	0.56	0.26	2	8.55	8.04	195	Dead	0							
8-9	0.96	0.56	0.25	13	8.10	8.01	368	Dead	0			0.59	0.26		0.83	
8-10	1.01	0.59	0.03	21	8.55	8.89	0		0			28.32	10.53	2.32	5.54	0.89
8-11	0.99	0.58	0.03	26	8.57	8.63	200	Dead	0			11.57	2.53	0.56	3.13	0.05
8-12	0.99	0.58	0.02	11	8.36	8.61	430	Dead	0			34.43	1.10	12.5	5.06	b.d.
8-13[e]	0.98	0.58	0.02	22	8.53	7.93	700	Live	0	2.5E + 08	18.0	15.49	3.37	4.05	8.83	1.56
E6-1	1.06	0.63	0.02	8	n.m.	8.99	0.0		0			21.41	6.82	3.77	7.49	0.48
E6-2	1.06	0.63	0.02	7	n.m.	8.74	870	Live	0	8.3E + 07	8.4	18.69	4.34	9.31	5.80	0.70
E6-3	1.06	0.63	0.02	12	n.m.	8.48	6500	Live	0		33.3	18.37	2.47	4.84	7.45	0.20
E4-1	1.16	0.68	0.02	13	n.m.	8.02	0.0		10			20.54	3.26	6.54	5.72	1.83
E4-2	1.16	0.68	0.02	12	n.m.	8.06	8900	Live	10			17.87	2.15	4.37	6.01	1.34
E4-3	1.16	0.68	0.02	6	n.m.	7.90	19,000	Live	10			18.65	2.47	4.69	13.04	2.61
10-1	0.99	0.58	0.03	15	10.05	9.99	0		0			117.89	31.47	8.51	18.2	1.07
10-2	0.93	0.55	0.03	14	10.02	9.83	100	Dead	0			100.99	23.31	13.65	14.92	1.04
10-3	0.93	0.55	0.03	11	9.94	9.01	430	Dead	0			68.81	11.60	11.88	8.38	1.40
10-4[e]	0.80	0.47	0.02	22	10.11	8.35	700	Live	0	3.3E + 07	17.5	14.99	6.31	5.10	68.35	0.39

n.m.: not measured.
b.d.: below detection limit.
[a] Each experimental series is denoted by the solid horizontal lines drawn in the table.
[b] Concentration of *Pseudomonas reactans* in inlet ($Bact_{in}$) and outlet ($Bact_{out}$) solution measured in mg_{wet}/L and colony-forming units (CFU/mL), respectively.
[c] Dead *Pseudomonas reactans* (dead) plus NaN_3 or live *Pseudomonas reactans* (live) ± nutrient broth was added to the inlet solution.
[d] Concentration of element determined from its concentration in the outlet fluid minus its concentration in the inlet fluid.
[e] The amount of Si, Al, Ca, Mg and Fe in the inlet solutions is estimated from the concentration of these ions in experiments with the same inlet electrolyte and bacteria concentration.

experiment, all reactor system parts including tubing were sterilized at 130 °C for 30 min and rinsed with sterile MilliQ water.

The experiments conducted within in this study can be divided into three categories 1) bacteria- and nutrient-free, 2) dead bacteria in nutrient-free media, and 3) live bacteria. Live bacteria experiments can further be subdivided into two categories: 3a) nutrients added and 3b) no nutrients added. Experiments were performed in series. At the beginning of each series 0.5–1 g of fresh basaltic glass powder was added to the reactor system. A sterile bacteria-free fluid was injected into the reactor at a constant flow rate until a steady-state outlet fluid composition was attained. This provided a reference point, to compare results with subsequent bacteria-bearing dissolution experiments. Once steady state was attained, live or dead bacteria ± nutrients or sodium azide (NaN_3) were added to this inlet solution. Sodium azide was added to the inlet fluids containing dead bacteria to avoid any possible external contamination and bacterial growth during the experiment. Additional live or dead bacteria were added to the inlet fluid after a second steady-state element release rate was attained. This step was repeated until the experimental series was stopped. To assess the effect of nutrients on rates, a 1:10 diluted Aldrich nutrient

Table 3b
Steady-state dissolution rates, log ($r_{+,I,j}$/(mol/cm^2/s)) for basaltic glass at 25 °C determined in the present study.

Exp. [a]	pH_{out} (25 °C)	$Bact_{in}$ [b] (mg/L)	Bact. status [c]	$Nutr_{in}$ (%)	A* [d,e] (kJ/mol)	Log $r_{+,Si,BET}$	Log $r_{+,Si,geo}$	Log $r_{+,Al,BET}$	Log $r_{+,Al,geo}$	Log $r_{+,Ca,BET}$	Log $r_{+,Ca,geo}$	Log $r_{+,Mg,BET}$	Log $r_{+,Mg,geo}$	Log $r_{+,Fe,BET}$	Log $r_{+,Fe,geo}$
4-1	4.33	0		0	18.15	−14.57	−13.20	−14.48	−13.11	−14.19	−12.82	−14.17	−12.80	−14.37	−13.00
4-2	4.63	100	Dead	0		−14.94	−13.57	−15.45	−14.08			−15.04	−13.67	−15.66	−14.29
4-3	4.58	430	Dead	0		−15.10	−13.73	−15.54	−14.17	−14.83	−13.46	−15.16	−13.79	−15.78	−14.41
4-4	7.44	700	Live	0		−15.11	−13.74	−16.11	−14.74	−15.24	−13.87	−14.95	−13.58	−16.09	−14.72
6-1	5.92	0		0	23.46 [f]	−14.96	−13.59								
6-2	5.98	0		0	22.20 [f]	−15.01	−13.64								
6-3	6.38	0		1		−15.18	−13.81								
6-4	6.44	0		10		−14.83	−13.46								
6-5	6.04	0		0	21.40 [g]	−14.87	−13.50	−15.93	−14.56			−14.93	−13.56		
6-6	6.15	11.8	Dead	0		−15.37	−14.00	−15.94	−14.57			−15.32	−13.95		
6-7	6.17	100	Dead	0		−15.38	−14.01	−15.68	−14.31						
6-8	6.19	198	Dead	0		−15.35	−13.98								
6-9	6.35	368	Dead	0				−15.40	−14.03			−14.71	−13.34		
6-10	6.19	0		0	15.81 [g]	−15.09	−13.72	−16.59	−15.22	−14.92	−13.55	−15.16	−13.79	−16.88	−15.51
6-11	6.32	200	Dead	0								−15.75	−14.38	−17.92	−16.55
6-12	6.24	430	Dead	0		−15.47	−14.10	−17.23	−15.87	−14.89	−13.52	−15.59	−14.22		
6-13	6.02	700	Live	0		−15.57	−14.20	−16.00	−14.63			−15.11	−13.74	−16.31	−14.94
E5-1	6.59	0		0	13.18 [g]	−14.87	−13.50	−15.95	−14.58	−14.79	−13.42	−14.84	−13.47	−15.54	−14.17
E5-2	6.22	870	Live	0		−15.06	−13.69	−16.34	−14.97	−14.62	−13.25	−15.28	−13.91	−16.00	−14.63
E5-3	7.15	6500	Live	0		−15.31	−13.94	−16.06	−14.69	−14.67	−13.30	−15.25	−13.88	−15.66	−14.29
E3-1	7.43	0		10		−15.00	−13.63	−15.00	−13.63	−14.80	−13.43	−14.67	−13.30	−15.19	−13.82
E3-2	7.78	8900	Live	10		−14.99	−13.62	−15.27	−13.90	−14.91	−13.54	−15.02	−13.65	−15.20	−13.83
E3-3	7.62	12,000	Live	10		−15.00	−13.63	−15.53	−14.17	−14.88	−13.51	−14.97	−13.60	−15.21	−13.84
8-1	7.92	0		0	23.17 [f]	−14.53	−13.17								
8-2	7.91	0		0	23.34 [f]	−14.73	−13.36								
8-3	7.34	0		1		−14.90	−13.53								
8-4	7.67	0		10		−15.13	−13.76								
8-5	8.37	0		0	20.72	−14.58	−13.21	−14.58	−13.21			−14.67	−13.30		
8-6	8.24	12	Dead	0		−14.73	−13.36	−14.76	−13.40			−14.89	−13.52		
8-7	8.04	70	Dead	0		−14.89	−13.52	−15.06	−13.69						
8-8	8.04	195	Dead	0											
8-9	8.01	368	Dead	0		−15.36	−13.99	−15.26	−13.89			−14.67	−13.30		
8-10	8.89	0		0	16.50	−14.70	−13.33	−14.68	−13.31	−15.21	−13.84	−14.88	−13.51	−15.48	−14.11
8-11	8.63	200	Dead	0		−15.08	−13.71	−15.29	−13.92	−15.82	−14.45	−15.12	−13.75	−16.72	−15.35
8-12	8.61	430	Dead	0		−14.73	−13.36	−15.77	−14.40	−14.59	−13.22	−15.03	−13.66		
8-13	7.93	700	Live	0		−14.99	−13.62	−15.20	−13.83	−14.99	−13.62	−14.70	−13.33	−15.26	−13.89
E6-1	8.99	0.0		0	16.15	−14.92	−13.55	−14.96	−13.59	−15.10	−13.73	−14.84	−13.47	−15.84	−14.47
E6-2	8.74	870	Live	0		−14.96	−13.59	−15.14	−13.77	−14.68	−13.31	−14.93	−13.56	−15.66	−14.29
E6-3	8.48	6500	Live	0		−14.95	−13.58	−15.36	−13.99	−14.95	−13.58	−14.81	−13.44	−16.18	−14.81
E4-1	8.02	0.0		10		−15.00	−13.63	−15.34	−13.97	−14.91	−13.54	−15.02	−13.65	−15.32	−13.95
E4-2	8.06	8900	Live	10		−15.08	−13.71	−15.54	−14.17	−15.11	−13.74	−15.02	−13.65	−15.48	−14.11
E4-3	7.90	19,000	Live	10		−15.08	−13.71	−15.51	−14.14	−15.10	−13.73	−14.70	−13.34	−15.21	−13.84
10-1	9.99	0		0	16.44	−14.06	−12.69	−14.18	−12.81	−14.62	−13.25	−14.33	−12.96	−15.37	−14.00
10-2	9.83	100	Dead	0		−14.11	−12.75	−14.30	−12.93	−14.40	−13.03	−14.41	−13.04	−15.37	−14.00
10-3	9.01	430	Dead	0		−14.26	−12.89	−14.58	−13.21	−14.45	−13.08	−14.64	−13.27	−15.23	−13.86
10-4	8.35	700	Live	0		−14.90	−13.53	−14.82	−13.45	−14.78	−13.42	−13.70	−12.33	−15.75	−14.38

[a] Each experimental series is denoted by the solid horizontal lines drawn in the table.
[b] Concentration of *Pseudomonas reactans* in inlet ($Bact_{in}$) solution measured in mg_{wet}/L.
[c] Either dead *Pseudomonas reactans* plus NaN_3 or live *Pseudomonas reactans* was added to the inlet solution.
[d] Chemical affinity of hydrated basaltic glass layer.
[e] Calculated by PHREEQC modeling version 2.17.
[f] Calculated with hypothetical stoichiometric release of [Al].
[g] Modeled with PHREEQC assuming same inlet solution as in experiments 6-1 to 6-4.

broth, comprised of 0.1 g/L glucose, 1.5 g/L peptone, 0.6 g/L NaCl, and 0.3 g/L yeast extract, was added to selected live bacteria experiments. These experiments were compared to live bacteria experiments performed with no added nutrients. During 4 of the experimental series (following experiments 4–3, 6–12, 8–12, and 10–3) less than 10% of the basaltic glass was removed for SEM analysis. In all other cases, all of the original basaltic glass remained in the reactor until the experimental series was completed.

The chemical compositions of each individual inlet solution used for the experiments in this study are listed in Appendix 1 along with its ionic strength and pH at 25 °C. Inlet fluids were comprised of MilliQ water and analytical grade chemicals including NH_4Cl, NH_4OH, Na-acetate, $C_6H_{13}NO_4S$ ('MES' buffer), $NaHCO_3$, Na_2CO_3, NaCl (99.5% pure), HCl, and NaOH. Experimental series were performed using four distinct inlet pH buffers: 4, 6, 8, and 10, comprised of a 0.01 M Na acetate–NaCl–HCl solution, a 0.001 M or 0.01 M MES solution, a 0.01 M $NaHCO_3$ solution, and a 0.004 M $NaHCO_3$ + 0.003 M Na_2CO_3 solution, respectively. The ionic strength was ~0.01 mol/kg for the pH 4, 8, and 10 inlet fluids and 0.001 or 0.01 mol/kg for the pH 6 inlet fluids. Inlet fluid pH generally remained stable within ±0.1 units throughout each experimental series. Outlet fluid pH varied within ±0.3 units, except for the live bacteria experiments performed at pH 4 and 10,

where pH changed by as much as ±3.0 units from the initial to the steady-state value. All outlet fluid samples were filtered through 0.45 μm Millipore acetate cellulose filters and acidified with ultrapure 2% HNO_3 before chemical analysis. The exception was samples collected for dissolved organic carbon determination, which were filtered and stored at 4 °C before the analysis. Inlet fluids were routinely analyzed at the beginning, in the middle, and at the end of each experiment and were filtered and processed using exactly the same protocol as the outlet fluids. All chemistry data for the outlet fluids at steady-state are provided in Tables 3a and 3b.

To assess possible adsorption of released aqueous metals to biomass surfaces additional non-filtered outlet fluid samples were collected, and 0.01 M EDTA was added to these unfiltered samples. After 10 min the biomass was separated using centrifugation. The amount of Mg, Ca, and Al released to the fluid after this EDTA treatment was considered to be reversibly adsorbed on the surface (e.g., Knauer et al., 1997; Le Faucher et al., 2005). This amount never exceeded 10% of total dissolved (<0.45 μm) filtered concentration of each metal and therefore was not considered in the mass balance calculations presented below.

Mechanical steady state was achieved in the BMFR after 24 h of reaction. Chemical steady state was assumed when measured Mg, Ca, Al, Si, and trace metal concentrations varied by less than 5% for concentrations of ≥5 μM but 15% for concentrations of <5 μM in 4 to 5 samples collected at least 24 h apart. Measured steady-state Mg, Ca, Al, Si, and trace metal concentrations and fluid flow rates (reproducibility of ±10%) were used for calculating dissolution rates. The largest uncertainty on reported rates generated in this study stem from the ΔC_i values in Eq. (2). As the analytical uncertainty was 5–10% and the experimental reproducibility was 10–20% the overall uncertainty on log $R_{Me,}$ and log R_{Si} values reported in this study range from 0.1 to 0.2 units.

3.4. Batch experiments performed to assess live bacteria interaction with mineral-free solutions in the presence of mineral constituents

These experiments were designed to quantify the amount of basaltic glass constituents (Mg, Ca, Al, Si, metals) retained by bacteria via both long-term intracellular uptake (e.g. active assimilation) and passive cell wall adsorption. They also provide insight into the bioprecipitation processes that might occur on the cell walls or in the media due to metabolically induced fluid chemistry changes. In addition, these experiments provide insight into potential element release originating from the bacterial biomass as a result of cell lyses. Duplicate experiments were performed in closed-system 250-mL polypropylene containers with 1 to 8.5 g_{wet}/L rinsed biomass of *P. reactans* HK 31.3 and initial concentrations of Si, Ca, Mg, Fe, Al, Sr, and As ranging from 2 to 3500 μg/L. Three types of aqueous fluids were used: 1) a 0.1 M NaCl and 0.01 M $NaHCO_3$ solution amended with a 10% NB protein-rich media to allow active bacterial growth and intracellular uptake in cells, 2) the same media with 0.01 M NaN_3 added to prevent bacterial metabolism to assess metal interaction with bacterial cell walls without active assimilation, and 3) a nutrient-free 0.1 M NaCl + 0.01 M $NaHCO_3$ solution with 0.01 M NaN_3 added to allow cell lysis but minimum element uptake. The typical duration of these experiments was 220 h. The 250-mL polypropylene reactor vessels with biomass were aerated and shaken in the dark at 25 °C and periodically sampled. For each sampling, 10 mL

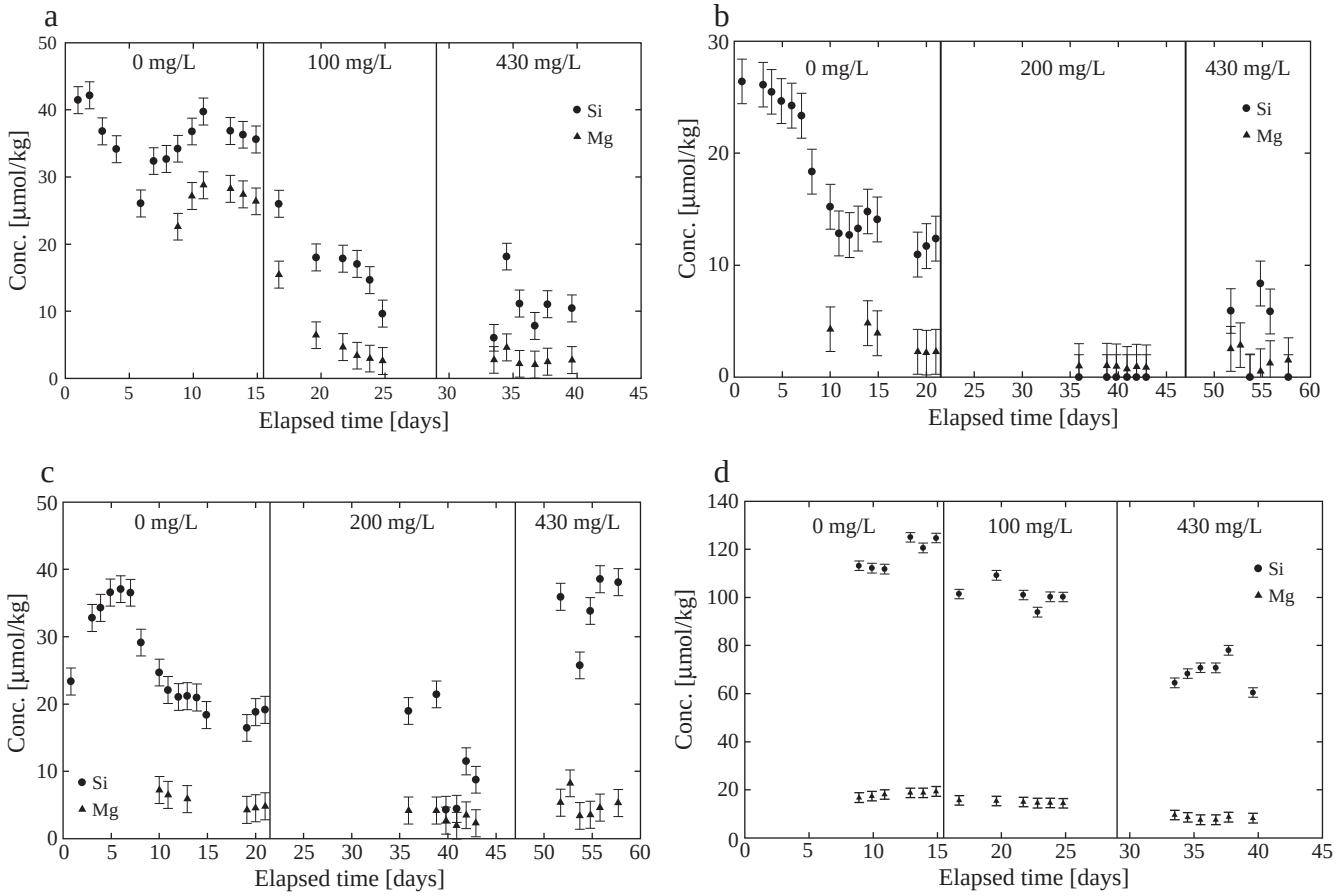

Fig. 3. Total dissolved Si and Mg concentration evolution as a function of time during basaltic glass dissolution experiments with 0, 100 or 200, and 430 mg_{wet}/L dead *Pseudomonas reactans* HK 31.3 added sequentially to the inlet fluid at 25 °C and (a) pH ~4 (exps. 4-1 to 4-3), (b) pH ~6 (exps. 6-10 to 6-12), (c) pH ~8 (exps. 8-10 to 8-12), and (d) pH ~10 (exps. 10-1 to 10-3). The filled circles and diamonds correspond to measured Si and Mg concentrations. The error bars in these plots correspond to ±2 μmol/kg uncertainty.

aliquots of homogeneous solution + bacteria were collected using sterile serological pipettes and transferred in sterile polystyrene vials for pH, optical density, bacterial number by agar plate counting. Aqueous metal concentrations were measured in these samples after they were filtered through a 0.45 μm membrane. The biomass/fluid ratio remained constant during experiments and the concentration of bacteria was not affected by the sampling. Sterile controls were routinely run using both nutrient media and 0.01 M NaCl solutions; no bacterial contamination was detected.

3.5. Analytic methods

Filtered solutions were analyzed for all elements using a Agilent 7500 Ion Coupled Plasma Mass Spectrometer (ICP-MS), the 'molybdate blue method' for silicon (Koroleff, 1976), and a Perkin Elmer Zeeman 5000 Atomic Absorption Spectrometer (AAS) for magnesium and aluminum. ICP-MS measurements were made with and without helium gas. Indium and rhenium were used as internal standards, and corrections for oxide and hydroxide ions were made for the rare earth elements (REE) and metals (Ariés et al., 2000). The international geostandard SLRS-4 (Riverine Water Reference Material for Trace Metals certified by the National Research Council of Canada) was used to check the accuracy and reproducibility of each analysis (Yeghicheyan et al., 2001). We obtained good agreement between replicated measurements of SLRS-4 and the certified values (relative difference<10%), except for B and P (30%).

Selected solid samples were examined using a JEOL 6360 LV and a JEOL JSM840a Scanning Electron Microscope (SEM) after gold or graphite metallization, and by X-ray Photoelectron Spectroscopy (XPS). Energy Dispersive X-ray Spectroscopy (EDS) was used together with SEM to identify primary and secondary mineral phases, and to detect organic signals originating from the bacteria itself or from bacterial processes. XPS analyses used to quantify the stoichiometry of the basaltic glass surface (<100 Å) layer, were performed using a Kratos Axis Ultra DLD instrument. The excitation energy was a monochromatic AlKα ($h\nu = 1486.6$ eV) at a power of 180 W. The base pressure in the chamber was 5×10^{-10} Torr and never exceeded 5×10^{-9} Torr. A charge balance system was used to compensate for surface charging and for the adventitious carbon. For survey scans, a pass energy of 160 eV and a step size of 0.5 eV was used, and for high resolution scans, these settings were 10 eV and 0.1 eV, respectively. Data interpretation was made with the commercial software CasaXPS, using a Shirley background. The uncertainty for these analysis methods is estimated to 5% for the ICP-MS, 3% for the spectrophotometer, 2% for the AAS analysis, and 10% for the XPS analysis.

4. Experimental results

In total 46 steady-state basaltic glass dissolution experiments were performed in this study. The steady-state fluid chemistry of these 46 experiments is listed according to pH in Tables 3a and 3b, and the

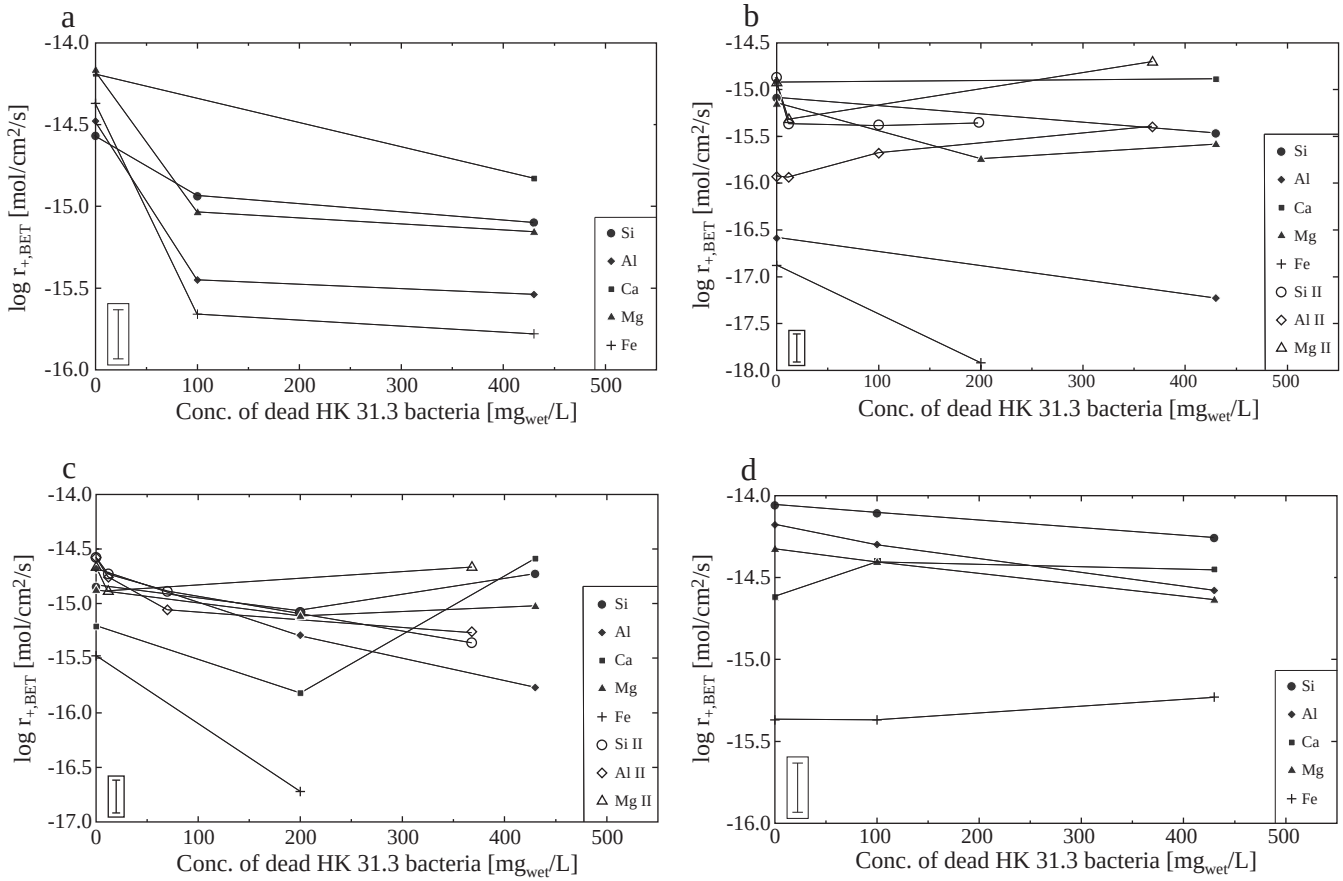

Fig. 4. Measured basaltic glass dissolution rates based on Si, Al, Ca, Mg and Fe during experiments with dead *Pseudomonas reactans* HK 31.3 sequentially added to the inlet fluids at 25 °C and (a) pH ~4 (exps. 4-1 to 4-3), (b) pH ~6 (exps. 6-10 to 6-12, and 6-5 to 6-9), (c) pH ~8 (exps. 8-10 to 8-12, and 8-5 to 8-9), and (d) pH ~10 (exps. 10-1 to 10-3). The symbols are defined in the legend shown in the figure. The error bars in the lower left of each plot correspond to ±0.15 log units uncertainty on the rates.

main results of these mixed-flow reactor experiments are described in Sections 4.1 and 4.2 below.

4.1. Basaltic glass dissolution in the presence of dead bacteria in BMFR

To test the effect of dead *P. reactans* on the basaltic glass dissolution rates over a broad pH-range, four dissolution experiment series were performed at pH ranging from 4 to 10 at 25 °C (experiments 4-1 to 4-3, 6-10 to 6-12, 8-10 to 8-12, and 10-1 to 10-3). Fig. 3 shows the fluid Si and Mg concentrations originating from basaltic glass dissolution as a function of elapsed time as the dead bacteria concentration was increased. Steady-state Si and Mg concentrations were attained within a few days after the bacteria were added to the system. There was a general trend of a decreasing Si concentration with increasing dead bacteria concentration in each series (see Fig. 3). This effect was less pronounced for Mg. Dissolution rates for these experiments based on the five major elements, Si, Al, Ca, Mg, and Fe are shown in Fig. 4. These plots suggest that the presence of dead bacteria inhibited basaltic glass dissolution rates by as much as a 0.5 log units during experiments 4-1 to 4-3. Some of this decrease likely stems from the shift in outlet solution pH due to cell lysis and organic matter release from the dead cells (see Section 5.1 below). The DOC concentration in the dead bacteria experiments typically varied from 10 to 30 mg/L for the biomass range from 1 to 6.5 g_{wet}/L, suggesting the presence of cell lysis products in the reactive fluids.

PHREEQC modeling of the initial bacteria-free system indicates that Al-phases (i.e. boehmite, diaspore, gibbsite) were supersaturated in the pH ~4 outlet fluids of experiments 4-1 to 4-3, which could explain, at least in part, the observed decrease in fluid phase Al concentration, when the dead bacteria were added (see Fig. 4a). There is no obvious saturated iron phase that could explain the decrease in Fe, but this could be due to Fe^{3+} and/or $FeOH^{2+}$ adsorption onto dead bacteria surfaces. At pH ~6 (experiments 6-10 to 6-12), both Al- and Fe-hydroxides (i.e. gibbsite, goethite) were highly supersaturated and most likely contributed to the initially low Al and Fe release rates observed in Fig. 4b. However, in an additional experimental series conducted at this pH (experiments 6-5 to 6-9), Al release exhibited slightly increasing rates (see Fig. 4b). The presence of cell lysis products could increase oxy(hydr)oxide solubility via aqueous complexing of Al and Fe with DOC. Unfortunately, this process cannot be quantified due to lack of knowledge of the identity of the organic ligands present and the paucity of metal–ligand stability constants. In contrast to Fe and Al, the Si, Mg and Ca dissolution rates did not show any distinct evolution with increasing dead bacteria concentration at near to neutral pH. According to thermodynamic calculations, the outlet solutions of experiments 10-1 to 10-3 were supersaturated with respect to several secondary phases including calcite, aragonite, gibbsite, kaolinite, smectite, mesolite, natrolite, scolecite, and stilbite. Nevertheless, the results of these pH ~10 experiments showed only a slight decrease in dissolution rates based on Si, Al, and Mg release of 0.2–0.4 log units in the presence of dead bacteria (see Fig. 4d), which is almost within the ±0.15 log unit experimental uncertainty of the combined measurements. The basaltic glass itself was strongly undersaturated in all of the initial bacteria-free experiments with an A* greater than 10 kJ/mol (see Table 3b),

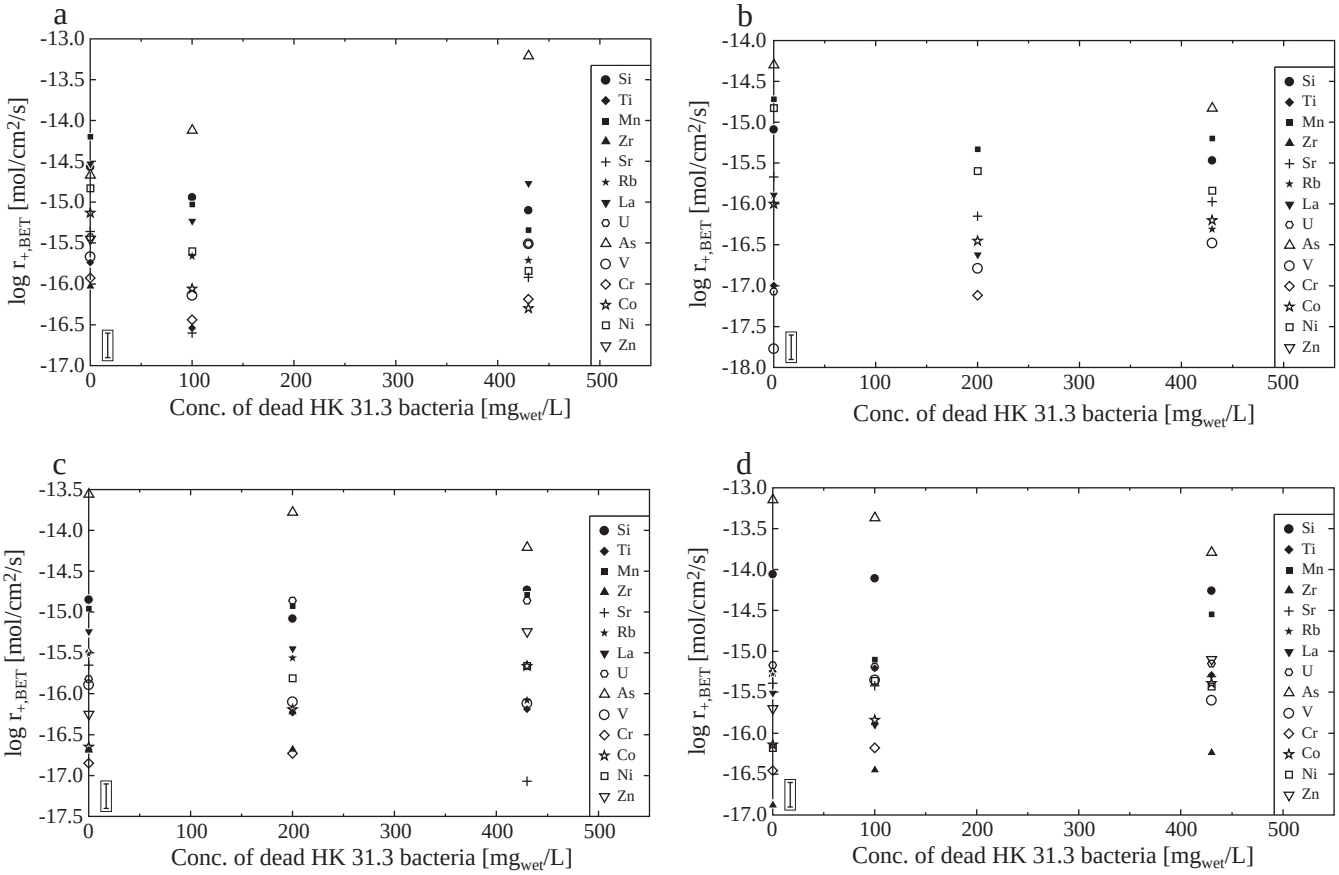

Fig. 5. Measured basaltic glass dissolution rates based on trace element release during experiments with dead *Pseudomonas reactans* HK 31.3 sequentially added to the inlet fluids at 25 °C and (a) pH ~4 (exps. 4-1 to 4-3), (b) pH ~6 (exps. 6-10 to 6-12), (c) pH ~8 (exps. 8–10 to 8-12), and (d) pH ~10 (exps. 10-1 to 10-3). The symbols are defined in the legend shown in the figure. The error bars in the lower right of each plot correspond to ±0.15 log units uncertainty on the rates.

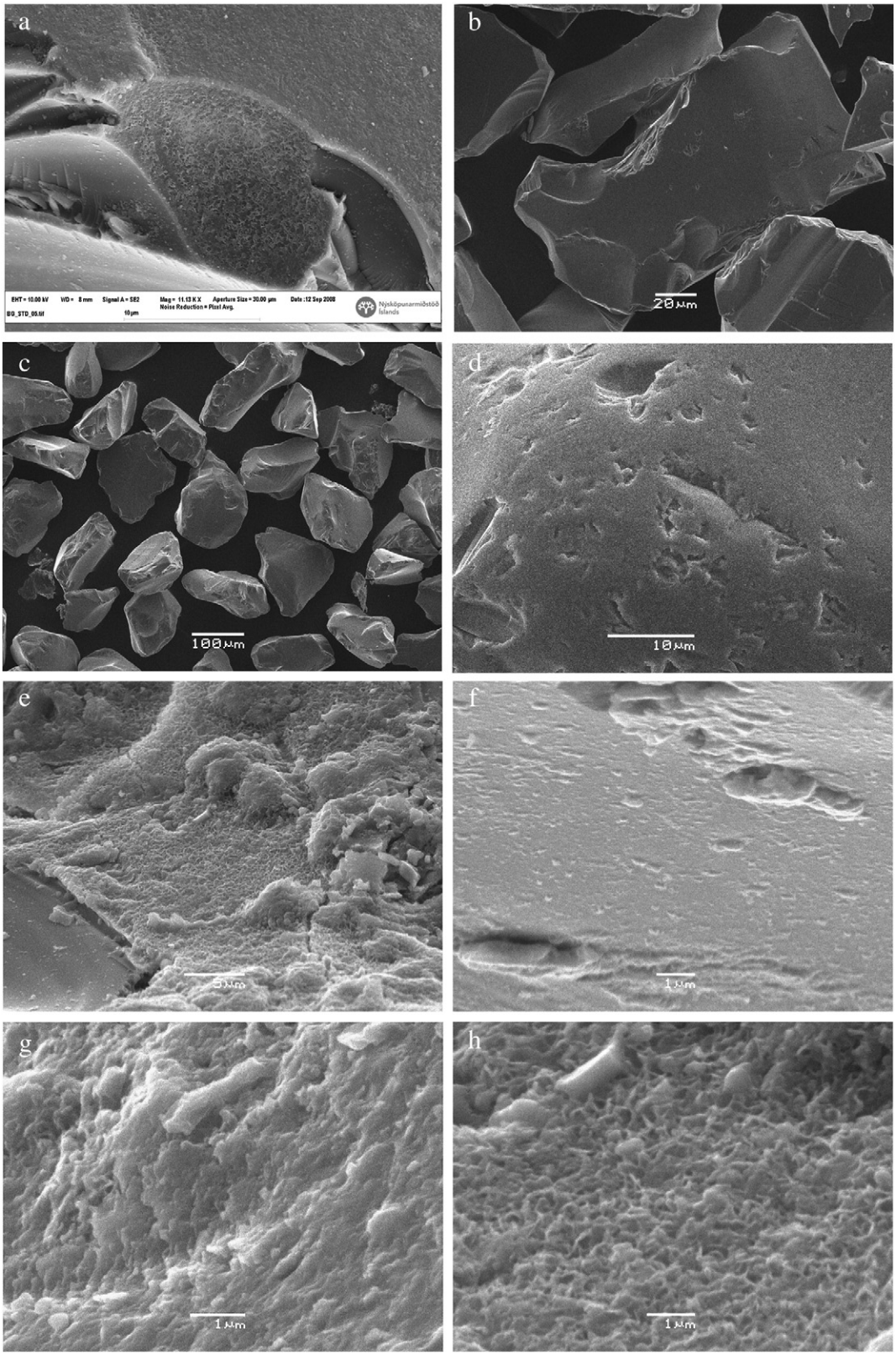

Fig. 6. Scanning Electron images of basaltic glass surfaces: a) basaltic glass surface prior to experiments, b) after experiments 10-1 to 10-3 performed in the presence of dead bacteria, c) and d) after experiments 8-10 to 8-13 performed in the presence of dead bacteria showing rounded particles and dissolution etch pits, e) after experiments E5-1 to E5-3 performed in the presence of live bacteria and nutrients showing biofilm-looking coverage of the surface, f) after experiments E3-1 to E3-3 performed in the presence of live bacteria experiment and nutrients showing bacterial "imprints", g) and h) close-up of biofilm coverage of glass surfaces after experiments E5-1 to E5-3 and E3-1 to E3-3, respectively.

where A* refers to the chemical affinity of the hydrated basaltic glass in Eq. (1).

Dissolution rates based on selected trace elements, Ti, Mn, Zr, Sr, Rb, La, U, As, V, Cr, Co, Ni and Zn are plotted on Fig. 5 as a function of fluid phase dead bacteria concentration. Among studied elements, only arsenic (As) at pH ~4 showed increasing release rates, of 0.5–1.5 log units, in the presence of dead bacteria (see Fig. 5a), whereas at pH 8–10, a 0.5-order of magnitude decrease in As release rate was observed (see Fig. 5c, d). Note also that there was an order of magnitude increase of Cr release rates with increasing dead biomass concentration at pH 8–10. Other than for these exceptions, the other trace elements generally showed the same pattern as the major elements. Their rates, however, tend to be lower than those predicted from Si rates and the stoichiometry of basaltic glass (see Table 1). Of the trace elements, only arsenic appeared to have higher stoichiometric release rates than Si based on XRF analysis (see Fig. 5a–d).

SEM photos of the basaltic glass prior to experiments were compared with glass from bacteria-free and post-bacterial experiments in Fig. 6a–d. The only dissolution features evident are etch pits (see Fig. 6d); there is no evidence of a specific effect due to either the dead bacteria or their lysis products. In general, the post-experimental glass surfaces appeared smooth and free of secondary precipitates.

4.2. Basaltic glass dissolution in the presence of live bacteria in BMFR

Similar experiments were performed in the presence of live bacteria. Fig. 7 illustrate the temporal evolution of Si and Mg concentration in the fluid phase as live bacteria were added to the inlet fluids. Note the presence of live bacteria shifts the inlet fluid pH from pH 4 and 10 towards neutral in the outlet fluid likely due to bacterial metabolism. As such these experiments were only run at pH 6 to 8.7 corresponding to the natural pH range of *P. reactans* growth (Shirokova et al., 2012). Various bacteria concentrations were tested in experiments with and without nutrients added to the inlet fluids to assess the effect of bacterial nutritional status on element release rates from basaltic glass.

No significant decrease in outlet fluid Si concentration was found for experiments with live bacteria (see Fig. 7), except for experiments E5–1 to E5–3 performed with no added nutrients (see Fig. 7a). In this one instance a 50% decrease in Si release rates with increasing bacteria concentration from 0 to 6.5 g_{wet}/L was observed. The release rates of the five major elements of basaltic glass shown in Fig. 8 depicts an interesting effect of nutrient addition. As described above for dead cells, Al- and Fe-hydroxide precipitates are almost unavoidable at pH 6 to 8. However, in the presence of nutrients, basaltic glass dissolution shows almost perfect stoichiometric behavior even at neutral pH. This is interpreted to be a consequence of the presence of organic molecules, originating from the nutrients, which contains peptone or yeast extract, which can complex Al and Fe ions in aqueous solution. This change of aqueous Fe and Al speciation increased the stability of these elements in the fluid phase preventing secondary precipitate formation.

Trace elements follow the same pattern as the major elements in response to the addition of live bacteria (not shown). Mn and Ti are released stoichiometrically when nutrients are added, but the remaining

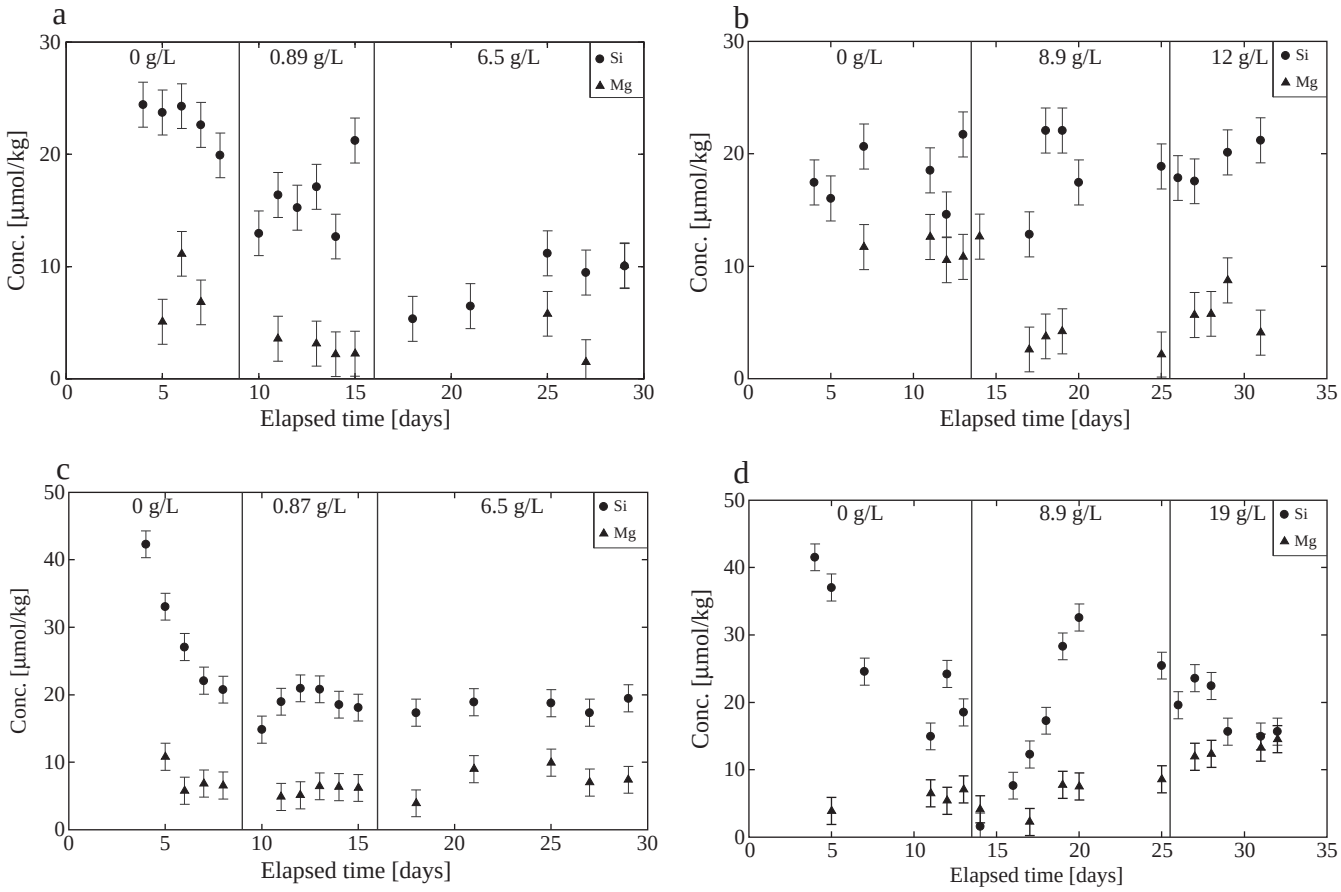

Fig. 7. Total dissolved Si and Mg concentration evolution as a function of time during basaltic glass dissolution experiments in the presence of selected live *Pseudomonas reactans* HK 31.3 concentrations at 25 °C and a) pH 6 to 7 without nutrients (exps. E5-1 to E5-3), b) pH ~7.5 with 10% nutrient broth (exps. E3-1 to E3-3), c) pH 8.5 to 9 without nutrients (exps. E6-1 to E6-3), and d) pH ~8 with 10% nutrient broth (exps. E4-1 to E4-3). The filled circles and diamonds correspond to measured Si and Mg concentrations. The error bars correspond to ±2 µmol/kg uncertainty.

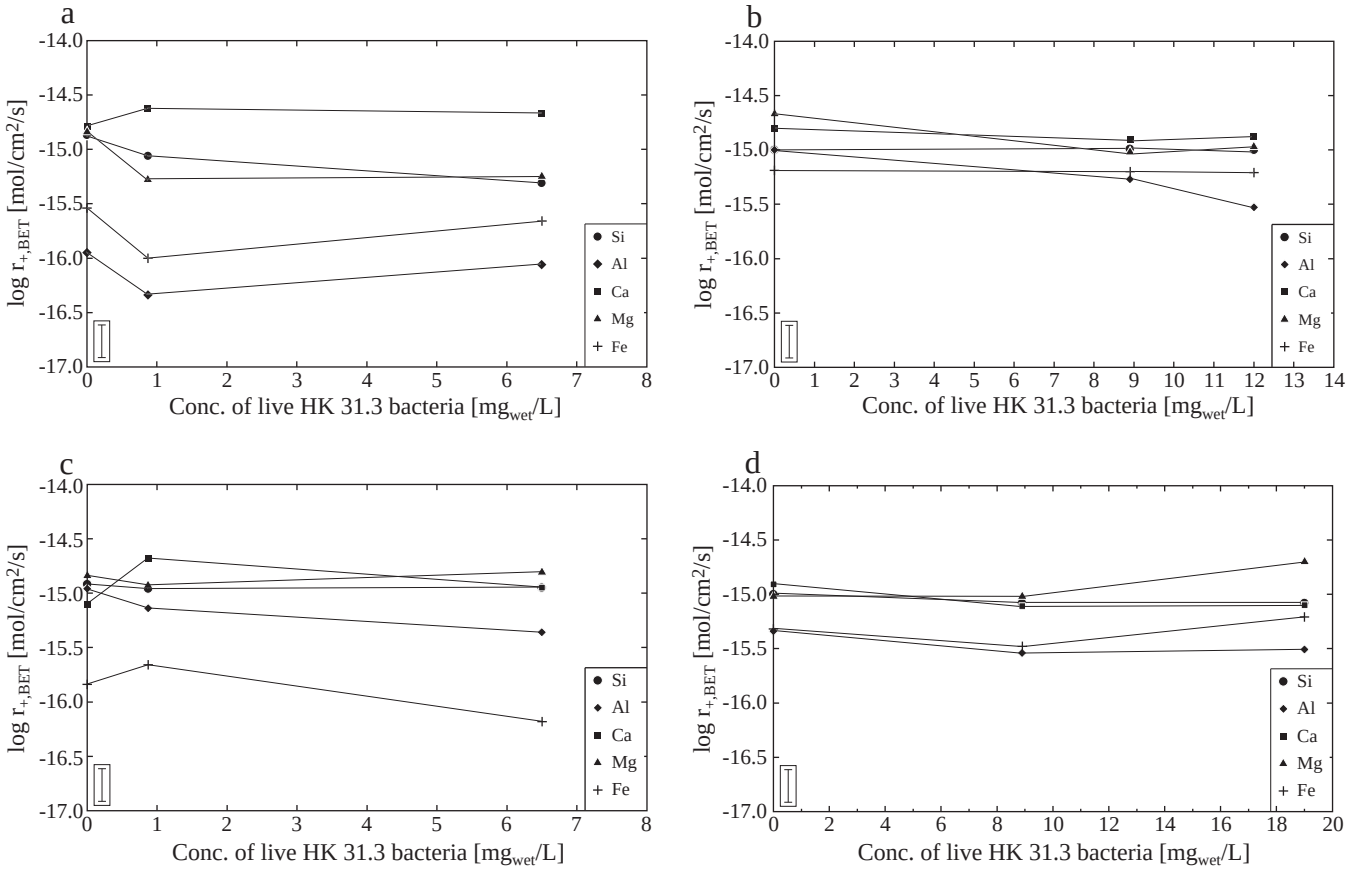

Fig. 8. Measured basaltic glass dissolution rates based on Si, Al, Ca, Mg and Fe release during experiments performed with live *Pseudomonas reactans* HK 31.3 added to the inlet fluids at 25 °C and at a) pH 6 to 7 without nutrients (exps. E5-1 to E5-3), b) pH ~7.5 with 10% nutrient broth (exps. E3-1 to E3-3), c) pH 8.5 to 9 without nutrients (exps. E6-1 to E6-3), and d) pH ~8 with 10% nutrient broth (exps. E4-1 to E4-3). The symbols are defined in the figure. The error bars in the lower right of each plot correspond to ±0.15 log units uncertainty on the rates.

trace elements do not show any distinct dissolution patterns. Arsenic concentration is below the analytical detection limit (~0.01 ppb) for the majority of the live bacteria experiments and therefore no substantial increase in its release rates is observed, in contrast with the experiments conducted with dead bacteria. The difficulty of quantifying trace element release rates in experiments with live bacteria may result from 1) their uptake by the bacteria (discussed below), 2) analytical uncertainty in the ICP-MS analysis (±5%), or 3) the small

Table 4
Results of X-ray photoemission spectroscopy (XPS) analysis of basaltic glass surfaces.

Sample:[a]	Atomic percentage ratio										
	C/Si	O/Si	Si/Si	Fe/Si	Mg/Si	Ca/Si	Na/Si	Ti/Si	P/Si	Al/Si	N/Si
Basaltic glass original 1	0.22	2.48	1.00	0.08	0.15	0.10	0.01	0.02	0.00	0.35	0.00
Basaltic glass original 2	0.21	2.56	1.00	0.09	0.17	0.09	0.02	0.02	0.00	0.34	0.00
Basaltic glass original av.	0.22	2.52	1.00	0.09	0.16	0.10	0.02	0.02	0.00	0.34	0.00
8-13[b]											
Post expt. 8-13 live 1	0.59	2.46	1.00	0.05	0.10	0.05	0.04	0.02	0.00	0.34	0.09
Post expt. 8-13 live 2	0.60	2.32	1.00	0.04	0.12	0.06	0.04	0.01	0.00	0.33	0.09
Post expt. 8-13 av.	0.60	2.39	1.00	0.05	0.11	0.06	0.04	0.02	0.00	0.33	0.09
E6-3[b]											
Post expt. pH 8 live, no nutr. 1	1.74	2.73	1.00	0.06	0.07	0.03	0.01	0.02	0.05	0.45	0.22
Post expt. pH 8 live, no nutr. 2	1.79	2.74	1.00	0.08	0.06	0.04	0.01	0.02	0.07	0.43	0.25
Post expt. pH 8 live, no nutr. av.	1.76	2.73	1.00	0.07	0.07	0.03	0.01	0.02	0.06	0.44	0.23
E4-3[b]											
Post expt. pH 8 live, 10% nutr. 1	2.66	2.63	1.00	0.04	0.10	0.03	0.00	0.01	0.00	0.39	0.41
Post expt. pH 8 live, 10% nutr. 2	2.49	2.47	1.00	0.04	0.11	0.03	0.00	0.01	0.00	0.40	0.36
Post expt. pH 8 live, 10% nutr. av.	2.57	2.55	1.00	0.04	0.10	0.03	0.00	0.01	0.00	0.40	0.38

[a] There is a duplicate ('2') of each analysis, and the average is listed in the line marked "sample name" and "av."
[b] Refers to exp. names in Tables 3a–3b.

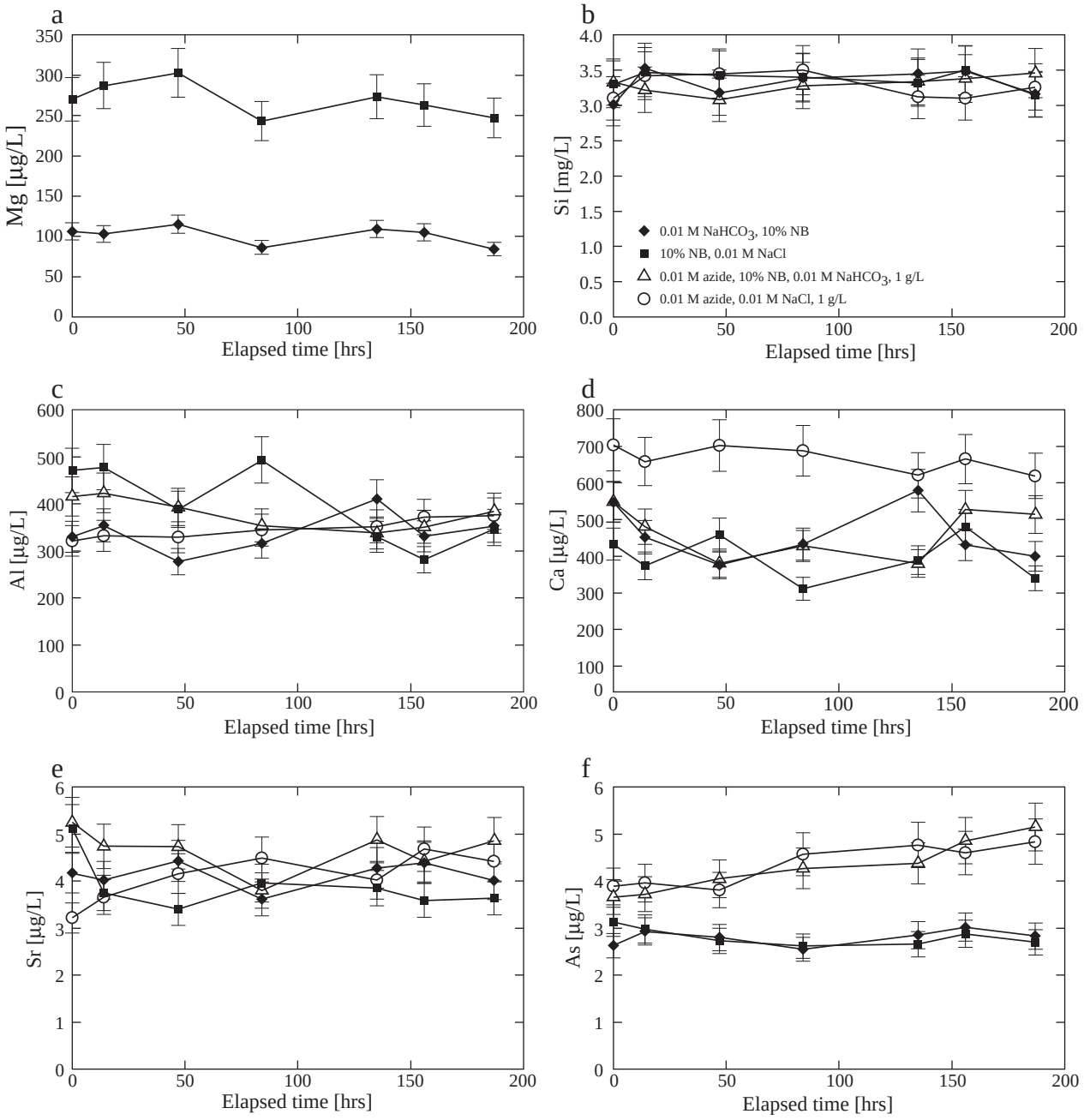

Fig. 9. Temporal evolution of dissolved Mg, Si, Al, Ca, Sr, and As concentration in closed system mineral-free experiments with live bacteria performed in an aqueous 0.01 M NaCl, 10% NB inlet fluid, and inactivated bacteria performed in an aqueous 0.01 M NaN_3 inlet fluid. The biomass concentration increased from 0.1 to 1.2 g_{wet}/L for live bacteria experiments (black diamonds and squares) and stayed constant at 1 g_{wet}/L for inactivated bacteria (white triangles and circles). The error bars correspond to the estimated uncertainty and reproducibility of the measurements, which ranged from 7 to 10%.

difference between the inlet and outlet concentration of these elements at steady-state. In any case, it is clear that the presence of live bacteria does not lead to any large increases (≥30%) in trace element release rates from basaltic glass into the fluid compared to bacteria-free experiments.

SEM images of basaltic glass samples collected after the live bacteria experimental series show the presence of a biofilm-looking layer on the glass surfaces (see Fig. 6e). Furthermore, some surface features suggestive of bacterial imprints are observed (see Fig. 6f) which contrast to typical dissolution features such as etch pits (see Fig. 6d). However, this biofilm-like layer is patchy and heterogeneous as most surfaces appear clear and smooth.

Results of post-experimental basaltic glass surface analysis by XPS provided in Table 4 show a depletion in surface Fe, Mg, and Ca concentration, consistent with cation leaching, and some Al enrichment, perhaps in the form secondary phases, not explicitly identified during SEM analyses. An enrichment in C and N, especially in experiments performed at pH ~8 with live cultures in nutrient media, confirms the presence of biofilms as inferred from the SEM observations (see Fig. 6e, g, h).

BET surface area measurements of the basaltic glass at the end of experiments with live bacteria yielded the value close to 3000 cm^2/g, which is ~50% lower than the initial BET surface area. It supports the observations made by comparing various SEM images that the

basaltic glass grains were smoothed and rounded during the experiments. There is therefore no indication that the presence of live *P. reactans* increased specific surface area.

4.3. Element assimilation and release by bacteria cells in basaltic glass free, closed-system batch experiments

The temporal evolution of fluid phase Mg, Ca, Al, Si, and trace element concentrations in basaltic glass-free, closed-system batch experiments with live and dead bacteria and in nutrient-free media is shown in Fig. 9; a summary is provided in the electronic annex. In Mg-poor fluids (100–300 μg/L) and nutrient-rich media there is a ≤10% decrease of Mg concentration, likely due to intracellular uptake of this element. Extrapolating these results to the typical bacterial concentrations used in the experiments suggest that ≤1 μmol/L of the Mg released to solution by basaltic glass dissolution was consumed by bacterial cells via intracellular uptake. The Si concentration evolution during bacterial growth does not exhibit a systematic variation within the experimental uncertainty (see Fig. 9b) confirming that Si uptake/adsorption and release due to cell lysis are negligible at the investigated conditions. The uptake of Ca, Mg, and Sr was also small and within the experimental reproducibility of 20–30%. The Al concentration did not exhibit any systematic change during of bacterial growth, although the assimilation of 100 μg Al/g_{wet} was observed in nutrient-bearing 0.01 M NaCl solution (see Fig. 9c). Bacterial uptake of As was absent, but there was a small release of As from the inactivated biomass with 1 μg As/g_{wet} over ~190 h. Taken together these results suggest that bacterial absorption and bacterial uptake play a minor role in the BMFR experiments performed in this study. Thus the observed changes in chemical composition of the solutions in the BMFR experiments mainly stems from dissolution of the basaltic glass.

5. Discussion

5.1. The effect of cell wall adsorption and bacterial assimilation on mass balance calculations

The elemental constituents released from the glass surface in the presence of bacteria can be incorporated into: (*i*) the <0.45 μm fluid fraction consisting of ions and molecules, simple organic complexes, and organic colloids of the lysis products and cell exometabolites; (*ii*) cell wall surfaces via adsorption, and (*iii*) bacteria interiors via assimilation (e.g. Hutchens et al., 2003; Neaman et al., 2005a,b, 2006). Whereas the mass of released elements incorporated into the fluid fraction was measured directly after these fluids were passed through 0.45 μm filters, the mass incorporated into cell walls or into bacteria could only be estimated via bacterial growth experiments in basaltic glass-free, Mg, Ca, Al, Si-bearing solutions. Measurement of the Mg, Ca, and Al desorbed from the cell surface upon EDTA treatment suggests that less than 20% of all elements released from our basaltic glass dissolution experiments were incorporated into cell walls or the bacteria interiors. As such this contribution to mass balance was neglected when calculating rates whose typical uncertainty was ±0.1 log *R* units.

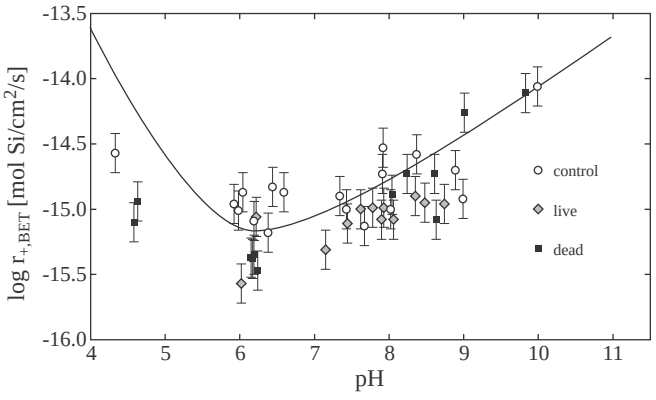

Fig. 10. Variation of measured steady-state BET normalized basaltic glass dissolution rates based on Si release as a function of pH. The symbols correspond to rates measured in the present study whereas the curve was generated from equations and parameters reported by Oelkers and Gislason (2001) for a total aqueous Al concentration of 10^{-6} mol/kg.

5.2. Effect of nutrients and bacteria on basaltic glass element release rates

The degree to which the presence of bacteria affects basaltic glass dissolution rates can be assessed with the aid of Fig. 10. Rates measured in the absence of bacteria are for the most part consistent with corresponding dissolution rates reported for this glass by Oelkers and Gislason (2001). Further comparison of Si release rates obtained in this and previous studies is shown in Table 5. The results shown in this table confirm that the rates obtained in this study are consistent with previous results (Oelkers and Gislason, 2001; Gislason and Oelkers, 2003; Stockmann et al., 2011).

Within the scatter of the data, the effect of the presence of either live or dead *P. reactans* is identical; rates in the presence of *P. reactans* are on average 0.3 log units lower than corresponding rates measured in bacteria-free experiments. This observation suggests that the influence of metabolic activity on basaltic glass dissolution rates at our experimental conditions is small. Note the average 0.3 log unit difference between rates measured in biotic versus abiotic experiments are within the combined uncertainty of the respective rate measurements.

Since both "starving" and "healthy" bacteria were tested (in nutrient-free and nutrient-rich media) over a wide range of biomass concentration, we suggest our experiments cover the likely range of conditions found in natural systems and as such these results can be extrapolated to basaltic glass during natural weathering.

There are several possible reasons why the presence of bacteria affects negligibly basaltic glass dissolution rates. First, the attachment of *P. reactans* exometabolites to basaltic glass surfaces may not be sufficient to facilitate the rupture of Si–O bonds, the main rate-controlling factor of glass dissolution. Moreover such effects may be balanced by the inhibiting effects of bacterial attachment blocking active sites on the basaltic glass surface; bacterial biofilm formation on surfaces is known to inhibit dissolution (Welch and Vandevivere, 1994; Ullman et al., 1996; Buchardt et al., 2001; Hutchens et al., 2006; Davis et al., 2007; Aouad et al., 2008; Hutchens, 2009; Hutchens et al., 2010), and the excretion of complex polysaccharides may also decrease dissolution rates (Welch and Vandevivere, 1994; Welch et al., 1999). It has also been suggested that microbially mediated dissolution may be less effective when bacteria are in direct contact with mineral surfaces (Hutchens et al., 2006). For example, a typical environmental bacterium, *Shewanella oneidensis* MR-1 was reported to decrease calcite dissolution rates via biofilm formation by inhibiting etch pit formation at screw or point dislocations (Lüttge and Conrad, 2004).

5.3. Comparison with literature data on the effect of bacteria on silicate minerals dissolution

Over the past decades, extensive research has focused on the effect of organic ligands on mineral dissolution rates (Ganor et al., 2009; Pokrovsky et al., 2009 and references therein). However, in contrast to our relatively good understanding of the effect of the presence of organic ligands on Ca, Mg-bearing silicate dissolution rates, there is relatively little quantitative literature data on the effect of bacteria on these rates. For example, it has been shown that a soil strain of *Pseudomonas* is capable of producing 2-ketogluconic acid from glucose and thus promoting the dissolution of the Ca, Zn, Mg silicates, wollastonite, apophyllite and olivine via formation of Ca-2 ketogluconate (Webley et al., 1960;

Table 5
Steady-state Stapafell basaltic glass dissolution rates obtained from abiotic experiments at 25 °C reported from various sources. All rates are given in units of mol/cm^2/s.

pH	Log $r_{+,Si,BET}$ [a]	Log $r_{+,Si,geo}$ [a]	Log $r_{+,Si,BET}$ [b]	Log $r_{+,Si,geo}$ [b]	pH [c]	Log $r_{+,Si,BET}$ [c]	Log $r_{+,Si,geo}$ [c]	pH [d]	Log $r_{+,Si,BET}$ [d]	Log $r_{+,Si,geo}$ [d]	Log $r_{+,Ca,Mg,BET}$ [d,e]	Log $r_{+,Ca,Mg,geo}$ [d,e]
4.5			−14.2	−12.2				4.3	−14.6	−13.2	−14.2	−12.8
6.0	−15.2	−13.2	−15.0	−13.0				6.0	−15.0	−13.6	−14.9	−13.6
6.5			−15.0	−13.0				6.6	−14.9	−13.5	−14.8	−13.4
7.0	−15.1	−13.1	−14.9	−12.9	7.0	−15.1	−13.7					
8.0	−14.8	−12.8	−14.6	−12.6	7.9	−14.7	−13.3	7.9	−14.6	−13.3		
8.5			−14.4	−12.4	8.6	−14.8	−13.4	8.4	−14.6	−13.2	−14.7	−13.3
9.0	−14.4	−12.4	−14.2	−12.2				8.9	−14.8	−13.4	−15.0	−13.6
10.0	−14.1	−12.1	−13.9	−11.9	10.1	−14.3	−13.0	10.0	−14.1	−12.7	−14.3	−13.0

[a] From Oelkers and Gislason (2001).
[b] From Gislason and Oelkers (2003). A roughness factor of 92 is used to calculate $r_{+,geo}$ from $r_{+,BET}$.
[c] From Stockmann et al. (2011). The basaltic glass roughness factor is 23.
[d] This study, bacteria- and nutrient-free experiments.
[e] This study, average of Ca and Mg dissolution rates. For the pH 10.0 experiment, only Mg rates are given.

Duff et al., 1962; Webley et al., 1963); however, no quantitative description of the process were generated. A recent study of soil rhizospheric bacteria *Pseudomonas aureofaciens* suggests these bacteria have little effect on wollastonite dissolution rates both in nutrient-free and nutrient-rich solutions (Pokrovsky et al., 2009). Fayalite (Fe_2SiO_4) dissolution at pH = 2 in the presence of acidophilic, iron-oxidizing bacteria was significantly inhibited compared to abiotic controls (Santelli et al., 2001). This inhibition was attributed to formation of unreactive laihunite-like ($Fe^{2+}Fe^{3+}{}_2(SiO_4)_2$) surface regions due to bacterial oxidation of released Fe^{2+} (Welch and Banfield, 2002). Such mechanisms, however, are unlikely to occur at the conditions of our experiments because of they were performed at higher pH, and, as a result, significantly lower dissolved Fe concentration.

xAluminosilicates and Fe-bearing minerals are generally considered to be much more susceptible to microbial-promoted dissolution than Ca, Mg-bearing orthosilicates (see Berner, 2010; Pokrovsky et al., 2010 for discussion). The main reason is the change of aqueous Al and Fe speciation due to the presence of bacterial exometabolites and siderophores. Aqueous complexation decreases the activity of aqueous Al^{3+} and Fe^{3+}, which (i) avoids secondary mineral formation, (ii) increases overall dissolution rates (Welch and Ullman, 1993; Vandevivere et al., 1994; Oelkers and Schott, 1998; Liermann et al., 2000a,b; Maurice et al., 2001) and (iii) increases the selective uptake of trace metals (Brantley et al., 2001). It is also worth noting that despite a common belief that microbes accelerate weathering (Robert and Berthelin, 1986; Thorseth et al., 1992; Uroz et al., 2009), there are numerous studies that conclude this effect is either rather weak or inhibiting (see Valsami-Jones and McEldowney, 2000; Balogh-Brunstad et al., 2008; Hopf et al., 2009; Hutchens, 2009; Sverdrup, 2009).

5.4. Application to subsurface CO_2 storage and soil weathering

The results of this study provide insight into the potential impact of heterotrophic bacteria on basaltic glass dissolution and during subsurface CO_2 storage efforts. Typical concentrations of live *P. reactans* cells used in the experiments presented above are 10^7–10^8 cells/mL. This is 6 orders of magnitude higher than the total concentration of culturable heterotrophic aerobic bacteria measured in the Icelandic groundwater samples used to separate *P. reactans* ($n \cdot 10 - n \cdot 100$ CFU/mL, Shirokova et al., 2009). However, the bacterial concentrations considered in our experiments are comparable with *i*) average bacterial populations in soils, which commonly range from 10^6 to 10^9 cells/cm^3 (Atlas and Bartha, 1993), *ii*) bacterial concentrations in shallow aquifers (10^6 cells/mL, Ehrlich, 1996), and (iii) in deep subsurface environments (Sinclair and Ghiorse, 1989; Stevens and McKinley, 1995; Pedersen, 1997). Although culturable bacteria represent only a small proportion of the species present in natural systems (e.g. Pedrós-Alió, 2006), the high concentrations of bacteria used in this present study allow straightforward evaluation of the degree to which the heterotrophic bacteria are capable of influencing glass dissolution in natural settings.

The relatively weak effect of bacteria and microbial exometabolites on basaltic glass observed in this study, together with similar observations on olivine (Shirokova et al., 2012), and other Ca–Mg-bearing silicates such as wollastonite (Pokrovsky et al., 2009) suggests that the impact of heterotrophic aerobic culturable bacteria on "basic" mineral and aluminosilicates chemical weathering rates in soils and during carbon sequestration efforts may be weaker than generally thought.

6. Conclusions

The experiments presented above show that the presence of live or dead bacteria affects only mildly basaltic glass dissolution rates based on Si release; constant pH rates were observed in this study to decrease by no more than a factor of 3 in the presence of *P. reactans*. Other major cations including Al, Ca, Mg, and Fe exhibit a similar behavior. A decrease in Al concentration due to the presence of *P. reactans* was observed in nearly all of the experiments. Al might be adsorbed on bacteria surfaces, but little aqueous Al-complexing with bacteria and exometabolites is indicated by the lack of acceleration in basaltic glass dissolution rates in their presence. The presence of nutrient components in solution prevented Al^{3+} and Fe^{3+} from forming secondary precipitates, most likely through organic molecular complexation. No increase of trace elements release from basaltic glass was observed, except for an increase in arsenic release rates at pH 4 in the presence of dead *P. reactans*. As little effect of their presence was found on laboratory dissolution rates it seems likely that *P. reactans* will have a little effect on basaltic glass dissolution rates during either soil weathering or subsurface CO_2 storage efforts in basalts.

Acknowledgments

We would like to thank several colleagues for their help, in particular Carole Causserand, Alain Castillo, and Phillippe de Parseval for technical assistance, and Therese K. Flaathen, Allison Stephenson, Sam Parry, Irina Bundeleva, Quentin Gautier, Giuseppe Saldi, Chris Pearce and Vasileios Mavromatis for lab assistance. Erik Sturkell is gratefully acknowledged for his graphical assistance and continued support. The Environmental and Energy Fund of Reykjavík Energy, the Research Fund of the University of Iceland, the Nordic Council of Ministers through NORDVULK, and the European Community through the MIN-GRO Research and Training Network (MRTN-CT-2006-035488) and the ERASMUS student mobility program are gratefully acknowledged for their financial support. Finally, we would like to thank Editor Jeremy Fein for his valuable comments, which greatly improved this manuscript.

Appendix 1. Chemical composition of the inlet fluids used in the BMFR experiments

Exp.	Inlet fluid (mol/kg)	Ionic strength (mol/kg)	Inlet pH (25 °C)	STDEV pH_{in}	Outlet pH (25 °C)	STDEV pH_{out}	Bacteria (mg_{wet}/L)	Bacteria status [d]	Nutrient (%)
4-1	0.003 m $NaOOCCH_3$ + 0.003 m NaCl + 0.003 m HCl	0.009	4.07	0.02	4.33	0.19	0		0
4-2	0.003 m $NaOOCCH_3$ + 0.003 m NaCl + 0.003 m HCl	0.009	4.58	0.04	4.63	0.19	100	Dead	0
4-3	0.003 m $NaOOCCH_3$ + 0.003 m NaCl + 0.003 m HCl	0.009	4.28	0.06	4.58	0.04	430	Dead	0
4-4	0.003 m $NaOOCCH_3$ + 0.003 m NaCl + 0.003 m HCl	0.009	4.18		7.28	1.43	700	Live	0
6-1	0.00998 m NH_4Cl + 0.000003 m NH_4OH	0.010	5.86	0.15	5.92	0.10	0		0
6-2	0.00998 m NH_4Cl + 0.000003 m NH_4OH	0.010	5.81	0.02	5.98	0.03	0		0
6-3	0.00998 m NH_4Cl + 0.000003 m NH_4OH	0.010	6.22	0.10	6.38	0.06	0		1
6-4	0.00998 m NH_4Cl + 0.000003 m NH_4OH	0.010	6.33	0.06	6.44	0.06	0		10
6-5[a]	0.001 m MES + 0.0004 m NaOH	0.001	6.05	0.01	6.04	0.04	0		0
6-6 [a]	0.001 m MES + 0.0004 m NaOH	0.001	6.12	0.01	6.15	0.03	11.8	Dead	0
6-7[a]	0.001 m MES + 0.0004 m NaOH	0.001	6.12	0.01	6.17	0.02	100	Dead	0
6-8[a]	0.001 m MES + 0.0004 m NaOH	0.001	6.16		6.19	0.02	198	Dead	0
6-9[a]	0.001 m MES + 0.0004 m NaOH	0.001	6.40		6.39	0.01	368	Dead	0
6-10[a]	0.001 m MES + 0.0004 m NaOH	0.001	6.10	0.04	6.19	0.05	0		0
6-11[a]	0.001 m MES + 0.0004 m NaOH	0.001	6.23	0.04	6.32	0.03	200	Dead	0
6-12[a]	0.001 m MES + 0.0004 m NaOH	0.001	6.10	0.03	6.24	0.02	430	Dead	0
6-13[a]	0.001 m MES + 0.0004 m NaOH	0.001	6.08		6.15	0.12	700	Live	0
E5-1[a]	0.01 m MES	0.01	n.m.		6.59	0.14	0		0
E5-2[a]	0.01 m MES	0.01	n.m.		6.22	0.10	870	Live	0
E5-3[a]	0.01 m MES	0.01	n.m.		7.15	0.25	6500	Live	0
E3-1[a]	0.01 m MES	0.01	n.m.		7.43	0.23	0		10
E3-2[a]	0.01 m MES	0.01	n.m.		7.78	0.07	8900	Live	10
E3-3[a]	0.01 m MES	0.01	n.m.		7.62	0.13	12,000	Live	10
8-1[b]	0.0096 m NH_4Cl + 0.0004 m NH_4OH	0.010	7.92	0.02	7.92	0.03	0		0
8-2[b]	0.0096 m NH_4Cl + 0.0004 m NH_4OH	0.010	7.94	0.01	7.91	0.02	0		0
8-3[b]	0.0096 m NH_4Cl + 0.0004 m NH_4OH	0.010	7.83	0.09	7.34	0.25	0		1
8-4[b]	0.0096 m NH_4Cl + 0.0004 m NH_4OH	0.010	7.89	0.08	7.47	0.25	0		10
8-5	0.01 m $NaHCO_3$	0.010	8.55	0.02	8.37	0.06	0		0
8-6	0.01 m $NaHCO_3$	0.010	8.46	0.03	8.24	0.07	12	Dead	0
8-7	0.01 m $NaHCO_3$	0.010	8.33	0.13	8.04	0.06	70	Dead	0
8-8	0.01 m $NaHCO_3$	0.010	8.55		8.04	0.06	195	Dead	0
8-9	0.01 m $NaHCO_3$	0.010	8.10		8.01	0.13	368	Dead	0
8-10	0.01 m $NaHCO_3$	0.010	8.55	0.04	8.89	0.02	0		0
8-11	0.01 m $NaHCO_3$	0.010	8.57	0.11	8.63	0.08	200	Dead	0
8-12	0.01 m $NaHCO_3$	0.010	8.36	0.16	8.61	0.08	430	Dead	0
8-13	0.01 m $NaHCO_3$	0.010	8.53		8.09	0.27	700	Live	0
E6-1	0.01 m $NaHCO_3$	0.010	n.m.		8.99	0.04	0.0		0
E6-2	0.01 m $NaHCO_3$	0.010	n.m.		8.74	0.11	870	Live	0
E6-3	0.01 m $NaHCO_3$	0.010	n.m.		8.48	0.15	6500	Live	0
E4-1	0.01 m $NaHCO_3$	0.010	n.m.		8.02	0.04	0.0		10
E4-2	0.01 m $NaHCO_3$	0.010	n.m.		8.06	0.06	8900	Live	10
E4-3	0.01 m $NaHCO_3$	0.010	n.m.		7.90	0.10	19,000	Live	10
10-1	0.003 m Na_2CO_3 + 0.004 m $NaHCO_3$	0.013	10.05	0.00	9.99	0.04	0		0
10-2	0.003 m Na_2CO_3 + 0.004 m $NaHCO_3$	0.013	10.02	0.01	9.83	0.12	100	Dead	0
10-3	0.003 m Na_2CO_3 + 0.004 m $NaHCO_3$	0.013	9.94	0.17	9.01	0.33	430	Dead	0
10-4	0.003 m Na_2CO_3 + 0.004 m $NaHCO_3$	0.013	10.11		8.37	0.45	700	Live	0

n.m. = not measured.

[a] MES is an organic buffer with the chemical composition $C_6H_{13}NO_4S$.

[b] N_2 was bubbled through the inlet solution for 30 min prior to use to minimize the amount of dissolved CO_2 in solution.

Appendix 2. Supplementary data

Supplementary data to this article can be found online at doi:10.1016/j.chemgeo.2011.12.011.

References

Alfredsson, H.A., Hadrarson, B.S., Franzson, H., Gislason, S.R., 2008. CO_2 sequestration in basaltic rock at the Hellisheidi site in SW Iceland: stratigraphy and chemical composition of the rocks at the injection site. Mining Magazine 72, 1–5.

Aouad, G., Crovisier, J.-L., Geoffroy, V.A., Meyer, J.-M., Stille, P., 2006. Microbially-mediated glass dissolution and sorption of metals by *Pseudomonas aeruginosa* cells and biofilm. Journal of Hazardous Materials B 136, 889–895.

Aouad, G., Crovisier, J.-L., Damidot, D., Stille, P., Hutchens, E., Mutterer, J., Meyer, J.-M., Geoffroy, V.A., 2008. Interactions between municipal solid waste incinerator bottom ash and bacteria (*Pseudomonas aeruginosa*). The Science of the Total Environment 393, 385–393.

Ariés, S., Valladon, M., Polvé, M., Dupré, B., 2000. A routine method for oxide and hydroxide interference corrections in ICP-MS chemical analysis of environmental and geological samples. Geostandards Newsletter 24, 19–31.

Atlas, R.M., Bartha, R., 1993. Microbial Ecology: Fundamentals and Applications. Benjamin/Cummings, Redwood City, Canada. 563 pp.

Bailey, B., Templeton, A., Staudigel, H., Tebo, B.M., 2009. Utilization of substrate components during basaltic glass colonization by *Pseudomonas* and *Shewanella* isolates. Geomicrobiology Journal 26, 648–656.

Balogh-Brunstad, Z., Keller, C.K., Dickinson, J.T., Stevens, F., Li, C.Y., Bormann, B.T., 2008. Biotite weathering and nutrient uptake by ectomycorrhizal fungus, *Suillus tomentosus*, in liquid-culture experiments. Geochimica et Cosmochimica Acta 72, 2601–2618.

Belkanova, N.P., Karavaiko, G.I., Avakyan, Z.A., 1985. Cleavage of the syloxane bond in quartz by *Bacillus mucilaginosus*. Microbiology 54, 27–30 (in Russian).

Belkanova, N.P., Eroschev-Shak, V.A., Lebedeva, E.V., Karavaiko, G.I., 1987. Dissolution of kimberlite minerals by heterotrophic microorganisms. Microbiology 56, 613–620 (in Russian).

Benedetti, M.F., Dia, A., Riotte, J., Chabaux, F., Gérard, M., Boulègue, J., Fritz, B., Chauvel, C., Bulourde, M., Déruelle, B., Ildefonse, P., 2003. Chemical weathering of basaltic lava flows undergoing extreme climatic conditions: the water geochemistry record. Chemical Geology 201, 1–17.

Bennett, P.C., Casey, W.H., 1994. Organic acids and the dissolution of silicates. In: Pittman, E.D., Lewan, M. (Eds.), The Role of Organic Acids in Geological Processes. Springer-Verlag, New York, pp. 162–201.

Bennett, P.C., Rogers, J.R., Choi, W.J., 2001. Silicates, silicate weathering, and microbial ecology. Geomicrobiology Journal 18, 3–19.

Berner, R.A., 2010. Comment: effect of organic ligands and heterotrophic bacteria on Wollastonite dissolution kinetics. American Journal of Science 310, 424.

Bourcier, W.L., Peiffer, D.W., Knauss, K.G., McKeegan, K.D., Smith, D.K., 1990. A kinetic model for borosilicate glass dissolution based on the dissolution affinity of a surface alteration layer. Materials Research Society Symposium Proceedings 176, 209–216.

Brantley, S., Liermann, L., Bau, M., 2001. Uptake of trace metals and rare earth elements from hornblende by a soil bacterium. Geomicrobiology Journal 18, 37–61.

Buchardt, B., Israelson, C., Seaman, P., Stockmann, G., 2001. Ikaite Tufa Towers in Ikka Fjord, southwest Greenland: their formation by mixing of seawater and alkaline spring water. Journal of Sedimentary Research 71, 176–189.

Davis, K.J., Nealson, K.H., Lüttge, A., 2007. Calcite and dolomite dissolution rates in the context of microbe–mineral surface interactions. Geobiology 5, 191–205.
Duff, R.B., Webley, D.M., Scott, R.O., 1962. Solubilization of minerals and related materials by 2-ketogluconic acid-producing bacteria. Soil Science 95, 105–114.
Edwards, K.J., Bach, W., McCollom, T.M., Rogers, D.R., 2004. Neutrophilic iron-oxidizing bacteria in the ocean: their habitats, diversity, and roles in mineral deposition, rock alteration, and biomass production in the deep-sea. Geomicrobiology Journal 21, 393–404.
Ehrlich, H.L., 1981. The geomicrobiology of silica and silicates, In: Ehrlich, H.L. (Ed.), Geomicrobiology, 2nd ed. Marcel Dekker, Inc., New York, pp. 131–135.
Ehrlich, H.L., 1996. How microbes influence mineral growth and dissolution. Chemical Geology 132, 5–9.
Fein, J.B., Daughney, C.J., Yee, N., Davis, T.A., 1997. A chemical equilibrium model for metal adsorption onto bacterial surfaces. Geochimica et Cosmochimica Acta 61, 3319–3328.
Flaathen, T.K., Gislason, S.R., Oelkers, E.H., 2010. The effect of aqueous sulphate on basaltic glass dissolution rates. Chemical Geology 277, 345–354.
Ganor, J., Reznik, I.J., Rosenberg, Y.O., 2009. Organics in water–rock interactions. Reviews in Mineralogy and Geochemistry 70, 259–369.
Gislason, S.R., Oelkers, E.H., 2003. Mechanism, rates and consequences of basaltic glass dissolution: II. An experimental study of the dissolution rates of basaltic glass as a function of pH and temperature. Geochimica et Cosmochimica Acta 67, 3817–3832.
Gislason, S.R., Wolff-Boenisch, D., Stefansson, A., Oelkers, E.H., Gunnlaugsson, E., Sigurdardóttir, H., Sigfússon, G., Brocker, W.S., Matter, J., Stute, M., Axelsson, G., Fridriksson, T., 2010. Mineral sequestration of carbon dioxide in basalt: a pre-injection overview of the CarbFix project. International Journal of Greenhouse Gas Control 4, 537–545.
Gout, R., Oelkers, E.H., Schott, J., Zwick, A., 1997. The surface chemistry and structure of acid-leached albite: new insights on the dissolution mechanism of the alkali feldspars. Geochimica et Cosmochimica Acta 61, 3013–3018.
Grantham, M.C., Dove, P.M., Dichristina, T.J., 1997. Microbially catalyzed dissolution of iron and aluminum oxyhydroxide mineral surface coatings. Geochimica et Cosmochimica Acta 61, 4467–4477.
Hopf, J., Langenhorst, F., Pollok, K., Mertean, D., Kothe, E., 2009. Influence of microorganisms on biotite dissolution: an experimental approach. Chemie der Erde 69, 45–56.
Hutchens, E., 2009. Microbial selectivity on mineral surfaces: possible implications for weathering processes. Fungal Biology Reviews 23, 115–121.
Hutchens, E., Valsami-Jones, E., McEldowney, S., Gaze, W., McLean, J., 2003. The role of heterotrophic bacteria in feldspar dissolution — an experimental approach. Mining Magazine 67, 1157–1170.
Hutchens, E., Valsami-Jones, E., Harouiya, N., Chairat, C., Oelkers, E.H., McEldoney, S., 2006. An experimental investigation of the effect of *Bacillus megaterium* on apatite dissolution. Geomicrobiology Journal 23, 177–182.
Hutchens, E., Gleeson, D., McDermott, F., Miranda-CasoLuengo, R., Clipson, N., 2010. Meter-scale diversity of microbial communities on a weathered pegmatite granite outcrop in the Wicklow Mountains, Ireland; evidence for mineral induced selection? Geomicrobiology Journal 27, 1–14.
Johnson, K.J., Ams, D.A., Wedel, A.N., Szymanowski, J.E.S., Weber, D.L., Schneegurt, M.A., Fein, J.B., 2007. The impact of metabolic state on Cd adsorption onto bacterial cells. Geobiology 5, 211–218.
Kalinowski, B.E., Liermann, L.J., Givens, S., Brantley, S.L., 2000. Rates of bacteria-promoted solubilization of Fe from minerals: a review of problems and approaches. Chemical Geology 169, 357–370.
Kenward, P.A., Goldstein, G.H., González, L.A., Roberts, J.A., 2009. Precipitation of low-temperature dolomite from an anaerobic microbial consortium: the role of methanogenic Archaea. Geobiology 7, 556–565.
Knauer, K., Behra, R., Sigg, L., 1997. Effects of free Cu^{+2} and Zn^{+2} ions on growth and metal accumulation in freshwater algae. Environmental Toxicology and Chemistry 16, 220–229.
Koroleff, F., 1976. Determination of silicon. In: Grasshoff, K. (Ed.), Methods of Seawater Analysis. Springer Verlag, New York, pp. 149–158.
Le Faucher, S., Behra, R., Sigg, L., 2005. Thiol and metal contents in periphyton exposed to elevated copper and zinc concentrations: a field and microcosm study. Environmental Science and Technology 36, 8099–8107.
Lee, J.-U., Fein, J.B., 2000. Experimental study of the effects of *Bacillus subtilis* on gibbsite dissolution rates under near-neutral pH and nutrient-poor conditions. Chemical Geology 166, 193–202.
Liermann, L.J., Kalinowski, B.E., Brantley, S.L., Ferry, J.G., 2000a. Role of bacterial siderophores in dissolution of hornblende. Geochimica et Cosmochimica Acta 64, 587–602.
Liermann, L.J., Barnes, A.S., Kalinowski, B.E., Zhao, X., Brantley, S.L., 2000b. Microenvironments of pH in biofilms grown on dissolving silicate surfaces. Chemical Geology 171, 1–16.
Lüttge, A., Conrad, P.G., 2004. Direct observation of microbial inhibition of calcite dissolution. Applied and Environmental Microbiology 70, 1627–1632.
Malinovskaya, I.M., Kosenko, L.V., Votselko, S.K., Podgorskii, V.S., 1990. Role of *Bacillus mucilaginosus* polysaccharide in degradation of silicate minerals. Mikrobiologiya 59, 70–78 (Engl. Transl. p. 49–55).
Martinez, R.E., Pokrovsky, O.S., Schott, J., Oelkers, E.H., 2008. Surface charge and zeta-potential of metabolically active and dead cyanobacteria. Journal of Colloid and Interface Science 323, 317–325.
Martinez, R.E., Gardés, E., Pokrovsky, O.S., Schott, J., Oelkers, E.H., 2010. Do photosynthetic bacteria have a protective mechanism against carbonate precipitation at their surfaces? Geochimica et Cosmochimica Acta 74, 1329–1337.
Maurice, P.A., Vierkorn, M.A., Hersman, L.E., Fulghum, J.E., Ferryman, A., 2001. Enhancement of kaolinite dissolution by an aerobic *Pseudomonas mendocina* bacterium. Geomicrobiology Journal 18, 21–35.
Nazina, T.N., Luk'yanova, E.A., Zakharova, E.V., Ivoilov, V.S., Poltaraus, A.B., Kalmykov, S.N., Belyaev, S.S., Zubkov, A.A., 2006. Distribution and activity of microorganisms in the deep repository for liquid radioactive waste at the Siberian chemical combine. Microbiology 75, 727–738.
Nazina, T.N., Luk'yanova, E.A., Zakharova, E.V., Konstantinova, L.I., Kalmykov, S.N., Poltaraus, A.B., Zubkov, A.A., 2010. Microorganisms in a disposal site for liquid radioactive wastes and their influence on radionuclides. Geomicrobiology Journal 27, 473–486.
Neaman, A., Chorover, J., Brantley, S.L., 2005a. Implications of the evolution of organic acid moieties for basalt weathering over geological time. American Journal of Science 305, 147–185.
Neaman, A., Chorover, J., Brantley, S.L., 2005b. Element mobility patterns records organics ligands in soils on early Earth. Geology 33, 117–120.
Neaman, A., Chorover, J., Brantley, S.L., 2006. Effects of organic ligands on granite dissolution in batch experiments at pH 6. American Journal of Science 306, 451–473.
Ngwenya, B.T., 2007. Enhanced adsorption of zinc is associated with aging and lysis of bacterial cells in batch incubations. Chemosphere 67, 1982–1992.
Oelkers, E.H., 2001. General kinetic description of multioxide silicate mineral and glass dissolution. Geochimica et Cosmochimica Acta 65, 3703–3719.
Oelkers, E.H., Gislason, S.R., 2001. The mechansim, rates and consequences of basaltic glass dissolution: I. An experimental study of the dissolution rates of basaltic glass as as function of aqueous Al, Si and oxalic acid concentration at 25 °C and pH = 3 and 11. Geochimica et Cosmochimica Acta 65, 3671–3681.
Oelkers, E.H., Schott, J., 1998. Does organic acid adsorption affect alkali–feldspar dissolution rates? Chemical Geology 155, 235–245.
Oelkers, E.H., Schott, J., 2005. Geochemical aspects of CO_2 sequestration. Chemical Geology 217, 183–186.
Oelkers, E.H., Gislason, S.R., Matter, J., 2008a. Mineral carbonation of CO_2. Elements 4, 333–337.
Oelkers, E.H., Schott, J., Gauthier, J.-M., Herrero-Roncal, T., 2008b. An experimental study of the dissolution rates of muscovite. Geochemical aspects of CO_2 sequestration. Geochimica et Cosmochimica Acta 72, 4948–4961.
Parkhurst, D.L., Appelo, C.A.J., 1999. User's guide to PHREEQC (version 2) — a computer program for speciation, batch-reaction, one-dimensional transport, and inverse geochemical calculations. Washington, DC: U.S. Geological Survey Water-Resources Investigations Report 99–4259. 312 pp.
Pedersen, K., 1997. Microbial life in deep granitic rock. FEMS Microbiology Reviews 20, 399–414.
Pedrós-Alió, C., 2006. Marine microbial diversity: can it be determined? Trends in Microbiology 14, 257–263.
Pokrovsky, O.S., Martinez, R.E., Golubev, S.V., Kompantseva, E.I., Shirokova, L.S., 2008. Adsorption of metals and protons on *Gloeocapsa* sp. cyanobacteria: a surface speciation approach. Applied Geochemistry 23, 2574–2588.
Pokrovsky, O.S., Shirokova, L.S., Bénézeth, P., Schott, J., Golubev, S.V., 2009. Effect of organic ligands and heterotrophic bacteria on wollastonite dissolution kinetics. American Journal of Science 309, 731–772.
Pokrovsky, O.S., Shirokova, L.S., Bénézeth, P., Schott, J., Golubev, S.V., 2010. Reply to Comment by R. A. Berner on "Effect of organic ligands and heterotrophic bacteria on Wollastonite dissolution kinetics". American Journal of Science 309, 731–772 Am. J. Sci. 310, 425–426.
Robert, M., Berthelin, J., 1986. Role of biological and biochemical factors in soil mineral weathering. In: Huang, P.M., Schnitzer, M. (Eds.), Interactions of Soil Minerals with Natural Organics and Microbes. Soil Science Society of America, Madison, Wisconsin, pp. 453–495.
Rogers, J.R., Bennett, P.C., 2004. Mineral stimulation of subsurface microorganisms: release of limiting nutrients from silicates. Chemical Geology 203, 91–108.
Santelli, C., Welch, S.A., Westrich, H.R., Banfield, J.F., 2001. The effect of Fe-oxidizing bacteria on Fe-silicate mineral dissolution. Chemical Geology 180, 99–115.
Schott, J., Pokrovsky, O.S., Oelkers, E.H., 2009. The link between mineral dissolution/precipitation kinetics and solution chemistry. Reviews in Mineralogy and Geochemistry 70, 207–258.
Shirokova, L.S., Bénézeth, P., Pokrovsky, O.S., 2009. Effect of heterotrophic bacteria extracted from groundwater on Ca silicate dissolution. Geochimica et Cosmochimica Acta 73, A1213.
Shirokova, L.S., Bénézeth, P., Pokrovsky, O.S., Gérard, E., Ménez, B., Alfredsson, H., 2012. Effect of the heterotrophic bacterium *Pseudomonas reactans* on olivine dissolution kinetics and implications for CO_2 storage in basalts. Geochimica et Cosmochimica Acta 80, 30–50. doi:10.1016/j.gca.2011.11.046.
Sinclair, J.L., Ghiorse, W.C., 1989. Distribution of aerobic bacteria, protozoa, algae, and fungi in deep subsurface sediments. Geomicrobiology Journal 7, 15–31.
Stevens, T.O., McKinley, J.P., 1995. Lithoautotrophic microbial ecosystems in deep basalt aquifers. Science 270, 450–454.
Stockmann, G.J., Wolff-Boenisch, D., Gislason, S.R., Oelkers, E.H., 2011. Do carbonate precipitates affect dissolution kinetics? 1: Basaltic glass. Chemical Geology 284, 306–316.
Sverdrup, H., 2009. Chemical weathering of soil minerals and the role of biological processes. Fungal Biology Reviews 23, 94–100.
Thorseth, I.H., Furnes, H., Heldal, M., 1992. The importance of microbiological activity in the alteration of natural basaltic glass. Geochimica et Cosmochimica Acta 56, 845–850.
Thorseth, I.H., Furnes, H., Tumyr, O., 1995. Textural and chemical effects of bacterial activity on basaltic glass: an experimental approach. Chemical Geology 119, 139–160.
Ullman, W.J., Kirchman, D.L., Welch, S.A., Vandevivere, P., 1996. Laboratory evidence for microbially mediated silicate mineral dissolution in nature. Chemical Geology 132, 11–17.
Uroz, S., Calvaruso, Ch., Turpault, M.-P., Frey-Klett, P., 2009. Mineral weathering by bacteria: ecology, actors and mechanisms. Trends in Microbiology 17, 378–387.

Urrutia Mera, M., Kemper, M., Doyle, R., Beveridge, T.J., 1992. The membrane-induced proton motive force influences the metal binding ability of *Bacillus subtilis* cell walls. Applied and Environmental Microbiology 58, 3837–3844.

Valsami-Jones, E., McEldowney, S., 2000. Mineral dissolution by heterotrophic bacteria: principles and methodologies. Environmental Mineralogy: Microbial Interactions, Anthropogenic Influences, Contaminated Land and Waste Management. Mineralogical Society Series, London, U.K., pp. 27–55.

Vandevivere, P., Welch, S.A., Ullman, W.J., Kirchman, D.L., 1994. Enhanced dissolution of silicate minerals by bacteria at near-neutral pH. Microbial Ecology 27, 241–251.

Webley, D.M., Duff, R.B., Mitchell, W.A., 1960. Plate method for studying the breakdown of synthetic and natural silicates by soil bacteria. Nature 188, 766–767.

Webley, D.M., Henderson, M.E.K., Taylor, I.F., 1963. The microbiology of rocks and weathered stones. Journal of Soil Science 14, 102–112.

Welch, S.A., Banfield, J.F., 2002. Modification of olivine surface morphology and reactivity by microbial activity during chemical weathering. Geochimica et Cosmochimica Acta 66, 213–221.

Welch, S.A., Ullman, W.J., 1993. The effect of organic acids on plagioclase dissolution rates and stoichiometry. Geochimica et Cosmochimica Acta 57, 2725–2736.

Welch, S.A., Vandevivere, P., 1994. Effect of microbial and other naturally occurring polymers on mineral dissolution. Geomicrobiology Journal 12, 227–238.

Welch, S.A., Barker, W.W., Banfield, J.F., 1999. Microbial extracellular polysaccharides and plagioclase dissolution. Geochimica et Cosmochimica Acta 63, 1405–1419.

Wolff-Boenisch, D., Gislason, S.R., Oelkers, E.H., 2004a. The effect of fluoride on the dissolution rates of natural glasses at pH 4 and 25 °C. Geochimica et Cosmochimica Acta 68, 4571–4582.

Wolff-Boenisch, D., Gislason, S.R., Oelkers, E.H., Putnis, C.V., 2004b. The dissolution rates of natural glasses as a function of their composition at pH 4 and 10.6, and temperatures from 25 to 74 °C. Geochimica et Cosmochimica Acta 68, 4843–4858.

Wolff-Boenisch, D., Gislason, S.R., Oelkers, E.H., 2006. The effect of crystallinity on dissolution rates and CO_2 consumption capacity of silicates. Geochimica et Cosmochimica Acta 70, 858–870.

Wolff-Boenisch, D., Wenau, S., Gislason, S.R., Oelkers, E.H., 2011. Dissolution of basalts and peridotite in seawater, in the presence of ligands, and CO_2: implications for mineral sequestration of carbon dioxide. Geochimica et Cosmochimica Acta 75, 5510–5525.

Wu, L., Jacobson, A.D., Chen, H.-C., Hausner, M., 2007. Characterization of elemental release during microbe–basalt interactions at T = 28 °C. Geochimica et Cosmochimica Acta 71, 2224–2239.

Wu, L., Jacobson, A.D., Hausner, M., 2008. Characterization of elemental release during microbe–granite interactions at T = 28 °C. Geochimica et Cosmochimica Acta 72, 1076–1095.

Yeghicheyan, D., Carignan, J., Valladon, M., Le Coz, M.B., Cornec, F.L., Castrec-Rouelle, M., Robert, M., Aquilina, L., Aubry, E., Churlaud, C., Dia, A., Deberdt, S., Dupré, B., Freydier, R., Gruau, G., Hénin, O., de Kersabiec, A.-M., Macé, J., Marin, L., Morin, N., Petitjean, P., Serrat, E., 2001. A compilation of silicon and thirty one trace elements measured in the natural river water reference material SLRS-4 (NRC-CNRC). Geostandards Newsletter 25, 465–474.

Chapter 5

The role of mineral surfaces on calcite nucleation kinetics

Gabrielle J. Stockmann, Eric H. Oelkers, Domenik Wolff-Boenisch, Nicolas Bovet and Sigurdur R. Gislason

(To be submitted upon completion of work)

ABSTRACT

Calcite was precipitated in flow-through experiments at 25 ºC from supersaturated aqueous solutions in the presence of seeds of calcite and six different silicates: augite, basaltic glass, enstatite, labradorite, olivine, and peridotite. The aim of the experiments was to determine how calcite nucleation and growth depends on the identity and structure of the growth substrate. Calcite saturation was achieved mixing a $CaCl_2$-rich solution with a $NaHCO_3$-Na_2CO_3 buffer in a mixed-flow reactor containing 0.5-2 grams of mineral grains. This led to a calcite saturation index of 0.6 and pH 9.1 for the reactive solution inside the reactor. Although chemical conditions, flow rate and temperature were identical for all experiments, the onset of calcite nucleation and the amount of calcite being precipitated depended on the identity of the mineral substrate. With calcite as the growth substrate, new calcite crystals formed instantaneously. Calcite nucleated relatively rapidly on olivine, enstatite, and peridotite (mainly composed of Mg-olivine). Scanning Electron Microscope images showed silicate crystals to be almost completed covered with calcite coatings at the end of the experiments. Less calcite growth was found on labradorite and augite, and least on basaltic glass. In all cases, calcite precipitation occurs on the mineral substrate and not adjacent to them. These findings indicate that calcite nucleation and its subsequent growth depends on the crystal structure of the silicate substrate. Orthorhombic silicate minerals (olivine and enstatite) are the easiest for trigonal calcite to nucleate on. Monoclinic augite and triclinic labradorite show intermediate behavior, whereas basaltic glass with its non-ordered crystal structure is the least favorable platform for calcite growth. The results have implications for CO_2 mineralization in ultramafic and basaltic rocks indicating that trigonal carbonates easier precipitate on crystalline rather than glassy rocks, but even glass surfaces can serve as a substrate for calcite nucleation.

The role of mineral surfaces on calcite nucleation kinetics

(*draft manuscript to be submitted to GCA upon completion of work*)

Gabrielle J. Stockmann [a,b,*], Eric H. Oelkers [b,c], Domenik Wolff-Boenisch [c], Nicolas Bovet [d] and Sigurdur R. Gislason [c]

[a] *Nordic Volcanological Center, Institute of Earth Sciences, University of Iceland, Sturlugata 7, 101 Reykjavík, Iceland*

[b] *GET-Université de Toulouse-CNRS-IRD-OMP, 14 Avenue Edouard Belin, 31400 Toulouse, France*

[e] *Institute of Earth Sciences, University of Iceland, Sturlugata 7, 101 Reykjavík, Iceland*

[d] *Nano-Science Center, Department of Chemistry, University of Copenhagen, Universitetsparken 5, 2100 Copenhagen, Denmark*

Abstract

Calcite was precipitated in flow-through experiments at 25 ºC from supersaturated aqueous solutions in the presence of seeds of calcite and six different silicates: augite, basaltic glass, enstatite, labradorite, olivine, and peridotite. The aim of the experiments was to determine how calcite nucleation and growth depends on the identity and structure of the growth substrate. Calcite saturation was achieved by mixing a $CaCl_2$-rich solution with a $NaHCO_3$-Na_2CO_3 buffer in a mixed-flow reactor containing 0.5-2 grams of individual mineral or rock grains. This led to a calcite saturation index of 0.6 and pH 9.1 for the reactive solution inside the reactor. Although chemical conditions, flow rate and temperature were identical for all experiments, the onset of calcite nucleation and the amount of calcite being precipitated depended on the identity of the mineral substrate. With calcite as the growth substrate, new calcite crystals formed instantaneously. Calcite nucleated relatively rapidly on olivine, enstatite, and peridotite (mainly composed of Mg-

*Corresponding author.
E-mail: gjs3@hi.is (G.J. Stockmann)
Present Address: Nordic Volcanological Center, Institute of Earth Sciences, University of Iceland, Sturlugata 7, 101 Reykjavik, Iceland. Tel.: +354 857 4079 ; fax: +354 562 9767.

olivine). Scanning Electron Microscope images showed silicate crystals to be almost completed covered with calcite coatings at the end of the experiments. Less calcite growth was found on labradorite and augite, and least on basaltic glass. In all cases, calcite precipitation occurs on the mineral substrate and not adjacent to them. These findings indicate that calcite nucleation and its subsequent growth depends on the crystal structure of the silicate substrate. Orthorhombic silicate minerals (olivine and enstatite) are the easiest for trigonal calcite to nucleate on. Monoclinic augite and triclinic labradorite show intermediate behavior, whereas basaltic glass with its non-ordered crystal structure is the least favorable platform for calcite growth. The results have implications for CO_2 mineralization in ultramafic and basaltic rocks indicating that trigonal carbonates precipitate easier on crystalline rather than glassy rocks, but even glass surfaces can serve as a substrate for calcite nucleation.

Keywords: Calcite coatings, silicates, nucleation kinetics, crystallography, mixed-flow reactors, CO_2 sequestration

1. Introduction

Calcite precipitation is a prerequisite for a successful and optimized carbon dioxide sequestration through carbonate mineralization as described by e.g. Oelkers et al. (2008); Wakahama et al. (2009); Gislason et al. (2010), and Flaathen et al. (2011). Thus understanding the effects and processes that controls calcite precipitation on silicates are important for the success of carbon mineralization efforts in basaltic rocks as currently carried out in Iceland (Oelkers et al., 2008; Alfredsson et al., 2008; Gislason et al., 2010; Matter et al., 2009; 2011; Gysi and Stefansson, 2011; 2012; Aradóttir et al., 2011; 2012). The results reported within this manuscript are a continuation of the calcium carbonate coating experiments carried out on basaltic glass and diopside described in Chapter 2 and 3 in this thesis. Simultaneous-run experiments on basaltic glass and diopside showed that identical experimental settings led to different results in how extensively the calcium carbonate coating was covering the primary surface. Whereas basaltic glass had no calcite precipitates on its surface, diopside crystals were extensively covered by carbonate growth. This indicated that

primary crystal structure might play a role in the nucleation and growth of secondary carbonate. Therefore, six different silicates, representing four different crystal structures, were selected for flow-through experiments in this study, where the inlet solution inside the reactor was supersaturated with respect to calcite. By applying identical chemical conditions to each silicate experiment, it was possible to deduce the effect of primary mineral structure on calcite nucleation and precipitation.

Mechanisms that control secondary mineral growth are; degree of saturation, chemical composition of primary and secondary phase, match of crystallographic properties between primary and secondary minerals, molar volume of both phases, and presence of aqueous ions that can either enhance or inhibit calcite growth (e.g. Velbel 1993; Lasaga, 1998; Cubillas et al., 2005; Benning and Waychunas, 2007; Putnis, 2009). The best-known examples of ions that can inhibit calcite growth are inorganic phosphate (Plant and House, 2002), Mg^{2+} ions (Zhang and Dawe, 2000) and natural organic materials (Lin et al., 2005). There are fewer examples of ions that enhance calcite growth, but these include aqueous Na_2SO_4 at basic pH (Vavouraki et al., 2008). However, Flaathen et al. (2011) reached the conclusion that the presence of 5 mM SO_4^{2-} in solution inhibited calcite precipitation rates by 40%.

Putnis (2009) noted that the replacement of one mineral by another is closely related to the mineral structure and the relative volumes of the phases involved, and emphasized the importance of structural control on secondary minerals formation on the surfaces of primary minerals. In addition, Putnis (2009) reported that mineral replacement reactions are favoured when the primary phase contributes elements to the secondary phase. Both diopside and basaltic glass contains Ca^{2+} and Mg^{2+} ions that could potentially form carbonates. The lack of carbonate precipitates on the glass suggests that a local source of elements is not itself sufficient to provoke secondary mineral precipitation on the dissolving mineral surface. This study aims to provide further insight into processes that control calcite precipitation on silicate mineral surfaces through a series of six different silicate (enstatite, olivine, augite, labradorite, basaltic glass and peridotite) dissolution experiments performed in the presence of co-precipitating calcite. A few experiments with calcite growth on calcite were carried out for comparison.

2. Theoretical Background

The standard state adopted in this study is that of unit activity of pure minerals and H_2O at any temperature and pressure. For aqueous species other than H_2O, the standard state is unit activity of species in a hypothetical 1.0 mol/kg solution referenced to infinite dilution at any temperature and pressure. Thermodynamic calculations reported in this study were performed using the PHREEQC 2.17 computer code (Parkhurst and Appello, 1999) together with its llnl.dat and minteqv4.dat databases. Calcite and the majority of the silicates (enstatite, augite, labradorite and olivine) used in this study were already included in one of the PHREEQC databases. Exceptions were the basaltic glass and the ultramafic rock, peridotite. In case of the basaltic glass, thermodynamic properties of hydrated leached basaltic glass with the composition, $SiAl_{0.35}O_2(OH)_{1.05}$, was added to the minteqv4 database. The equilibrium constant (K) for the leached glass dissolution reaction was calculated from the stoichiometric sum of the equilibrium constants of amorphous SiO_2 and amorphous $Al(OH)_3$ hydrolysis reactions to be Log K = 1.07 and its corresponding ΔH_r = -22.47 kJ/mol at 25 ºC (Stockmann et al., 2012).

Calcite precipitates readily when supersaturated in solution by the reaction:

$$Ca^{2+} + CO_3^{2-} = CaCO_3(s) \quad (1)$$

Calcite dissolution and precipitation kinetics are traditionally described as a function of the degree of disequilibrium in aqueous solution by using a mechanistic model formulated by Plummer et al. (1978) for calcite dissolution. This can be expressed by the following empirical equation for precipitation reactions:

$$r = k(\Omega - 1)^n \quad (2)$$

where r is the precipitation rate normalized to reacting surface, k is the apparent rate constant, $(\Omega - 1)$ represents the degree of supersaturation of solution, and n designates the empirical order of reaction, which is indicative of the growth mechanism of mineral surfaces. The Ω defines the saturation state of solution, equal to the ratio of the ion activity product of dissolved mineral components (Q) to the thermodynamic

solubility product (K_{sp}). For calcite, the saturation state is defined as:

$$\Omega = \frac{Q}{K_{sp}} = \frac{a_{Ca^{2+}} \cdot a_{CO_3^{2-}}}{K_{sp}} \quad (3)$$

where a_i refers to the activity of the subscripted aqueous species.

3. Materials and methods

3.1 Silicate minerals and rocks

Six different silicates were used for combined silicate dissolution and calcite precipitation experiments in this study; augite, enstatite, olivine, labradorite, basaltic glass and peridotite. Enstatite from Bamble, Norway, augite from Harcourt, Ontario, Canada and labradorite from Sonora, Mexico were bought as mm-large crystals and crushed with agate mortar and pestle to a smaller size fraction. The 45-125 um size fraction for each of the three minerals were obtained through first sieving and then cleaning in several cycles of acetone, discarding the fine particles in each cleaning cycle until the acetone liquid appeared clear. Powders of olivine (Fo93) and peridotite from Gusdal in Norway, mainly composed of Mg-rich olivine and minor amounts of pyroxene, were bought in the 65-125 μm and 45-125 μm size fractions, respectively, and thus only went through the acetone cleaning cycles described above. The basaltic glass was collected from the Stapafell Mountain in Southwest Iceland and is the same material as was previously described by Oelkers and Gislason (2001), Gislason and Oelkers (2003), Wolff-Boenisch et al. (2011) and Stockmann et al. (2011; 2012). The preparation of the 45-125 μm size fraction of the basaltic glass is described in detail in Stockmann et al. (2011). After cleaning, all silicates were dried in the oven overnight at 60 °C. The chemical composition of the six silicates, determined by X-ray Fluorescence spectrometry, is listed in Table 1. The specific surface area, A_{BET}, of each cleaned silicate powder was determined by the multi-point krypton adsorption BET method and are listed in Table 2, together with the calculated geometric surface area, A_{geo} and roughness factor.

3.2 Calcite

The calcite powder used in this study were originally large transparent Iceland spar calcite crystals collected from hydrothermal veins in basaltic traps in Central Siberia, and is the same material as was described by Pokrovsky et al. (2005) and Flaathen et al. (2011). These authors reported that electron microprobe and total chemical analysis showed their samples contained less than 0.5% impurities and that no other phases were detected by X-ray diffraction (XRD). The size fraction of this calcite powder was 100-200 μm and the specific surface area of the resulting calcite powder was 370 cm^2/g (Pokrovsky et al., 2005) as determined by multi-point krypton absorption using the BET method. For a detailed description of preparation and cleaning of this calcite powder see Pokrovsky et al. (2005) and Flaathen et al. (2011).

3.3 Dissolution-precipitation experiments in mixed-flow reactors

The silicate dissolution / calcite precipitation experiments conducted within this study were split into three experimental series; 1) short-term precipitation of calcite on silicates, 2) short-term pure dissolution experiments of silicates with no precipitation of secondary phases taking place, and 3) long-term precipitation of calcite on the same silicate samples as dissolved in series 2, a continuation of that project. All three experimental series used mixed-flow polypropylene reactors with a volume of 30 mL in experimental series 1, and a volume of 300 mL in experimental series 2 and 3. The experimental setup for experimental series 1 is illustrated on Fig. 1. Experimental series 2 and 3 used a similar setup just with another type of reactors. A weighed mass of silicate powders or calcite seeds were inserted into the mixed-flow reactor and induced into a water bath kept at 25 ± 2 °C. Reactors were continuously stirred with floating Teflon stirring bars, and sample solution left the reactor through a 2.5 μm polypropylene filter. Additional filtering through a 0.2 μm cellulose acetate membrane filters was performed on the outlet fluid samples before chemical analysis. Calcite precipitation was achieved by mixing two solutions inside the reactor; 1) an aqueous Na-carbonate solution and 2) an aqueous $CaCl_2$ solution leading to a mixed solution inside the reactor of pH 9.1, and a calcite saturation index of 0.6. In the pure silicate dissolution experiments (series 2) only the aqueous Na-carbonate solution

with a pH of 9 was used as inlet. In experimental series 3, the reactors were not continuously flow-through experiments as the inlet flows were stopped during weekends for practical reasons, whereas reactor stirring and water bath temperature control ran continuously for the two months duration of these experiments. The main purpose of these experiments was to see if long-term exposure to a calcite-saturated solution would create even more calcite precipitation on the silicate surfaces.

The Na-carbonate solution comprised of demineralised H_2O, $NaHCO_3$ (99.5%) and Na_2CO_3 (>99%) from Sigma-Aldrich. The Ca-bearing solution comprised of $CaCl_2$ (1000 ppm standard) from Merck, and this acidic $CaCl_2$ stock solution was neutralized using 1 mol/kg NaOH from Merck. Concentrations of $NaHCO_3$ and Na_2CO_3 in the carbonate solution were 0.0169 and 0.00129 mol/kg, respectively, and the $CaCl_2$ solution had a Ca concentration of 0.277 mmol/kg.

By use of Gilson peristaltic pumps, the two inlet solutions were injected simultaneously and at identical flow rates into the reactors creating a 1:1 mixture. The injection of two separate solutions was essential to avoid calcite precipitation prior to solution entry into the reactor. At the onset of each experiment, the reactor was filled with 0.25-2 g of silicate or calcite seed crystals and a 1:1 mixture of the two inlet solutions. Outlet solution pH was measured at 23 ± 2 °C immediately after sampling. The short-term calcite precipitation experiments typically ran for 2-10 days (series 1), whereas the pure silicate dissolution experiments ran for 14 days (series 2), and the long-term calcite coating experiments for two months (series 3).

3.4 Analytic methods

Sample solutions from experimental series 1 were analysed using a Varian SpectrAA 300 atomic absorption spectrometer for Ca content of the inlet and outlet solutions, the 'molybdate blue method' for silicon (Koroleff, 1976), and a Perkin Elmer Zeeman 5000 Atomic Absorption Spectrometer (AAS) for magnesium. The major element concentrations of inlet and outlet fluids from experimental series 2 and 3 were determined using a Spectro Ciros Vision Inductively Coupled Plasma Optical Emission Spectrometer (ICP-OES).

Selected solid samples were examined by a HITACHI S3400N Scanning Electron Microscope (SEM) after gold metallization, and by X-ray Photoelectron Spectroscopy (XPS). Energy Dispersive X-ray Spectroscopy (EDS) was used together with SEM to

identify primary and secondary mineral phases. Cleaned silicate powders were analyzed by X-ray Fluorescence spectroscopy and X-ray diffraction prior to experiments to determine their chemical composition and pureness. XPS analyses were used to quantify the stoichiometry of the silicate surface layers (<100 Å) with and without carbonate coatings using a Kratos Axis Ultra DLD instrument. One set of post-experimental powder samples was cleaned with demineralised H_2O (MilliQ) and the other with a calcite-saturated solution (Cc). Data interpretation of XPS results was made with the commercial software CasaXPS, using a Shirley background. Analytical uncertainties on the analysis methods used in this study are estimated to be 2% for the AAS analysis, 3% for the spectrophotometer, 3-5% for the ICP-OES analyses, and 10% for the XPS analysis.

4. Experimental results

All experiments were run at pH ~9 and 25 ºC using mixed-flow reactors. An overview of the experimental conditions and the steady-state results obtained from the three experimental series is provided in Table 3a-b. The results of XPS surface analysis of the pre- and post-experimental silicate powders are listed in Table 4.

Steady-state calcite precipitation rates was calculated from the measured steady-state Ca concentration from the formula:

$$r = \frac{\Delta[Ca] \cdot fr}{A_{BET} \cdot m} \quad (4)$$

where $\Delta[Ca]$ stands for the concentration of Ca in the outlet fluid minus the Ca concentration in the inlet fluid, *fr* refers to the fluid flow rate, A_{BET} designates the BET specific surface area of the calcite, and *m* denotes the initial mass of calcite used in the experiment.

Silicate concentration were measured for all outlet solution samples in this study, except the calcite powder experiments, and the silicate mineral and glass dissolution rates based on the release of the *i*th element ($r_{+,i,j}$) were calculated from:

$$r_{+,i,j} = \frac{\Delta C_i \cdot fr}{\nu_i \cdot A_j \cdot m} \quad (5)$$

where ΔC_i stands for the concentration of the *i*th element in the outlet fluid minus its concentration in the inlet fluid, *fr* refers to the fluid flow rate, ν_i is a stoichiometric factor equal to the number of moles of the *i*th element in one mole of the material, A_j designates the specific surface area of the material, and *m* denotes the mass of material used in the experiment. The index *j* refer to rates calculated either using the measured BET surface area, A_{BET} or the geometric surface area, A_{geo}. In this study, only BET rates are provided.

4.1 Short-term calcite precipitation (Experimental series 1)

Six experimental series were carried out on calcite and five different silicates (augite, enstatite, olivine, basaltic glass, labradorite) under identical experimental conditions for 2-10 days. The temporal evolution of the Ca outlet concentration in each individual experiment is shown in Figs. 2a-f. Inlet solution concentrations of Ca are marked as a solid line on these plots, and a decrease in Ca outlet concentration compared to the inlet is interpreted to be due to calcite precipitation removing Ca from solution. In the experiments were calcite is the solid phase, the Ca outlet concentration reaches a new steady-state value within one day of experiment, as shown on Fig. 2a. For the silicates, on the other hand, a new steady-state Ca concentration is first reached after 4-5 days in the case of olivine and enstatite (Fig. 2b and d, respectively), and after 8 days for labradorite (Fig. 2f), whereas basaltic glass and augite never reaches a new steady-state Ca concentration within the ~10 days duration of the experiments (Fig. 2c and e, respectively). On Figure 3, selected data series from the plots on the figs. 2 are plotted together for comparison. Judging from this figure it looks like the Ca outlet concentration for both the majority of the calcite experiments and the silicate experiments reaches a new steady-state value around ~0.04 mmol/kg. This concentration corresponds to SI calcite = 0.35 ± 0.10 (see Table 3). Only the first calcite experiment, C-1 (Fig. 2a) had a final steady-state Ca concentration close to calcite saturation, SI calcite = 0.10 ± 0.10 (Table 3).

The Si and Mg concentration in the outlet solutions were also measured for the silicate experiments, and the calculated mineral/glass dissolution rates based on Si ±

Mg are shown in Figs. 3a-e. The rates are calculated according to the stoichiometry mineral/glass formulas provided in Table 3. However, element release rates uncorrected for stoichiometry are also listed in the table. These silicate experiments were not set up with the purpose of determining mineral dissolution rates at 25 ºC, but judging from the plots they all end up on a steady-state dissolution. A chemical steady state for these experiments should theoretically be reached within 3 residence times, 3τ, where the residence times is defined as the reactor volume divided by the fluid flow rate. For these experiments this corresponds to 3 * (30 ml / 0.5 ml/min) = 3 hours. Measured steady state is generally defined as the outlet fluid concentration remaining constant, within analytical uncertainty, for at least 10 residence times, in this case 10 hours. Thus, it is realistic that steady-state dissolution of these silicate minerals and basaltic glass was indeed reached.

Figures 4a and b illustrate calcite precipitation rates as a function of elapsed time, and initial mass of calcite powder, respectively. Calcite precipitation rates reach a steady state almost instantly, and they are clearly correlated to amount of calcite powder present (Fig. 4b).

4.2 Short-term silicate mineral/rock dissolution experiments (Experimental series 2)

These experiments were run as pure silicate dissolution experiments using only one inlet solution comprised of 8.36 mM $NaHCO_3$ / 0.64 mM Na_2CO_3 (pH 9). The silicate powders used in these experiments were olivine, enstatite, augite, labradorite and peridotite. The majority of these silicates contain low amounts of Ca (see Table 1), thus release of Ca from the silicates in reaction with the carbonate-containing inlet are not expected to lead to calcite precipitation. SEM analysis of the post-experimental powders did not detect calcite or any secondary phases. Figures 5a-d illustrates the temporal evolution of the silicate mineral dissolution rates of olivine, enstatite, augite and labradorite. Figure 5e show the Si and Mg element release rates from dissolution of peridotite. Both dissolution rates and element release rates for each silicate phase are listed in Table 3. The rates from series 2 are referred to as the '[silicate initial] 1-C' names. There is a consistency between the rates obtained from experimental series 1 and series 2 (see Table 3).

4.3 Long-term calcite precipitation on silicate minerals/rock (Experimental series 3)

Experimental series 3 was a continuation of series 2, where the mixed-flow reactors containing the same silicate powders were connected to two inlets instead of the previous one carbonate-bearing inlet. These two new inlet solutions comprised of 1) 0.1461 mM $CaCl_2$ + 14 ml 0.058 M NaOH and 2) 16.72 mM $NaHCO_3$ / 1.30 mM Na_2CO_3. The solution inside the reactor was a 1:1 mixture of the two inlets with a pH of 9.1 at 25 ºC, and identical to the inlet solutions used in experimental series 1. However, the main purpose of experimental series 3 was to expose the silicate powders to long-term exposure to a calcite-saturated solution to maximize calcite growth on the silicate surfaces. The experiments ran for approximately 70 days, and element concentration in the outlet solutions were frequently measured as illustrated on figures 7a-e. Temporal evolution of element concentrations are generally stable or increasing after ~30 days of experiment, thus calcite precipitation does not seem to decrease element release from the silicates although SEM photos show extensive calcite growth on some of the silicate surfaces (see Fig. 8).

4.4 Results of SEM and XPS analysis

All pre- and post-experimental powders from this study were exposed to SEM and XPS analysis. Both analysis techniques confirmed the precipitation of calcite on the silicate surfaces as was previously interpreted from changes in the Ca concentration of the solution samples. The most extensive growth of calcite was found on enstatite, olivine (Mg-rich) and peridotite (mainly composed of Mg-rich olivine), and least on basaltic glass as illustrated by the SEM images in Fig. 8. Labradorite and augite showed intermediate calcite coverage. Surface analysis of the silicates by XPS (Table 4) shows predominantly changes in the Ca/Si ratio from olivine, enstatite and peridotite, confirming the results of solution chemistry and SEM that these are the silicate phases most extensively covered by calcite precipitates.

4.5 Comparison with silicate dissolution rates from the literature

The dissolution rates obtained from this study are compared to rates from the literature in Table 5. Dissolution rate data are extensively reported in the literature for

olivine (e.g. Grandstaff, 1977; Kuo and Kirkpatrick, 1985; de Leeuw et al., 2000; Pokrovsky and Schott, 2000a,b; Rosso and Rimstidt, 2000; Oelkers, 2001; Morales and Herbert, 2002; Olsen and Rimstidt, 2008; Prigiobbe et al., 2009), diopside (e.g. Knauss et al., 1993; Chen and Brantley, 1998; Golubev et al., 2005; Golubev and Pokrovsky, 2006; Dixit and Carroll, 2007; Daval et al., 2010), enstatite (e.g. Oelkers and Schott, 2001; Halder and Walther, 2011) and basaltic glass (e.g. Oelkers and Gislason, 2001; Gislason and Oelkers, 2003; Wolff-Boenisch et al., 2004a,b; 2006; 2011; Stockmann et al., 2011; 2012), whereas only limited data are available for augite (e.g. Siegel and Pfannkuch, 1984; Schott and Berner, 1985; Sverdrup, 1990; McAdam et al., 2008) and labradorite (Sjoberg, 1989; Welch and Ulman, 1993; McAdam et al., 2008) and none at basic pH. Augite is compared to the dissolution rate of diopside ($CaMgSi_2O_6$), another more simple clinopyroxene, although results were previously reported at pH 5.8 and 25 ºC (Hoch et al., 1996) indicating rates of augite could be faster than diopside's under oxidizing conditions due to a higher Fe content in augite. These authors concluded that the dissolution rate is directly related to oxidation of iron favouring faster augite dissolution rates over the more iron-poor diopside. Conclusively, it can be seen from Table 5 that both augite and enstatite dissolution rates from this study are ~ 0.5-1.0 log unit faster than rates reported in the literature, whereas dissolution rates of basaltic glass and olivine are identical to previous findings. Importantly, none of the rates from the experiments, where calcite was precipitating are lower than expected from the rates reported in the literature, thus the calcite precipitates are not decreasing the dissolution rates.

5. Conclusions

The results of this study indicate that calcite nucleation onsets at different times depending on the identity of the primary mineral. If the primary mineral is calcite itself, calcite nucleation and growth starts immediately. In case of the silicates, the fastest nucleation and most extensive growth of calcite was found on enstatite, olivine and peridotite, representing minerals belonging to the orthorhombic crystal structure. Intermediate growth of calcite was found on labradorite and augite, representing a triclinic and monoclinic mineral, respectively. Least calcite was found on basaltic

397 glass, which has a non-ordered silicate framework. Hence, of the silicates typically
398 present in mafic and ultramafic rocks, the orthorhombic minerals will act as the best
399 mineral platforms for calcite growth. Its implications for CO_2 sequestration efforts in
400 these rocks indicate that crystalline rocks could be faster covered by carbonate
401 coatings than the basaltic glassy rocks.
402
403 This draft manuscript will be submitted after completion of additional data
404 processing and modelling work.
405

406 ## Acknowledgements

407 We would like to thank several colleagues for their help, in particular Carole
408 Causserand, Alain Castillo, and Phillippe de Parseval for technical assistance, and
409 Therese K. Flaathen, Allison Stephenson, Sigurdur Markusson, Svava Arnardottir,
410 Sam Parry, Quentin Gautier, Giuseppe Saldi, Chris Pearce and Vasileios Mavromatis
411 for lab assistance. We are most grateful for the SEM technical support provided by
412 David Cornell and Johan Hogmalm at Geovetarcentrum, University of Gothenburg in
413 Sweden. Finally, we would sincerely like to thank Erik Sturkell for graphical
414 assistance and continued support. The Environmental and Energy Fund of Reykjavík
415 Energy, the Research Fund of the University of Iceland, the Nordic Council of
416 Ministers through NORDVULK, and the European Community through the MIN-
417 GRO Research and Training Network (MRTN-CT-2006-035488) and the ERASMUS
418 student mobility program are gratefully acknowledged for their financial support.
419

420 **References**

421 Alfredsson, H.A., Hadrarson, B.S., Franzson, H., Gislason, S.R., 2008. CO_2
422 sequestration in basaltic rock at the Hellisheidi site in SW Iceland: stratigraphy and
423 chemical composition of the rocks at the injection site. Min. Mag. 72, 1–5.

424 Aradóttir, E.S.P., Sigurdardóttir, H., Sigfússon, B., Gunnlaugsson, E., 2011. CarbFix -
425 a CCS pilot project imitating and accelerating natural CO_2 sequestration.
426 Greenhouse Gases: Science and Technology 1, 105–118.

427 Aradóttir, E. S., Sonnenthal, E., Bjornsson, G., Jonsson, H., 2012. Multidimensional
428 reactive transport modeling of CO_2 mineral sequestration in basalts at the
429 Hellisheidi geothermal field, Iceland. Int. J. Greenhouse Gas Control 9, 24-40.

430 Benning, L.G., Waychunas, G.A., 2008. Nucleation, growth, and aggregation of
431 mineral phases. Mechanism and kinetic controls.259-333. In (S.L.Brantaley,
432 J.D.Kubiki and A. F. White eds.) Kinetics of Water-Rock Interactions. Springer.

433 Chen, Y., Brantley, S.L., 1998. Diopside and anthophyllite dissolution at 25° and
434 90°C and acid pH. Chem. Geol. 147, 233-248.

435 Cubillas, P., Köhler, S., Prieto, M., Causserand, C., Oelkers, E.H., 2005. How do
436 mineral coatings affect dissolution rates? An experimental study of coupled $CaCO_3$
437 dissolution – $CdCO_3$ precipitation. Geochim. Cosmochim. Acta 69, 5459–5476.

438 Daval, D., Hellmann, R., Corvisier, J., Tisserand, D., Martinez, I., Guyot, F., 2010.
439 Dissolution kinetics of diopside as a function of solution saturation state:
440 Macroscopic measurements and implications for modeling of geological storage of
441 CO_2. Geochim. Cosmochim. Acta 74, 2615–2633.

442 de Leeuw, N.H., Parker, S.C., Catlow, C.R.A., Price, G.D., 2000. Modelling the effect
443 of water on the surface structure and stability of forsterite. Phys. Chem. Miner. 27,
444 332–341.

445 Dixit, S., Caroll, S.A., 2007. Effect of solution saturation state and temperature on
446 diopside dissolution. Geochem. Trans. doi:10.1186/1467-4866-8-3.

447 Flaathen, T.K., Oelkers, E.H., Gislason, S.R., Aagaard, P., 2011. The effect of
448 dissolved sulphate on calcite precipitation kinetics and consequences for
449 subsurface CO_2 storage. Energy Procedia 4, 5037–5043.

450 Gislason, S.R., Oelkers, E.H., 2003. Mechanism, rates and consequences of basaltic
451 glass dissolution: II. An experimental study of the dissolution rates of basaltic glass
452 as a function of pH and temperature. Geochim. Cosmochim. Acta 67, 3817-3832.

453 Gislason, S.R., Wolff-Boenisch, D., Stefansson, A., Oelkers, E.H., Gunnlaugsson, E.,
454 Sigurdardóttir, H., Sigfússon, G., Brocker, W.S., Matter, J., Stute, M., Axelsson,
455 G., Fridriksson, T., 2010. Mineral sequestration of carbon dioxide in basalt: A pre-
456 injection overview of the CarbFix project. Int. J. Greenhouse Gas Control 4, 537-
457 545.

458 Golubev, S.V., Pokrovsky, O.S., Schott, J., 2005. Experimental determination of the
459 effect of dissolved CO_2 on the dissolution kinetics of Mg and Ca silicates at 25 °C.
460 Chem. Geol. 217, 227-238.

461 Golubev, S.V., Pokrovsky, O.S., 2006. Experimental study of the effect of organic
462 ligands on diopside dissolution kinetics. Chem. Geol. 235, 377-389.

463 Grandstaff, D.E., 1977. Some kinetics of forsterite olivine dissolution. Trans. Am.
464 Geophys. Union 58, 539.

465 Gysi, A.P., Stefansson, A., 2011. CO_2–water–basalt interaction. Numerical simulation
466 of low temperature CO_2 sequestration into basalts. Geochim. Cosmochim. Acta 75,
467 4728–4751.

468 Gysi, A.P., Stefansson, A., 2012. CO_2-water-basalt interaction. Low temperature
469 experiments and implications for CO_2 sequestration into basalts. Geochim.
470 Cosmochim. Acta. 81, 129-152.

471 Halder, S., Walther, J.V., 2011. Far from equilibrium enstatite dissolution rates in
472 alkaline solutions at earth surface conditions. Geochim. Cosmochim. Acta 75,
473 7486–7493.

474 Hoch, A.R., Reddy, M.M., Drever, J.I., 1996. The effect of iron content and dissolved
475 O_2 on dissolution rates of clinopyroxene at pH 5.8 and 25°C: preliminary results.
476 Chem. Geol. 132, 151-156.

Knauss, K.G., Nguyen, S.N., Weed, H.C., 1993. Diopside dissolution kinetics as a function of pH, CO_2, temperature, and time. Geochim. Cosmochim. Acta 57, 285-294.

Koroleff, F., 1976. Determination of silicon. In: Grasshoff, K. (Ed.), Methods of seawater analysis. Springer Verlag, New York. pp. 149–158.

Kuo, L.C., Kirkpatrick, R.J., 1985. Kinetics of crystal dissolution in the system diopside–forsterite–silica. Am. J. Sci. 285, 51–90.

Lasaga, A.C., 1984. Chemical kinetics of water-rock interactions. J. Geophys. Res. 89(B6), 4009-4025.

Lin, Y.P., Singer, P-C., Aiken, R., 2005. Inhibition of calcite precipitation by natural organic material: Kinetics, mechanism and thermodynamics. Env. Sci. Tech. 39, 6420-6428.

Matter, J.M., Broecker, W.S., Stute, M., Gíslason, S.R., Oelkers, E.H., Stefánsson, A., Wolff-Boenisch, D., Gunnlaugsson, E., Axelsson, G., Björnsson, G., 2009. Permanent carbon dioxide storage into basalt: the CarbFix pilot project, Iceland. Energy Procedia 1, 3641–3646.

Matter, J.M., Broecker, W.S., Gislason, S.R., Gunnlaugsson, E., Oelkers, E.H., Stute, M., Sigurdardóttir, H., Stefansson, A., Alfredsson, H.A., Aradóttir, E.S., Axelsson, G., Sigfusson, B., Wolff-Boenisch, D., 2011. The CarbFix Pilot Project – Storing Carbon Dioxide in Basalt. Energy Procedia 4, 5579-5585.

McAdam, A.C., Zolotov, M.Y., Sharp, T.G., Leshin, L.A., 2008. Preferential low-pH dissolution of pyroxene in plagioclase–pyroxene mixtures: Implications for martian surface materials. Icarus 196, 90–96.

Morales, T.A., Herbert, R., 2002. Surface chemistry and acidic dissolution of forsterite. Geochim. Cosmochim. Acta 66, A521.

Oelkers, E.H., 2001. An experimental study of forsterite dissolution rates as a function of temperature and aqueous Mg and Si concentrations. Chem. Geol. 175, 485–494.

Oelkers, E.H., Schott, J., 2001. An experimental study of enstatite dissolution rates as a function of pH, temperature, and aqueous Mg and Si concentration, and the mechanism of pyroxene/pyroxenoid dissolution. Geochim. Cosmochim. Acta 65, 1219-1231.

Oelkers, E.H., Gislason, S.R., 2001. The mechansim, rates and consequences of basaltic glass dissolution: I. An experimental study of the dissolution rates of basaltic glass as as function of aqueous Al, Si and oxalic acid concentration at 25 °C and pH = 3 and 11. Geochim. Cosmochim. Acta 65, 3671-3681.

Oelkers, E.H., Gislason, S.R., Matter, J., 2008. Mineral carbonation of CO_2. Elements 4, 333-337.

Olsen, A.A., Rimstidt, J.D., 2008. Oxalate-promoted forsterite dissolution at low pH. Geochim. Cosmochim. Acta 72, 1758–1766.

Parkhurst, D.L., Appelo, C.A.J., 1999. User's guide to PHREEQC (version 2) — A computer program for speciation, batch-reaction, one-dimensional transport, and inverse geochemical calculations.Washington, DC: U.S. Geological Survey Water-Resources Investigations Report 99-4259, 312 p.

Plant, L.J., House, W.A., 2002. Precipitation of calcite in the presence of inorganic phosphate. Colloids and Surfaces A: Physiochemical and Engineering Aspects 203, 143-153.

Plummer, L.N., Wigley, T.M.L., Parkhurst, D.L., 1978. Kinetics of calcite dissolution in CO_2-water system at 5 °C to 60 °C and 0.0 to 1.0 atm CO_2. Am. J. Sci. 278, 179-216.

Pokrovsky, O.S., Schott, J., 2000a. Forsterite surface composition in aqueous solutions: a combined potentiometric, electrokinetic, and spectroscopic approach. Geochim. Cosmochim. Acta 64, 3299–3312.

Pokrovsky, O.S., Schott, J., 2000b. Kinetics and mechanism of forsterite dissolution at 25 °C and pH from 1 to 12. Geochim. Cosmochim. Acta 64, 3313–3325.

Pokrovsky, O.S., Golubev, S.V., Schott J., 2005. Dissolution kinetics of calcite, dolomite and magnesite at 25°C and 0 to 50 atm pCO_2. Chem. Geol. 217, 239-255.

Prigiobbe, V., Costa, G., Baciocchi, R., Hanchen, M., Mazzotti, M., 2009a. The effect of CO_2 and salinity on olivine dissolution kinetics at 120 °C. Chem. Eng. Sci. 64, 3510–3515.

Putnis, A., 2009. Mineral Replacement Reactions. Rev. Min. Geochem. 70, 87-124.

Rosso, J.J., Rimstidt, J.D., 2000. A high resolution study of forsterite dissolution rates. Geochim. Cosmochim. Acta 64, 797–811.

Schott, J., Berner, R.A., 1985. Dissolution mechanisms of pyroxenes and olivines during weathering. In The Chemistry of Weathering (ed. J. J. Drever) pp. 35–53. D. Riedel Publ. Co.

Siegel, D.I., Pfannkuch, H.O., 1984. Silicate mineral dissolution at pH 4 and near standard temperature and pressure. Geochim. Cosmochim. Acta 48, 197–201.

Sjoberg, L., 1989. Kinetics and stoichiometry of labradorite dissolution. In: Miles, D.L. (Ed.), Proc. of the 6th Int. Symp. on Water–Rock Inter., Malvern, UK, pp. 639–642.

Stockmann, G.J., Wolff-Boenisch, D., Gislason, S.R., Oelkers, E.H., 2011. Do carbonate precipitates affect dissolution kinetics? 1: Basaltic glass. Chem. Geol. 284, 306-316.

Stockmann, G.J., Shirokova, L.S., Pokrovsky, O.S., Bénézeth, P., Bovet, N., Gislason, S.R., Oelkers, E. H., 2012. Does the presence of heterotrophic bacterium *Pseudomonas reactans* affect basaltic glass dissolution rates? Chem. Geol. 296-297, 1-18.

Sverdrup, H.U., 1990. The Kinetics of Base Cation Release Due to Chemical Weathering. Lund University Press, Lund, Sweden.

Vavouraki, A., Putnis, C., Putnis, A., Koutsoukos, P.G., 2008. An Atomic Force Microscopy study of the growth of calcite in the presence of sodium sulfate. Chem. Geol. 253, 243-251.

Velbel, M.A., 1993. Formation of protectiye surface layers during silicate-mineral weathering under well-leached oxidizing conditions. Am. Min. 78, 405-414.

Wakahama, H., Mito, S., Ohsumi, T., Ueda, A., Yajima, T., Satoh, H., Sugiyama, K., Ozawa, A., Ajima, S., Todaka, N., Sato, T., Kato, M., Kaji, Y., Tokumarui, T.,

564 Kaieda, H., Kubota, K., 2009. A concept of CO_2 Georeactor sequestration at the
565 Ogachi HDR site, NE Japan. Energy Procedia 3683–3689.

566 Welch, S.A., Ullman, W.J., 1993. The effect of organic acids on plagioclase
567 dissolution rates and stoichiometry. Geochim. Cosmochim. Acta 57, 2725-2736.

568 Wolff-Boenisch, D., Gislason, S.R., Oelkers, E.H., Putnis, C.V., 2004a. The
569 dissolution rates of natural glasses as a function of their composition at pH 4 and
570 10.6, and temperatures from 25 to 74°C. Geochim. Cosmochim. Acta 68, 4843–
571 4858.

572 Wolff-Boenisch, D., Gislason, S.R., and Oelkers, E.H., 2004b. The effect of fluoride
573 on the dissolution rates of natural glasses at pH 4 and 25°C. Geochim. Cosmochim.
574 Acta 68, 4571–4582.

575 Wolff-Boenisch D., Gislason S.R., Oelkers, E.H., 2006. The effect of crystallinity on
576 dissolution rates and CO_2 consumption capacity of silicates. Geochim.
577 Cosmochim. Acta, 70, 858-870.

578 Wolff-Boenisch, D., Wenau, S., Gislason, S.R., Oelkers, E.H., 2011. Dissolution of
579 basalts and peridotite in seawater, in the presence of ligands, and CO_2:
580 Implications for mineral sequestration of carbon dioxide. Geochim. Cosmochim.
581 Acta 75, 5510-5525.

582 Zhang, Y., Dawe, R.A., 2000. Influence of Mg^{2+} on the kinetics of calcite
583 precipitation and calcite crystal morphology. Chem. Geol. 163, 129-138.

584

584

Table 1

Chemical composition of investigated minerals and rocks (in wt%) obtained from XRF analysis [a]

Mineral	SiO_2	Al_2O_3	Fe_2O_3	MgO	CaO	Na_2O	K_2O	TiO_2	MnO	P_2O_5	LOI	Total
Augite	53.15	0.87	10.86	11.74	23.15	0.48	0.003	0.029	0.266	0.004	-0.78	99.76
Basaltic glass	48.55	14.43	12.08	9.51	11.94	1.91	0.274	1.570	0.192	0.199	-0.66	100.00
Enstatite	57.59	0.70	7.73	30.05	1.75	0.23	0.024	0.073	0.048	1.022	0.49	99.71
Labradorite	53.54	29.42	0.40	0.00	12.15	4.28	0.370	0.093	0.005	0.015	0.03	100.30
Olivine	42.76	0.27	7.81	48.15	0.36	0.01	0.019	0.021	0.110	0.010	0.45	99.97
Peridotite	43.06	0.46	7.01	48.99	0.04	0.00	0.000	0.013	0.101	0.008	0.24	99.92

[a] Analyzed at the Grant Institute, University of Edinburgh, 2011

Table 2

Specific surface area of the mineral and rock powders used in this study

Mineral [a]	Specific surface area (cm^2/g)			Density	Surface roughness
	A_{BET} [c]		A_{geo} [d]	(g/cm^3)	(A_{BET}/A_{geo})
Augite	1528	±20	225	3.40	7
Basaltic glass	5878	±40	251	3.05	23
Enstatite	4505	±30	239	3.20	19
Labradorite	694	±20	285	2.69	2
Olivine	3672	±40	200	3.27	18
Peridotite	3286	±40			
Calcite [b]	370	±20	153	2.71	2

[a] The powders are in the 45-125 µm size fraction except for peridotite (65-125 µm) and calcite (100-200 µm)

[b] A_{BET} from Pokrovsky et al. (2005)

[c] determined by multi-point krypton adsorption using the B.E.T. method

[d] calculated using equations in Wolff-Boenisch et al. (2004a)

Table 3a

Experimental conditions and steady-state results of the mineral/rock dissolution experiments performed in this study

Exp. name	Temp. (ºC)	Mass of glass (g)	Init. BET surface area (m^2)	Flow rate (g/min)	Duration of exp. (days)	Outlet pH (25 ºC)	[Si] (µmol/kg)	[Mg] (µmol/kg)	[Al] (µmol/kg)	[Ca] (µmol/kg)
Calcite	**$CaCO_3$**									
C-1	25	0.23	0.01	0.42	7.1	9.11				22.5
C-3	25	0.57	0.02	0.44	2.8	9.11				41.0
C-4	25	0.18	0.01	0.46	2.8	9.10				41.9
C-6	25	0.26	0.01	0.43	7.0	9.11				40.1
Blank	25	0.00	0.00	0.46	3.0	9.12				67.3
Olivine	**$Mg_{1.75}Fe_{0.14}Si_{1.04}O_4$ (Fo93)**									
O-2	25	0.27	0.10	0.44	7.1	9.14	0.69	1.05		43.6
O-3	25	0.25	0.09	0.44	5.7	9.15				41.6
O 1-C	25	1.98	0.73	0.92	14.0	9.16	2.04	2.42		
O 100-P	25	1.98	0.73	~1.0	66.1	9.21	0.59	1.23		23.7
Basaltic glass	**$Si_{1.000}Al_{0.350}Fe_{0.187}Mn_{0.003}Mg_{0.292}Ca_{0.263}Na_{0.076}K_{0.007}Ti_{0.024}P_{0.004}O_{3.371}$**									
BG-2	25	0.26	0.15	0.43	8.7	9.13	1.98	0.50		66.1
BG-3	25	0.26	0.15	0.45	4.0	9.13				65.6
Enstatite	**$Mg_{0.78}Fe_{0.10}Ca_{0.03}Si_{1.01}O_3$**									
E-1	25	0.27	0.12	0.42	8.7	9.11	0.64	0.36		33.0
E-2	25	0.26	0.12	0.47	4.0	9.17				57.8
E-3	25	0.25	0.11	0.40	5.5	9.17				42.7
E 1-C	25	1.99	0.90	0.96	14.0	9.17	1.77	1.53		
E 100-P	25	1.99	0.90	~1.0	66.1	9.19	0.66	1.00		26.2
Augite	**$Ca_{0.94}Mg_{0.66}Fe_{0.31}Si_2O_6$**									
A-1	25	0.25	0.04	0.47	9.0	9.14	0.73			64.6
A-2	25	0.26	0.04	0.45	2.7	9.14				65.7
A-3	25	0.25	0.04	0.24	1.5	9.14				69.8
A-4	25	0.25	0.04	0.42	1.9	9.17				68.0

A 1-C	25	1.98	0.30	0.88	14.0	9.18	1.49	1.02		
A 100-P	25	1.98	0.30	~1.0	66.1	9.28	0.93	0.90		63.2
Labradorite	**$Ca_{0.59}Na_{0.38}Al_{1.57}Si_{2.42}O_8$ (An% 60)**									
L-1	25	0.26	0.02	0.47	9.0	9.14	0.61			41.0
L 1-C	25	2.01	0.14	0.90	14.0	9.16	1.81		1.47	
L 100-P	25	2.01	0.14	~1.0	66.1	9.21	1.15		0.86	37.2
Peridotite	**release rates**									
P 1-C	25	2.05	0.67	0.90	14.0	9.18	1.29	1.78		
P 100-P	25	2.05	0.67	~1.0	66.1	9.21	0.55	1.00		27.9

Table 3b

Steady-state results of the mineral/rock dissolution experiments performed in this study

			Silicate dissolution rates based			Element release rates of silicates		
	SI Calcite	Calcite prec.	Si	Mg	Al	Si	Mg	Al
Exp. name	log Ω	Log $r_{+,BET, Ca}$ (mol/cm^2/s)	Log $r_{+,BET}$ (mol/cm^2/s)	Log $r_{+,BET}$ (mol/cm^2/s)	Log $r_{+,BET}$ (mol/cm^2/s)	Log $r_{+,BET}$ (mol/cm^2/s)	Log $r_{+,BET}$ (mol/cm^2/s)	Log $r_{+,BET}$ (mol/cm^2/s)
Calcite								
C-1	0.10	-11.39						
C-3	0.35	-12.01						
C-4	0.36	-11.45						
C-6	0.34	-11.69						
Blank								
Olivine								
O-2			-14.30	-14.34		-14.28	-14.10	
O-3								
O 1-C			-14.38	-14.54		-14.37	-14.29	
O 100-P								
Basaltic glass								
BG-2			-14.04	-14.10		-14.04	-14.63	
BG-3								
Enstatite								
E-1			-14.44	-14.57		-14.43	-14.68	
E-2								
E-3								
E 1-C			-14.50	-14.46		-14.50	-14.56	
E 100-P								

Augite						
A-1	-14.12			-13.82		
A-2						
A-3						
A-4						
A 1-C	-14.44	-14.13		-14.14	-14.31	
A 100-P						
Labradorite						
L-1	-13.95			-13.56		
L 1-C	-14.09		-14.00	-13.71		-13.80
L 100-P						
Peridotite						
P 1-C				-14.54	-14.40	
P 100-P						

Table 4

Results of X-ray Photoemission Spectroscopy (XPS) analysis on silicate surfaces

Sample: [a]	ATOMIC PERCENTAGE RATIO										
	C/Si	O/Si	Si/Si	Fe/Si	Mg/Si	Ca/Si	Na/Si	Ti/Si	Cl/Si	Al/Si	N/Si
Olivine											
Original powder	0.43	3.23	1.00	0.08	1.59	0.00	0.00	0.00	0.00	0.00	0.00
O-2 MilliQ	1.31	3.46	1.00	0.10	1.44	0.03	0.02	0.00	0.03	0.00	0.12
O-2 Cc	1.84	3.69	1.00	0.09	1.40	0.04	0.22	0.00	0.04	0.00	0.14
O-100P MilliQ	0.72	3.23	1.00	0.12	1.52	0.02	0.00		0.03		
O-100P Cc	0.71	3.39	1.00	0.12	1.43	0.05	0.03		0.02		
Augite											
Original powder	0.35	2.15	1.00	0.09	0.37	0.16	0.01	0.00	0.00	0.00	0.00
A-1 MilliQ	0.85	2.18	1.00	0.10	0.33	0.17	0.02	0.00	0.04	0.00	0.03
A-1 Cc	1.25	2.13	1.00	0.08	0.28	0.15	0.04	0.00	0.03	0.00	0.07
A-100P MilliQ	0.67	2.42	1.00	0.12	0.27	0.20	0.02		0.00		
A-100P Cc	0.51	2.32	1.00	0.11	0.27	0.19	0.06		0.00		
Basaltic glass											
Original powder	0.22	2.52	1.00	0.09	0.16	0.10	0.02	0.02	0.00	0.34	0.00
BG-2 MilliQ	0.99	2.37	1.00	0.11	0.08	0.10	0.01	0.02	0.25	0.32	0.07
BG-2 Cc	0.90	2.66	1.00	0.16	0.10	0.10	0.14	0.03	0.11	0.33	0.05
Enstatite											
Original powder	0.13	2.15	1.00	0.07	0.60	0.00	0.00	0.00	0.00	0.00	0.00
E-1 MilliQ	1.04	2.14	1.00	0.06	0.59	0.07	0.00	0.00	0.14	0.00	0.08
E-100P MilliQ	0.42	2.32	1.00	0.10	0.62	0.03	0.00		0.00		
E-100P Cc	0.35	2.24	1.00	0.08	0.59	0.02	0.03		0.00		

Labradorite											
Original powder	0.61	2.35	1.00	0.00	0.00	0.12	0.04	0.00	0.00	0.59	0.00
L-1 MilliQ	1.12	2.25	1.00	0.00	0.00	0.10	0.17	0.00	0.00	0.57	0.00
L-1 Cc	0.95	2.35	1.00	0.00	0.00	0.10	0.22	0.00	0.00	0.54	0.02
L-100P MilliQ	0.57	2.32	1.00	0.00	0.00	0.13	0.07		0.00	0.58	
L-100P Cc	1.51	2.51	1.00	0.00	0.00	0.10	0.16		0.00	0.55	
Peridotite											
Original powder	0.13	2.82	1.00	0.05	1.55	0.00	0.00		0.00	0.00	
P-100P MilliQ	0.58	3.11	1.00	0.14	1.43	0.04	0.00		0.00	0.00	
P-100P Cc	0.67	3.29	1.00	0.15	1.39	0.03	0.06		0.00	0.00	

[a] Duplicate analysis were performed on each sample, and it is the average values that are listed in this table. The terms “MilliQ” and “Cc” refer to the post-experimental powders were cleaned with either MilliQ water or with a calcite saturated solution.

Table 5

Comparison of steady-state dissolution rates (Log r_+) based on Si release in mol/cm^2/s at 25 °C

Mineral/rock [a]	This study (pH 9.1) Log $r_{+,BET}$ [a]	Literature (pH 9) Log $r_{+,BET}$ [b]	Comments	Reference
Basaltic glass	-14.0	-14.2		Gislason and Oelkers (2003)
Augite [b]	-14.3	-15.1	for diopside ($Ca_{0.99}Mg_{0.98}Fe_{0.02}Cr_{0.01}Si_2O_6$) at pH 8.7	Golubev et al. (2005)
Enstatite	-14.5	-15.2	for $Mg_{0.849}Fe_{0.136}Ca_{0.004}Si_{1.002}O_3$	Oelkers and Schott (2001)
Labradorite [b]	-14.0			
Peridotite [c]	-14.5		as olivine is the dominant mineral phase, it can be compared to the olivine value below from Pokrovsky and Schott (2000)	
Olivine (Fo93)	-14.3	-14.5	for $Mg_{1.82}Fe_{0.18}SiO_4$ (Fo91) at pH 9.3	Pokrovsky and Schott (2000)

[a] Chemical composition of solid phases provided in Table 1 and 3

[b] No literature data available for dissolution at alkaline pH

[c] Si element release rate. The peridotite is mainly composed of Mg-rich olivine and minor amounts of pyroxene.

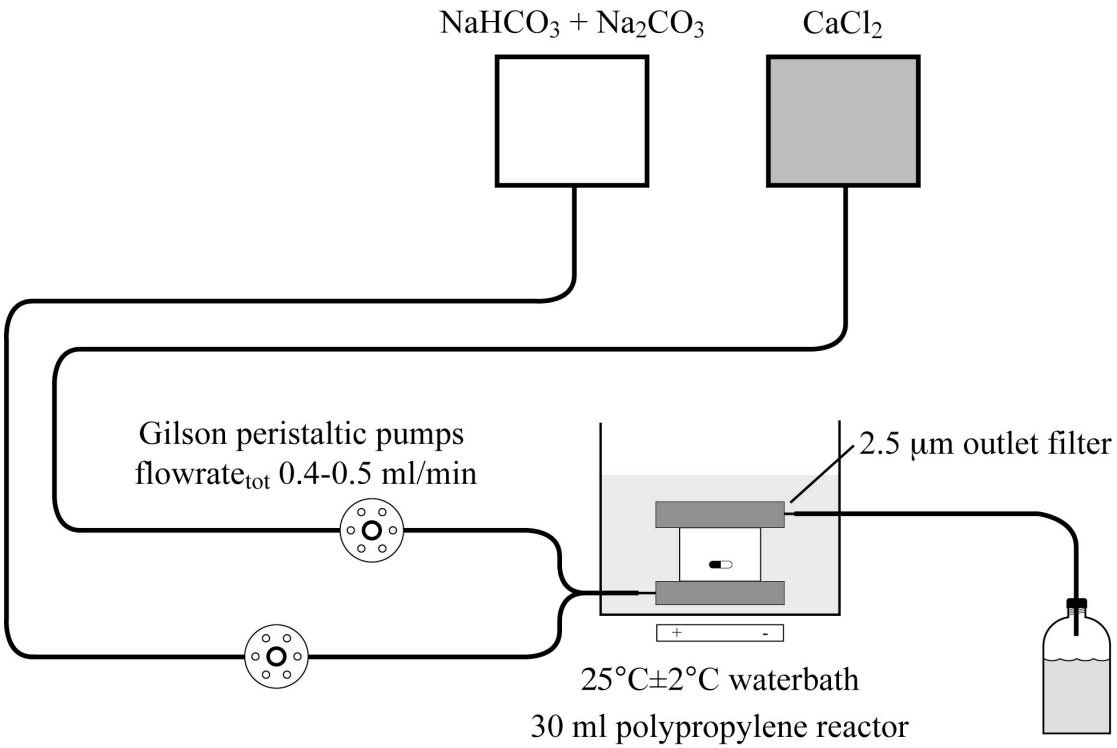

Fig. 1. Schematic illustration of the 30 mL reactors used in Experimental series 1 in the present study. Experimental series 2 and 3 used bigger 300 mL reactors of a different kind (shown in Stockmann et al., 2011) and higher flow-rates (~1 ml/min), but otherwise the same setup. Calcite saturation in the experiments is obtained by mixing two inlet solutions comprised of Na_2CO_3/$NaHCO_3$ and $CaCl_2$, respectively, inside the reactor. Each reactor contained ~0.25-2 grams of silicate or calcite powder.

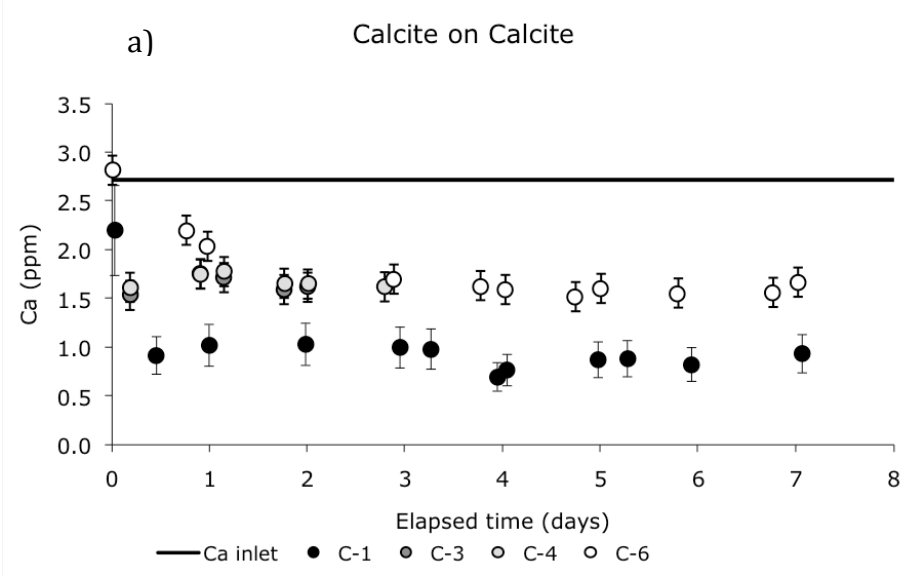
a)
Calcite on Calcite
Ca (ppm)
Elapsed time (days)
Ca inlet
C-1
C-3
C-4
C-6

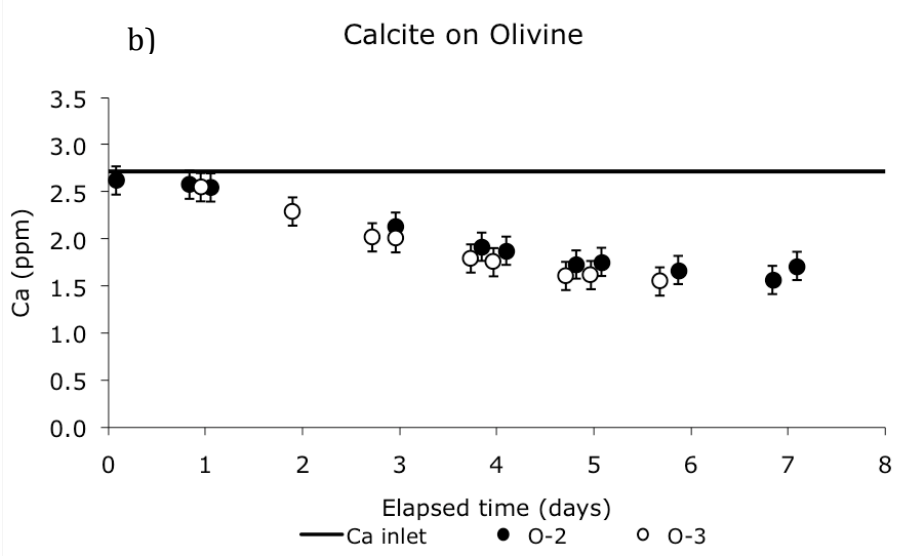
b)
Calcite on Olivine
Ca (ppm)
Elapsed time (days)
Ca inlet
O-2
O-3

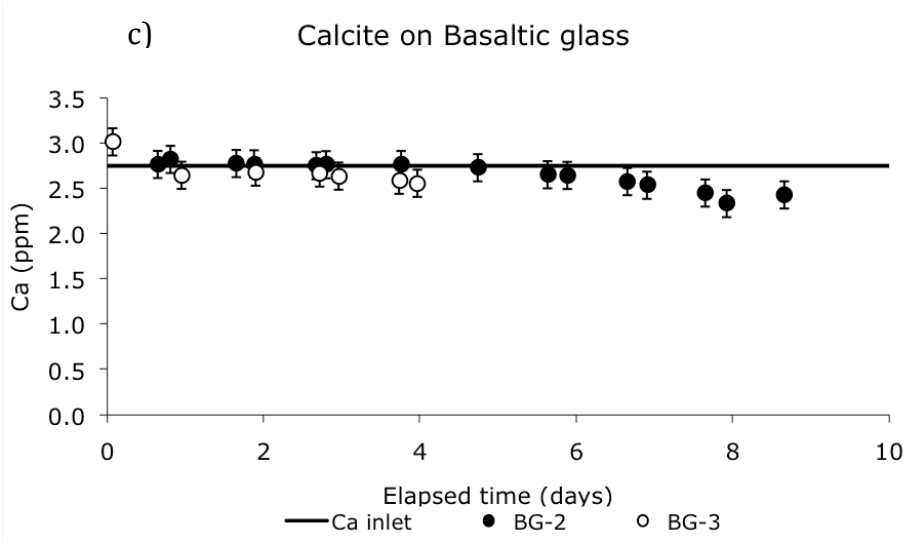
c)
Calcite on Basaltic glass
Ca (ppm)
Elapsed time (days)
Ca inlet
BG-2
BG-3

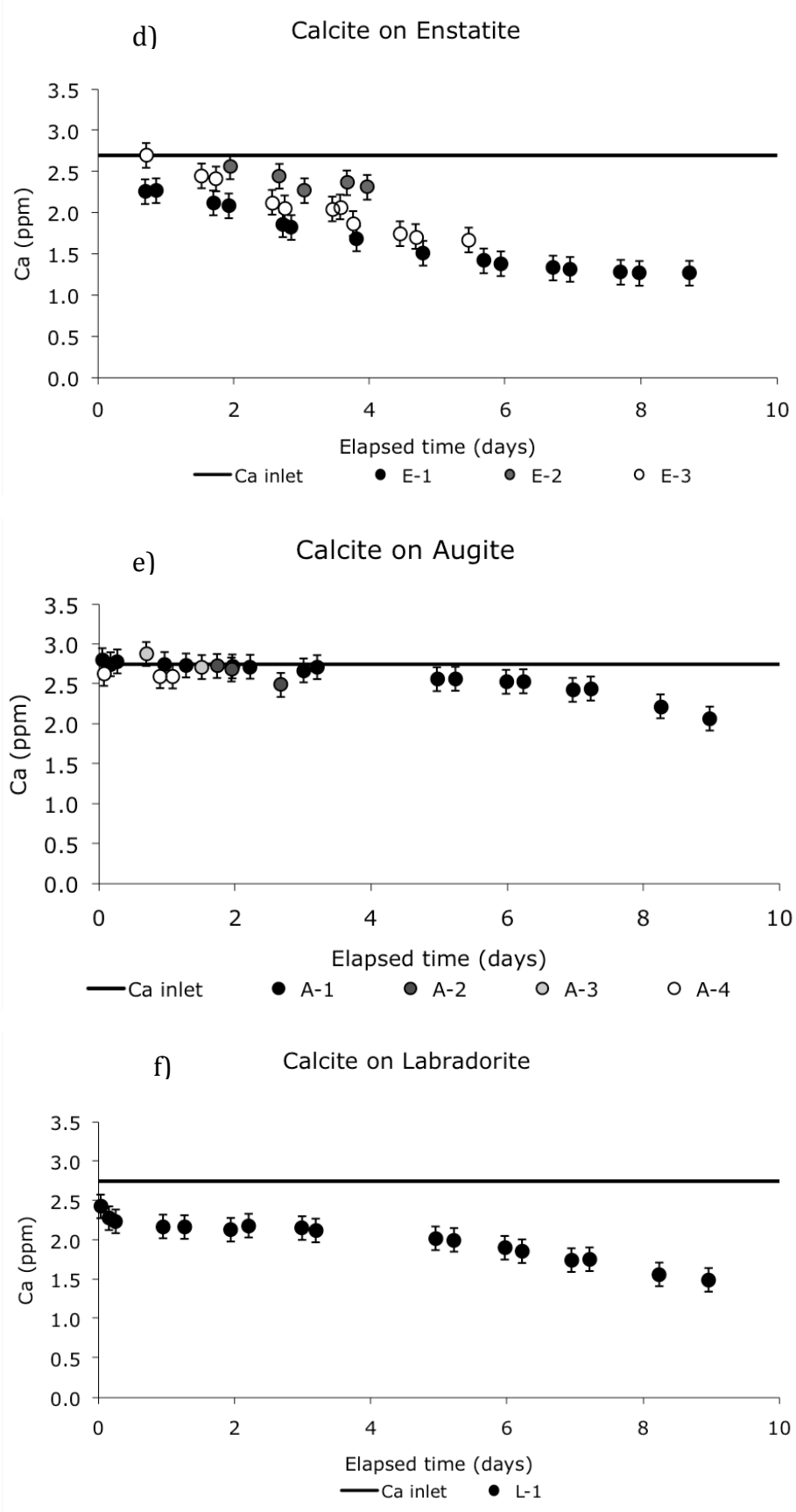

Fig. 2. Temporal evolution of Ca concentration in inlet and outlet solutions from mixed-flow reactors containing calcite and different silicates at pH 9.1 and 25 ºC. The solid lines represent the Ca concentration of the inlet solutions. The difference between inlet and outlet Ca is interpreted as caused by calcite precipitation.

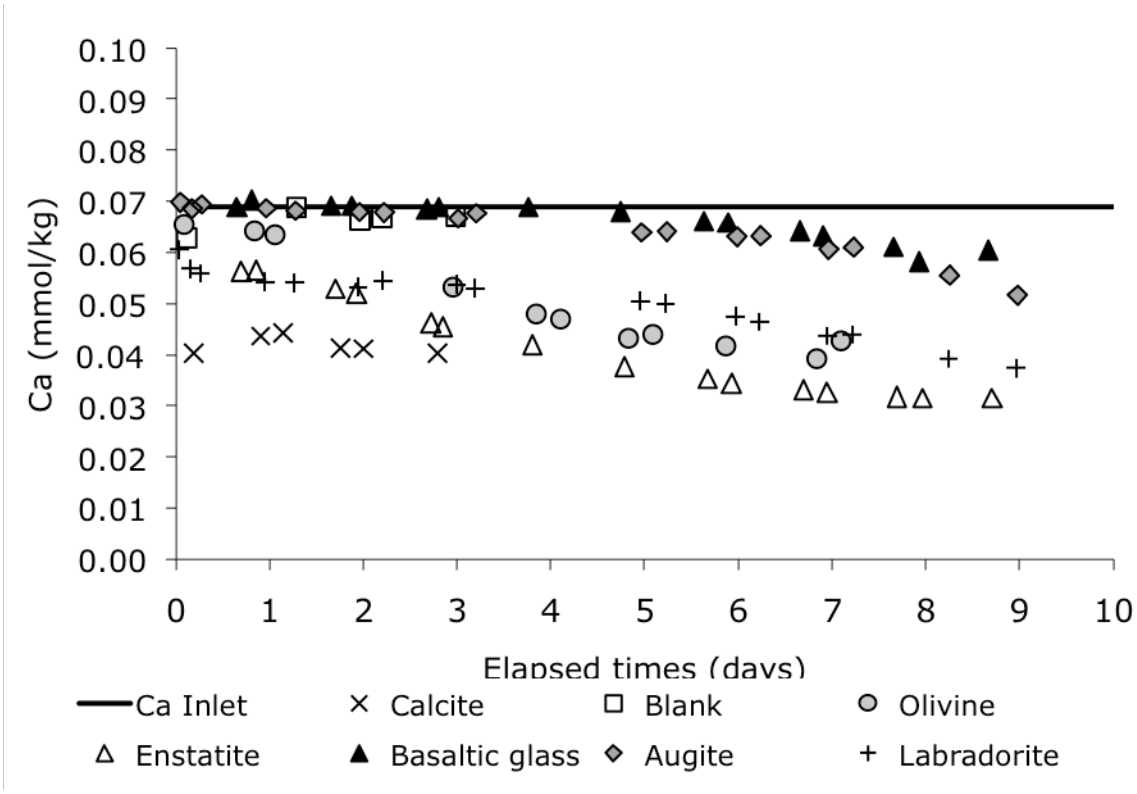

Fig. 3. Compilation of data from figure 2 illustrating the temporal evolution of Ca concentration in the outlet solutions from the mixed-flow reactors containing silicates and calcite. Additionally, a blank experiment was performed without any presence of a solid phase. The solid line represents the Ca concentration of the inlet solutions.

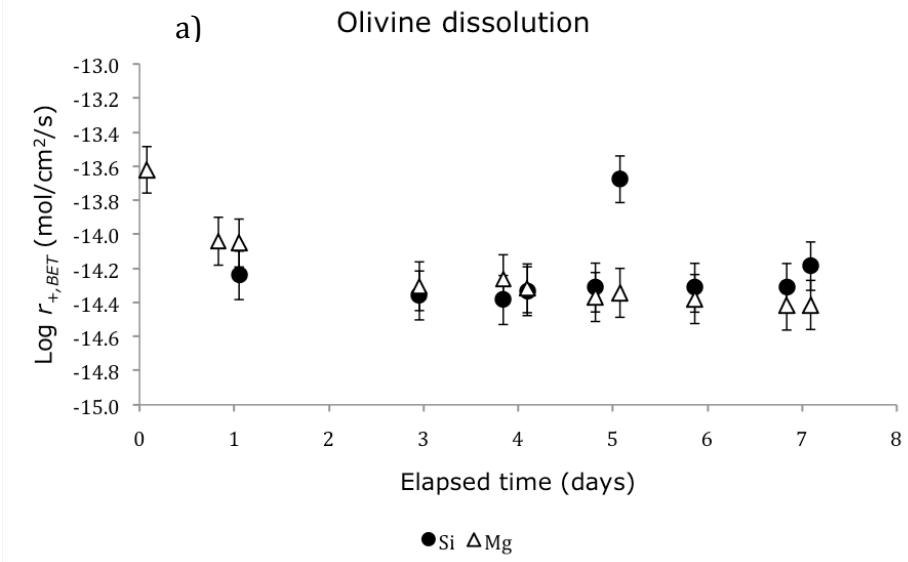
a)
Olivine dissolution
Log $r_{+,BET}$ (mol/cm²/s)
-13.0
-13.2
-13.4
-13.6
-13.8
-14.0
-14.2
-14.4
-14.6
-14.8
-15.0
0 1 2 3 4 5 6 7 8
Elapsed time (days)
●Si △Mg

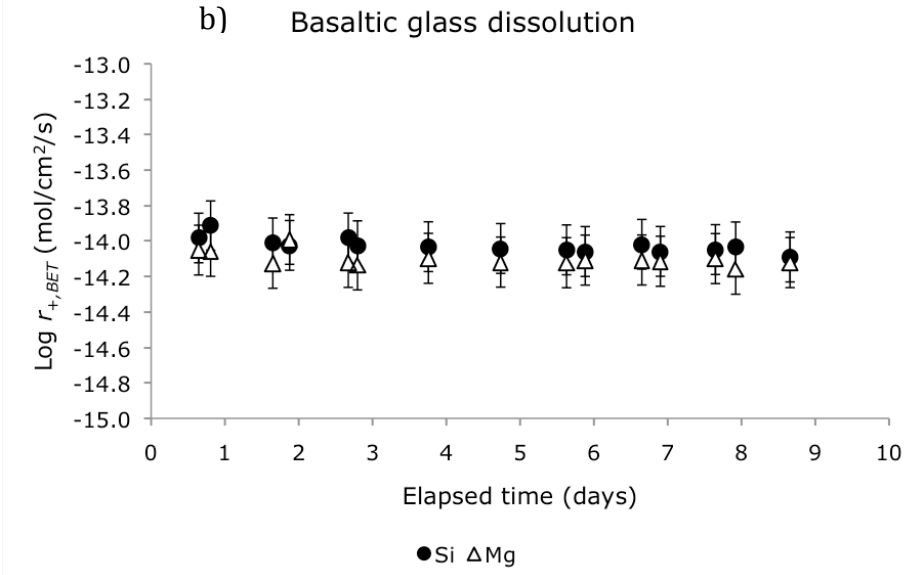
b)
Basaltic glass dissolution
Log $r_{+,BET}$ (mol/cm²/s)
-13.0
-13.2
-13.4
-13.6
-13.8
-14.0
-14.2
-14.4
-14.6
-14.8
-15.0
0 1 2 3 4 5 6 7 8 9 10
Elapsed time (days)
●Si △Mg

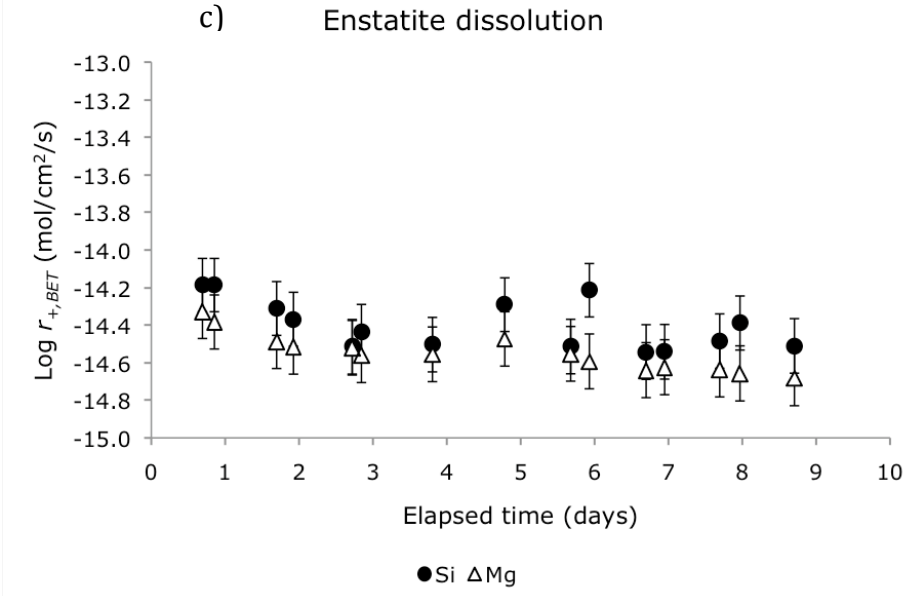
c)
Enstatite dissolution
Log $r_{+,BET}$ (mol/cm²/s)
-13.0
-13.2
-13.4
-13.6
-13.8
-14.0
-14.2
-14.4
-14.6
-14.8
-15.0
0 1 2 3 4 5 6 7 8 9 10
Elapsed time (days)
●Si △Mg

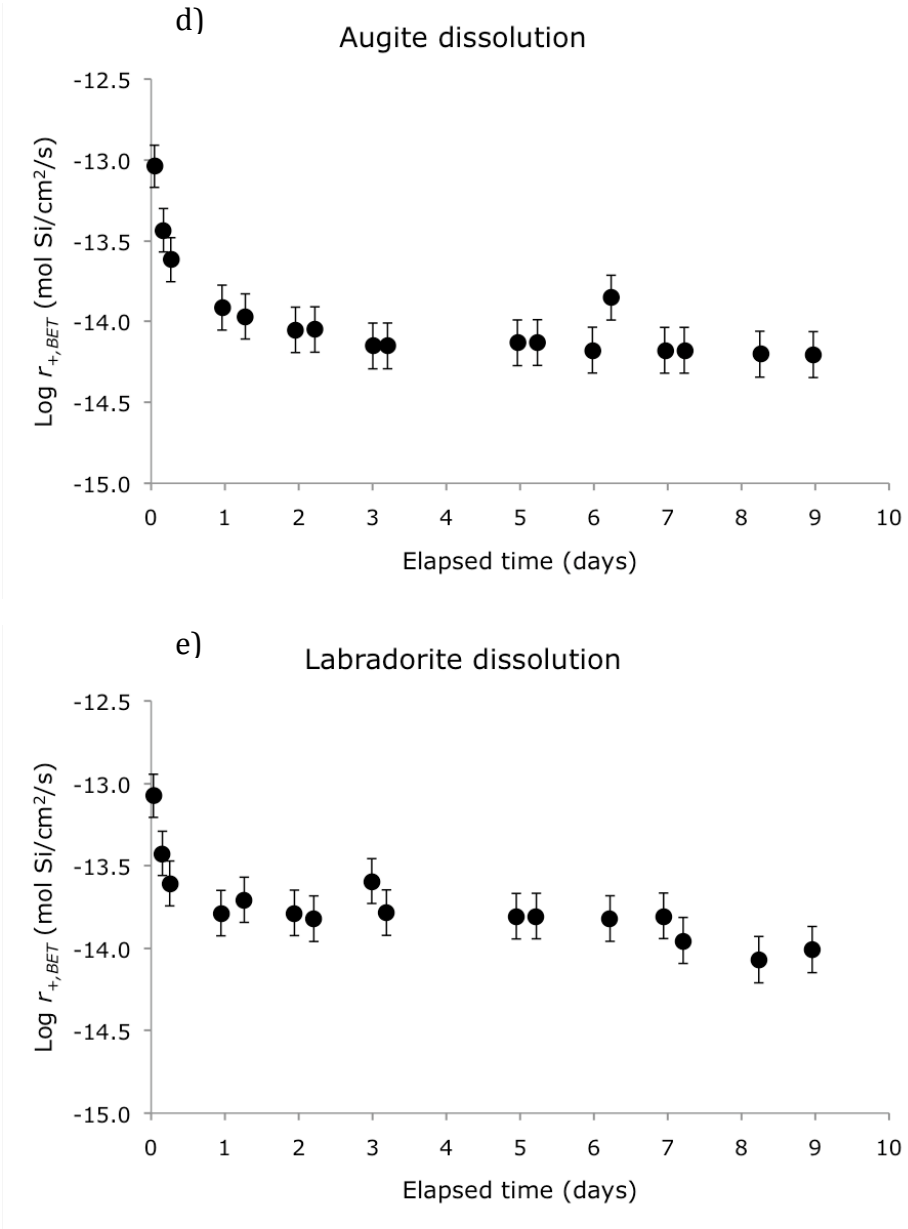

Fig. 4. Temporal evolution of primary silicate dissolution rates based on Si ± Mg of; a) olivine, b) basaltic glass, c) enstatite, d) augite and e) labradorite during calcite precipitation experimental series 1 at pH 9.1 and 25 °C.

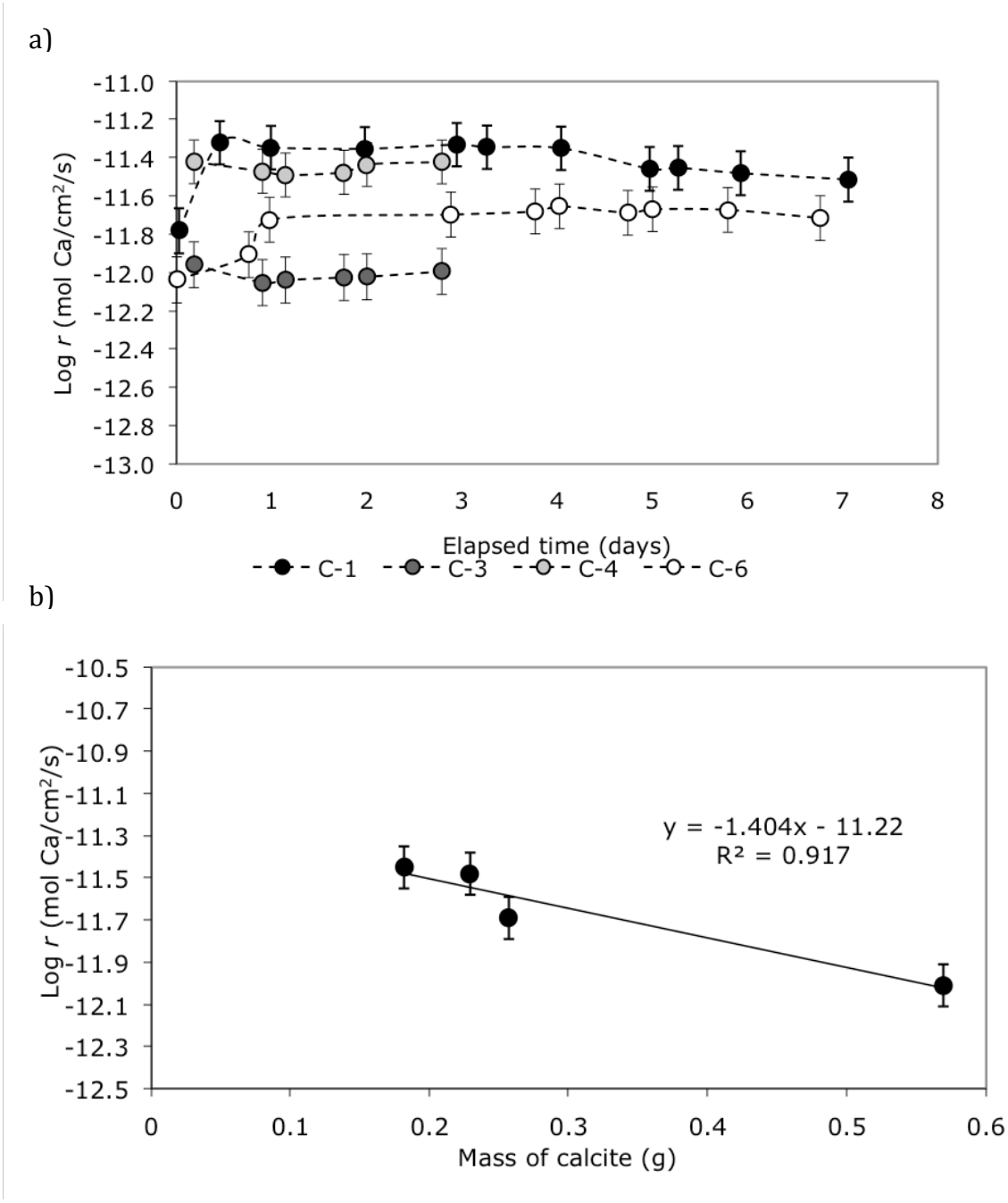

Fig. 5. a) Temporal evolution of calcite precipitation rates based on $\Delta[Ca]_{out\text{-}in}$ in the four "calcite on calcite" experiments from experimental series 1 at pH 9.1 and 25 °C. b) Correlation between mass of initial calcite and measured steady-state calcite precipitation rates.

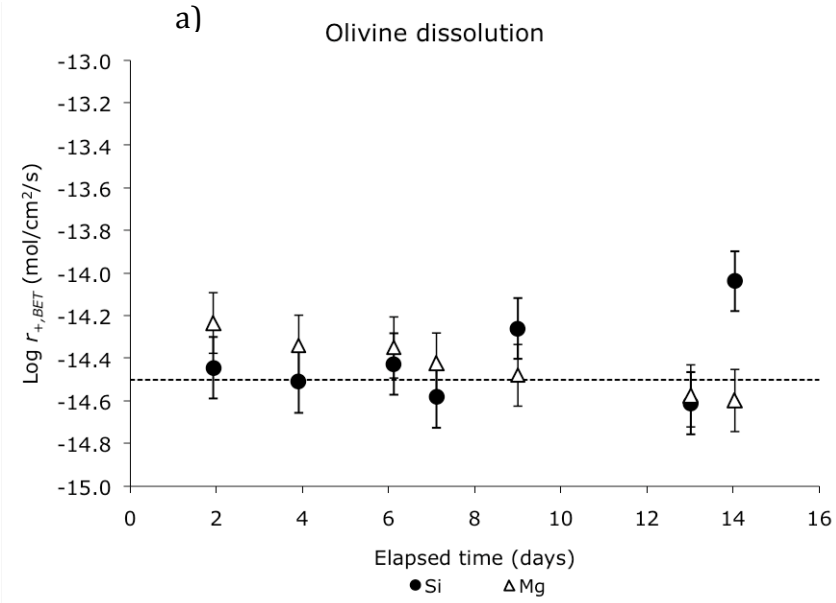
a)
Olivine dissolution
Log $r_{+,BET}$ (mol/cm²/s)
-13.0
-13.2
-13.4
-13.6
-13.8
-14.0
-14.2
-14.4
-14.6
-14.8
-15.0
0
2
4
6
8
10
12
14
16
Elapsed time (days)
Si
Mg

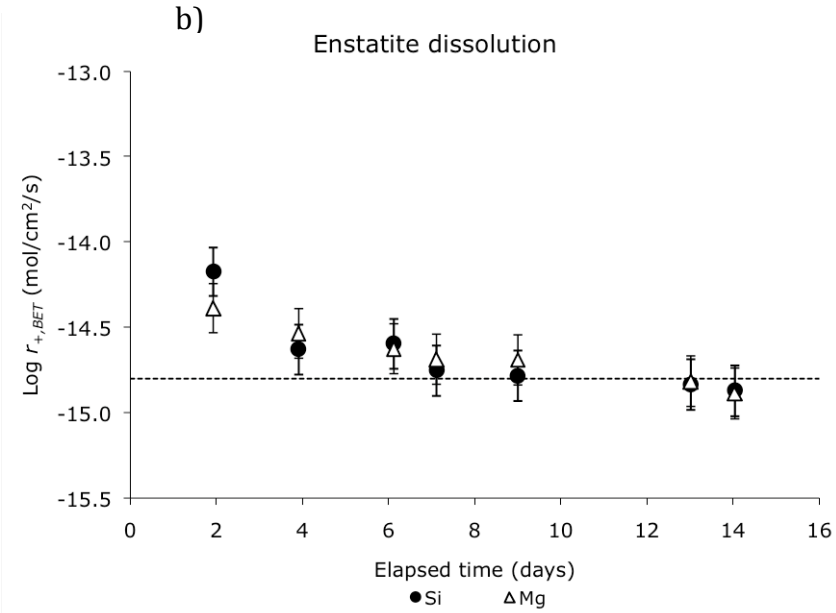
b)
Enstatite dissolution
Log $r_{+,BET}$ (mol/cm²/s)
-13.0
-13.5
-14.0
-14.5
-15.0
-15.5
0
2
4
6
8
10
12
14
16
Elapsed time (days)
Si
Mg

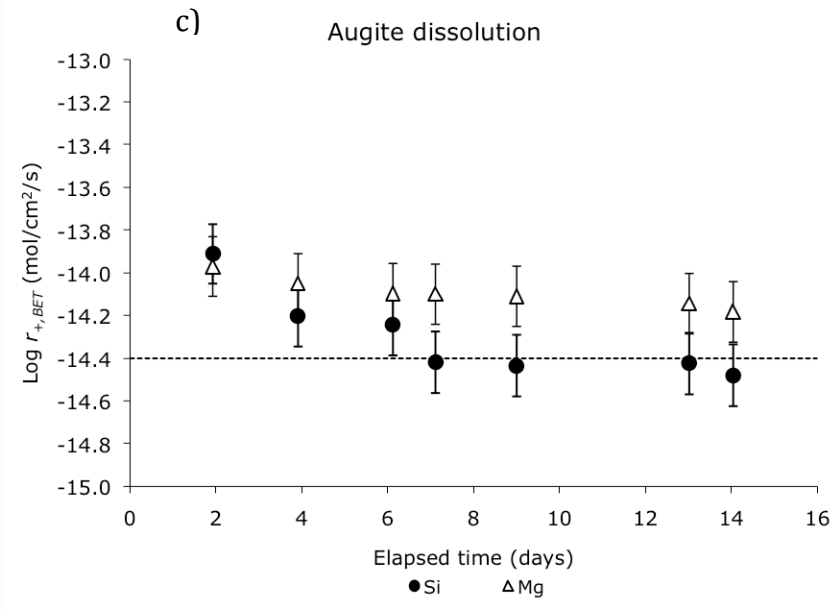
c)
Augite dissolution
Log $r_{+,BET}$ (mol/cm²/s)
-13.0
-13.2
-13.4
-13.6
-13.8
-14.0
-14.2
-14.4
-14.6
-14.8
-15.0
0
2
4
6
8
10
12
14
16
Elapsed time (days)
Si
Mg

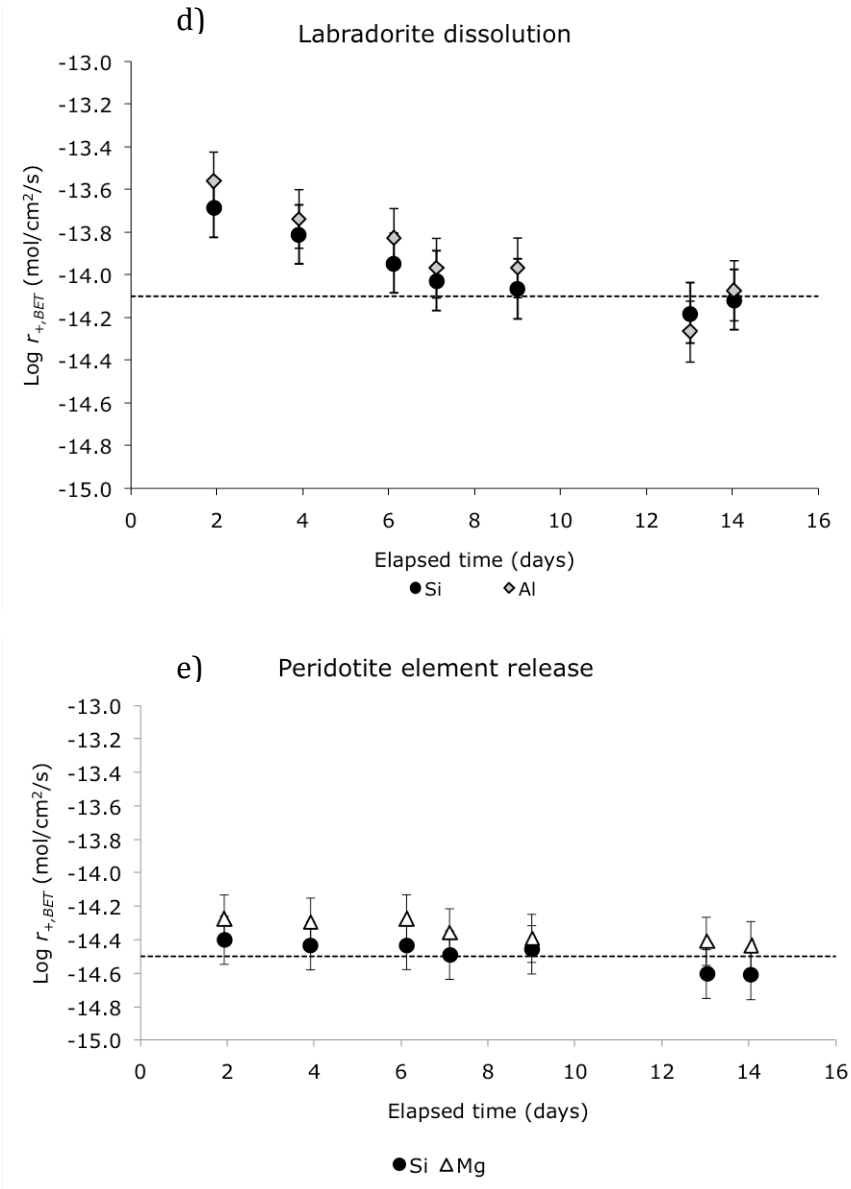

Fig. 6. Temporal evolution of primary silicate mineral dissolution rates based on Si ± Mg or Al of; a) olivine, b) enstatite, c) augite, and d) labradorite, and e) element release rates of peridotite during experimental series 2 at pH 9 and 25 °C. These were pure dissolution experiments with no calcite or other secondary phases precipitating. The inlet solution comprised of 8.36 mM $NaHCO_3$ / 0.64 mM Na_2CO_3. The dashed lines on the plots represent steady state.

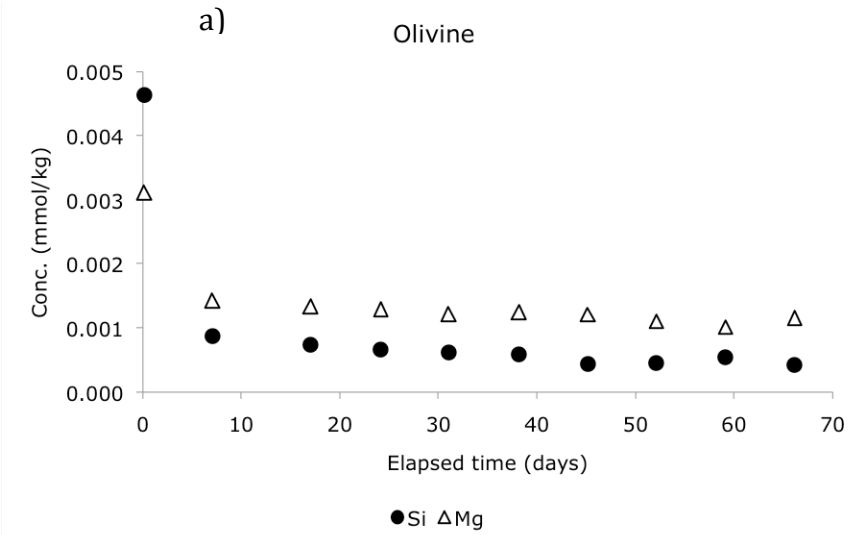
a)
Olivine
Conc. (mmol/kg)
0.005
0.004
0.003
0.002
0.001
0.000
0
10
20
30
40
50
60
70
Elapsed time (days)
Si Mg

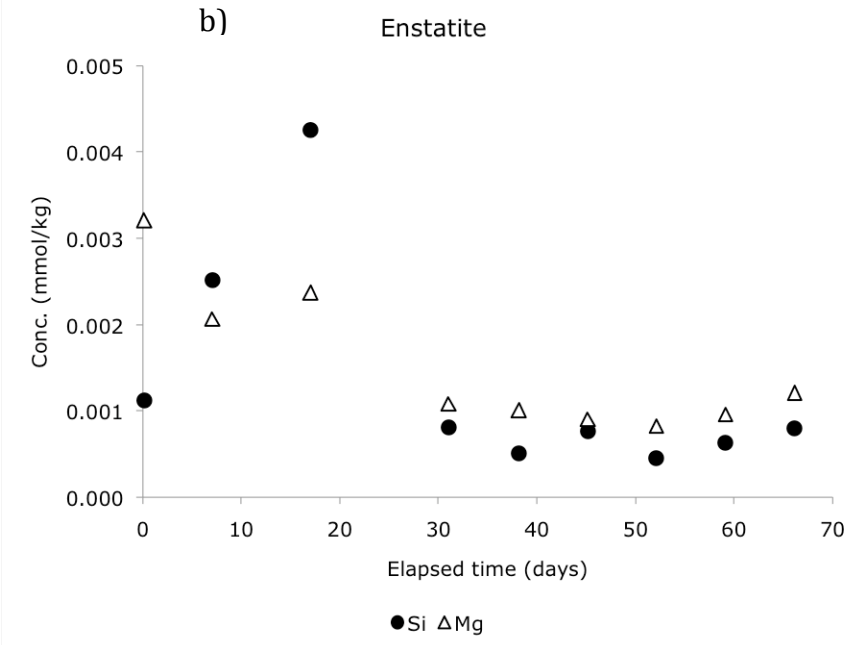
b)
Enstatite
Conc. (mmol/kg)
0.005
0.004
0.003
0.002
0.001
0.000
0
10
20
30
40
50
60
70
Elapsed time (days)
Si Mg

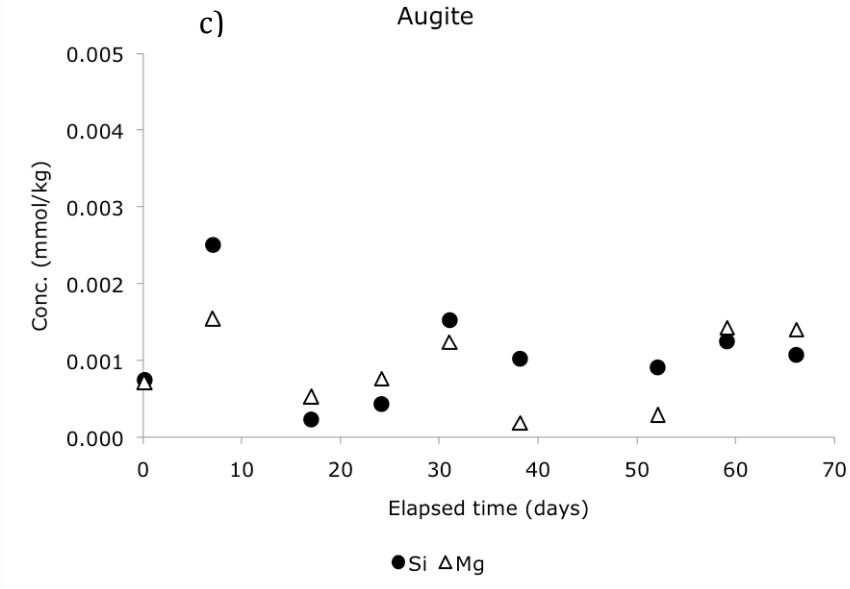
c)
Augite
Conc. (mmol/kg)
0.005
0.004
0.003
0.002
0.001
0.000
0
10
20
30
40
50
60
70
Elapsed time (days)
Si Mg

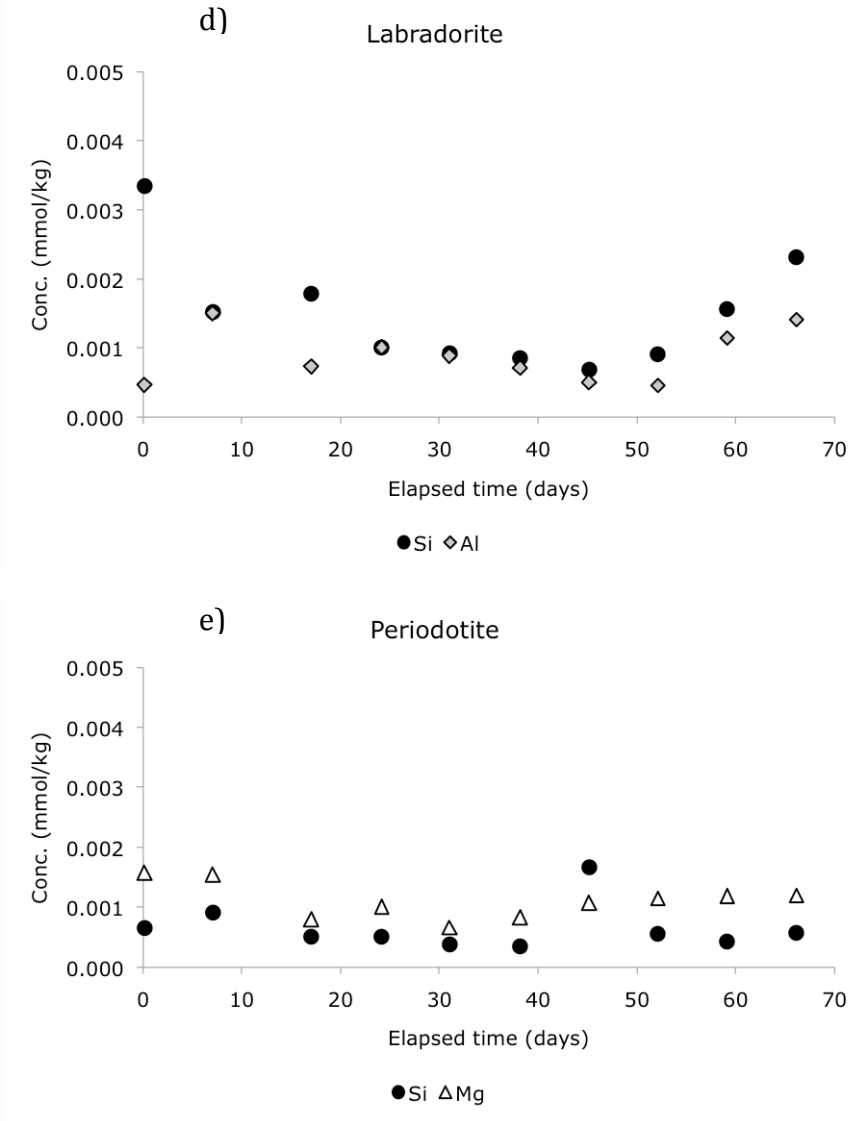

Fig. 7. Temporal evolution of Si, Mg and Al concentration in the outlet solutions from the; a) olivine-, b) enstatite-, c) augite-, d) labradorite-, and e) peridotite experiments of experimental series 3 at pH 9 and 25 °C. These experiments used two inlets of $CaCl_2$ and $NaHCO_3/Na_2CO_3$, respectively, to create calcite saturation inside the reactors.

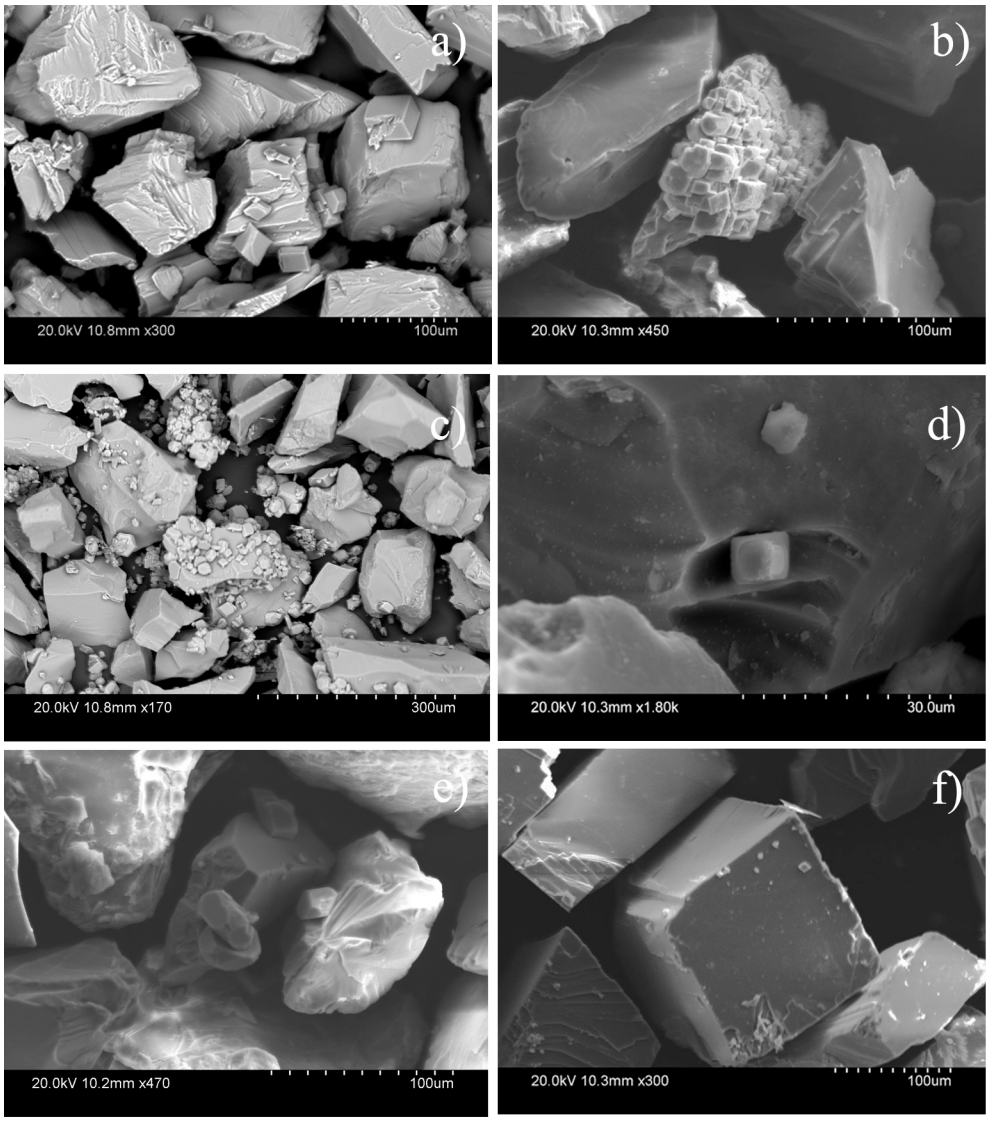

Fig. 8. Scanning Electron Microscope images of post-experimental solid samples of a) augite, b) enstatite, c) olivine, d) basaltic glass, e) peridotite and f) calcite crystals after having been exposed to inlet solutions saturated with respect to calcite.

Conclusions and perspectives

The major findings of this thesis are as follows:

- Calcium carbonate precipitates either on or adjacent to basaltic glass and diopside do not affect the dissolution rates of these primary phases
- Calcium carbonate (calcite and aragonite) precipitates grew on the basaltic glass in experiments performed in Ca-free inlet solutions, but nucleated and grew independently of the glass surfaces in experiments performed in Ca-bearing inlet solutions; no pervasive $CaCO_3$ layers were observed
- Calcite is observed to precipitate both in the form of discrete prisms and as pervasive coatings covering the whole diopside surface
- The measured steady-state BET rates of basaltic glass and diopside match those previously reported in the literature, supporting their application to reaction path modeling of natural systems
- Morphology and location of the secondary precipitates seem to be a function of a) the relative structures of the primary and secondary phases, b) the degree of supersaturation of the reactive fluid with respect to the secondary phase, and c) the location of the source of the elements comprising the secondary phase
- The observation that basaltic glass and diopside dissolution rates are unaffected by calcium carbonate precipitation, favors carbon storage in glassy volcanic rocks as well as in crystalline basaltic and ultramafic rocks
- Calcite nucleation and its subsequent growth depends on the crystal structure of the silicate substrate
- Orthorhombic silicate minerals (olivine and enstatite) are the easiest for trigonal calcite to nucleate on, monoclinic augite and triclinic labradorite show intermediate behavior, whereas basaltic glass with its non-ordered crystal structure is the least favorable platform for calcite growth

- Implications for CO_2 mineralization in ultramafic and basaltic rocks are that trigonal carbonates precipitate more readily on crystalline rather than glassy basalts, but even glass surfaces can serve as a substrate for calcite nucleation
- The presence of live or dead bacteria, *Pseudomonas reactans* affects only mildly basaltic glass dissolution rates based on Si release at pH 4 to 10
- No increase of trace elements release from basaltic glass was observed, except for an increase in arsenic release rates at pH 4 in the presence of dead *Pseudomonas reactans*
- As little effect of their presence was found on laboratory dissolution rates it seems likely that *Pseudomonas reactans* will have little effect on basaltic glass dissolution rates during either soil weathering or subsurface CO_2 storage efforts in basalts

This study is one of several PhD projects and studies connected to the CarbFix project at the Hellisheiði geothermal power plant in Iceland. By now, the knowledge base has become quite extensive with respect to host rock geology, hydrology, downhole well sampling, numerical modeling of water-rock interaction, dissolution rates of primary silicates, secondary mineral formation, effect of carbonate coatings, impact of biological life, expectancy of toxic metal release; all of these providing a good understanding of the reactions expected during and after CO_2 injection (Alfredsson et al., 2008; 2011; Khalilabad et al., 2008; Oelkers et al., 2008; Flaathen et al., 2009; 2010; 2011; Matter et al., 2009; 2011; Gislason et al., 2010; Gudbrandsson et al., 2011; Wolff-Boenisch, 2011; Wolff-Boenisch et al., 2011; Gysi and Stefansson, 2011; 2012a,b,c, Stockmann et al., 2011; 2012; Aradottir et al., 2011, 2012a,b; Shirokova et al., 2012).

One of the former unknowns, which has now been resolved, is the element release rates of crystalline basalt, mainly composed of olivine, Ca-plagioclase and olivine (Gudbrandsson et al., 2011). The CO_2-loaded water is running through basaltic formations of both glassy and crystalline composition after injection (e.g. Alfredsson et al., 2008, Gislason et al., 2010). Whereas the basaltic glass dissolution rates are well described (Oelkers and Gislason, 2001; Gislason and Oelkers, 2003), and the individual mineral dissolution rates of olivine, plagioclase and pyroxene are reported

in the literature as well (e.g. Chou and Wollast, 1985; Blum and Stillings, 1995; Stillings and Brantley, 1995; Pokrovsky and Schott, 2000; Oelkers and Schott, 2001; Hänchen et al., 2006), the overall element release rates of the mineral composite basaltic rock was until recently unknown. Basaltic glass has a non-ordered silica structure that easy breaks and weathers, and it is therefore characterized by relatively high reactivity and fast dissolution rates (e.g. Gislason and Eugster, 1987 a,b), and it was expected that crystalline rocks would be slower to dissolve than their glassy counterparts. Gudbrandsson et al. (2011) measured far-from-equilibrium element release rates of crystalline basalt at pH 2-11 and temperatures from 5 to 75 ºC, and found Si release rates were comparable to those of glass at acidic pH and temperatures ≤ 25 ºC, but slower at basic conditions and temperatures ≥ 50 ºC. They also noticed that Fe and Mg release continues to decrease with increasing pH, whereas Ca release showed at U-shaped curve. This was interpreted as stemming from the dissolution of the three major mineral components; olivine, pyroxene and Ca-rich plagioclase, respectively. The results are quite promising for the CO_2 sequestration process and indicate that even crystalline basalt is rather readily dissolving and providing divalent cations at all pH to potential carbonate formation.

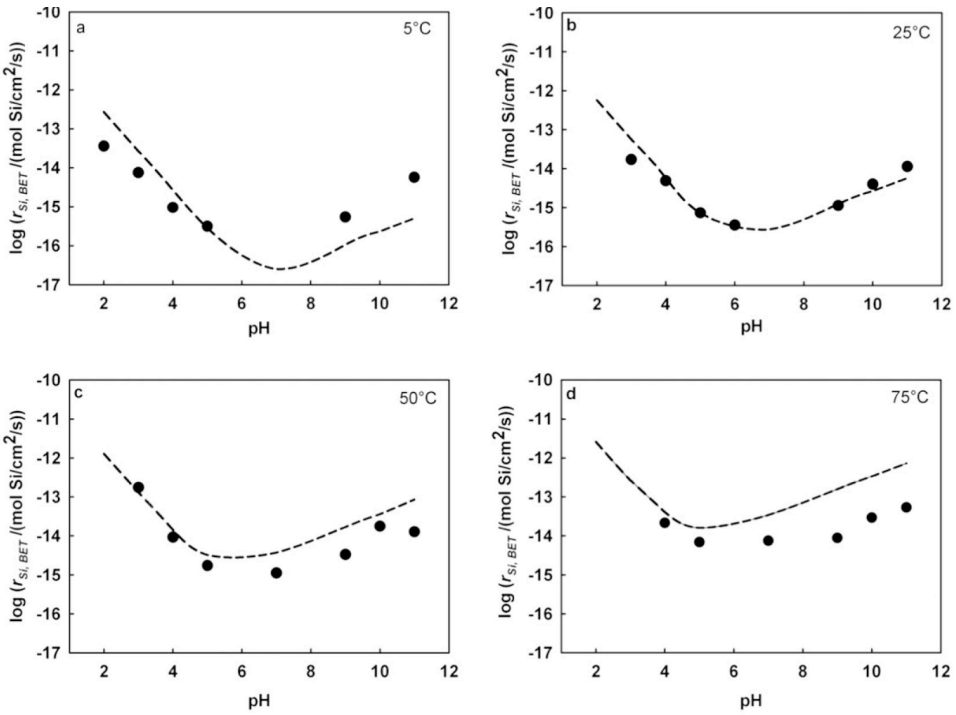

Fig. 1 Steady-state Si release rates of crystalline basalt (black circles) at different temperatures compared to the steady-state Si release rates of basaltic glass (dashed curves). *Source: Gudbrandsson et al. (2011).*

Another important part of the CarbFix project has been to look into ways and means to increase the dissolution of basaltic glass, as this is considered the rate-limiting process of the CO_2 sequestration process (c.f. Oelkers et al., 2008). According to Gislason and Oelkers (2003), the far-from-equilibrium basaltic glass dissolution rate can be described by:

$$r_{+,BET} = A_A \exp^{\frac{E_A}{RT}} \left(\frac{a^3_{H^+}}{a_{Al^{3+}}} \right)^{\frac{1}{3}} \quad (1)$$

where $r_{+,BET}$ describes the basaltic glass dissolution rate normalized to the BET surface area, A_A refers to a constant equal to $10^{-5.6}$ (mol Si)/cm^2/s, E_A refers to a temperature independent activation energy of 25.5 kJ/mol, R is the gas constant, T is the temperature measured in Kelvin (K), and a_i represents the activity of the subscripted aqueous species. Equation (1) illustrates the rate dependency on the ($a^3{}_{H}{}^{+}/a_{Al}{}^{3+}$) ratio and the temperature. Thus, increasing rates can either be obtained by 1) increasing the temperature, but this has the disadvantage that secondary minerals like zeolites and clays become saturated and scavenge divalent cations, or 2) change of the ($a^3{}_{H}{}^{+}/a_{Al}{}^{3+}$) ratio. This can be done by decreasing the pH or by complexing Al^{3+} with other ions. Wolff-Boenisch et al. (2004; 2011) and Flaathen et al. (2010) showed basaltic glass dissolution rates can be increased at acidic pH by Al^{3+} complexation by F^- - and SO_4^{2-} ions, respectively. At basic pH, the Al^{3+} concentration is very low because of complexation with OH^- ions, and additional complexing with other ions has very little effect (Wolff-Boenisch et al., 2004; 2011; Flaathen et al., 2010). These complexing ions could potentially be added to the water stream dissolving CO_2 gas. However, at Hellisheiði, a gas mixture consisting of 75% CO_2 and 25% H_2S (another gas byproduct of geothermal exploitation) is to be injected in the future. The H_2S will oxidize in water to aqueous SO_4^{2-} leading to a low pH, and the combined effect of pH and SO_4^{2-} should result in rapid dissolution of glassy and crystalline basalt.

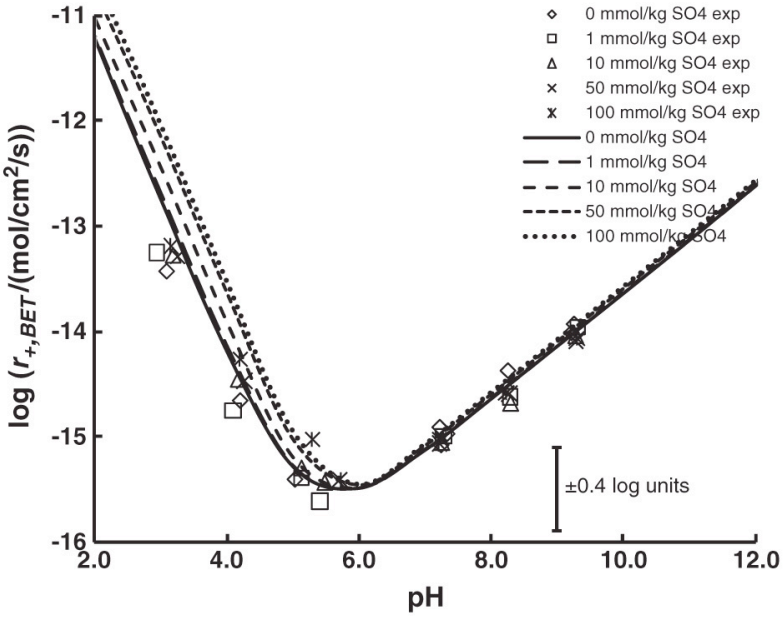

Fig. 2 Steady-state basaltic glass dissolution rates at 50 ºC, in the presence of increasing [SO_4^{2-}]. *Source: Flaathen et al. (2010).*

Once the basalt starts to dissolve, the question follows whether geochemical conditions will allow precipitation of carbonates, thus trapping the CO_2 in minerals. Precipitation of other secondary minerals like clays and zeolites competing for divalent cations should be avoided or at least minimized if possible. Numerical modeling and experiments of CO_2-water-basaltic glass interactions have been studied at temperatures and pCO_2 of relevance to the CarbFix project (Gysi and Stefansson, 2011; 2012a). These authors showed that a mixture of (Fe,Mg,Ca) carbonates precipitated on basaltic glass along with Fe-hydroxides / oxyhydroxides and Fe-Mg-Ca smectites in batch reactor experiments at 40 ºC, and pCO_2 of 2 to 13 bar (Gysi and Stefansson, 2012a). Numerical modeling on CO_2-water-basaltic glass reactions at an initial pCO_2 of 2 bar and 30 bar, respectively, favored the more CO_2-rich conditions for a carbon dioxide storage scenario. Modeling indicate the Ca^{2+}, Mg^{2+} and Fe^{2+} ions are predominantly scavenged in carbonates, with co-precipitation of SiO_2, and lesser formation of clays and zeolites at an initial pCO_2 of 30 bar (see Fig. 3) (Gysi and Stefansson, 2011).

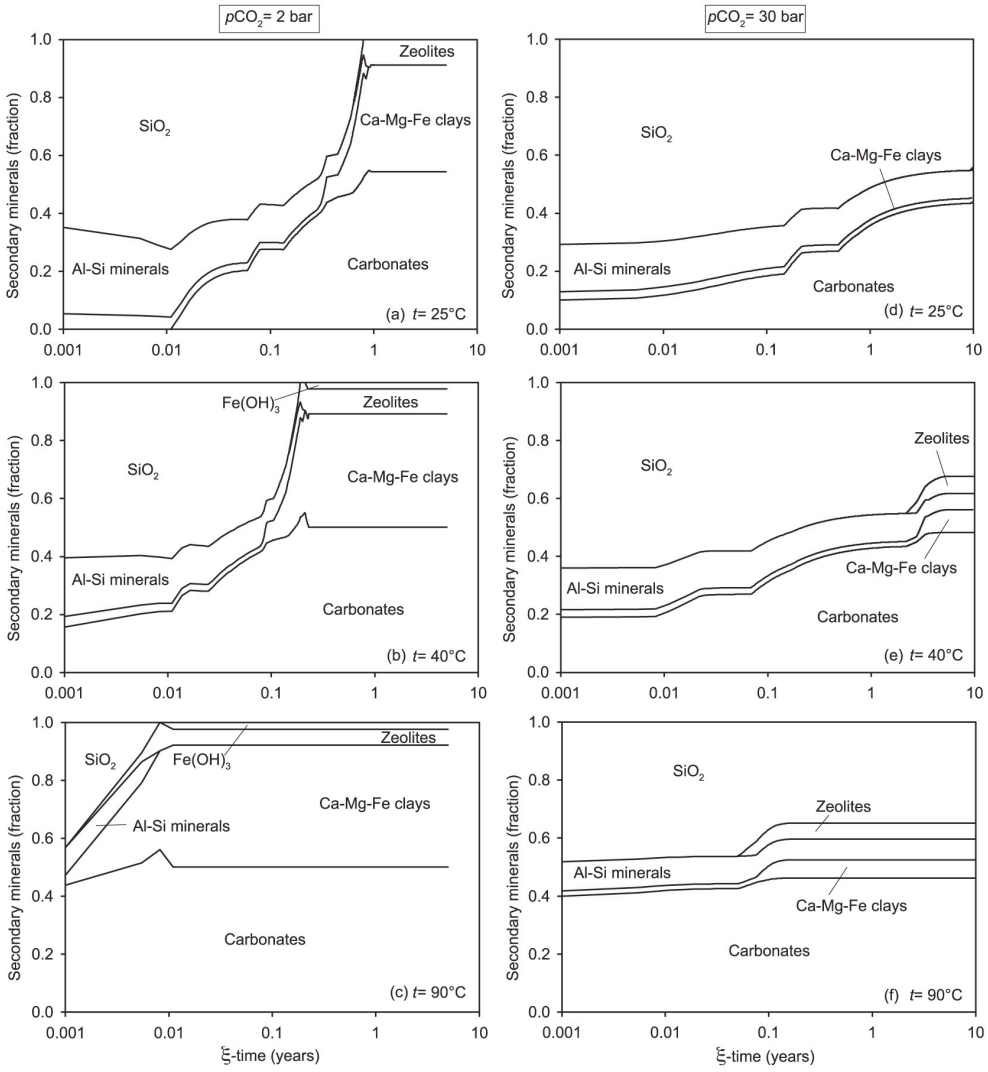

Fig. 3 The mole fraction of secondary mineral formation as a function of reaction progress (ξ) at an initial pCO_2 of 2 and 30 bar, and temperatures of 25, 40 and 90 ºC, respectively, from numerical modeling of CO_2-water-basaltic glass interaction. *Source: Gysi and Stefansson (2011).*

CO_2 sequestration experiments have also been conducted on the Columbia River basalts (CRB) in the US (McGrail et al., 2006; Schaef and McGrail, 2009; Schaef et al., 2009; 2010; 2011) as this geological formation offers possibilities for CO_2 storage like the basaltic formations of Iceland. The CRB consists predominantly of crystalline parts but also contains minor glassy fractions (Schaef and McGrail, 2009). McGrail et al. (2006) let the CRB react with water and supercritical CO_2 in batch reactors for up to 1334 days and showed that rapid and extensive calcite precipitation formed on the surface of the basalt grains. After a year a phase transition was observed in these long-term experiments from calcite to ankerite ($Ca(Fe,Mg)(CO_3)_2$). Unfortunately, element release was not measured in the previous

experiments conducted on the CRB, so it is not known whether these coatings affected the basalt dissolution.

It would be interesting to expose the crystalline basalt from Iceland, described in Gudbrandsson et al. (2011) to solutions supersaturated with respect to calcite, similar to those experiments carried out on basaltic glass (Stockmann et al., 2011) to see if crystallinity plays a role in how extensive and how rapid the basalt surface gets covered with calcium carbonate precipitates. Furthermore, it would be relevant to conduct long-term calcite precipitation experiments on both basaltic glass and crystalline basalt like those of Columbia River basalt (McGrail et al., 2006) to test if carbonate precipitates will eventually cover the whole primary surface and block dissolution. Since it has been observed that it makes a difference whether the Ca source comes from the glass or an external source, using the glass as the sole divalent cation source should be preferred.

A lot of water is required to fully dissolve CO_2 gas like at the Hellisheiði power plant, and the higher the temperature or the lower the pCO_2, the more water is required to dissolve the gas. Water supply is not a problem in Iceland, but other countries, where the *in-situ* CO_2 mineralization technique could be applied (e.g. India) are generally not so fortunate in water resources. Hence, if seawater could be used instead of groundwater, this would provide a global, more sustainable solution, where Earth's groundwater resources are spared for drinking water purposes. However, more seawater than groundwater is needed to dissolve CO_2, thus where 27 tons of groundwater dissolve one ton of CO_2 at a pCO_2 of 25 bar and a temperature of 25 ºC, 31 tons of seawater are required (Gislason et al., 2010). However, seawater has the advantage that it is a plentiful resource on Earth. Wolff-Boenisch et al. (2011) measured Si release rates of basaltic glass, crystalline basalt and peridotite in the presence of real seawater, and in artificial seawater where ions and organic ligands were added one at a time to determine their effect on the basaltic glass, crystalline basalt and peridotite Si release rates. Their results indicate that CO_2-loaded seawater injection and carbonatization should be equally efficient in basalt and in peridotite formations, and the use of seawater looks promising.

Both seawater and groundwater contain biological life in the form of bacteria and fungi, which is normally ignored in mineral-solution experiments performed in

the laboratory. However, to simulate real-case scenarios of what is going to happen after CO_2 injection into an aquifer, it is important to have an idea of the impact of the biological life present. Complementary to the bacterial experiments conducted within this thesis work, dissolution studies have been carried out on olivine in the presence of *Pseudomonas reactans* (Shirokova et al., 2012), and on basaltic glass in the presence of fungi (Pokrovsky, personal communication). It would be ideal to test additional bacterial species extracted from the wells at Hellisheiði in dissolution experiments similar to those described in Shirokova et al. (2012) and Stockmann et al. (2012). Unfortunately, only a very limited number of bacteria species are cultivatable in the laboratory, thus it is not possible to test all of the bacteria species present in the groundwater aquifer in Iceland. As with the carbonate coatings, it could be interesting to see what long-term effects might be on basalt in the presence of bacteria. We observed initial formation of biofilm on basaltic glass surfaces in Stockmann et al. (2012), and maybe long-term exposure to bacteria would lead to more extensive growth of biofilm that could potentially cover the whole primary silicate surface and affect the basalt dissolution.

After all of these experiments conducted in the laboratory it is now essential to test these results in small-scale field studies, like the one recently initiated at Hellidheiði. During CO_2 injection it is of importance to monitor the release of toxic metals as a result of basalt dissolution at low pH that may threaten groundwater resources. Furthermore, it is important to monitor CO_2 fluxes on the surface above the injection area. So far, fully dissolved CO_2 in water has proven a successful method during injection (Gislason, personal communication), and chemical analysis of water samples from monitoring wells and a camera inserted into the wells are going to shed light on how the solution chemistry and mineral precipitation is developing.

Along the ideas of this thesis an additional project has been formulated with the purpose of looking into naturally precipitating calcite and aragonite in Iceland, to study primary-secondary mineral contacts and compare them with laboratory calcite growth on silicates from this thesis work. Drill cuttings from Hellisheiði and the Krafla volcanic area in North Iceland, as well as Icelandic Spar samples from Helgustaðir in East Iceland, among others, are proposed for this aim.

References

Alfredsson, H.A., Hadrarson, B.S., Franzson, H., Gislason, S.R., 2008. CO_2 sequestration in basaltic rock at the Hellisheidi site in SW Iceland: stratigraphy and chemical composition of the rocks at the injection site. Min. Mag. 72, 1–5.

Alfredsson, H.A., Wolff-Boenisch, D., Stefansson, A., 2011. CO_2 sequestration in basaltic rocks in Iceland: Development of a piston-type downhole sampler for CO_2 rich fluids and tracers. Energy Procedia 4, 3510–3517.

Aradóttir, E.S.P., Sigurdardóttir, H., Sigfússon, B., Gunnlaugsson, E., 2011. CarbFix - a CCS pilot project imitating and accelerating natural CO_2 sequestration. Greenhouse Gases: Science and Technology 1, 105–118.

Aradóttir, E.S.P., Sonnenthal, E.L., Jónsson, H.I., 2012a. Development and evaluation of a thermodynamic dataset for phases of interest in CO_2 sequestration in basaltic rocks. Chem. Geol. 304–305, 26–38.

Aradóttir, E. S., Sonnenthal, E., Bjornsson, G., Jonsson, H., 2012b. Multidimensional reactive transport modeling of CO_2 mineral sequestration in basalts at the Hellisheidi geothermal field, Iceland. Int. J. Greenhouse Gas Control 9, 24-40.

Blum, A.E., Stillings, L.L., 1995. Feldspar dissolution kinetics. In Chemical Weathering Rates of Silicate Minerals (eds. A. F. White and S. L. Brantley). Mineralogical Society of America, Washington, DC.

Chou, L., Wollast, R., 1985. Steady-state kinetics and dissolution mechanisms of albite. Am. J. Sci. 285, 963–993.

Flaathen, T.K., Gislason, S.R., Oelkers, E.H., Sveinbjörnsdóttir, A.E., 2009. Chemical evolution of the Mt. Hekla, Iceland, groundwaters: A natural analogue for CO_2 sequestration in basaltic rocks. Appl. Geochem. 24, 463-474.

Flaathen, T.K., Gislason, S.R., Oelkers, E.H., 2010. The effect of aqueous sulphate on basaltic glass dissolution rates. Chem. Geol. 277, 345–354.

Flaathen, T.K., Oelkers, E.H., Gislason, S.R., Aagaard, P., 2011. The effect of dissolved sulphate on calcite precipitation kinetics and consequences for subsurface CO_2 storage. Energy Procedia 4, 5037–5043.

Gislason, S.R., Eugster, H.P., 1987a. Meteoric water–basalt interactions. 2: A field-study in NE Iceland. Geochim. Cosmochim. Acta 51, 2841–2855.

Gislason, S.R., Eugster, H.P., 1987b. Meteoric water–basalt interactions. 2: A laboratory study. Geochim. Cosmochim. Acta 51, 2827–2840.

Gislason, S.R., Oelkers, E.H., 2003. Mechanism, rates and consequences of basaltic glass dissolution: II. An experimental study of the dissolution rates of basaltic glass as a function of pH and temperature. Geochim. Cosmochim. Acta 67, 3817-3832.

Gislason, S.R., Wolff-Boenisch, D., Stefansson, A., Oelkers, E.H., Gunnlaugsson, E., Sigurdardóttir, H., Sigfússon, G., Brocker, W.S., Matter, J., Stute, M., Axelsson, G., Fridriksson, T., 2010. Mineral sequestration of carbon dioxide in basalt: A pre-injection overview of the CarbFix project. Int. J. Greenhouse Gas Control 4, 537-545.

Gudbrandsson, S., Wolff-Boenisch, D., Gislason, S.R., Oelkers, E.H., 2011. An experimental study of crystalline basalt dissolution from 2 ≤ pH ≤ 11 and temperatures from 5 to 75 °C. Geochim. Cosmochim. Acta 75, 5496-5509.

Gysi, A.P., Stefansson, A., 2011. CO_2–water–basalt interaction. Numerical simulation of low temperature CO_2 sequestration into basalts. Geochim. Cosmochim. Acta 75, 4728–4751.

Gysi, A.P., Stefansson, A., 2012a. CO_2-water-basalt interaction. Low temperature experiments and implications for CO_2 sequestration into basalts. Geochim. Cosmochim. Acta. 81, 129-152.

Gysi, A.P., Stefansson, A., 2012b. Mineralogical aspects of CO_2 sequestration during hydrothermal basalt alteration - An experimental study at 75 to 250 °C and elevated pCO_2. Chem. Geol. 306-307, 146–159.

Gysi, A.P., Stefansson, A., 2012c. Experiments and geochemical modeling of CO_2 sequestration during hydrothermal basalt alteration. Chem. Geol. 306-307, 10–28.

Hänchen, M., Prigiobbe, V., Storti, G., Seward, T.M., Mazzotti, M., 2006. Dissolution kinetics of fosteritic olivine at 90–150 ºC including effects of the presence of CO_2. Geochim. Cosmochim. Acta 70, 4403–4416.

Khalilabad, M.R., Axelsson, G., Gislason, S.R., 2008. Aquifer characterization with tracer test technique; permanent CO_2 sequestration into basalt, SW Iceland. Min. Mag. 72, 121–125.

Matter, J.M., Broecker, W.S., Stute, M., Gíslason, S.R., Oelkers, E.H., Stefánsson, A., Wolff-Boenisch, D., Gunnlaugsson, E., Axelsson, G., Björnsson, G., 2009. Permanent carbon dioxide storage into basalt: the CarbFix pilot project, Iceland. Energy Procedia 1, 3641–3646.

Matter, J.M., Broecker, W.S., Gislason, S.R., Gunnlaugsson, E., Oelkers, E.H., Stute, M., Sigurdardóttir, H., Stefansson, A., Alfredsson, H.A., Aradóttir, E.S., Axelsson, G., Sigfusson, B., Wolff-Boenisch, D., 2011. The CarbFix Pilot Project – Storing Carbon Dioxide in Basalt. Energy Procedia 4, 5579-5585.

McGrail, B.P., Schaef, H.T, Ho, A.M., Chien, Yi-Ju, Dooley, J.J., Davidson, C.L., 2006. Potential for carbon dioxide sequestration in flood basalts. JGR Research 111. B12201, doi:10.1029/2005JB004169.

Oelkers, E.H., Schott, J., 2001. An experimental study of enstatite dissolution rates as a function of pH, temperature, and aqueous Mg and Si concentration, and the mechanism of pyroxene/pyroxenoid dissolution. Geochim. Cosmochim. Acta 65, 1219–1231.

Oelkers, E.H., Gislason, S.R., 2001. The mechansim, rates and consequences of basaltic glass dissolution: I. An experimental study of the dissolution rates of basaltic glass as as function of aqueous Al, Si and oxalic acid concentration at 25 °C and pH = 3 and 11. Geochim. Cosmochim. Acta 65, 3671-3681.

Oelkers, E.H., Gislason, S.R., Matter, J., 2008. Mineral carbonation of CO_2. Elements 4, 333-337.

Pokrovsky, O.S., Schott, J., 2000. Kinetics and mechanism of forsterite dissolution at 25 °C and pH from 1 to 12. Geochim. Cosmochim. Acta 64, 3313–3325.

Schaef, H.T., McGrail, B.P., Owen, A.T., 2009. Basalt-CO_2-H_2O Interactions and Variability in Carbonate Mineralization Rates. Energy Procedia 1, 4899-4906.

Schaef, H.T., McGrail, B.P., 2009. Dissolution of Columbia River Basalt under mildly acidic conditions as a function of temperature: Experimental results relevant to the geological sequestration of carbon dioxide. Appl. Geochem. 24, 980-987.

Schaef, H.T., McGrail, B.P., Owen, A.T., 2010. Carbonate mineralization of volcanic province basalts. Int. J. Greenhouse Gas Control 4, 249-261.

Schaef, H.T., McGrail, B.P., Owen, A.T., 2011. Basalt Reactivity Variability with Reservoir Depth in Supercritical CO_2 and Aqueous Phases. Energy Procedia 4, 4977–4984.

Shirokova, L.S., Bénézeth, P., Pokrovsky, O.S., Gérard, E., Ménez, B., Alfredsson, H., 2011. Effect of the heterotrophic bacterium *Pseudomonas reactans* on olivine dissolution kinetics and implications for CO_2 storage in basalts. Geochim. Cosmochim. Acta 80, 30-50.

Stillings, L.L., Brantley, S.L., 1995. Feldspar dissolution at 25 °C and pH 3 – reaction stoichiometry and the effect of cations. Geochim. Cosmochim. Acta 59, 1483–1496.

Stockmann, G.J., Wolff-Boenisch, D., Gislason, S.R., Oelkers, E.H., 2011. Do carbonate precipitates affect dissolution kinetics? 1: Basaltic glass. Chem. Geol. 284, 306-316.

Stockmann, G.J., Shirokova, L.S., Pokrovsky, O.S., Benezeth, P., Bovet, N., Gislason, S.R., Oelkers, E.H., 2012. Does the presence of heterotrophic bacterium Pseudomonas reactans affect basaltic glass dissolution rates? Chem. Geol. 296-297, 1-18.

Wolff-Boenisch, D., Gislason, S.R., Oelkers, E.H., 2004. The effect of fluoride on the dissolution rates of natural glasses at pH 4 and 25°C. Geochim. Cosmochim. Acta 68, 4571–4582.

Wolff-Boenisch, D., 2011. On the buffer capacity of CO_2-charged seawater used for carbonation and subsequent mineral sequestration. Energy Procedia 4, 3738–3745.

Wolff-Boenisch, D., Wenau, S., Gislason, S.R., Oelkers, E.H., 2011. Dissolution of basalts and peridotite in seawater, in the presence of ligands, and CO_2: Implications for mineral sequestration of carbon dioxide. Geochim. Cosmochim. Acta 75, 5510–5525.

Appendices

Appendix I. Stockmann, G., Wolff-Boenisch, D., Gíslason, S.R. and Oelkers, E.H. (2008). Dissolution of diopside and basaltic glass: the effect of carbonate coating. Mineralogical Magazine 72, 135-139
(Extended abstract).

Appendix II. Chemistry of solutions from diopside dissolution experiments at 70 °C (Chapter 3, Diopside manuscript)

Appendix III. Growth of *Pseudomonas reactans* (HK 31.3) in the presence of extract of basalt (filtered solution) at different conditions
(Chapter 4, Stockmann et al., 2012)

Mineralogical Magazine, February 2008, Vol. 72(1), pp. 135–139

Dissolution of diopside and basaltic glass: the effect of carbonate coating

G. Stockmann[1,*], D. Wolff-Boenisch[1], S. R. Gíslason[1] and E. H. Oelkers[2]

[1] Institute of Earth Sciences, University of Iceland, Askja, Sturlugata 7, 101 Reykjavik, Iceland
[2] Géochimie et Biogéochimie Expérimentale, Université Paul Sabatier, CNRS-UMR 5563, 14 rue Edouard Belin, 31400 Toulouse, France

ABSTRACT

Far-from-equilibrium dissolution experiments with diopside and basaltic glass in mixed-flow reactors at 70ºC and pH 8.2 show that solute concentrations do not reach steady state over the experimental duration of 45–60 days. Chemical modelling indicates that during the dissolution experiments, solutions have become supersaturated with respect to carbonates in the case of diopside, and carbonates, clay minerals and zeolites in the case of the basaltic glass. Decreasing dissolution is therefore interpreted as a result of secondary surface precipitates blocking the reactive surface area. Calcite formation was supported in both experiments by a significant increase in Ca (and Sr) concentrations as pH was abruptly lowered from 8.2 to 7 because this change increased carbonate solubility and caused all potential carbonate precipitates to re-dissolve. The reduction in pH also led to an increase in Si concentration for diopside and a decrease in Si concentration for basaltic glass. This observation is in accordance with previous experiments on the pH-dependent dissolution rates of pyroxenes and basaltic glass.

Keywords: dissolution, diopside, basaltic glass, carbonate coating, carbon dioxide sequestration, mixed-flow reactor.

Introduction

Increasing emission of industrial carbon dioxide (CO_2) into the atmosphere has been identified as one of the biggest challenges of this century because of its effect on the global climate (Hoffert *et al.*, 2002; Broecker, 2005). One solution to solve this problem is to inject CO_2 into a geological stable environment, where it can be stored safely. The Hellisheidi geothermal power plant in Iceland and its vicinity has been suggested as a good testing ground for trapping CO_2 directly from the power plant and storing it in the underlying basaltic rocks. Basalt is known for its high reactivity and easy weathering (e.g. Gíslason and Oelkers, 2003; Gíslason *et al.*, 2006). There are several examples in nature and laboratory experiments of carbonates being formed by chemical weathering of basalts (e.g. McGrail *et al.*, 2006).

Prior to the CO_2 injection a series of laboratory experiments and modelling are required to optimize the injection conditions at the Hellisheidi site. The main components of basaltic rocks are pyroxenes, plagioclase and basaltic glass rich in Ca, Mg and Fe, and chemical modelling predicts that these minerals will dissolve in contact with CO_2-saturated water and form carbonates, clays and zeolites (Gysi and Stefánsson, 2008). The dissolution rates of basaltic glass and pyroxenes are known at far-from-equilibrium conditions (Oelkers and Gíslason, 2001; Gíslason and Oelkers, 2003; Wolff-Boenisch *et al.*, 2004; Knauss *et al.*, 1993; Golubev *et al.*, 2005), but it is unknown how dissolution of these components will evolve in a solution saturated with carbonates, clays and zeolites. A decrease in dissolution of basaltic

* E-mail: gjs3@hi.is
DOI: 10.1180/minmag.2008.072.1.135

rocks caused by precipitation will have implications for the amount and rate of CO_2 being sequestered. In this paper we report on an experiment conducted to study the changes in dissolution kinetics of basaltic glass and diopside in a solution saturated with calcite ($CaCO_3$).

Method and materials

Natural crystals of diopside from the Transbaikal region in Russia and basaltic glass from Stapafell in SW Iceland were used in this experiment. Previous electron microprobe analysis showed the diopside composition to be $Ca_{0.99}Mg_{0.98}Fe_{0.02}Cr_{0.01}Si_2O_6$ (Golubev *et al.*, 2005). Acid and deionized water-washed crystals of diopside were ground with an agate mortar and pestle and sieved, whereas the basaltic glass was crushed in plastic bags with a soft plastic hammer and then sieved. For both mineral and glass, the 45 to 125 μm size fraction was ultrasonically cleaned in cycles of deionized water and acetone, separating and discarding the ultra fine suspension at the end of each cleaning cycle, and finally dried overnight at 60ºC.

10 g of each material were transferred into a 300 ml polyethylene mixed-flow reactor. Both reactors were placed in a 70ºC water bath heated by a thermo heater (Thermo-Haake C10) and kept at constant temperature during the 60 days of the experiment. Teflon™-coated floating stir bars from Nalgene™ were placed on the bottom of the reactors and propelled by a multi-position magnetic stirrer located underneath the water bath. A constant pumping rate of 0.6 ml/min was maintained using a Masterflex™ cartridge pump. Inlet solutions comprised Millipore™ water and Merck analytical grade $NaHCO_3$ and HCl. The ionic strength of the inlet solution was 0.035. The outlet solution was filtered through a 0.2 μm cellulose acetate membrane filter, acidified with concentrated supra-pure HNO_3 and analysed for Si, Ca and Mg content by ICP-OES spectrometry (Spectro Ciros Vision).

TABLE 1. Summary of diopside dissolution experiments performed at 70ºC.

Sample no.	Duration (days)	pH[a]	[Si] (μM)	[Ca^{2+}] (μM)	[Mg^{2+}] (μM)	[Sr^{2+}] (μM)
D-1	1	8.2	65.2	22.2	27.5	0.15
D-3	3	8.2	28.3	12.7	10.6	0.09
D-5	5	8.2	21.7	9.0	7.7	0.06
D-7	7	8.2	19.4	8.1	7.1	0.05
D-9	8	8.2	19.6	7.8	7.0	0.04
D-11	10	8.2	19.1	6.3	6.6	0.04
D-13	18	8.2	17.3	5.9	6.0	0.03
D-15	20	8.2	20.3	8.2	6.6	0.05
D-17	23	8.2	18.7	7.7	7.2	0.04
D-19	25	8.2	18.8	7.8	7.3	0.04
D-21	27	8.2	16.4	6.1	6.1	0.03
D-23	31	8.2	17.3	5.5	5.6	0.03
D-25	33	8.2	15.2	4.7	5.1	0.03
D-27	35	8.2	14.7	4.4	4.7	0.03
D-29	39	8.2	14.1	4.6	4.9	0.03
D-31	41	8.2	14.1	5.3	5.3	0.03
D-33	45	8.2	11.1	3.7	3.9	0.02
D-35	47	8.2	11.3	3.8	4.1	0.02
D-37	52	8.2	8.3	4.0	4.0	0.02
D-38	53	8.2	7.1	3.6	4.0	0.02
D-39	56	7.0	44.6	30.9	27.7	0.15
D-40	57	7.0	33.7	20.5	20.1	0.10
D-41	58	7.0	28.3	15.5	16.1	0.08
D-42	59	7.0	23.4	11.8	13.3	0.06
Change in conc. D-39/D-38			6.3	8.6	7.0	8.6

[a] Background electrolyte was a $NaHCO_3$/HCl buffer.

In this study, dissolution experiments of diopside and basaltic glass ran for 60 and 45 days, respectively. The pH of the inlet solution was kept constant at pH 8.2 during the main part of the experiments. One final batch of pH 7 inlet solution over four days ended both experiments.

Results and discussion

The results of the diopside dissolution experiment are listed in Table 1. The values show a continuous decrease in Si, Ca and Mg concentrations with time and did not reach a steady state (Fig. 1). In contrast, Knauss *et al.* (1993) reported a steady state for diopside dissolution under similar experimental conditions (but in the absence of bicarbonate) within 10–15 days. Dissolution rates are known to slow down in near-equilibrium solutions; however, our experiments were carried out in far-from-equilibrium conditions with respect to diopside. Rather, we interpret this discrepancy as a result of calcite precipitation in our experiments, covering the diopside surface and impeding the dissolution process and the achievement of a steady state. A similar tendency has been reported by Cubillas *et al.* (2005) who observed decreasing dissolution rates of calcite by overgrowth of otavite ($CdCO_3$).

Not only calcite would hamper dissolution, but probably any kind of precipitate (e.g. Hodson, 2002). The reason we favour calcite as the dominating precipitate is because chemical modelling with *PHREEQC* (Parkhurst and Appelo, 1999) shows calcite (and dolomite) to be the only saturated phases in the initial solution. Ca release rates from diopside were estimated using the formula given in Golubev *et al.* (2005). A temperature of 70ºC was chosen because *PHREEQC* calculations indicated that from this temperature on, sufficient material would dissolve and provide the required amount of Ca ions to assure calcite saturation in combination with a 35 mM $NaHCO_3$ inlet solution. As for dolomite, it rarely forms in laboratory experiments and has therefore been tentatively ruled out in this study.

At the end of the experiment a 4-day pulse of pH 7 solution was injected into the reactors by adding HCl to the $NaHCO_3$ inlet solution. The purpose was to dissolve potential carbonates that might have precipitated on the surface. This pulse led to a consistent increase in solute concentrations of Si, Ca and Mg by a factor of 6–9 (cf. Table 1 and Fig. 1). The change in Sr concentration is also listed in Table 1 as Sr is known to substitute for Ca in calcite. Both ions increased by a factor 8.6, suggestive of calcite precipitation. The observed increase in Si concentration by lowering pH is in accordance with results from Knauss *et al.* (1993) who showed that dissolution rates of diopside based on the Si concentration follow a linear trend where dissolution rates (and by extension the Si solute concentrations) increase with lowering pH (see Fig. 2).

Table 2 reports a summary of the results from dissolution of basaltic glass at 70ºC. The trend was similar to the experiment with diopside; i.e., decreasing Si, Ca, Mg and Sr concentrations over time and no attainment of a steady state. Again, we attribute this to precipitates on the surface of basaltic glass crystals that limited the dissolution. PHREEQC modelling of the 31 samples indicated

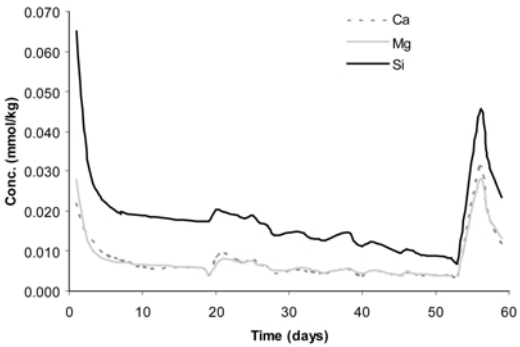

FIG. 1. Dissolution of diopside at 70ºC.

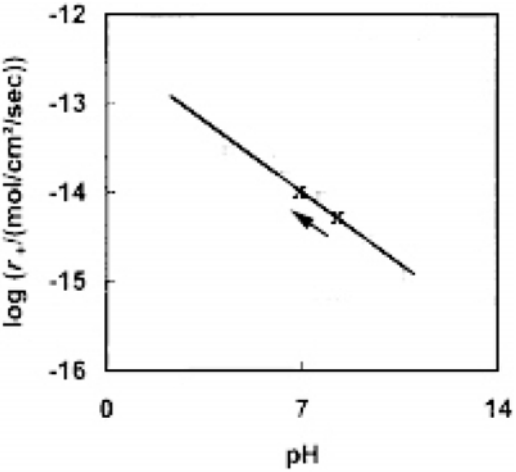

FIG. 2. Dissolution rates of diopside at 70ºC as a function of pH. The arrow marks the route from pH 8 to 7 in the experiment in this study. Modified from Knauss *et al.* (1993) and Oelkers and Schott (2001).

TABLE 2. Summary of basaltic glass dissolution experiments performed at 70ºC.

Sample no.	Duration Days	pH[a]	[Si] µM	[Ca^{2+}] µM	[Mg^{2+}] µM	[Sr^{2+}] µM
B-1	6	8.2	317.6	16.7	69.3	0.02
B-3	8	8.2	308.9	23.6	81.1	0.03
B-5	11	8.2	298.2	21.0	73.1	0.03
B-7	13	8.2	291.7	21.2	73.4	0.03
B-9	15	8.2	280.9	19.5	69.1	0.02
B-11	19	8.2	258.0	21.7	70.0	0.03
B-13	21	8.2	250.2	20.8	64.0	0.03
B-15	23	8.2	256.9	18.9	66.9	0.03
B-17	27	8.2	237.2	19.6	60.7	0.03
B-19	29	8.2	228.3	22.2	64.1	0.03
B-21	33	8.2	229.7	18.5	61.1	0.03
B-23	35	8.2	208.9	20.6	55.8	0.03
B-25	37	8.2	221.5	17.9	54.2	0.03
B-27	41	8.2	207.4	18.0	50.8	0.03
B-28	42	7.0	198.1	758.2	66.8	1.33
B-29	43	7.0	168.3	450.7	58.0	0.68
B-30	44	7.0	147.3	228.5	42.8	0.36
B-31	45	7.0	110.8	108.2	25.8	0.17
Change in conc. B-28/B-27			1.0	42	1.3	46

[a] Background electrolyte was $NaHCO_3$/HCl.

supersaturation not only with respect to calcite and dolomite but also clay minerals and zeolites. However, of these minerals calcite and dolomite were the only phases containing Ca.

Analogously to the diopside experiments, lowering the pH to 7 resulted in a major increase in Ca and Sr concentrations. The magnitude of this rise was very similar, indicating again the close link between stoichiometric Sr and Ca substitution. As to Si, its concentration kept on deceasing (Fig. 3), which was again consistent with findings in the literature (Gíslason and Oelkers, 2003). In contrast to diopside and other pyroxenes, basaltic glass dissolution rates were expected to decrease when going from pH 8.2 to 7 (Fig. 4) and this behaviour was observed in our experiments.

In the future, a characterization of the precipitates present on the silicate surface will be performed in order to unequivocally confirm and quantify the amount of carbonates. In these preliminary experiments, interpretations have been based on a combination of chemical

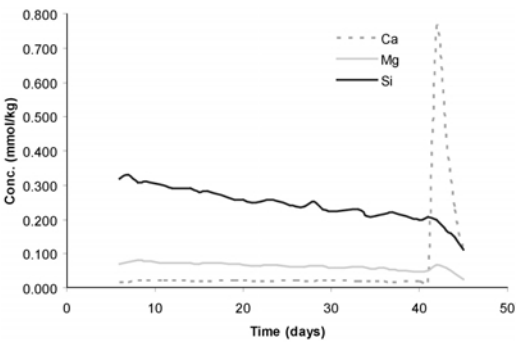

FIG. 3. Dissolution of basaltic glass at 70ºC.

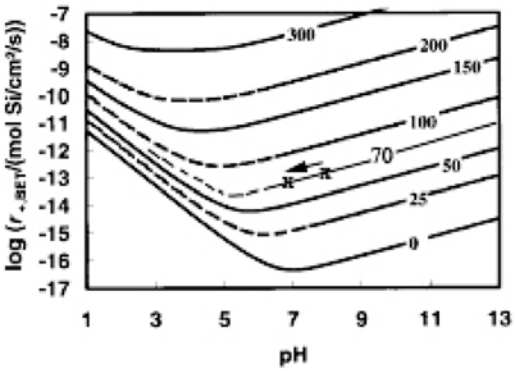

FIG. 4. Dissolution rate of Si in basaltic glass at 0–300ºC. The 70ºC curve has been added and the arrow marks the route from pH 8 to 7 (modified from Gíslason and Oelkers, 2003).

modelling and consistent observations of solute concentrations as a function of small pH changes.

Conclusion

The preliminary results displayed a decrease in dissolution concentrations for Si, Ca and Mg over time for diopside and basaltic glass in a solution saturated with calcite at a constant temperature of 70ºC and pH 8.2, thus indicating that carbonate coatings will slow down the dissolution rates of diopside and basaltic glass.

The implication for the CO_2 sequestration project at Hellisheidi is that, if coatings reduce the dissolution rates of basaltic minerals, this could affect the amount of Ca, Mg and Fe being released by CO_2-supersaturated water and thereby limit the amount of CO_2 being trapped as carbonate minerals.

Acknowledgements

We would like to thank Reykjavík Energy, Nordural and Hitaveita Sudurnesja for their financial support. This study is part of the Carb-Fix project. We thank many colleagues for their help, in particular Helgi Alfredsson for XRF analysis, Eydís Salome Eiríksdóttir, Snorri Gudbrandsson and Ingvi Gunnarsson at the University of Iceland, and Hólmfridur Sigurdardóttir at Reykjavík Energy.

References

Broecker, W.S. (2005) Global warming: Take action or wait? *Jökull*, **55**, 1–16.

Cubillas, P., Köhler, P., Prieto, P. and Oelkers, E. H. (2005) Experimental determination of the dissolution rates of calcite, aragonite and bivalves. *Chemical Geology*, **216**, 59–67.

Gíslason, S.R. and Oelkers, E.H. (2003) The mechanism, rates and consequences of basaltic glass dissolution: II. An experimental study of the dissolution rates of basaltic glass as a function of pH and temperature. *Geochimica et Cosmochimica Acta*, **67**, 3817–3832.

Gislason, S.R., Oelkers, E.H. and Snorrason, Á. (2006) The role of river suspended material in the global carbon cycle. *Geology*, **34**, 49–52.

Golubev, S.V., Pokrovsky, O.S. and Schott, J. (2005) Experimental determination of the effect of dissolved CO_2 on the dissolution kinetics of Mg and Ca silicates at 25ºC. *Chemical Geology*, **217**, 227–238.

Gysi, A.P. and Stefánsson, A. (2008) Numerical simulation of CO_2-water basalt interaction. *Mineralogical Magazine*, **72**, 55–59.

Knauss, K.G., Nguyen, S.N. and Weed, H.C. (1993) Diopside dissolution kinetics as a function of pH, CO_2, temperature, and time. *Geochimica et Cosmochimica Acta*, **57**, 285–294.

Hodson, M. (2002) The influence of Fe-rich coatings on the dissolution of anorthite at pH 2.6. *Geochimica et Cosmochimica Acta*, **67**, 3355–3363.

Hoffert, M.I., Caldeira, K., Benford, G., Criswell, D.R., Green, C., Herzog, H., Jain, A.K., Kheshgi, H.S., Lackner, K.S. Lewis, J.S., Lightfoot, H.D., Manheimer, W. Mankins, J.C., Mauel, M.E., Perkins, L.J., Schlesinger, M.E., Volk, T. and Wigley, T.M.L. (2002) Advanced technology paths to global climate stability. Energy for a greenhouse planet. *Science*, **298**, 981–987.

McGrail, B.P., Schaef, H.T., Ho, A.M., Chien, Y.-J., Dooley, J.J. and Davidson, C.L. (2006) Potential for carbon dioxide sequestration in flood basalts. Journal of Geophysical Research, **111**, B12201, doi:10.1029/2005JB004169.

Oelkers, E.H. and Gíslason, S.R. (2001) The mechanism, rates and consequences of basaltic glass dissolution: I. An experimental study of the dissolution rates of basaltic glass as a function of aqueous Al, Si and oxalic acid concentration at 25ºC and pH = 3 and 11. *Geochimica et Cosmochimica Acta*, **65**, 3671–3681.

Oelkers, E.H. and Schott, J. (2001) An experimental study of enstatite dissolution rates as a function of pH, temperature, and aqueous Mg and Si concentration, and the mechanism of pyroxene/pyroxenoid dissolution. *Geochimica et Cosmochimica Acta*, **65**, 1219–1231.

Parkhurst, D. L. and Appelo, C.A.J. (1999) *User's guide to PHREEQC (Version 2) – A computer program for speciation, batch-reaction, one-dimensional transport, and inverse geochemical calculations*. USGS, Water Resources Investigation Report, 99–4259.

Wolff-Boenisch, D., Gíslason, S.R., Oelkers, E.H. and Putnis, C.V. (2004) The dissolution rates of natural glasses as a function of their composition at pH 4 and 10.6, and temperatures from 25 to 74ºC. *Geochimica et Cosmochimica Acta*, **68**, 4843–4858.

Diopside dissolution rates based on Si, Ca and Mg - Experiment 1a-b at 70 °C

	Elapsed time	pH	log *r*+, Si (BET)	log *r*+, Ca (BET)	log *r*+, Mg (BET)	ΔG_r Diopside	log (a^2_{H+}/a_{Ca2+})	log (a^2_{H+}/a_{Mg2+})
Exp. no.	days	70 °C	mol/cm^2/s	mol/cm^2/s	mol/cm^2/s	kJ/mol		
D-1	0.9	8.34	-13.52	-13.69	-13.59	-21.92	-11.29	-11.59
D-2	1.9	8.36	-13.73	-13.85	-13.82	-26.88	-11.15	-11.40
D-3	2.9	8.38	-13.89	-13.94	-14.00	-30.32	-11.09	-11.25
D-4	3.9	8.39	-13.96	-14.03	-14.09	-32.25	-11.02	-11.18
D-5	4.9	8.44	-14.00	-14.08	-14.13	-32.33	-11.05	-11.23
D-6	5.9	8.43	-14.03	-14.12	-14.17	-33.40	-10.99	-11.19
D-7	6.9	8.47	-14.06	-14.15	-14.18	-33.36	-11.01	-11.23
D-8	7.1	8.47	-14.04	-14.17	-14.18	-33.31	-11.00	-11.23
D-9	8.1	8.50	-14.05	-14.17	-14.19	-32.91	-11.04	-11.27
D-10	8.9	8.49	-14.06	-14.23	-14.21	-33.77	-10.96	-11.23
D-11	10.0	8.52	-14.07	-14.26	-14.22	-33.49	-10.98	-11.29
D-12	11.0	8.56	-14.07	-14.29	-14.23	-33.15	-11.01	-11.33
D-13	18.0	8.56	-14.10	-14.28	-14.26	-33.71	-11.02	-11.30
D-14	18.9	8.55	-14.10	-14.50	-14.41	-36.49	-10.76	-11.13
D-15	19.9	8.36	-14.04	-14.15	-14.22	-35.66	-10.85	-10.97

D-16	20.9	8.36	-14.05	-14.10	-14.14	-34.85	-10.91	-11.06
D-17	23.0	8.53	-14.07	-14.19	-14.18	-32.70	-11.07	-11.33
D-18	23.9	8.43	-14.08	-14.21	-14.19	-34.93	-10.91	-11.13
D-19	24.9	8.42	-14.07	-14.17	-14.18	-34.52	-10.93	-11.15
D-20	25.9	8.46	-14.11	-14.24	-14.24	-35.25	-10.92	-11.15
D-21	26.9	8.44	-14.13	-14.29	-14.26	-36.20	-10.84	-11.10
D-22	27.9	8.49	-14.19	-14.41	-14.34	-37.36	-10.80	-11.11
D-23	30.9	8.39	-14.16	-14.29	-14.27	-37.64	-10.76	-11.01
D-24	31.9	8.42	-14.17	-14.32	-14.28	-37.52	-10.76	-11.05
D-25	32.9	8.56	-14.20	-14.32	-14.29	-35.57	-10.98	-11.27
D-26	33.9	8.43	-14.21	-14.36	-14.32	-38.29	-10.76	-11.01
D-27	34.9	8.47	-14.21	-14.37	-14.33	-37.84	-10.79	-11.08
D-28	38.1	8.44	-14.15	-14.27	-14.27	-36.52	-10.86	-11.09
D-29	39.0	8.49	-14.23	-14.35	-14.32	-37.69	-10.84	-11.10
D-30	39.9	8.51	-14.27	-14.44	-14.37	-38.58	-10.78	-11.11
D-31	40.9	8.41	-14.23	-14.31	-14.29	-38.67	-10.77	-11.00
D-32	41.9	8.41	-14.24	-14.31	-14.30	-38.64	-10.77	-11.01
D-33	44.9	8.50	-14.32	-14.44	-14.41	-39.80	-10.77	-11.06
D-34	45.9	8.53	-14.31	-14.35	-14.34	-37.90	-10.91	-11.19
D-35	46.9	8.37	-14.33	-14.39	-14.38	-41.73	-10.62	-10.87

D-36	47.9	8.47	-14.37	-14.42	-14.41	-40.82	-10.74	-11.00
D-37	52.1	8.37	-14.42	-14.42	-14.42	-43.29	-10.59	-10.82
D-38	53.0	8.37	-14.48	-14.47	-14.42	-44.53	-10.53	-10.82
D-39	55.9	6.70	-13.69	-13.54	-13.59	-61.61	-8.52	-8.49
D-40	57.1	6.73	-13.81	-13.72	-13.73	-64.47	-8.40	-8.42
D-41	58.0	6.83	-13.89	-13.84	-13.82	-64.35	-8.48	-8.52
D-42	59.1	7.19	-13.97	-13.96	-13.91	-57.58	-9.06	-9.14

Diopside dissolution rates based on Si, Ca and Mg - Experiment 2 at 70 °C

	Elapsed time	pH	log $r+,Si$ (BET)	log $r+,Ca$ (BET)	log $r+,Mg$ (BET)	ΔG_r Diopside	log (a^2_{H+}/a_{Ca2+})	log (a^2_{H+}/a_{Mg2+})
Exp. no.	days	70 °C	mol/cm^2/s	mol/cm^2/s	mol/cm^2/s	kJ/mol		
D-100	4.0	8.39	-14.08	-14.44	-14.31	-38.09	-10.59	-10.93
D-101	5.9	8.25	-14.11	-14.45	-14.37	-41.54	-10.39	-10.66
D-102	6.9	8.29	-14.19	-14.52	-14.42	-42.53	-10.38	-10.68
D-103	9.9	8.22	-14.25	-14.57	-14.45	-45.48	-10.21	-10.51
D-104	11.9	8.30	-14.36	-14.89	-14.60	-48.67	-9.99	-10.48
D-105	13.8	8.24	-14.35	-14.73	-14.57	-48.09	-10.09	-10.44
D-106	16.9	8.24	-14.41	-14.77	-14.60	-49.65	-10.04	-10.37
D-107	19.0	8.35	-14.41	-14.95	-14.67	-48.97	-10.05	-10.48
D-108	25.8	8.51	-14.43	-15.29	-14.83	-49.41	-9.90	-10.67

Diopside dissolution rates based on Si, Ca and Mg - Experiment 3 at 70 °C

Exp. no.	Elapsed time days	pH 70 °C	log $r+,Si$ (BET) mol/cm^2/s	log $r+,Ca$ (BET) mol/cm^2/s	log $r+,Mg$ (BET) mol/cm^2/s	ΔG_r Diopside kJ/mol	log (a^2_{H+}/a_{Ca2+})	log (a^2_{H+}/a_{Mg2+})
D-200	3.0	8.29	-13.99	-14.28	-14.14	-49.02	-10.31	-10.56
D-201	3.9	8.35	-14.06	-14.29	-14.18	-49.06	-10.39	-10.63
D-202	4.8	8.23	-14.05	-14.31	-14.21	-51.96	-10.17	-10.38
D-203	5.9	8.28	-14.09	-14.38	-14.24	-51.98	-10.19	-10.44
D-204	6.9	8.30	-14.12	-14.38	-14.25	-52.07	-10.23	-10.47
D-205	7.9	8.33	-14.16	-14.61	-14.35	-54.06	-10.05	-10.42
D-206	9.9	8.21	-14.16	-14.43	-14.32	-55.50	-10.02	-10.22
D-207	10.9	8.26	-14.14	-14.47	-14.31	-54.16	-10.07	-10.34
D-208	12.8	8.34	-14.21	-14.56	-14.38	-54.34	-10.12	-10.41

Growth of *Pseudomonas reactans* (HK 31.3) in the presence of extract of basalt (filtered solution) at different conditions [a]

Experiment:	10% NB, 0.01 M $NaHCO_3$, 1% NaCl, 40 mL of basalt-extract (0.01 M $NaHCO_3$)						
Sample:	G3-1	G3-2	G3-3	G3-4	G3-5	G3-6	G3-7
Elapsed time, hrs	0	14	47	84	135	156	187
Biomass, CFU/mL	22000000	141500000	269500000	321000000	336000000	336500000	329500000
OD at 600 nm	0.044	0.283	0.539	0.642	0.672	0.673	0.659
pH	8.05	7.91	8.15	8.07	8.44	8.31	8.2
Si (mg/L)	3.007	3.53	3.18	3.39	3.45	3.49	3.16
B	16	20	11	14	17	16	46
Na	5982116	6289184	6383092	6484464	6519904	6797392	6738345
Mg	106	103	115	86	109	105	84
Al	330	354	277	316	410	331	353
P	59519	61156	61005	60930	62401	63198	65164
K	32914	31990	32870	32726	45250	44171	55029
Ca	547	452	376	433	579	431	400
Ti	54	51	50	50	50	52	52
V	3.484	3.400	3.528	3.560	3.513	3.968	3.716
Cr	2.652	2.069	1.991	2.170	3.303	2.447	2.804
Mn	0.784	1.785	0.446	0.205	0.402	0.096	1.038
Fe	57.9	51.6	6.7	3.9	8.4	2.2	7.1
Co	<d.l.	0.147	0.081	0.069	0.157	0.159	0.168
Ni	0.860	1.364	1.260	1.451	2.501	1.536	2.003
Cu	25.4	13.1	17.0	10.4	17.4	19.2	14.6
Zn	67	81	82	78	71	80	72
As	2.625	2.930	2.802	2.549	2.852	3.022	2.827
Rb	12.219	11.974	12.098	11.811	12.097	12.156	12.262
Sr	4.174	4.016	4.433	3.624	4.275	4.390	4.013
Y	0.011	0.001	0.001	0.016	0.030	0.009	0.009
Zr	0.455	0.442	0.298	0.333	0.387	0.336	0.460
Mo	0.872	0.375	0.196	0.083	0.046	0.067	0.213
Sb	0.405	0.261	0.099	0.069	0.161	0.065	0.029
Cs	0.178	0.198	0.159	0.172	0.183	0.172	0.189
Ba	0.914	2.777	4.152	0.997	1.697	1.795	2.298
La	2.563	2.970	2.069	2.464	3.379	2.865	2.657
Ce	0.019	0.031	0.020	0.017	0.026	0.009	0.025
Nd	0.045	0.010	0.012	0.033	0.019	0.003	0.042
Pb	1.393	1.391	1.156	0.803	1.275	1.060	1.309
Th	0.005	0.002	0.007	0.001	0.003	0.000	0.001
U	0.092	0.087	0.064	0.063	0.084	0.070	0.065

[a] *All element concentrations are in µg/L, except for Si*

Experiment:	**10% NB, 1% NaCl, 40 mL of 0.005 M basalt-extract Na Acetate**						
Sample:	G5-1	G5-2	G5-3	G5-4	G5-5	G5-6	G5-7
Elapsed time, hrs	0	14	47	84	135	156	187
Biomass, CFU/mL	23000000	150000000	294500000	365000000	362500000	374000000	376000000
OD at 600 nm	0.046	0.3	0.589	0.73	0.725	0.748	0.752
pH	7.85	7.62	7.57	7.79	7.94	8.01	7.91
Si (mg/L)	3.3	3.47	3.43	3.4	3.32	3.5	3.15
B	25	32	14	22	23	21	18
Na	5846052	5998410	6301906	6404352	6448128	6756837	6702384
Mg	270	287	303	243	273	263	247
Al	471	478	388	493	330	281	346
P	64027	63545	63822	61229	62403	65572	65749
K	35105	33290	34995	33623	51887	41496	44519
Ca	433	374	458	311	389	480	340
Ti	57	56	53	51	51	55	52
V	2.5	2.9	2.8	2.8	2.7	2.5	2.8
Cr	6.8	4.5	5.6	4.2	4.3	5.6	4.6
Mn	16.3	14.8	9.3	3.0	2.4	1.1	1.8
Fe	248.9	230.7	164.7	134.0	120.8	108.0	104.8
Co	0.742	0.998	0.692	0.591	0.698	0.496	0.681
Ni	4.407	5.171	4.520	4.361	4.580	4.835	4.879
Cu	13.87	20.88	12.71	8.37	11.42	22.80	11.13
Zn	117	59	55	45	51	91	86
As	3.127	2.984	2.729	2.622	2.660	2.882	2.701
Rb	12.249	11.926	12.093	11.569	12.052	12.104	11.711
Sr	5.123	3.751	3.399	3.961	3.847	3.586	3.641
Y	0.033	0.017	0.025	0.018	0.007	0.019	0.009
Zr	0.677	0.610	0.475	0.477	0.478	0.359	0.353
Mo	1.021	0.407	0.150	0.165	<d.l.	<d.l.	<d.l.
Sb	0.351	0.211	0.159	0.151	0.100	0.102	0.058
Cs	0.144	0.132	0.141	0.142	0.164	0.142	0.149
Ba	0.939	1.255	1.300	0.962	4.716	1.174	3.416
La	2.161	2.093	1.168	2.063	3.624	0.082	2.274
Ce	0.035	0.015	0.023	0.019	0.002	0.027	0.012
Nd	0.016	0.002	0.019	0.022	<d.l.	<d.l.	<d.l.
Pb	1.097	0.835	0.816	1.345	1.191	1.069	1.099
Th	0.010	0.017	0.003	0.003	0.014	0.009	0.011
U	0.073	0.049	0.052	0.040	0.049	0.076	0.071

[a] *All element concentrations are in µg/L, except for Si*

d.l.: detection limit

Experiment:	**No-growth of HK 31.3, in 0.01 M Na Azide, 10% NB, 1% NaCl, 0.01 M $NaHCO_3$; added 40 mL of basalt extract in 0.01 M $NaHCO_3$**						
Sample:	G6-1	G6-2	G6-3	G6-4	G6-5	G6-6	G6-7
Elapsed time, hrs	0	14	47	84	135	156	187
Biomass, CFU/mL	252900000	262500000	234500000	182500000	198000000	207000000	201500000
OD at 600 nm	0.5058	0.525	0.469	0.365	0.396	0.414	0.403
pH	7.21	7.25	7.37	7.68	7.83	7.91	8.05
Si (mg/L)	3.33	3.22	3.08	3.28	3.34	3.38	3.46
B	24.113	21.169	18.559	17.507	16.912	22.206	19.916
Na	6295030	6589560	6829934	6915150	6875044	7070124	7276923
Mg	521	533	560	621	715	746	760
Al	416	423	393	354	338	351	384
P	55148	56961	59955	60668	62136	63757	67142
K	29019	32078	35051	34703	47367	41978	43722
Ca	549	481	381	428	380	527	514
Ti	48.2	49.1	52.3	49.8	49.0	52.4	52.8
V	2.663	2.390	2.379	2.327	2.947	2.664	2.714
Cr	11.784	5.733	5.594	4.411	4.167	4.160	5.020
Mn	16.8	14.3	12.9	12.6	10.4	11.0	10.6
Fe	208.8	214.8	206.2	195.9	179.6	187.9	184.2
Co	0.634	0.640	0.564	0.597	0.746	0.767	0.868
Ni	8.149	4.244	3.859	4.185	5.063	28.160	5.444
Cu	12.832	50.242	20.061	28.410	30.692	37.521	32.666
Zn	132	89	81	85	63	61	56
As	3.656	3.724	4.048	4.268	4.379	4.863	5.149
Rb	10.320	10.039	10.907	10.681	11.117	10.969	11.155
Sr	5.254	4.739	4.725	3.803	4.880	4.421	4.859
Y	0.022	0.016	0.017	0.019	0.018	0.023	0.017
Zr	0.740	0.464	0.357	0.362	0.363	0.367	0.331
Mo	1.132	0.763	0.703	0.628	0.719	1.047	1.096
Sb	0.804	0.250	0.167	0.116	0.109	0.155	0.079
Cs	0.130	0.156	0.152	0.154	0.135	0.154	0.145
Ba	11.951	7.577	5.988	4.449	4.865	8.590	4.705
La	1.101	2.523	1.249	2.125	3.005	2.307	2.182
Ce	0.092	0.009	0.010	0.015	0.019	0.014	0.019
Nd	0.118	0.024	0.047	<d.l.	<d.l.	0.031	0.058
Pb	71.695	2.131	2.137	0.925	0.917	0.610	0.661
Th	0.056	0.038	0.031	0.019	0.030	0.022	0.019
U	0.043	0.052	0.067	0.063	0.073	0.075	0.101

[a] *All element concentrations are in µg/L, except for Si*

d.l.: detection limit

Experiment:	**No growth of HK 31.3, in 0.01 M Na Azide, 10% NB, 1% NaCl, 0.01 M $NaHCO_3$; added 40 mL of basalt extract in Acetate**						
Sample:	G4-1	G4-2	G4-3	G4-4	G4-5	G4-6	G4-7
Elapsed time, hrs	0	14	47	84	135	156	187
Biomass, CFU/mL	238950000	250000000	247000000	240500000	227000000	229000000	221000000
OD at 600 nm	0.4779	0.5	0.494	0.481	0.454	0.458	0.442
pH	7.85	7.83	8.04	8.24	8.38	8.21	8.18
Si (mg/L)	3.10	3.42	3.45	3.5	3.12	3.1	3.26
B	18	25	21	21	18	25	22
Na	7025130	7005076	7388910	7921110	7540191	7985775	7662375
Mg	276	323	354	400	481	521	486
Al	321	332	329	344	352	372	375
P	55036	57587	60980	65779	63354	64840	64619
K	29141	29806	34901	37029	46111	50763	43555
Ca	704	658	702	688	621	665	619
Ti	46.357	47.811	51.286	53.603	51.365	53.439	52.804
V	3.636	3.612	3.711	3.938	4.271	4.207	4.093
Cr	2.463	1.727	1.934	1.653	1.865	1.206	2.103
Mn	0.151	0.767	0.535	0.480	0.151	0.270	0.338
Fe	33.707	31.960	19.579	35.783	18.254	18.885	19.631
Co	0.111	0.066	0.142	0.188	0.139	<d.l.	<d.l.
Ni	1.258	1.718	1.514	2.201	2.121	1.966	1.950
Cu	11.287	8.585	12.955	19.520	52.305	80.001	28.726
Zn	59	59	66	65	46	49	55
As	3.888	3.960	3.810	4.568	4.766	4.598	4.842
Rb	10.017	10.054	10.984	11.426	10.872	11.229	10.627
Sr	3.224	3.663	4.155	4.490	4.022	4.682	4.421
Y	0.037	0.035	0.030	0.020	0.027	0.028	0.016
Zr	0.309	0.360	0.306	0.303	0.243	0.247	0.203
Mo	1.322	0.459	0.394	0.193	0.662	0.487	0.560
Sb	0.424	0.240	0.153	0.171	0.149	0.137	0.070
Cs	0.156	0.169	0.172	0.177	0.201	0.185	0.163
Ba	7.230	6.710	7.259	7.719	5.527	5.658	4.891
La	1.143	2.361	0.335	2.480	1.784	2.285	2.135
Ce	0.020	0.017	0.021	0.028	0.023	0.020	0.016
Nd	0.067	0.027	0.049	<d.l.	0.026	0.044	<d.l.
Pb	0.739	0.634	1.045	1.277	1.115	1.154	0.729
Th	0.039	0.037	0.012	0.028	0.018	0.011	0.011
U	0.062	0.104	0.116	0.098	0.104	0.131	0.105

[a] *All element concentrations are in µg/L, except for Si, d.l.: detection limit*